

1983

Electrocatalysis of the anodic oxidation of As(III) on platinum and other noble-metal electrodes

Tim D. Cabelka
Iowa State University

Follow this and additional works at: <https://lib.dr.iastate.edu/rtd>

 Part of the [Analytical Chemistry Commons](#)

Recommended Citation

Cabelka, Tim D., "Electrocatalysis of the anodic oxidation of As(III) on platinum and other noble-metal electrodes " (1983).
Retrospective Theses and Dissertations. 7699.
<https://lib.dr.iastate.edu/rtd/7699>

This Dissertation is brought to you for free and open access by the Iowa State University Capstones, Theses and Dissertations at Iowa State University Digital Repository. It has been accepted for inclusion in Retrospective Theses and Dissertations by an authorized administrator of Iowa State University Digital Repository. For more information, please contact digirep@iastate.edu.

INFORMATION TO USERS

This reproduction was made from a copy of a document sent to us for microfilming. While the most advanced technology has been used to photograph and reproduce this document, the quality of the reproduction is heavily dependent upon the quality of the material submitted.

The following explanation of techniques is provided to help clarify markings or notations which may appear on this reproduction.

1. The sign or "target" for pages apparently lacking from the document photographed is "Missing Page(s)". If it was possible to obtain the missing page(s) or section, they are spliced into the film along with adjacent pages. This may have necessitated cutting through an image and duplicating adjacent pages to assure complete continuity.
2. When an image on the film is obliterated with a round black mark, it is an indication of either blurred copy because of movement during exposure, duplicate copy, or copyrighted materials that should not have been filmed. For blurred pages, a good image of the page can be found in the adjacent frame. If copyrighted materials were deleted, a target note will appear listing the pages in the adjacent frame.
3. When a map, drawing or chart, etc., is part of the material being photographed, a definite method of "sectioning" the material has been followed. It is customary to begin filming at the upper left hand corner of a large sheet and to continue from left to right in equal sections with small overlaps. If necessary, sectioning is continued again—beginning below the first row and continuing on until complete.
4. For illustrations that cannot be satisfactorily reproduced by xerographic means, photographic prints can be purchased at additional cost and inserted into your xerographic copy. These prints are available upon request from the Dissertations Customer Services Department.
5. Some pages in any document may have indistinct print. In all cases the best available copy has been filmed.

**University
Microfilms
International**
300 N. Zeeb Road
Ann Arbor, MI 48106

8323268

Cabelka, Tim D.

ELECTROCATALYSIS OF THE ANODIC OXIDATION OF ARSENIC(III) ON
PLATINUM AND OTHER NOBLE-METAL ELECTRODES

Iowa State University

PH.D. 1933

University
Microfilms
International 300 N. Zeeb Road, Ann Arbor, MI 48106

Electrocatalysis of the anodic oxidation of As(III) on platinum
and other noble-metal electrodes

by


Tim D. Cabelka

A Dissertation Submitted to the
Graduate Faculty in Partial Fulfillment of the
Requirements for the Degree of
DOCTOR OF PHILOSOPHY

Department: Chemistry
Major: Analytical Chemistry

Approved:

Signature was redacted for privacy.

In Charge of Major 

Signature was redacted for privacy.

For the Major Department

Signature was redacted for privacy.

For the Graduate College

Iowa State University
Ames, Iowa

1983

TABLE OF CONTENTS

	Page
I. INTRODUCTION	1
II. LITERATURE REVIEW	4
A. The Electrochemistry of As(III) and As(V)	4
B. Anodic Oxidation of Pt, Au, Pd, and Ir	19
C. Oxide Participation in Anodic Reactions on Noble-Metal Electrodes	64
III. EXPERIMENTAL	109 -
A. Electrodes and Rotators	109
B. Potentiostats	110
C. Triple-Pulse Amperometry Apparatus	110
D. Lock-In Amplifiers	110
E. Chemicals	111
F. Miscellaneous	111
IV. THEORY OF MIXED KINETICS OF ELECTROCHEMICAL REACTIONS AT ROTATING DISC ELECTRODES	112
A. Introduction	112
B. Heterogeneous Rate Constant of a Charge Transfer Step	114
C. Heterogeneous Rate Constant of a Step not Involving Charge Transfer	117
D. Homogeneous Rate Constant for a Preceding First-Order Reaction	117
E. Homogeneous Rate Constant of a Following First-Order Reaction	119
F. Macroscopically Nonhomogeneous Surface	120
G. Summary	122

V. POTENTIODYNAMIC AND RING-DISC STUDIES OF AS(III,V)	124
A. As(III) Electrochemistry on a Pt RDE in Acidic Media	124
1. The effects of changing the As(III) concentration	124
2. The effects of changing the negative scan limit	126
3. The effects of changing the positive scan limit	128
4. The effects of changing the electrode rotation speed	128
5. The effects of changing the potential scan rate	131
6. Summary	135
B. As(III) Electrochemistry on a Pt Disc/Au Ring RRDE in Acidic Media	136
1. Introduction	136
2. Potentiodynamic experiments at the RRDE	140
3. Transient RRDE experiments: evidence for As(III) adsorption	149
4. Adsorption pseudocapacitance in the As(III)-Pt system	152
C. As(V) Electrochemistry on Pt in Acidic Media	159
1. Potentiodynamic studies at a Pt RDE	159
2. As(V) underpotential deposition and isopotential points	163
3. RRDE studies	172
D. As(III) Electrochemistry on a Au RDE in Acidic Media	174
E. As(III) Electrochemistry on Ir and Pd RDEs in Acidic Media	180
F. As(III) Electrochemistry on a Pt RDE in Basic Media	184

G. As(III) Electrochemistry on a Au RDE in Basic Media	192
VI. POTENTIOSTATIC STUDIES OF As(III) OXIDATION	195
VII. STUDIES USING HYDRODYNAMIC MODULATION OF A ROTATING DISC ELECTRODE	225
A. Theory	225
B. Studies of As(III) Oxidation on Pt Oxidizing SHMRDE	231
C. Brief Study of As(V) Electrochemistry on Pt Utilizing SHMRDE	240
D. Study of As(III) Oxidation on Ir Utilizing SHMRDE	241
E. Brief Comments on As(III) Oxidation of Au and Glassy Carbon	242
VIII. THE MECHANISM OF As(III) OXIDATION ON PT AND OTHER NOBLE METAL ELECTRODES	246
A. Introduction	246
B. Slow Heterogeneous Charge Transfer	247
C. Slow Homogeneous Chemical Reaction	250
D. Nonlinear Diffusion to Active Sites	252
E. Slow Heterogeneous Reaction Not Involving Charge Transfer	255
F. Detailed Discussion of the Mechanism of Anodic Oxidation	257
IX. SUMMARY	282
X. SUGGESTIONS FOR FUTURE RESEARCH	284
XI. BIBLIOGRAPHY	286
XII. ACKNOWLEDGEMENTS	306

LIST OF FIGURES

	Page
Figure IV-1. Diffusion volume of Landsberg model of a nonhomogeneous surface	120
Figure V-1. Cyclic voltammograms at a Pt RDE in acidic solution as a function of [As(III)]	125
Figure V-2. Cyclic voltammograms of As(III) at a Pt RDE in acidic solution as a function of E_c	127
Figure V-3. Cyclic voltammograms of As(III) at a Pt RDE in acidic solution as a function of E_a	129
Figure V-4. Cyclic voltammograms of As(III) at a Pt RDE in acidic solution as a function of ω	130
Figure V-5. Cyclic voltammograms of As(III) at a Pt RDE in acidic solution at low ω	132
Figure V-6. Cyclic voltammograms of As(III) at a Pt RDE in acidic solution as a function of scan rate	133
Figure V-7. Theoretical $i_d - E_d$ and $i_r - E_d$ behavior	139
Figure V-8. RRDE cyclic voltammograms for As(III) with $E_d < 1.4$ V	141
Figure V-9. RRDE cyclic voltammograms for As(III) with $E_d > 1.4$ V	144
Figure V-10. Transient ring current response for As(III) oxidation following potential step at the disc	151
Figure V-11. As(III) adsorption isotherm on Pt	153
Figure V-12. Cyclic voltammograms of As(V) at a Pt RDE in acidic solution as a function of E_c	161
Figure V-13. Cyclic voltammograms of As(V) at a Pt RDE in acidic solution as a function of E_a	164
Figure V-14. Cyclic voltammograms of As(V) at a Pt RDE in acidic solution as a function of ω	168

Figure V-15.	Ring current-disc potential response in As(V) solution as a function of E_a	173
Figure V-16.	Cyclic voltammogram of As(III) at a Au RDE in acidic solution	175
Figure V-17.	Cyclic voltammograms of As(III) at a Au RDE in acidic solution as a function of E_a	177
Figure V-18.	Cyclic voltammograms of As(III) at a Au RDE in acidic solution as a function of ω	179
Figure V-19.	Cyclic voltammograms of As(III) at a Au RDE in acidic solution as a function of scan rate	181
Figure V-20.	Cyclic voltammograms of As(III) at a Pt RDE in basic solution as a function of E_a	185
Figure V-21.	Cyclic voltammograms of As(III) at a Pt RDE in basic solution as a function of ω	187
Figure VI-1.	Potentiostatic i-t response as a function of [As(III)]	212
Figure VI-2.	Potentiostatic i-t response as a function of $\omega^{1/2}$	214
Figure VII-1.	SHMRDE voltammogram of As(III) at Pt as a function of E_a	235
Figure VII-2.	SHMRDE voltammogram of As(III) at Pt at high values of E_a	238
Figure VIII-1.	Plot of $\log k$ vs. $\log t$ for long times	269
Figure VIII-2.	Plot of $\log k$ vs. $\log t$ for short times as a function of [As(III)]	270
Figure VIII-3.	Plot of $\log k$ vs. $\log t$ for short times as a function of ω	271

LIST OF TABLES

	Page
Table V-1. Anodic current for As(III) oxidation on Pt as a function of pH	191
Table VI-1. Summary of data collected to test the theory developed for a macroscopically inhomogeneous electrode surface	200
Table VI-2. Summary of the parameters from linear regression analysis performed on data from potentiostatic experiments at steady-state rotation speeds	202
Table VI-3. Calculated values for $k(\text{cm s}^{-1})$ at various times after a potential step at $t=0$	203
Table VI-4. Summary of parameters from linear regressions on As(III) data obtained by linearly ramping the rotation speed. ASR rotator	205
Table VI-5. Summary of parameters from linear regressions on Br^- data obtained by linearly ramping the rotation speed. ASR rotator	205
Table VI-6. Summary of parameters from linear regressions on As(III) data obtained by linearly ramping the rotation speed. MSR rotator	207
Table VI-7. Summary of parameters from linear regressions on Br^- data obtained by linearly ramping the rotation speed. MSR rotator	207
Table VI-8. Values of $k(\text{cm s}^{-1})$ as a function of time and the ionic strength I at constant pH. Applied potential 1.10 V vs. SCE	208
Table VI-9. Values of $k(\text{cm s}^{-1})$ as a function of time and pH at a constant ionic strength and a constant overpotential	209
Table VI-10. Summary of parameters of linear regressions of k vs. $\log t(\text{s})$. $\omega^{1/2} = 10.00 \text{ rad}^{1/2} \text{ s}^{-1/2}$	218
Table VI-11. Summary of parameters of linear regressions of k vs. $\log t(\text{s})$. $C^* = 2.039 \text{ mM}$	218

I. INTRODUCTION

Two broad categories of solid materials are used with anodic reactions. Carbon, in a variety of forms, is used widely, especially in the oxidation of organic compounds whose oxidation potential is not too positive. Most of the applications of liquid chromatography with electrochemical detection (LC-EC) utilize a carbon working electrode. The noble metals (plus Ni under some circumstances) have been used for many years in the study of anodic reactions. Platinum is by far the most commonly used noble metal. Gold is used to a much lesser extent; all of the other noble metals are used infrequently. It is to be expected that the use of carbon and the noble metals have advantages and disadvantages that must be considered individually by the electrochemist in choosing the appropriate electrode material for a given application.

One of the most important considerations in choosing an electrode material is the long term "activity" of the electrode at the required potential. Poisoning of the electrode surface by surfactants, halides, or the products of the oxidation is common to both carbon and the noble metals. In addition, one must contend with thin oxide films on noble metal electrodes if the required potential is positive enough to oxidize the substrate surface to the corresponding oxide. Some anodic reactions occur only on a reduced (i.e., bare metal) surface, some occur only on an oxidized surface, and some reactions can occur on either surface.

The purpose of this dissertation is to examine a specific anodic reaction, the oxidation of As(III) in aqueous solutions, on some of the

noble metals. Of particular interest is the role that thin oxide films on the metals have in the oxidation of As(III). Is an oxide film necessary for the oxidation to occur? If so, is the oxide a direct participant in the reaction, or does it simply act as an electron sink? Can the oxide actually inhibit the oxidation of As(III)? How do the oxides of different noble metals effect the oxidation of As(III)? While the use of noble metals as working electrodes for anodic reactions has many advantages, there is relatively little known about the way in which the oxide films on these electrodes effect the electrode process. It is hoped that a more detailed understanding of the mechanisms of anodic reactions occurring on noble-metal oxides will lead to methods of optimizing the rate of such reactions. This, in turn, has important implications for applications as diverse as energy storage and transformation, electrochemical synthesis, and electroanalytical methodology.

Several electrochemical techniques will be presented for study of the oxidation of As(III) on noble-metal electrodes. For the most part, the transport of As(III) to the electrode surface is precisely controlled through the use of rotating disc electrodes. Methods are presented which permit the evaluation of the rate of As(III) oxidation under a variety of conditions. A relatively new technique is described to examine the oxidation of As(III) in a range of positive potentials that was previously inaccessible. The majority of the data presented in this dissertation deals with the oxidation of As(III) on Pt, primarily because of the widespread use of Pt and the exceptionally large body of literature on the

anodic electrochemistry of Pt. A detailed mechanism for the anodic oxidation of As(III) is proposed.

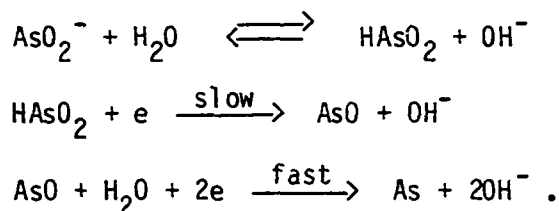
II. LITERATURE REVIEW

A. The Electrochemistry of As(III) and As(V)

The electrochemistry of arsenic in its' various oxidation states has not been subjected to a large number of fundamental investigations. This is undoubtedly related to the irreversibility of the reactions as well as the tendency for As(III) to interact with the electrode substrate. The majority of the studies that have been performed are related to electro-analytical methods for the determination of arsenic. Two excellent reviews of the polarographic determination of arsenic are available (1,2); however, it is not the purpose of this literature review to survey analytical methodology, but rather to focus on the electrochemical reaction mechanisms.

There is still a great deal of variation in the literature on the structure given for "arsenious acid" and arsenites in aqueous solutions. Much of this is undoubtedly related to the use of the Pourbaix diagram (3) for arsenic. However, two studies (4,5) have conclusively established by Raman spectroscopy that $\text{As}(\text{OH})_3$ is the only major component in an acidic aqueous solution of As(III). Additionally, in solutions where the $[\text{OH}^-]$ was increased according to Job's method of continuous variations, the species $\text{As}(\text{OH})_3$, $\text{AsO}(\text{OH})_2^-$, $\text{AsO}_2(\text{OH})^{-2}$, and AsO_3^{-3} were all observed. The existence of HAsO_2 was ruled out. These results did unambiguously establish the nature of the As(III) species in solution; however, in this review, the formulas given by the original authors will be used.

Mechanistic information can be obtained from several studies that were predominantly analytical in nature. In their review article, Arnold and Johnson (1) state that many polarographic studies are consistent with the reduction of As(III) on Hg to give an adsorbed layer of arsenic metal on the surface of the Hg drop. A limiting current is obtained when the surface is covered with an adsorbed monolayer. Susic and Pjescic (6) investigated the polarographic reduction of As(III) in ammoniacal solutions at a series of pH values. They concluded that the overall three-electron reduction is irreversible and that H^+ participates in the reaction since the $E_{1/2}$ became more negative as the pH was increased. For the rate determining step they found that $\alpha_a = 0.54$ and that one proton participates in the mechanism up to and including the rate-determining step. The reduction mechanism they proposed is

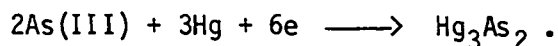


In the first study of the determination of As(III) using differential pulse polarography, Myers and Osteryoung (7) compared the theoretical and experimental values for the ratio peak current/bulk concentration (i_p/C) and also concluded that the reduction is irreversible. They also attributed the negative deviations in the calibration curves at high $[\text{As(III)}]$ to the absorption of As(0) on the electrode surface. The three

peaks obtained were explained as a reduction to the zero state, a polarographic maxima, and a reduction to the -3 state.

The determination of As(III) by polarography frequently is accomplished in supporting electrolytes of salts of organic acids. Soviet workers (8) have reported that an As(III) complex with citrate is electroactive. Reduction currents are usually not obtained for As(III) in unbuffered neutral solutions; addition of La(III) to unbuffered 0.1 M KCl does result in a reduction, probably due to formation of $\text{La}(\text{AsO}_2)^{2+}$ ion-pairs in the bulk solution (9).

While almost all workers state that the first As(III) reduction wave corresponds to the production of an As(0) species, Zhdanov and co-workers (10) maintain that the first wave is the surface-controlled reaction



The second wave then corresponds to the reduction of the mercuric arsenide.

Watson (11) has recently reviewed the polarographic behavior and analysis of some organoarsenic compounds. The reactions for the most part are irreversible four- and two-electron reductions that are followed by chemical reactions in solution.

It was observed in some of the earliest polarographic studies that As(V) is electroinactive on Hg. All attempts to electrochemically reduce As(V) on Zn, graphite, sintered Ni, Pt, Pb, Pb-Sn, and amalgamated Cu in

various acidic and alkaline media were unsuccessful, as were chemical reductions with Mg and Al(12). Most electrochemical determinations of As(V) therefore have been based on the prior reduction of As(V) to As(III) with reducing agents such as Cd, I^- , $SnCl_2$, Cu(I), SO_3^{-2} , or hydrazine sulfate. Nevertheless, there have been a small number of cases where an As(V) reduction current was observed.

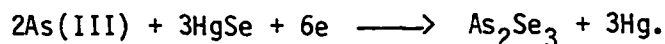
The first electroreduction of As(V) was reported by Meites (13). The supporting electrolyte was 11.5 M HCl. Two distinct waves were obtained, the total current being 8/3 times the magnitude of an equimolar As(III) signal; therefore, the overall reduction was concluded to be from the +5 to the -3 state. The first wave was ascribed to the +5 to 0 reduction since the current was approximately 5/8 of the total wave and the potential was negative of the $E_{1/2}$ for the +3/0 couple. Diluting the HCl concentration to 9 M resulted in a complete elimination of the wave. Experiments with other electrolytes showed that both H^+ and Cl^- have to be present at a very high activity. Meites speculated that some or all of the oxygen atoms in the As(V) specie in solution are replaced by Cl^- in 11.5 HCl. It is interesting to note that a recent attempt to reproduce these results was unsuccessful (10).

The addition of La(III) to a solution of AsO_4^{-3} gave two reduction waves in 0.1 M KCl (9). Presumably, ion-pairs are formed that are similar to those formed between La(III) and As(III). At low [La(III)] the waves correspond to the reductions +5 to 0 and to -3; As(III) is not formed for the reason given by Meites.

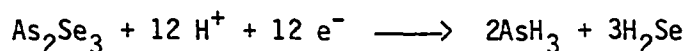
The polarographic analysis of an As(V)-pyrogallol complex gives three well-defined waves in 2 M HClO₄ containing 0.5 M pyrogallol (14). The diffusion currents are found to be in a ratio of about 2:3:3 and are attributed to the reductions +5 to +3, +3 to 0, and 0 to -3. The +5 to +3 and +3 to 0 reductions were irreversible, but the 0 to -3 reduction was reversible. The $E_{1/2}$ for the As(V) complex was -0.10 V vs. SCE and the diffusion coefficient was evaluated as 1.7×10^{-7} cm²/sec, which is indicative of a large, bulky complex. (Note: The structure of the As(V) complex has been elucidated since this study was performed (15)). Pyrogallol does not form a complex with As(III).

Anodic stripping voltammetry (ASV) and cathodic stripping voltammetry (CSV) at Hg electrodes has been performed in three cases. As previously discussed, arsenic deposition on Hg is generally considered to stop at a monolayer coverage due to the relative insolubility of As in Hg and the nonconducting nature of As. Toropova et al. (16) reported that arsenic could be determined using a hanging Hg-drop electrode.

At higher [As(III)], two stripping peaks were obtained which were attributed to the oxidation of surface arsenic and the As/Hg amalgam. Henze (17) used differential pulse cathodic stripping voltammetry to determine As(III). The As(III) was co-deposited with Cu(II) (at 120 ppm) at -0.55 V vs. SCE. Some interesting electrochemistry was utilized by Holec (18) in a cathodic stripping voltammetric determination of As(III). If a small amount of Se(IV) is added to the sample, Se(IV) is reduced to mercuric selenide at about -0.1 V. Deposition of As(III) occurs on the surface of mercuric selenide according to the reaction



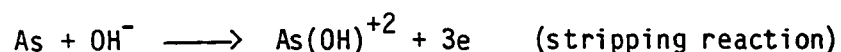
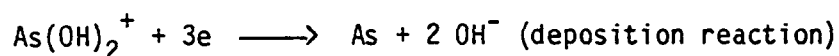
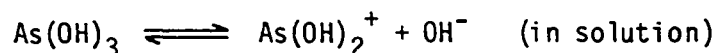
At -0.72 V, the As_2Se_3 is stripped from the electrode by the reaction



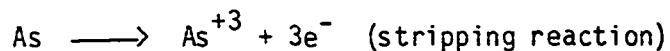
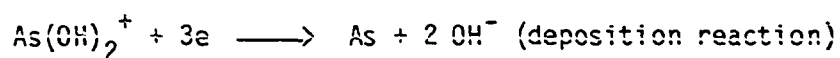
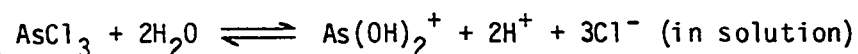
Solid electrodes are used more frequently than Hg electrodes for the determination of As(III) by ASV. Once again it is essential that the arsenic be in the +3 state. One of the first studies was conducted by Trushina and Kaplin (19) using a Pt electrode. Two anodic waves were obtained in 0.5 M KHCO_3 and 0.1 N KH_2PO_4 ; only one peak was obtained in 1.0 N HCl. Based on the peak width at half-height, the electrooxidation in 1.0 N HCl was found to be nearly reversible. Kaplin et al. (20) later found that a Au cathode was superior to a Pt cathode. This same conclusion was reached by Forsberg et al. (21), who performed differential pulse ASV as well. These workers found Hg and Ag to be completely unsatisfactory as electrodes. They also determined that 1 M HClO_4 was a satisfactory supporting electrolyte. Cyclic voltammetry experiments showed that both electroreduction and electrooxidation were much more reversible on Au than on Pt. These authors recognized that oxide films on the electrodes presented difficulties, so a pretreatment step was included in the experimental procedure to ensure that deposition occurred on a reproducible, reduced surface. A negative deviation in the calibration curve of high [As(III)] was attributed to "the formation of a monolayer of adsorbed As, a poor electrical conductor, at the electrode surface" (21). Finally, Forsberg et al. (21) saw an enhancement in the stripping peak area on a Pt electrode when a Au(III) salt was added to the

electrolyte. This could be due to either a partial As deposition on a deposited Au surface, thereby enhancing the reversibility, or to an increase in the real surface area which would lead to a less-hindered deposition.

Kaplin et al. (22) have continued their work on pure Au cathodes. There is no significant interaction between As and Au. In a series of HCl solutions with pH 0 to 3, the As(III) specie in solution was found to be As(OH)_3 and Cl^- was not contained in the species involved in the electrode reactions. The proposed mechanism in this pH range was



In the pH range 0 to -0.9, the proposed mechanism was

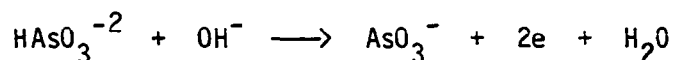


Kaplin et al. (22) were able to calculate the rate constants for the discharge (7×10^{-8} cm/sec) and the ionization (1×10^{-10} cm/sec), values which are indicative of irreversible reactions.

Co-deposition on solid electrodes has been used in a number of studies. Kaplin and co-workers (20) could satisfactorily determine arsenic on a graphite cathode when it was co-deposited with Cu, Au, Pd, and Pt. The familiar deviation in the linearity of a plot of peak current

vs. [As(III)] was probably due to a change in the deposition kinetics on transferring from a micro- to a macrophase. Another group of Soviet workers investigated the ASV of As(III) with co-deposited Cu on a graphite cathode (23). The sensitivity of the method with co-deposition was ten times better than for deposition of As(III) on a Cu substrate. The increased amount of deposited As was ascribed to the formation of Cu-As solid solutions. Later work identified Cu_3As as the composition of the solid solution (24). The original state of the surface of a Pt cathode could be restored only after a long period of anodic or cathodic polarization; this was due to a penetration of the As into the Pt. Kaplan *et al.* (24) were also able to obtain two stripping peaks on Au as well as on Pt, corresponding to the oxidation of a bulk-phase arsenic and to oxidation of arsenic bound to the support. Arsenic was again found to have a greater affinity for Pt than for Au. A similar study was conducted by Japanese workers who co-deposited As(III) and Cu(II) at constant current on a Pt rotating disc electrode (25). Two stripping peaks, at 0.0 V and 0.5 V vs. SCE were obtained. The peak at 0.5 V was due to stripping of Cu_3As , the existence of which was confirmed by x-ray diffraction and chemical analysis.

The anodic oxidation of As(III) can be observed on Hg in solutions of strong bases (26-29). The waves are quasi-reversible and have $E_{1/2}$ values of about -0.29 V vs. SCE. Addition of complexing agents such as tartrates, succinates, malates, glycerol, and mannitol shift the $E_{1/2}$ toward more negative potentials, especially the latter two reagents. Haight (28) stated that the most likely oxidation mechanism was



but once again the validity of the mechanism must be questioned in light of the structure of As(V) species present in aqueous solutions.

The oxidation of As(III) to As(V) has been examined on several other electrode materials. In the report of a study of the As(III)-As(V) couple on spectral graphite, the authors state that the reduction of AsO_4^{-3} is strongly affected by the solution pH (30). The reduction and oxidation processes are irreversible with the transfer coefficient $\alpha < 0.12$, an exchange current density of 10^{-8} A/cm², and a standard heterogeneous rate constant of 10^{-9} cm/sec. It was also reported that the steady-state potentials are reversible and that H⁺ participates in the As(III)-As(V) equilibrium.

The earliest investigations of the anodic oxidation of As(III) were aimed at the industrial preparation of arsenates (31-35). Alkaline media were used almost exclusively. MacNevin and a series of co-workers were the first to examine the As(III) oxidation in some detail. MacNevin and Martin (36) found that the current efficiency was 100% on Pt in strong acid solutions, but was low (as low as 22%) in the pH range 3-11. No evidence was found for the oxidation of As(III) by dissolved O₂ in acidic solutions, nor was there any indication of an intermediate (i.e., +4) oxidation state. MacNevin and Baker (37) later developed a coulometric method for the determination of As(III).

The variation in the anodic current obtained under supposedly constant conditions caused these authors to investigate the effects of anode pre-polarization (38). "Hydrogen" or "oxygen" pre-polarization of the electrode caused at least a ten-fold variation in the anodic currents obtained for the oxidation of As(III) and Fe(II) on Pt. The pre-polarizations were carried out at ± 4.0 V, while the anode was potentiostated at 1.0 V for the As(III) oxidation. The pre-polarized electrode was not changed (with respect to the i - t behavior for either As(III) or Fe(II)) by remaining in the supporting electrolyte for several hours. It was observed that if an oxygen pre-polarized electrode (i.e., oxidized surface) was allowed to stand for a period of time in an As(III) or Fe(II) solution (presumably this was in an open-circuit condition) that the electrode reverted to a state similar to that of a hydrogen pre-polarized electrode (i.e., reduced surface). This occurred very quickly in the Fe(II) solution but very slowly in the As(III) solution. MacNevin and Baker (36) explained these results by reasoning that the presence of "platinum oxides" has an effect on the current efficiency and that under open-circuit conditions As(III) and Fe(II) can chemically reduce the platinum oxide and give a clean (i.e., reduced) surface.

Zakharov and Songina (39) examined the anodic oxidation of arsenite at a rotating Pt electrode (it is not clear whether this was a disc or wire electrode) in 1964. The i - E curves presented are actually "pseudo- i - E " curves because the current was measured following a predetermined time period after the applied potential had been set. All of the i - E curves (with one exception) were developed for increasing values of the applied

potential. The oxidation waves began at about 0.6 V vs. the HgI₂/Hg reference electrode; the wave shifted to more positive potentials as the pH was decreased. The waves exhibited a maxima at +1.0 - 1.3 V, again dependent on electrolyte pH. The shift in potential was consistent with the Nernst equation

$$E = E^{\circ} - 0.059 \text{ pH} + 0.059 \log ([\text{AsO}_4^{-3}]/[\text{AsO}_3^{-3}]).$$

The peak current initially increased as the H₂SO₄ electrolyte concentration was increased, but decreased for concentrations greater than 1 M. The current obtained on the single "reverse scan" (i.e., applied potential becoming less positive) was much lower than that on the "forward scan" and did not exhibit a maxima. The current also decreased if the time following the application of the potential increments was increased, or if the electrode was pre-anodized at 1.7 V. Zakharov and Songina concluded that the oxidation of arsenite was irreversible, involves oxygen from platinum oxides, and can be represented by



They were not specific about the nature of the PtO[0] specie. However, based on the coincidence of the forward and reverse scans in the potential region 0.8-0.9 V, they could not eliminate an electron-transfer mechanism involving an As(IV) specie. From a plot of $\log [i/(i_{\text{max}}-i)]$ vs. E, they calculated the number of electrons involved in this electrode reaction to be 0.4; this was taken as additional evidence of irreversibility. Iodide, either in solution or previously adsorbed on the electrode, caused the entire wave to shift to more positive values and decreased the anodic

current. An iodized electrode could be "activated" by the addition of Hg(II).

Catherino (40) analyzed plots of $\log i$ vs. E for the oxidation of As(III) in the potential region where concentration polarization effects are negligible. The results were consistent with a theoretical treatment of a mechanism involving two consecutive one electron-transfer steps. The study was interpreted as supporting the evidence for the existence of an As(IV) intermediate product which had been postulated previously from kinetic effects observed in homogeneous solutions (41,42). The data in this study were collected in experiments where a stationary Pt electrode was immersed in a flowing stream of the electrolyte solution containing As(III) under laminar flow conditions.

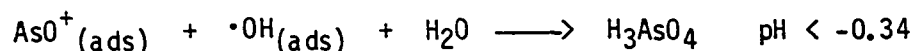
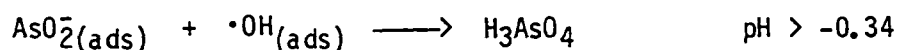
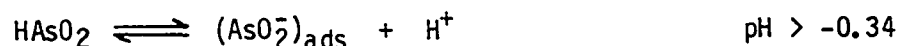
In a paper on the contamination of Pt electrodes by arsenic, Sutyagina et al. (43) state that oxidation currents obtained in 0.1 N H₂SO₄ in the potential range 0.38 V to 0.80 V vs. RHE vary with the degree of poisoning. The electrodes were poisoned by cathodic polarization at constant current which resulted in the deposition of arsenic. In this potential region, it was observed that no arsenic passed into solution, leading to the speculation that some species such as As₂O₃ is formed on the electrode surface. Oxidation of a similarly prepared electrode in a KOH solution led to removal of arsenic, indicated by the increase in hydrogen adsorption. The anodic current obtained in the potential region 0.8 V to 1.4 V was attributed to simultaneous oxidation and desorption of arsenic as As(V) and surface oxidation. The removal of arsenic from the surface was studied as a function of the upper (anodic) limit of the

potential scan in cyclic voltammetric experiments. No As was removed from the surface unless the anodic limit was greater than 0.8 V, which is once again the potential where As(III) oxidation and Pt oxide formation begin. The rate of desorption increases with potential up to 1.2 V.

Loucka (44) has examined the adsorption, oxidation and reduction of As(III) on stationary Pt and Au electrodes. The supporting electrolyte was 0.5 M H_2SO_4 ; cyclic voltammetric and potentiostatic methods were used. On Pt, As(III) can be adsorbed with reduction to As(0) at potentials from 0.1 to 0.7 V vs. NHE; in cyclic voltammetry experiments, this reduced As gives an anodic peak with a peak potential of 0.8 V and results in an adsorbed As(III) specie. At more positive potentials, there is a simultaneous oxidation and partial desorption of As as As(V) and platinum oxide formation. On Au, adsorbed As(III) is reduced to As(0) with a peak potential of 0.1 V. This As(0) is re-oxidized once again at 0.4 V to the adsorbed state; if the potential is swept to more positive values, the adsorbed As(III) is oxidized to As(V) which is desorbed. The As(III) oxidation occurs at potentials negative of that where any appreciable phase gold oxide is formed.

Zakharov, Songina and Kal'nitskaya (45) studied the oxidation of arsenite on a rotating gold-wire electrode as well as on Pt. The oxidation wave on a Au electrode begins 400 mV positive of the wave on a Pt electrode. The current on the reverse scan indicates that the gold electrode surface is passivated at positive potentials, undoubtedly due to the formation of the surface oxide. The reaction order was found to be 0.65; this was ascribed to the oxidation of the As(III) adsorbed on a

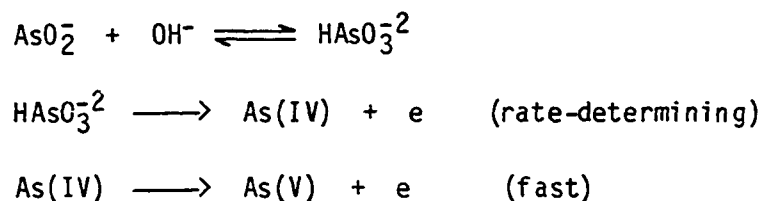
"uniformly inhomogeneous electrode surface." They also observed that the height of the anodic wave obtained on the forward scan was a function of the scan rate. The reaction mechanism proposed involved adsorbed hydroxyl radicals and varies slightly according to pH as follow:



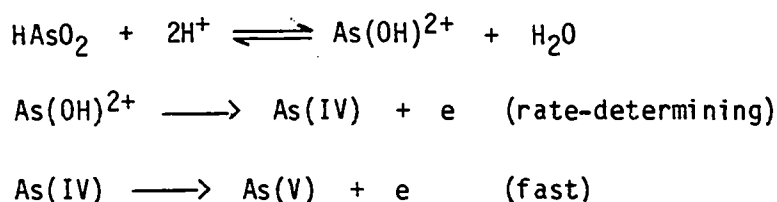
The reaction between the adsorbed As(III) and $\cdot\text{OH}_{(\text{ads})}$ was postulated to be the rate-determining step. They went on to state that the reaction undoubtedly takes place sequentially via an As(IV) specie, which may be oxidized by a second $\cdot\text{OH}_{(\text{ads})}$ or which may undergo disproportionation to As(III) and As(V).

Two Polish scientists have studied the oxidation of As(III) to As(V) on a Au electrode in a series of perchlorate and phosphate solutions with pH from 0 to 14 (46). Cyclic voltammetry on a stationary Au foil was used exclusively. The authors assume that the oxidation is an irreversible process that is controlled by the rate of charge transfer. Based on peak currents obtained as a function of scan rate, bulk $[\text{As(III)}]$, and pH, values were calculated for the transfer coefficient and the heterogeneous rate constant as a function of potential. The reaction orders with respect to H^+ and OH^- were calculated from the values of $(d \log k/d \text{pH})_E$.

Their proposed mechanism was also dependent on solution pH. For pH 2-14, the proposed mechanism was:



In the pH range 2-1.4, the proposed mechanism was



The anodic oxidation of As(III) on Pt and Pb was recently studied in H_2SO_4 suspensions that also contained Fe(II), Zn(II), Cd(II) and Cl^- (47). The Cl^- was reported to promote the more complete oxidation of As(III). Loodma and Past (48) briefly examined the oxidation of As(III) on Ag and Ni anodes in 0.5 M KOH. On Ag, anodic maxima were obtained at 0.37-0.5 V and at 0.54-0.60 V vs. NHE. These currents were a function of $[\text{As(III)}]$. A maxima at 0.50 V is obtained on a Ni anode as well.

Nikitin et al. (49,50) oxidized a number of organoarsenic compounds on Pt anodes in acetonitrile solutions. In the oxidation of EtAs(OBu)_2 , for example, EtAs(OBu)_2 was postulated as an intermediate product in the overall reaction; however, the oxygen atom probably results from a homogeneous reaction with H_2O in the solvent rather than from any participation of a surface oxide.

B. Anodic Oxidation of Pt, Au, Pd, and Ir

Involvement of surface oxide in the oxidation of As(III) at noble-metal electrodes has been implied, as presented in the previous section (II.A). Literally hundreds of papers have been published on the anodic oxidation of the surfaces of noble-metal electrodes in aqueous solutions. The vast majority of this work, perhaps 70%, has dealt with platinum; gold has been the subject of another 15-20%, with the study of all other metals making up the remaining 10-15%. The purpose here is to review with reasonable detail the electrochemical oxidation of the surface of platinum, gold, palladium, and iridium electrodes, with special emphasis on the more recent studies that have not been included in review articles. Several older general reviews are still useful (51-54), as is one more recent review (55).

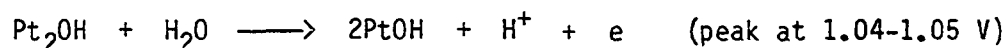
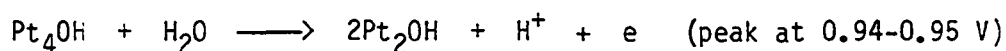
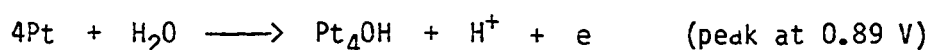
Platinum will be reviewed first. In the following discussions, the term "coverage" will have a rather specific meaning. Coverage (denoted by θ) will be defined as the ratio of the charge passed to form a given quantity of adsorbed oxygen or surface oxide to the charge required to form a monolayer of adsorbed $\cdot\text{H}$. A coverage of 1.0 signifies that the surface has a surface stoichiometry corresponding to PtOH , while $\theta=2$ means that the surface stoichiometry corresponds to PtO . Since it is assumed that H adsorbs 1:1 with Pt atoms on the surface, a coverage of two means that two electrons have been transferred for every surface Pt atom.

Most of the early workers found no limiting coverage for anodic potentials up to 2.0 V (53) and, for a limited range of times (t), found

that the oxide charge was a linear function of $\log t$ (56). It should be noted that in the middle 1960s the nature of the anodic film was vigorously debated between those who believed that the film was an adsorbed layer of oxygen or an oxygen-containing specie and those who believed it to be a phase oxide.

In the late 1960s and early 1970s, a considerable amount of progress was made in understanding the anodic oxidation of Pt. Although many workers contributed to this progress, the two leaders were Conway's group in Canada and Vetter's group in Germany.

Conway and co-workers developed a theory for the formation and reduction of the first 1-2 monolayers of surface oxide based on electrochemical and optical data as well as computer simulations (57-59). Only the major points of this theory will be presented here. In H_2SO_4 electrolytes of very high purity, three anodic peaks are obtained between 0.85 V and 1.1 V vs. NHE in potentiodynamic experiments. These three peaks correspond to the step-wise oxidation of the electrode surface according to



This sequence is intended to represent "surface site occupancy ratios" and not necessarily actual stable species. Extremely good agreement was obtained between the theoretical and experimental charges at each of the three peaks. In potentiodynamic experiments at a scan rate of 100 mV

sec^{-1} , $\theta=1$ at 1.1 V and $\theta=2$ at about 1.4 V. Scan reversal at $\theta < 1$ leads to the conclusion that the first anodic peaks are due to the formation of reversible species; polarization beyond $\theta=1$ or for long periods of time at $\theta \approx 1$ leads to the familiar hysteresis in the oxide reduction peak. The initial reversibility is also shown by the invariance of the anodic peak potentials with scan rate. A computer simulation of the sequence given above, assuming that each step is reversible and including two interaction parameters, gave a i - E profile with three anodic peaks having peak potentials independent of scan rate.

Anodic oxidation beyond one electron per Pt atom leads to hysteresis and irreversibility because of an induced surface rearrangement, or "place-exchange". This place-exchange leads to a thermodynamically more stable specie and hence a more negative reduction potential. Place-exchange occurs with both PtOH (to give "HOPt") and PtO (to give "OPt"). Belanger and Vijn (55) state that Goldstein et al. (60) did not reach conclusions similar to Angerstein-Kozłowska et al. (57) based on potentiostatic experiments with oxide growth times of 150-1150 μsec . In fact, the data of Goldstein et al. can be interpreted in a manner consistent with Conway's theory, since it was only at potentials where place-exchange can occur that Goldstein et al. were able to resolve the oxide reduction peak into two peaks.

Conway and co-workers also examined in detail the oxide reduction peak. It is known that the slope of a plot of peak potential vs. log scan rate is related to the steady-state Tafel slope (61). Conway's group found that the Tafel slopes varied from 0 at $\theta < 0.15$ to 27 mV for 0.15

$\alpha < 0.9$ to 40 mV for $\alpha > 2$. The low values of the Tafel slope are indicative of a complicated reduction mechanism. In general, the reduction process is not the reverse of the oxidation process; a generalized scheme is presented by Conway and Angerstein-Kozłowska (62) in a later paper.

Differential reflectance and ac impedance measurements were also used by Conway and Gottesfeld (59). The data obtained from both of these techniques as a function of potential, scan direction, and holding time are consistent with his theory of monolayer oxide formation and reduction.

As Belanger and Vijn (55) have correctly pointed out, the aim of the work performed by Vetter and Schultze (63-65) was different from that of Conway's group in that Vetter and Schultze were not concerned with the mechanism of the initial oxide formation. They found that the oxide charge (Q_{ox}) is proportional to $\log t$ for t from 2 msec to 1000 sec in potentiostatic experiments with potentials between 1.0 V and 2.0 V, and that Q_{ox} is proportional to potential for polarization times between 2 msec and 1000 sec. Again, no limiting oxide coverage was observed. Different Tafel slopes were obtained for the processes of oxide formation and reduction. They concluded that only a phase platinum oxide is present on the surface and that the oxide increases in thickness with time and/or potential. The overall mechanism of growth is concluded to be one of a field-assisted growth in which there is a place-exchange between a Pt(II) and an oxide ion to give a phase oxide lattice. For $\alpha < 1$, the rate-determining step (rds) is between the Pt(II) at the metal surface and oxide ion in the inner Helmholtz layer. At higher coverages, the place-

exchange mechanism is still operative, but the rds cannot unambiguously be assigned; it could occur at either the metal-metal oxide interface or the metal oxide-inner Helmholtz layer interface. This field-assisted growth mechanism had been proposed earlier by Visscher and Devanathan (66) and by Ord and Ho (67).

The field-assisted growth mechanism has been criticized on two grounds. The adsorption of oxide (O^{2-}) ions would seem to be unlikely, especially in highly acidic solutions. (Using this model, Vetter and Schultze calculated the coverage of O^{2-} to be 0.1 at 1.5 V.) This mechanism also cannot account for the limiting oxide coverage that has been observed by many workers (68-78). The limiting oxide coverage is observed when the data are recorded in potentiodynamic experiments and not when galvanostatic reductions are used. A limiting coverage is obtained when Q_H , the charge required to form a monolayer of adsorbed H, is not assumed to be a constant. The increase in Q_H can be attributed to either a surface roughening following oxide reduction or incomplete oxide reduction at the potential where hydrogen adsorption begins. Limiting coverages as high as 2.66 ($\theta=1$ corresponds to PtO) have been reported (68), but values closer to 2 are much more common. Biegler and co-workers (78) performed a very careful study and obtained limiting coverages at 2.15 and 2.08 for platinized platinum. This coverage could consist of either one monolayer of PtO₂ or two monolayers of PtO since there is no simple reason that phase oxide growth should stop at two monolayers. Biegler, Rand, and Woods concluded that a chemisorbed monolayer of oxygen (O₂) is formed. However, ellipsometric measurements of the thickness of

this limiting coverage have been given as 8 Å (77) and 13 Å (79), which tend to support theory that two monolayers of PtO are present.

Belanger and Vijn (55) seem to disparage the potential-step experiments of Momot and Bronoel (80-81) in which the presence of PtOH was postulated in the range 0.4 V to 0.8 V. While their results are significantly different from that of Icenhower et al. (82), it is not obvious that the experimental techniques and data treatments (e.g., compensation for double-layer charging) used by Icenhower et al. are superior to that of Momot and Bronoel.

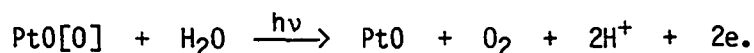
In addition to the Pt(II) oxide that has been discussed up to this point, it is possible to form a second type of platinum oxide (72,73,75, 83-90). This oxide is formed on electrodes polarized for long periods of time at potentials greater than 2 V; the reduction peak potential occurs at 0.03 to 0.4 V (i.e., in the H adsorption region). The most comprehensive study of this oxide was conducted by Balej and Spalek (75), who found that a mechanical stress in the electrode favors its formation, that it grows linearly with polarization time, and that the initial growth rate is a function of potential. This oxide does not reach a limiting thickness. While Pt(IV) oxide produced by chemical oxidation does not exhibit the same electrochemical behavior as this type of oxide, electron diffraction spectra indicate the presence of PtO₂ (91). In very recent work, Burke and Roche (92) have reported that the PtO₂ oxide can be formed without inducing mechanical stress by cycling between 0.50 V and 2.82 V at 1 Hz (i.e., 4.7 V sec⁻¹) for 10 minutes. Burke and Roche (92) believe that a hydrated Pt(IV) oxide is formed, but disagree with Shibata and

Sumino (93), Shibata (94) and Vinnikov et al. (79) on the physical location of the Pt(IV) oxide. While Burke and Roche hold that the Pt(IV) oxide is the outermost layer, the others have stated that the Pt(IV) state is beneath the one or two monolayers of Pt(II) oxide formed during initial anodization. The Pt(IV) oxide is reduced directly to Pt(0); this is similar to the reduction of the higher oxidation state on Au, but different from the behavior of Ir and Rh.

One optical method (differential reflectance) has already been mentioned. The first optical technique that was applied to the study of anodic oxidation was ellipsometry, where the amplitude ratio (ψ) and relative phase retardation (Δ) of elliptically polarized light is measured as the light passes from one medium into another through a thin film and is then reflected back into the original medium. Ellipsometry was first utilized by Reddy et al. in 1964 (95) and was used frequently in the latter part of the 1960s and early part of the 1970s. There is remarkably good agreement between ellipsometric data and coulometric data obtained at a relatively high scan rate (96). There is a slight decrease in the relative phase retardation between 0.5 V and 0.9 V, a much greater rate of decrease between 0.9 V and 1.15 V, and then a slightly smaller rate of decrease as the potential is swept toward more positive potentials. Other workers also have observed these discontinuities in the slope of Δ -E curves at approximately 1.1 V (67,97). This discontinuity can be attributed to a change in the index of refraction of the film as the oxide is transformed from PtOH to PtO; these results correlate very nicely with the electrochemical data of Conway and Gottesfeld (59). On the reverse

(negative) scan, Δ is constant until the potential has decreased to 0.8 V, whereupon Δ rapidly increases until it attains the values observed on the forward scan; this behavior, of course, is related to the hysteresis present in the reduction of the surface oxide. These ellipsometric data are generally considered to have been the first unambiguous data that established the anodic film as a phase oxide. However, these data are subject to some uncertainty due to the constancy (or lack thereof) of the index of refraction as a function of potential.

Vinnikov and co-workers (98) have measured the photocurrents obtained when the Pt(II) oxide and the Pt(IV) oxide are illuminated with light at 605 nm. An anodic photocurrent is obtained only when Pt(II) oxide is present, which they attribute to the reaction



The PtO[0] specie evidently represents a local site where there has been some oxidation beyond a single monolayer of PtO. If Pt(IV) oxide is present, a cathodic photocurrent is obtained; this was assigned to the reduction of Pt(II) oxide via a charge-transfer complex formed by the Pt(II) and Pt(IV) oxides.

In addition to the optical techniques just described, some spectroscopic techniques were applied to the study of electrochemical oxidation in the early 1970s. The most heavily utilized of these spectroscopic techniques has been x-ray photoelectron spectroscopy (XPS) (99-105). Unfortunately, the studies come to mutually contradictory conclusions due to differences in electrolytes, anodization potentials, anodization times,

pretreatments, and most importantly of all, spectra deconvolution.

Belanger and Vihj (55) concluded that the studies available to them (99-103) did not permit a satisfactory interpretation; subsequent publications (104,105) have not improved the situation.

Johnson and Heldt (106) claim to have detected a PtO-like oxide using Auger spectroscopy.

Shibata (107) has used low energy electron diffraction (LEED) to study the electrochemical oxidation of platinum. The LEED pattern for electrochemically-formed Pt(IV) oxide was identical to that of chemically prepared Pt(IV) oxide. When the electrode was polarized beyond 1.15 V, the electrode surface following oxide reduction gave a LEED pattern resembling Pt black. It is precisely at this potential where the Conway mechanism postulates that place-exchange becomes significant; the LEED data would, therefore, tend to confirm Conway's theory of platinum oxidation.

Ord and co-workers (108) have compared the values for the formal potential, exchange current density, and Tafel slope obtained from open-circuit transient experiments and galvanostatic oxidation experiments. While these experiments should give identical values, they were, in fact, significantly different. These workers prefer the values derived from the less-common open-circuit transient experiments. These data are interpreted as strengthening the case for field-assisted growth beyond a monolayer coverage.

Shibata (94) has measured the conductivity of the Pt(II) and Pt(IV) oxides. The outermost (Pt(II) oxide) monolayer has a conductivity that is

very similar to Pt metal. The inner multilayer oxide (Pt(IV) oxide) has a much lower conductivity, the specific conductance being $1.1-2.1 \times 10^{-3} \Omega^{-1} \text{cm}^{-1}$.

Appleby (109,110), in the course of developing a theory for successive electron transfers in cyclic voltammetry, has developed a theory for the oxidation of Pt. His theory basically states that oxidation is a two-stage process. The rate constant for the first step (denoted by Appleby as PtOH formation) decreases exponentially with coverage. This decrease is associated with a rearrangement of the surface phase and is accompanied by very rapid PtO formation. The decrease in the rate constant is a factor in addition to changes in the Temkin terms present in both the forward and backward rate expressions. The position (i.e., potential) and shape of the oxide reduction peak is determined by PtO reduction, but the overall rate is determined by PtOH reduction.

Fujihara and Kuwana (111) have examined the surface conductance of thin (100-300 Å) Pt films as a function of potential in H_2SO_4 and HClO_4 electrolytes. A plot of $\Delta C/C$ vs. $\Delta Q/Q$ (where C is the conductance and Q is the integrated charge) is linear with a slope of 1.0, as is predicted by theory, for potentials up to about 1.0 V; the slope is 0.46 at 1.1 V. Fujihara and Kuwana interpret this change in slope as a change in the surface characteristics due to a change in the valence of the adsorbed oxygen.

Battalova et al. (112) examined the reduction of the Pt(II) and Pt(IV) oxides formed at high potentials following relatively short

anodization times. They found that Pt(IV) oxide formed in acidic solutions was not reduced if the electrode was placed in 1 N NaOH. They concluded that the Pt(IV) oxide reduction is catalyzed by hydronium ion.

Gilroy (113) has authored an excellent paper on oxide growth at potentials less than 1.7 V. The quantity of oxide was determined by both galvanostatic reduction and current integration, with oxide growth times varying from 10 msec to 10^3 sec. Extrapolation of the plot of Q_{Ox} vs. $\log t$ to $Q_{Ox} = 0 \mu C$ gave a common intercept (to within 0.7 decade) for eight different potentials. A plot of $dQ_{Ox}/d \log t$ vs. potential gave a straight line with an intercept of 0.75 V. Plots of Q_{Ox} vs. potential (for a fixed t) exhibited some curvature, as opposed to the results obtained by other investigators. A very interesting plot of Q_{Ox} vs. $\log t$ for $t < 10$ ms is included, as is a plot of Q_{Ox} vs. $\log t$ following a penultimate step that was either positive or negative of the final step. The quantity of oxide found in these experiments were found to be higher for the current integration method than for the galvanostatic reduction method; the most likely explanation was judged to be an incomplete oxide reduction prior to the onset of hydrogen evolution. From his data, Gilroy derived an equation for oxide growth at constant potential

$$i = C\eta/t_0 \exp(-Q/C\eta),$$

where η is the overpotential, and C and t_0 are arbitrary constants.

Gilroy then noted that this equation is similar in form to that derived by Fleischmann and Thirsk (114) for film growth based on nucleation as the rate-determining step. This theory can explain the $Q_{Ox} - \log t$ results as

well as the slight convexity of the Q-E plots. Also included in this paper is a discussion of the theories for oxide growth presented by Gilman, Feldberg, Conway, Volker, and Damjanovic, and re-evaluations of the data of these and other investigators.

Ward et al. (115) looked at the kinetics of extended oxide growth on Pt. The growth was monitored by chronoellipsometry; two regions of growth were observed. The first region could be described by a high-field model with migration of ions through the oxide phase; the current was described by

$$i = i_0 \exp[\alpha(V-V_0)/d],$$

where d is the oxide thickness and V_0 is the potential (~ 0.9 V) where d is equal to 0. In this region, oxide growth is the only reaction occurring; d reaches 4-5Å. The second region of oxide growth begins when O_2 evolution begins and is described by

$$i = i_0 \exp\left[\frac{-d(t)}{d_0} + \frac{(V-V_0)}{V_0}\right],$$

where $d_0 = \alpha V$. It can be seen from this second equation that the oxide film grows at a greatly reduced rate. Ward et al. (115) could only speculate on the reason for the evident change in the mechanism of growth. One possibility is that the onset of electronic current through the oxide causes a redistribution of the potential drop across the interface such that drop across the oxide is significantly reduced. This removes the driving force for the field-assisted growth mechanism.

Gilroy (116) continued his earlier work by studying oxide formation in the potential region for oxygen evolution. Corrections were made for double-layer charging and incomplete galvanostatic reduction, and O_2 was removed by purging with Ar while holding the potential at an intermediate value prior to oxide reduction. The effect of this intermediate step was also carefully studied. Gilroy's previously developed theory (113) was found to provide a satisfactory explanation for oxide growth up to 2.2 V. No evidence was found for a change in the oxide structure at about 1.5 V, which was the same conclusion reached by Vetter and Schultze (63).

In his study of the reduction of multilayer oxides, Shibata (117) observed four arrests in the galvanostatic curve and four corresponding peaks in the potentiodynamic profile. These were attributed to the reduction of an oxygen monolayer adsorbed on the oxide surface, two monolayers of Pt(II) oxide, and the reduction of the multilayer Pt(IV) oxide.

Yamamoto et al. have recently looked at the oxidation of three single-crystal Pt electrodes (118). Cycling the potential of a Pt single-crystal electrode into the oxide region several times does not change the surface orientation, as shown by reflection high energy electron diffraction (RHEED); this is different than the behavior of Au single crystals. Oxygen appears to be most strongly bound to the (100) orientation and least strongly bound to the (111) orientation; the (110) orientation is intermediate. The quantity of oxide formed prior to O_2 evolution on the (111) surface is less than that formed on the other surfaces. Over long periods of time, the (110) surface appeared to be the

most stable and the (111) surface the least stable towards surface rearrangements.

Damjanovic and Yeh (119) studied the oxide growth on Pt as a function of pH in acidic solutions, again within the context of the high field-assisted growth mechanism. They found that the exchange current and Tafel parameters were not a function of pH, but that the potential at which the oxide film growth began was a function of pH.

Angerstein-Rozlowska et al. (120), in the course of studying the general features of noble-metal oxidation in the presence of specifically-adsorbed anions, has been able to arrive at some additional conclusions on the mechanism of Pt electrooxidation. The distinct oxidation stages observed at $\theta < 1$ are associated with "successive overlay structures of minimum free energy." These structures are initially electrochemically reversible, but irreversibility due to place-exchange of the metal and oxygen species is induced by increasing coverage, lateral repulsions of the surface dipoles, increasing positive potentials, and the presence of adsorbed anions which cause perturbations of the local fields. The tendency for both place-exchange and anion adsorption is determined by the thermodynamic potential for metal oxidation relative to the point of zero charge, the donor/ acceptor properties of the metal and the anion, and the hydrophilicity of the metal. Cations, on the other hand, can have a stabilizing effect on the unrearranged surface states and thereby diminish the tendency for place-exchange to occur.

Four recent papers by Damjanovic, Yeh, and Wolf (121-124) have called into question the high field-assisted theory of oxide growth. In the

first of these papers (121), the rate equation for anodic growth above 1.0 V in an alkaline solution (1 M KOH) was found to be of the same form as in acidic solutions. The exchange current density in 1 M KOH was determined to be $1.3 \times 10^{-7} \text{ A cm}^{-2}$ in 1 M KOH, while previous work in acidic solutions had given an exchange current density of $2 \times 10^{-10} \text{ A cm}^{-1}$. If the process at the metal/oxide interface is the rate-determining step, the Carbera-Mott model (125) predicts that the exchange-current density is given by

$$i_0 = N\nu ze \exp[-W/RT],$$

where N is the density of metal ions in the metal surface, ν is the vibrational frequency, ze is the charge on the migrating ion, and W is the activation energy. All of these factors should be independent of the conditions in solution and at the oxide/solution interface. If the second step (i.e., diffusion of the ions through the oxide) were the rate-determining step, then N would be the density of interstitial cations in a reaction plane within the oxide (126). But this latter density can only be less than or equal to the density of metal ions in the metal surface, so it would therefore appear that the activation energy for growth in alkaline solutions should be significantly less than the activation energy in acidic solutions. In the temperature study, Damjanovic et al. (122) found that W was about $6.5 \text{ kcal mol}^{-1}$ smaller than the corresponding activation energy in an acidic solution, while N_{alk} was about 1.5% of N_{acid} . Since both N and W are different, it would at first seem that the rate-determining step in alkaline solutions is the migration step, instead

of the ion-formation step as is the case in acidic solutions. The real difficulty is that there are no a priori reasons to believe that ion migration in the oxide should be effected by conditions in solution and there is evidence that identical phase oxides are formed in both cases. When the formation of oxide films was studied as a function of pH in alkaline solutions, it was found that the exchange current density decreased by one order of magnitude for a decrease of one pH unit (123). The rate-determining step must therefore occur at the oxide/solution interface, with the "pulling" of a Pt^{+2} out of its position in the surface of the oxide into a position in the immediate vicinity of an adsorbed OH^- or a $\text{Pt}^{+2}/\text{OH}^-$ place exchange suggested as possibilities. These results also suggest that the rate-determining step of oxide growth in acid solutions occurs at the oxide/solution interface. The differences in N and W are attributed to difference in the species reacting in the rate-determining step: H_2O in acidic and neutral solutions, OH^- in basic solutions.

Bagotzky and Tarasevich (127) presented a reasonably short review on the subject of "oxygen adsorption". This review stressed the Soviet orientation on the anodic electrochemistry of Pt. The oxygen chemisorption process was concluded to be a two-step discharge of water via a hydroxyl radical intermediate. A thermodynamic method developed in the middle-1930s by Slygin and Frumkin (128) and an electrochemical adsorption isotherm developed by Temkin (129) are the basis of an extended kinetic theory that allows the calculation of a wide variety of experimental parameters. Bagotzky and Tarasevich (127) claim that this treatment gives

better agreement with the experimental data than do the theories of Vetter and Schultze, or Conway.

Folquer et al. (130) and Arvia (131) in Argentina have investigated the kinetics of aging of oxide films on Pt. In this work, the oxide was aged by a potentiodynamic perturbation sequence where approximately one-half of the oxide was alternately formed and then reduced by a triangular waveform operating at a scan rate of greater than 0.4 V sec^{-1} . Following the aging sequence, a cathodic potentiodynamic scan showed that three different oxide species were present. It was speculated that the dynamic aging allows some oxygen to penetrate into the metal to the first and second crystallographic planes. Note that the aging referred to here is different from the simpler open-circuit and potentiostatic aging.

Facci and Murray (132) formed between 0.3 and 2.5 layers of PtO by polarizing a Pt electrode between 0.8 V and 2.0 V vs. SSCE in 1 M H_2SO_4 . When the electrode was removed from the aqueous solution under potentiostatic control and placed in a very dry acetonitrile solvent, they observed two reduction peaks at -1.2 V and -1.6 V vs. SSCE. If the electrode surface was silanized with trimethylchlorosilane following oxide growth in 1 M H_2SO_4 , only the peak at -1.6 V was obtained when the electrode was reduced in CH_3CN . Since the $\text{PtOSi}(\text{CH}_3)_3$ linkage is not reducible at an available potential, Facci and Murray conclude that the oxide reduced at -1.2 V lies on the outer surface and that subsequent oxide growth (that oxide reduced at -1.6 V) occurs between the metal and the first oxide state. It would be interesting to repeat these

experiments under conditions where a Pt(IV) oxide was unambiguously formed.

Facci and Murray briefly comment that their results are consistent with the requirement that most of the outer oxide layer must be reduced before significant reduction of the subsurface oxide layer commences. This observation was also made by Shibata and Sumino (133) working in aqueous HF, HClO₄, and H₂SO₄ solutions. Thick oxide films gave only one potential arrest when reduced at a high galvanostatic current density. Decreasing the current density led to two well-defined potential arrests. Increasing the acid concentration or agitating the solution caused the second arrest to be shifted to even more negative potentials. This was attributed to blocking of the reduction of the inner-layer oxide by anions that adsorb on the surface exposed by the reduction of the outer oxide layer at the first arrest. The order of adsorption was HSO₄⁻ > ClO₄⁻ > F⁻.

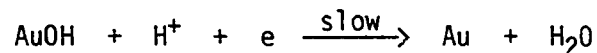
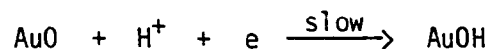
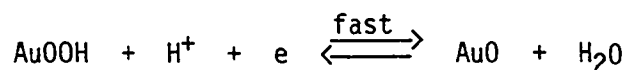
Very recently, Novak and Conway (134), and Conway and Mozota (135) studied the oxidation of Pt in the presence of co-adsorbed halide ions. The presence of Cl⁻ selectively inhibits the initial deposition of the PtOH monolayer and thereby favors the growth of the irreversible component of the oxide. Bromide and iodide block the formation of the oxide non-selectivity over a wide range of potentials. This is consistent with the previously known differences in the electrosorption valencies of Cl⁻, Br⁻, and I⁻.

Conway and Novak (136) recently completed a study of the formation and reduction of submonolayer quantities of Pt oxide in a trifluoroacetic acid solvent where the water concentration was controlled at very low

concentrations. The extent of hysteresis observed for submonolayer coverages was comparable to that obtained at very high coverages in aqueous solutions. This behavior was attributed to adsorption of the trifluoroacetate ion, but nucleation of the oxide into two-dimensional islands stabilized by lateral attractive interactions was also discussed.

While the body of literature concerning anodic oxide films on gold is much smaller than that for platinum, it has many of the same characteristics: some contradictions in the earlier investigations, a considerable increase in the quality and quantity of data in the last 15-20 years, and the application of a variety of nonelectrochemical techniques in the hope of arriving at a clear picture of the nature of the film. Two general reviews are recommended (51,55). At first it was believed that a Au(III) oxide or hydrated oxide was formed in acidic solutions; the reduction exhibited a high degree of hysteresis. Hoare's review (51) states that at most one monolayer of Au_2O_3 is formed in basic solutions. There was some evidence of multiple galvanostatic arrests at very low current densities (137), but it was not at all clear that intermediate oxidation states existed.

Brummer and Makrides (138,139) combined galvanostatic and potentiostatic methods in the study of Au oxidation. Under potentiostatic control, they found a linear relationship between oxide charge and potential for a given formation time. The Tafel slope for the oxide reduction was 39-42 mV and was pH invariant in strongly acidic solutions. They proposed the following mechanism for the reduction:



Gold oxide was found to undergo a rearrangement with time (i.e., aging) similar to platinum oxide.

Schultze and Vetter (140), and Dickertman et al. (141) have examined Au oxidation more recently, again using potentiostatic, galvanostatic, and potentiodynamic techniques. Polycrystalline gold (111) and (100) single crystal surfaces were used. They found that the Tafel slope for reduction was a linear function of the oxide coverage; the complete Tafel relation was given by

$$\log i = \log i_0 + \frac{E - E^0}{b^0(1 + g\theta)}$$

where $\log i_0$ was equal to $2 \times 10^{-11} \text{ A cm}^{-2}$, b^0 is the Tafel slope at zero coverage and was equal to 25 mV, g was an experimental constant equal to 3.0, and E^0 was 1.15 V. The anodic currents obtained in the cyclic voltammograms of the two single crystals were significantly different, the anodic peak for the (111) surface being about 200 mV positive of the anodic peak for the (100) surface. These data led Schultze and Vetter to propose a high-field ionic conduction mechanism for the formation of Au oxide (directly analogous to their theory for Pt oxidation) when the oxide thickness was greater than or equal to 3 Å. Surface orientation effects

were judged to be important for oxide thicknesses less than 2 Å. Schultze and Vetter described oxide reduction as essentially a de-nucleation phenomenon.

Arvia's group began a long series of studies on the anodic oxidation of Au in the middle-1970s (142-145). The anodic wave could be resolved into as many as three peaks, depending on scan rate, temperature, and electrolyte; this behavior was not observed by Capon and Parsons (146) in their study of several noble metals. At lower temperatures, a shoulder on the oxide reduction peak was observed. There was considerable oxide dissolution/desorption that occurred at the open-circuit potential; this was a first-order process and increased with temperature. Using relatively high scan rates, a number of aging times, and *i*-*E* curves obtained where the anodic scan rate was not equal to the cathodic scan rate, Ferro et al. (145) were able to deduce a mechanism in which the first step is the formation of an adsorbed OH radical, followed by aging effects which give a Au(III) oxide and a partial regeneration of the free metal surface. This is in some respects similar to the mechanism of oxide growth on Pt proposed by Conway and co-workers but there are some very significant differences (57-59). On Pt, the peak potentials of the three anodic peaks formed at $\theta < 1$ are scan-rate independent, indicative of reversible species; this is clearly not the case on Au.

When gold oxide formed at $E < 1.4$ V vs. SCE was potentiodynamically reduced, Cadle and Bruckenstein (147) found evidence that a Au(III) specie was present. When the electrode was polarized at $E > 1.4$ C, a Au(I) specie was also detected.

Goldstein et al. (148,149) have applied the technique of potentiostatic growth for very short periods of time followed by potentiodynamic reduction at high scan rates to the study of Au as well as Pt. Multiple peaks were observed. The oxide that is reduced at the most positive potential is rapidly converted to a form that is reduced at potentials 300 mV more negative. This suggested the successive oxidation of the Au(I) and Au(II) oxides. This conversion was a function of both time and polarization potential. These results are consistent with Arvia's work cited above and that of Gruneberg (150).

Hoare (151,152) obtained some controversial results on the formation of Au oxides. Hoare claims, based on differential double-layer capacitance measurements, that an oxide can exist at potentials as low as 0.80 V. This contradicts most common experience, where potentiodynamic experiments routinely show Au oxide formation beginning at about 1.30 V. In fact, some have claimed that no oxide is present below 1.20 V (153). Belanger and Vijn (55) suggest that this discrepancy was caused by Hoare's electrode pretreatment. Hoare also showed that the oxygen evolution reaction was inhibited by the formation of Au_2O_3 on the electrode surface.

Many of the same optical and spectroscopic techniques that were used to study Pt oxidation have been applied to Au. Ellipsometry and reflectance methods were the first to be applied. In an acidic solution, the ellipsometric parameter Δ slowly decreased with E between 0.5 V and 0.9 V, decreased more rapidly between 0.9 V and 1.2 V, and even more rapidly at $E > 1.2$ V (154-156). In a 1 M KOH solution, there was only one break in the Δ -E plot at 1.2 V. Since Sirohi and Genshaw (154) had ruled

out anion effects, the interpretation given for the Δ -E behavior was that chemisorption of oxygen giving AuOH or AuO occurs at $E < 1.2$ V and that oxide film formation occurs at $E > 1.2$ V. This interpretation is strengthened by the low values for the refractive index and absorption coefficient determined by Sirohi and Genshaw (154); it would appear that the adsorbed species are simply modifying the optical properties of the metal. Both of these properties were found to be significantly larger when a true phase oxide was present.

Reflectance data also confirm the essential features of Au surface oxidation that have been described above (157-160). In acid, the reflectivity-potential curve exhibits a slight negative slope between 0.0 V and 1.30 V, followed by much larger negative slope between 1.30 V and 1.45 V. A second break at 1.45 V was interpreted as the potential where a complete monolayer of AuO was formed. In 0.5 M NaOH, Takamura et al. (160) observed that a significant break in the reflectivity-potential curve occurred 600 mV negative of the potential where significant anodic current begins.

Kim, Sell, and Winograd (161) have detected a highly hydrated Au(III) oxide on a Au electrode anodized 1.8 V vs. SCE by subjecting it to analysis by XPS.

Lohrongal and Schultze (162,163) continued the work of Schultze and Vetter in two papers published in 1976. These were potentiostatic experiments at potentials from 1.4 V to 2.3 V, growth times from 10^{-4} s to 10^3 s, and pH from 0 to 6.2. At low coverages formed at low potentials, the vanishing of an unstable species and the growth of a stable oxide can

be separated. The unstable species was assigned to O^{-2} or OH^{-} reversibly adsorbed. For $E < 2.0$ V, a "mono-molecular" oxide layer of "Oxide I" can be formed upto a limiting thickness of 10 Å. This thickness increases by the direct logarithmic growth law for thicknesses up to 6 Å, so it would appear that Oxide I growth is predominantly by the high-field mechanism of Schultze and Vetter. At $E > 2.0$ V, continuous oxide growth of "Oxide II" occurs. Oxide II may grow to a thickness of 600 Å or more and is heavily hydrated. Oxides I and II exhibit different optical, electronic, and ionic conductivity behaviors; in fact, Oxide I is a semi-conductor, while Oxide II is essentially a conductor. Oxide II is probably compact (i.e., no pores or fissures) for thicknesses less than about 100 Å.

Sotto (164,165) has carefully studied the oxidation of Au single-crystal electrodes. He holds that the three reduction peaks that he observes are due to the step-wise formation of Au(I) ($AuOH$ or Au_2O), Au(II) ($Au(OH)_2$ or AuO), and Au(III) ($Au_2O_3 \cdot nH_2O$) species. All three of the species are strictly located on the surface and can co-exist at all potentials less than that potential that gives a certain, critical total coverage. Above that critical potential, the surface is essentially covered by a homogeneous $Au_2O_3 \cdot nH_2O$ film.

Sumino and Shibata (166) applied a reflection electron diffraction technique to the study of galvanostatically-formed oxides on Au and Pd. The analyses established that Au_2O_3 and PdO of poorly crystalline natures were formed.

A group of French workers has studied the anodic oxidation of Au by measuring the differential capacitance and the thin-film resistance

(167,168). In the first of these studies, the differential double-layer capacitance curves were obtained in HClO_4 and KClO_4 solutions. After determining that ClO_4^- was only slightly specifically adsorbed at positive charge densities, Clavilier and Huong (167) found that the electrode was covered by an oxygen specie at potentials negative of that where "classical" oxide formation begins. In the second of these studies (168), the electrical resistance of a thin (500 Å) Au film with a (111) orientation was studied as a function of applied potential. They found that adsorption/desorption of oxygen obeyed the Fuchs-Sondheimer relation, thus establishing it as a surface process. Deviation in the resistance was first observed at 0.0 V vs. SCE; bulk oxidation at 0.5 V, as indicated by an i - E curve recorded simultaneously, was accompanied by a sharp change in the resistance-potential curve. These features in the resistogram have also been reproduced by Tucceri and Posadas (169) and by Rath (170). Tucceri and Posadas (169) have also obtained modulated surface conductance data, in which a 1×10^{-2} V rms, 30 Hz ac signal was superimposed on the dc triangular waveform. The potential resolution of the modulated resistogram is clearly superior to either normal resistograms or voltammograms. In particular, a small anodic peak at 1.5 V in 0.5 M H_2SO_4 is very clear in the modulated data, as are the anodic peaks in the oxide-formation region.

Another group of French workers has used ellipsometry with surface plasmon excitation (171). They also saw a gradual change in the ellipsometric parameters Δ and ψ starting at about 0.4 V up to a potential

of about 1.5 V, where there was a sharp decrease with potential corresponding to the formation of the oxide.

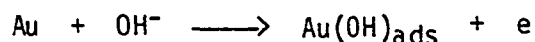
Arvia's group has continued to pursue the phenomenon of potentiodynamic aging at gold electrodes in acidic and basic solutions (172-175). In general, a monolayer of $\cdot\text{OH}_{\text{ads}}$ is formed just after exceeding the point-of-zero charge. Under the potentiodynamic aging perturbation, further oxidation and chemical transformations leads to a complex layer of the type $\text{Au}(\text{OH})_3$. The ionic composition of the latter is determined by the anodic switching potential and the ratio of the anodic and cathodic sweep rates of the perturbation program.

Huong, Hinnen, and LeCoeur (176) have published an excellent paper on "the incipient oxidation of gold electrode[s]." They used very careful cyclic voltammetry and differential capacitance measurements to study the small anodic peak that occurs about 400 mV negative of the major anodic waves. Electrodes of (110) and (111) single crystals were used throughout. Comparisons of several sources of Au by both electrochemical and spectroscopic means eliminated the possibility of a contaminant from the metal being the source of the peak. The possibility that the peak was due to the stripping of a metallic impurity originating in the solution was eliminated by comparing the electroreflectance spectra of the electrodes exposed to solutions doped with Bi(III) and Pb(II) with the spectra obtained following "incipient oxidation". The authors conclude that in neutral or basic media, OH^- is specifically adsorbed in a slow adsorption reaction, covering 10-20% of the electrode surface. This is thought to take place on active sites liberated in the course of cleaning

the electrode (i.e., cathodic and/or anodic polarization). In acidic solutions, water is the source of strongly adsorbed form of OH^- . This investigation is consistent with the resistivity measurements (168) that indicated that "superficial" oxidation begins at potentials considerably more negative than that normally observed in cyclic voltammetry.

Fujishima, Masuda, and Honda of the University of Tokyo and Bard of the University of Texas have collaborated (177) in applying laser photothermal spectroscopy to the study of Au oxidation. While the ΔT -potential curve has the same general shape as that obtained by ellipsometry or differential reflectance, it appears to be much less sensitive to changes occurring at the onset of oxidation.

Kirk, Foulkes, and Graydon (178) have also postulated the existence of a $\text{Au}(\text{OH})_{\text{ads}}$ specie. At fast scan rates (e.g., 10 V sec^{-1}), three distinct peaks were observed in what is usually considered to be the double-layer region. Impurity oxidation was eliminated as a source of these peaks. After correcting for double-layer charging, it was found that total charge for the three peaks were always = 1 electron per surface atom. The potentials of each of these peaks was a function of $\log [\text{OH}^-]$, indicating OH^- participation. Calculations for the number of coulombs for monolayer hydroxyl coverage on (110), (100), and (111) crystal faces agreed very well with the experimentally determined values. The three peaks were therefore identified with the reaction



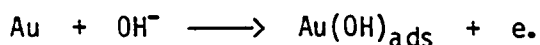
giving monolayer coverage on each of the three crystal faces.

Watanabe and Gerischer (179) have used anodic photocurrent measurements (incident wavelengths 340-730 nm) as a means to study gold oxide films. They examined the potential range 1.0 to 2.1 V vs. RHE in 0.2 M NaClO_4 at pH 6 in this paper. They were able to identify three characteristic potential regions. Between 1.0 V and 1.4 V, there was a low coverage of either a lower surface oxide or a chemisorbed hydroxyl species but not Au_2O_3 . Between 1.5 V and 1.8 V, Au_2O_3 was formed to a thickness of about 1 nm. Above 1.9 V, thickening of the Au_2O_3 layer occurred. In a subsequent paper (180), Watanabe and Gerischer slightly modified these conclusions. The first stage, the so-called incipient oxidation, occurs between 0.85 V and 1.35 V. In this region, the formation of chemisorbed species (Au-OH and/or Au-O) occurs up to a surface coverage of ca. 20%. The formation of islands or clusters is suggested. The second stage, formation of Au_2O_3 , begins at 1.35 V and is the predominate specie at 1.45 V. Thickening of the Au_2O_3 layer begins at 1.9 V, but there is also evidence that indicates that more than one kind of surface species exists at these high potentials.

Photoacoustic spectroscopy has recently been applied to the study of gold electrooxidation (181). This in situ technique used either a Xe lamp or an Ar^+ ion laser as an illumination source ($\lambda = 514.5$ nm); 1 M HClO_4 was used as the electrolyte. Unfortunately, the results are very similar to those obtained with photothermal spectroscopy, i.e., relatively insensitive to any oxidation occurring on the surface other than the formation of the Au(III) oxide, the existence of which was never in doubt.

It is now clear that Hoare (51) was in error when he stated that only one monolayer of Au_2O_3 is formed in base; the growth of thick films has been further investigated by Burke's group (182). Up to 100 monolayers can be formed with steady-state polarization. As in acidic solutions, the oxide consists of a compact, anhydrous inner film at the metal surface plus a much thicker, porous, and highly hydrated outer film. Onset of thick film growth occurs at the point (> 2.0 V) where a linear Tafel behavior for O_2 evolutions begins; this simultaneous reaction presumably enhances conversion of the oxide to the highly hydrated form. Oxide growth is slower than in acid solutions, but is more difficult to reduce. These workers also observed three peaks in the early stages of growth and subscribe to the theory given by Kirk et al. (178). The main anodic peak observed in cyclic voltammetry is therefore due to the conversion of Au(I) to Au(III). A later paper (183) by this same group studied the influence of pH on the reduction on these thick anodic films.

Newman and Burstein (184) have applied the "scratched electrode" technique to the study of Au oxidation in 1 M KOH. In these experiments, a transient current is obtained when a 1.5 mm long, 40 μm wide, 3 μm deep scratch is made in a rotating disc electrode with a diamond stylus. At +200 mV (NHE), evidence was obtained for monolayer coverage of adsorbed hydroxyl by the reaction

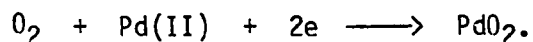
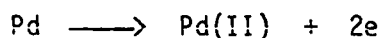


As potentials positive of +200 mV, evidence for monolayer coverage of Au_2O_3 was obtained.

Compared to Pt or even Au, the literature on the anodic oxidation of Pd is truly sparse. The reviews by Hoare (51) and Belanger and Vijn (55) also treat the oxidation of Pd.

The earliest works with Pd were analyses of galvanostatic charging curves (185,186). Hickling and Vrjosek (186) concluded that 2-3 monolayers of a hydrated PdO were formed in neutral or acidic solutions, but 3-4 monolayers were formed in base. They also stated that PdO₂ (formed just prior to O₂ evolution) was unstable in acid. There was one major cathodic arrest, corresponding to the reduction of PdO.

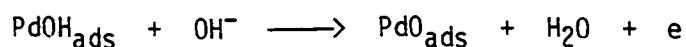
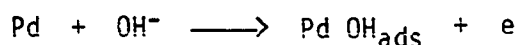
Hoare (187) studied Pd in oxygen-saturated solutions and found that the rest potential was about 0.86 V vs. RHE. However, the rest potential was dependent on the partial pressure of oxygen and solution pH. To account for the oxygen pressure dependence, Hoare theorized that the rest potential was a mixed potential such as would correspond to the simultaneous reactions



This mechanism was consistent with Hoare's early theory of PdO formation, i.e., that Pd(II) is formed at the metal surface, which then reacts with an oxygen specie to give PdO.

Cadle (188) and Llopis et al. (189) have studied the corrosion of Pd under anodic conditions, the former using a rotating ring-disc electrode and the latter using a radiotracer method. Cadle potentiostated a Pt ring at 0.24 V and scanned the potential applied to the Pd disc. A cathodic

ring current was obtained when the disc potential exceeded 0.7 V, which was the same potential where the disc *i*-E curve showed that Pd oxidation had begun. It was determined that this current was due to the reduction of Pd(II) from the disc. The ring current reached a steady (cathodic) value as the potential was scanned toward more positive values. Following scan reversal at the anodic limit, a steady ring current was also obtained, but at a value less than that on the forward scan; this indicates that Pd dissolution is decreased (or the surface is passivated somewhat) by PdO. A very large ring current spike (again cathodic) is obtained when the PdO on the disc is reduced. Rand and Woods (190) have criticized Cadle's method of determining the real surface area of his Pd electrode and have given a good general discussion of this difficult problem. Rand and Woods maintain that the best method is to oxidize the electrode under conditions that give a coverage plateau. Llopis et al. (189) concluded that the Pd oxidation reaction in base is described by



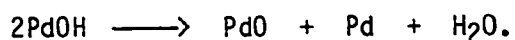
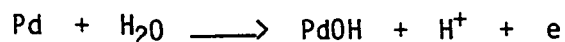
The PdO_{ads} specie is "the first step in formation of PdO on the surface".

Capon and Parsons (191) noted that the *i*-E curve of Pd was complicated by the absorption of hydrogen. The potential range of the double-layer region could be extended by increasing the concentration of the H₂SO₄ electrolyte. They also observed the familiar hysteresis in the cyclic voltammogram. Chloride ion had a very large influence on the curve, suppressing the hydrogen wave, giving a huge anodic wave in the

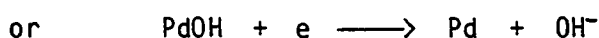
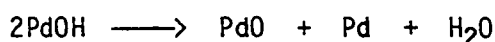
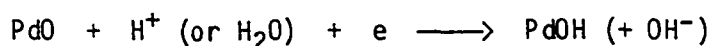
oxide region, and shifting the oxide reduction peak to more negative values. Increasing the sulfate concentration had the effects of slightly inhibiting the onset of oxidation and decreasing the size but not potentials of the oxide reduction peak and the hydrogen waves.

Potentiodynamic and potentiostatic methods were used by Rand and Woods (192) to study Pd behavior. A plot of Q_{oxide} vs. E (for oxidation times of 10^1 , 10^2 , and 10^3 s) gave a small plateau at $Q_{\text{oxide}} \approx 690 \mu\text{C}/\text{geometric cm}^2$ and $E \approx 1.7$ V vs. RHE. No limiting coverage was observed at higher E . When Q_{oxide} was large, the cathodic behavior consisted of a series of broad peaks that extended into the H region; this also resulted in a great deal of surface roughening. Rand and Woods interpreted their results as showing the oxygen chemisorption occurred at lower potentials, with nucleation and growth of phase oxide(s) at higher potentials.

A group of Soviet workers performed a more extensive study of Pd oxide electrochemistry (193). Both the formation and reduction of the oxide in both acidic and basic solutions was examined. In an acid solution, only one anodic wave was seen; the corresponding reduction showed hysteresis. In base, however, two anodic peaks were seen. The first anodic peak exhibited a reversible nature, while the second (more positive) was reduced with hysteresis. They proposed an oxidation mechanism of the type



In this mechanism, the second recombination step was considered to be the slow step. In basic solutions, OH^- (rather than H_2O) could be the source of oxygen; they pointed out that oxygen adsorption from OH^- discharge does take place at more cathodic potentials. They determined the scan rate dependence of the reduction peak potential; this was 30-60 mV/decade at low scan rates, but was 120 mV/decade at high scan rates. This led them to propose the two-step reduction mechanism



At the higher scan rates, the disproportionation step becomes rate-determining, thus leading to the observed scan-rate dependence.

Morcos (194) has compared the oxidation of Pd as a bulk metal and as an electrodeposit on a pyrolytic graphite substrate. Compared to the bulk metal, the oxidation of electrodeposited Pd begins at potentials slightly more negative. More remarkable is the dramatic increase in the quantity of oxide present at a given potential on the electrodeposited electrodes. The difference in oxide coverage was not solely due to an increase in surface roughness, as demonstrated by differential capacitance measurements. The quantity of oxide was also highly dependent on the current density for Pd deposition. Morcos attributes the differences in electrocatalytic activity to differences in the specific surface energy.

Spanish workers have recently pursued Pd oxidation studies (195, 196). Anodic potentiodynamic curves were used to determine the energy of

activation of Pd \longrightarrow Pd⁺² + 2e. This was 6.6 kcal/mole at pH 0 and 7.3 kcal/mole at pH 1. In alkaline solutions at high temperatures, the formation of PdO₂ is favored over PdO. At potentials greater than that for O₂ evolution, colored films are formed that increase in thickness with time; these films contain not only PdO and PdO₂, but in some cases may also contain PdO₃.

Gossner and Mizera (197) have recently taken some electrochemical data and have tried to correlate it with gas-phase Pd oxidation. The anodic charge measured in potentiodynamic experiments is a function of both scan rate and positive scan limit. The cathodic charge for oxide reduction and the "nonreducible" charge (i.e., the charge due to corrosion as Pd⁺²) was also plotted as a function of scan rate and scan limit. For a given growth potential and growth time, the charge due to oxide reduction is independent of scan rate. A plot of the oxide reduction peak potential vs. positive scan limit is discontinuous, showing five separate regions. The authors ascribe these five regions to: 1) preferential adsorption of •OH at energetically favorable sites such as dislocations, kinks, or steps; 2) adsorption of •OH at low coverages giving a reversible surface specie; 3) further oxidation of the PdOH by either PdOH \rightleftharpoons PdO + H⁺ + e or 2PdOH \rightleftharpoons PdO + Pd + H₂O; 4) formation of a stable PdO phase oxide; and 5) massive bulk oxidation. Gossner and Mizera also present evidence for bulk oxygen absorption. They conclude that "the border line between adsorption and oxide formation cannot be drawn unambiguously" and that the diffusion of oxygen into the bulk of the electrode has been completely underestimated in previous studies.

Chierchie, Mayer, and Lorenz (198) have even more recently published a paper which complements that of Gossner and Mizera. For anodic limits less than 1.05 V vs. NHE, three reduction peaks can be observed; the first two appear to be reversible, while the third is highly irreversible. This third peak increases in size and shifts toward negative potentials as the anodic limit is made positive of 1.1 V. A plot of the cathodic charge vs. the anodic scan limit shows three linear sections, with breaks at $210 \mu\text{C}/\text{cm}^2$ and $405 \mu\text{C}/\text{cm}^2$. According to these workers, these breaks correspond to the reduction of monolayers of PdOH and PdO, respectively. The PdOH is present on the surface as "extended superlattices" and are responsible for the reversible cathodic peaks observed at scan limits less than 1.1 V. The growth of the oxide species in potentiostatic experiments gave a logarithmic growth law. Chierchie, Mayer, and Lorenz concluded that polycrystalline Pd is oxidized in a stepwise fashion, the initially-formed PdOH transformed by potential and time into the more stable PdO. This relatively slow transformation process includes surface reconstruction as the initial step for the diffusion of oxygen into the bulk metal.

As opposed to the cases of Pt and Au oxidation, very little has been done in the areas of optical and spectroscopic investigations of Pd oxidation. Kim, Gossmann, and Winograd (199) did record the x-ray photoelectron spectra of Pd electrodes oxidized under a variety of conditions. Electrodes oxidized below 800 mV indicated a complete lack of any phase oxide. Electrodes oxidized at 900 mV for 1000 sec gave XPS data that were interpreted as showing that two monolayers of PdO and a PdO₂-type specie

were present; the authors could not obtain a spectra of chemically produced PdO₂. When Pd was oxidized at 1.28 V for 60 sec, a Pd(IV) specie was still in evidence and the PdO layer was estimated to be 4-5 layers thick. Oxidation at still higher potentials gave PdO layers up to 40 Å thick with a relatively small amount of PdO₂. Kim et al. (199) speculated that this was due to either the decomposition of PdO₂ or its' spontaneous reduction as the electrode was removed from solution.

Iridium has been studied to a somewhat greater extent than Pd, but again to a much lesser extent than Pt or Au. The reversible nature of the i-E curves for Ir was noticed very early in the development of cyclic voltammetry by Bold and Breiter (200). This nature was observed in both acidic and basic solutions, with the peaks in base being much more distinct. Capon and Parsons (191) were next to examine Ir, as part of a study of several noble metals in acidic solutions. They saw relatively little change in the shape of the i-E curves, as the concentration of sulfuric acid electrolyte was increased, other than the suppression of the oxide peak at about 1.0 V. They also observed sharper peaks in base. Addition of Cl⁻ or SO₄²⁻ had little effect on the Ir i-E curves, in contradiction to the behavior of the other Pt metals. Capon and Parsons (191) seem to have been one of the first to observe a characteristic of Ir that has been extensively studied ever since: the continuing oxidation of Ir under potentiodynamic conditions, giving (evidently) thicker and thicker oxide films, the thickness increasing as a function of the number of potential cycles. They observed this phenomenon in 1 M H₂SO₄ with scan

limits of 0.05 V and 1.4 V; this phenomenon diminished as the acid concentration was increased.

In 1974, Otten and Visscher (201,202), and Rand and Woods (203), published significant new studies on Ir which examined this abnormally large amount of surface oxide. In their first paper (201), Otten and Visscher found that ellipsometric parameter Δ was approximately a linear function of the number of cycles, suggesting that the thickness was also a function of the number of cycles. Since the quantity of adsorbed H actually decreased (~20%) with cycling, a simple surface roughing could not account for the increase in the oxide charge. To account for the difference in the thickness values given by ellipsometry and by coulometry (assuming a uniform oxide film), they proposed that the oxidation occurred in pits that were several nanometers thick. In their second paper (202), they found that both the $Q_{\text{Oxide}}-E$ and the $\Delta-E$ curves had breaks in their respective shapes at 1.1 - 1.2 V. This is in substantial agreement with Damjanovic, Dey, and Bockris (204), who found a break in the oxide coverage at 1.3 V (vs. HE in 1 M HClO₄) during a study of O₂ evolution on Ir. These breaks were interpreted in terms of their "pit model".

The cyclovoltammetric study of Rand and Woods (203) led them to propose a quite different mechanism of growth. They also observed continuous anodic growth in 1 M and 0.1 M H₂SO₄, but only if the anodic scan limit was greater than 1.4 V. Since the electrode was not roughened to a large extent in these experiments, they reasoned that the complete reduction of a reversible oxide film to the base metal on each cathodic scan could not be occurring. They proposed that an oxide phase did exist

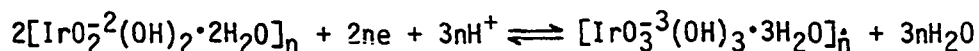
on the surface, but that the reversible nature was due to changes in stoichiometry occurring in the oxide. Since the hydrogen adsorption charge decreased by only 25% when about 60 monolayers of oxide was formed, they also concluded that oxide layer was porous.

Soviet electrochemists, primarily Kurnikov and Vasil'ev, have studied Ir in some detail (205-209). Three anodic peaks were obtained at fairly low scan rates in both acid and base; a fourth peak was observed just prior to O_2 evolution in some cases (205). Oxygen adsorption and desorption was judged to be slow relative to that for Pt. There was no "strengthening" of the Ir-O bond with potential or time; this behavior was strikingly different from that of Pt, Pd, and Rh. The Tafel slope for the first step, the formation of adsorbed OH radicals, was independent of the oxygen coverage, while the Tafel slope for the subsequent step was (unexpectedly) a strong function of the oxygen coverage θ for all values of θ (206). The kinetics of growth of the oxide (i.e., the second step) did not seem to depend on the potential where the first step took place or the length of time at this potential. The rate of reduction was also insensitive to formation potential or time, again demonstrating that strengthening of the Ir-O bond does not occur (207). The reduction was stepwise, the first step involving H^+ discharge. In their final paper on Ir, Kurnikov and Vasil'ev (208) summarized their previous data into the following scheme: for pH from 0 to 14, the oxidation and reduction of Ir follows the common stage sequence IrOH, IrO, IrOOH, IrO₂. The IrOH wave cannot be observed in acid, but the IrO is more distinct in acid than in base. The Ir(III) anodic wave is distinct in 1 N H₂SO₄ but not in a

phosphate buffer or in base. The Ir(III) cathodic wave is not observed in any of the electrolytes tested; the Ir(III) specie either readily decomposes or is masked by other maxima. In neutral or alkaline solutions, the formation of IrO₃ can be noted just prior to O₂ evolution; the inability to observe it in acidic solutions is consistent with the stability studies of chemically-prepared IrO₃. Podlovchenko and Epstein (209) found that "oxygen deposition" occurred at lower potentials in HF solutions than in H₃SO₄ solutions, in agreement with observation that the adsorptivity of F⁻ is less than that of SO₄⁻².

Burke and a whole series of co-workers have contributed several papers to the on-going examination of Ir oxidations (210-214). Buckley and Burke (210) found that the amount of oxide formed (which they also call "charge storage") can be accelerated by scanning at a very high sweep rate between 0.01 V and 1.50 V. They concur with Rand and Woods in postulating the formation of an irreversible oxide with subsequent stoichiometry changes. The reversibility of the peaks further indicates that proton migration (an oxide/hydroxide transition) is occurring. Buckley and Burke held that the observed H adsorption results from a partial reduction of the outer layer of oxide. The loss of charge storage capacity when the electrode was polarized above 1.6 V was attributed to corrosion of the outer active layer of oxide. Oxygen evolution on Ir in both acid and base was significantly higher than on Pt (211). At constant potential, the oxygen evolution current was constant in acidic solutions, but continuously decreased in basic solutions. (The oxygen current on Pt continuously decreases in both cases.) This decrease was ascribed to a

continuous slow oxidation of the metal substrate with consequent inhibition of electron transfer or radical reaction at the electrode surface. The rate of growth of the thick oxide on Ir is a function of the scan rate, upper and lower potential limits, and the pH of the electrolyte (212). The very thick films could not be formed in base, presumably due to oxide dissolution. The oxide layer was regarded as a polymeric layer of oxygen-bridged hydrated oxyhydroxide species. Burke and O'Sullivan (213) have discussed the H adsorption and double-layer capacitance characteristics of thick oxide films on Ir and have suggested that the oxygen evolution reaction on this kind of hydrous oxide is an example of three-dimensional electrocatalysis. Finally, Burke and Wheelan (214) have recently advocated the reaction



as the one responsible for the reversible charge-storage reaction. The above reaction is written for an acidic electrolyte; a similar reaction, involving the expulsion of a hydroxide ion may be written for base. This reaction was proposed to account for the observed dependence of 90 mV/pH unit. The model of Burke and Wheelan for the thickened oxide is one of an aggregate of linked oxyhydroxy octahedral species which form a mixture of linear chains with a relatively small amount of cross-linking. The entire polymer-like chain is permeated by H_2O , H^+ , OH^- , and other ions such as Na^+ . Electrons are delocalized but confined to a strand; there is some resistance encountered in transferring electrons between strands. The density of (electronic) states in a strand is small, so oxidation or

reduction requires injecting an electron into a much higher energy level or generating a vacancy in a much lower level. When Ir(IV) is the predominant specie in the chain, some Ir(V) and Ir(VI) states are also present.

Woods and others in Australia have continued to pursue this subject (215-217). In a study with Michell and Rand (215), cyclic voltammetry, x-ray emission, electron diffraction, and electron microscopy were utilized. Following formation of a thick film, electron microscopy showed that the rutile structure of IrO₂ was not present; a hexagonal arrangement with some ordering of the metal ions was found. X-ray emission was used to calculate the oxide thickness. For example, with a positive limit of 1.5 V, the oxide was 22 nm thick following 3,600 potential cycles. They concluded that 2 electrons were transferred per Ir atom during a typical potential scan, probably involving a conversion of Ir(OH)₂ to IrO₂ via a continuous series of reversible de-protonation steps. The electron microscopy results of Michell, Rand, and Woods are somewhat in conflict with the field-ion microscopy studies of Schubert et al. (218), who anodized Ir at 1.5 V in 0.1 N H₂SO₄. Schubert et al. saw no crystallographic development, the oxide appearing to be either amorphous or consisting of very fine microcrystallites. They did observe considerable anisotropy in the oxide penetration, reaching 10 nm in places. Woods (216) compared the thick oxides formed on Ir with those formed on Ru and on Rh in base. Woods also criticized Burke's theory of partial reduction of the outer oxide layer, but supports the theory of Arvia (see below) and later endorsed by Burke and O'Sullivan (213). Woods also states that IrO₂

is present at the foot of the O_2 evolution wave (but see reference (208)) and that the major peaks shift by 78-80 mV/pH unit, which is in reasonably good agreement with Burke's 90 mV/pH unit. Frazer and Woods (217) have speculated that IrO_3 is formed at high potentials and that IrO_3 participates directly in the oxygen evolution reaction.

Gottesfeld and Srinivasan (219) conducted ellipsometric and reflectometric measurements of the Ir anodic film. Increasing the positive scan limit to 1.40 V causes the optical parameters to increase to values typical of semiconductors. The phase oxide formed in the oxygen evolution region seemed to have a high level of bulk defects (see Mozota and Conway below) and a high surface concentration of active sites, both of these related to a gradual variation of the oxidation state of Ir in the oxide. The evolution of oxygen was proposed to proceed via a higher oxidation state of Ir in the oxide, much like the O_2 evolution reaction on Ni in base. The reflectance measurements given in this paper are identical to those given earlier by Conway and Gottesfeld (59).

As mentioned above, Arvia's group has developed the most convincing mechanism for thick Ir oxide formation (220,221). For a positive limit less than a certain critical value, one sees normal oxygen adsorption and desorption. However, if the critical potential is exceeded and a certain oxygen coverage is obtained, then some fraction of the oxygen will not be desorbed even at negative potentials. This oxygen is retained near the metal surface as an iridium oxide formed by the breaking of metal-metal bonds beneath the site where the oxygen had been adsorbed; thus, a new H adsorption site is generated for each molecule of oxide produced. When a

thick oxide is present, oxygen chemisorption occurs on Ir atoms at the metal/metal oxide interface, the source of oxygen being H_2O present in the hydrated oxide. On the negative scan, most of the oxygen is desorbed to leave sites for hydrogen adsorption, but some of the metal-oxygen species are transferred to the overlying layer resulting in oxide growth. Holding the potential at a constant value passivates the base metal surface; it is only when the oxygen ad-layer is partially reduced and hydrogen deposited that an oxide phase can separate and grow. Thus, multicycling into the hydrogen region is required for oxide growth. Zerbino and Arvia (221) also examined the different rates of growth and different fine structures of Ir i -E curves obtained in 0.1 M H_2SO_4 (pH 0.74), 0.15 M $HClO_4$ (pH 0.70), and 1 M H_3PO_4 (pH 0.67). The reversible valency interconversion (primarily involving $Ir(OH)_4$ units according to these authors) and the associated proton-transfer processes are effected by the ions that are in intimate contact with the polymer-like oxide. The differences in the rate of growth are due to differences in the dissolution rate caused by anion-oxide and anion-metal interactions.

Glarum and Marshall (222) found that their ac data were best explained by assuming that the anodic layer was a highly porous film with essentially all of the oxide sites accessible to the electrolyte phase. At equilibrium, this layer is electrically neutral and adopts the potential of the external electrolyte; the electrochemical potential of the oxide sites is determined at the metal/oxide interface. Aging is probably due to a rearrangement from $Ir(OH)_4$ to $IrO_2 \cdot 2H_2O$. Due to the highly porous nature, Glarum and Marshall warned investigators of

comparisons between films present in aqueous solutions and those that have been dehydrated by high vacuums.

Mozota and Conway (223-225) have been actively investigating Ir oxidation. These workers define the charge enhancement factor (CEF) as the ratio of the anodic charge on a given cycle to the anodic charge for initial oxygen monolayer formation on the bare metal. For a "fresh" electrode, a monolayer of IrOH is formed at 1.1 V and a monolayer of IrO is nearing completion when O₂ evolution begins (223). After a few cycles, the hydrated Ir(III)/Ir(IV) transitions become predominant; the oxide does not change in nature with further cycling, but does increase in thickness. At CEF > 100, macroscopic cracks are formed. Oxygen evolution at 50 mA cm⁻² for 10 minutes on an electrode with CEF = 50 caused wholesale macroscopic cracking and "peeling" of the oxide down to the base metal. The oxide was also a great deal rougher and more spongy in appearance than an identical electrode where Cl₂ evolution occurred. Mozota and Conway attribute these changes the direct participation of the oxide in the oxygen evolution reaction. Like Kurnikov et al. (205) Mazota and Conway could observe three anodic peaks on Ir, corresponding to three different OH species (224). The first two peaks were reversible while the third (most positive) was irreversible. Hydroxyl radicals are formed at less positive potentials than on Pt, but •OH/•OH repulsive forces are greater on Ir. They also found that •OH formation on Ir was less sensitive to anion competition than Au or Pt, but that the rearranged Ir-O bonds were stronger than Au-O or Pt-O. In their final paper (225), Mozota and Conway discuss the i-E curves in greater detail and reconcile the data to a

coherent picture of the entire oxide film. A high-area, porous, rough oxide lies on top of the Ir substrate, with about 70% of the substrate surface area exposed to the electrolyte via pores and cracks. Due to the potential-dependent change in the oxide conductivity (at least 4 orders of magnitude), the oxide can be either "turned on" or "turned off", in the sense that a redox process can occur on or in the oxide. This change in conductivity occurs at about 0.8 V on an activated electrode. At $E < 0.8$ V, the exposed metal/electrolyte interface undergoes normal double-layer charging and hydrogen processes, leading to essentially constant values for the double-layer capacitance and the hydrogen adsorption and desorption charge. At $E > 0.8$ V, the entire oxide/electrolyte interface also is subject to double-layer charging, thus leading to the very high value of C_{∞} ($> 800 \mu\text{F}/\text{cm}^2$ at 1.1 V) observed by Glarum and Marshall (222). Chloride concentration greater than 10^{-2} M stops continuing oxide growth (but does not change the redox characteristics of the film already formed) by adsorbing at the metal/oxide interface and thereby interfering with the Ir-O place exchange necessary for growth.

A brief summary of the anodic oxidation of Pt, Au, Pd, and Ir in aqueous solutions is in order. It is clear that both the formation and reduction of oxide films are complicated processes. These processes are influenced by many variables, such as pH, ion adsorption, applied potential, and time. Results obtained from several of the newer and more sophisticated techniques indicate that "incipient" oxidation of the surface can begin as much as 500-600 mV negative of the potential where oxidation is generally considered to begin. An exact structural

description of these "incipient" oxides is not yet available. At somewhat more positive potentials, a reversible hydroxyl species is often formed. The well-known electrochemical irreversibility of noble-metal oxides is introduced by potential- and/or time-induced surface rearrangements that produce more thermodynamically-stable species. The rate-determining step for oxide growth probably occurs at the metal oxide/electrolyte interface and probably involves the discharge of H_2O in acidic solutions and OH^- in basic solutions. The oxide films formed on Ir are unique in many respects.

C. Oxide Participation in Anodic Reactions on Noble-Metal Electrodes

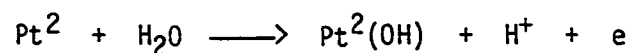
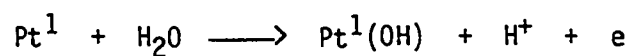
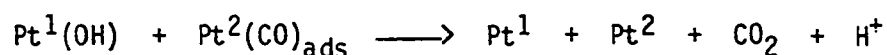
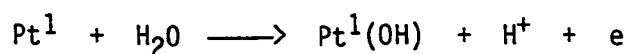
In this section of the literature review, a specific type of anodic reaction will be surveyed. Anodic reactions on noble-metal electrodes frequently take place not on the metallic surface, but rather on the corresponding metal oxide surface. In the last few years, it has become clear to an increasing number of workers that the metal oxide is not simply a passive electron sink, but may actually be an active participant in one or more of the elementary reactions in the overall electrode process. It is these reactions that will be covered in this section. In addition, the scope of this review has been limited to the relatively recent literature, primarily from 1973 to date, and to those earlier papers that have a special significance.

Compared to the large number of reaction mechanisms known in inorganic and especially organic chemistry, the number of well-

characterized reaction mechanisms in electrochemistry is small. This is undoubtedly related to the experimental difficulties encountered in elucidating the course of a complex process that occurs in a zone that is only the equivalent of 2-3 atomic layers in thickness. For anodic reactions at solid electrodes, a fairly complete list of the well-studied mechanisms would consist primarily of the oxidation of those simple organic molecules which have the potential to be used as fuels, and the oxygen evolution reaction (OER).

As was the case in the previous section, the volume of literature in which Pt is used as an electrode material far exceeds that of Au, Pd, and Ir combined.

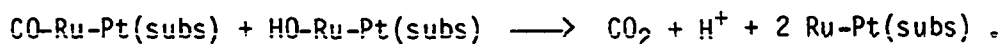
McCallum and Pletcher (226) studied CO oxidation on smooth Pt in 1 M HClO₄, utilizing a potential-step technique. Their results are consistent with the "reactant-pair" mechanism proposed by Gilman (227). In this mechanism, the reaction between the adsorbed CO and the oxidized Pt species occurs at the edge of expanding two-dimensional islands of Pt oxide. The mechanism can be represented by



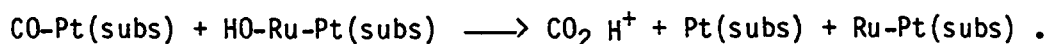
The superscripts 1 and 2 denote particular Pt sites. McCallum and Pletcher state that a steady-state oxidation of CO can take place on a

complete monolayer of oxide, but do not give any details other than to say that it is substantially different from the mechanism given above, and that it may still involve adsorbed species. Gibbs, McCallum and Pletcher (228) continued this work, using ca. 250 Å thick films of Au and Pt sputtered onto 3-23 μm thick sheets of a polymeric material. On Pt at short polarization times (i.e., a few seconds), the electrochemical response is dominated by the oxidation of the adsorbed CO according to the reactant-pair mechanism. This is entirely consistent with their earlier results. At longer times, it is likely that the oxidation still includes a surface reaction with either an oxide of Pt or an adsorbed hydroxyl radical. The reaction on the Au electrode is diffusion controlled. Gibbs, McCallum, and Pletcher could offer no likely mechanism for the reaction on Au. They believed that no surface oxidation occurred in the potential region where the reaction was relatively simple and therefore that a mechanism analogous to the one proposed for Pt was impossible.

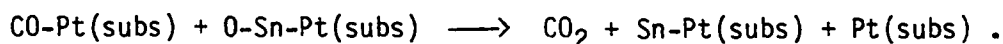
Matoo and Watanabe have studied the oxidation of CO on Pt for a number of years. In 1975, they oxidized CO on Pt having a sub-monolayer coverage of Ru ad-atoms (229). The mechanism depends on the Ru coverage. The more favorable reaction occurs at high Ru coverages, and is characterized by the reaction



The less favorable reaction occurs at low Ru coverages and is characterized by the reaction



Here, Ru-Pt(subs) represents a Ru ad-atom on the Pt substrate, and HO-Ru-Pt(subs) represent a hydroxyl radical adsorbed on a Ru ad-atom. The reactions given above are the rate-determining steps; the formation of the adsorbed hydroxyl is assumed to be fast. Motoo, Shitata, and Watanabe (230) later continued these experiments with Sn ad-atoms. In this case, the rate-determining step is



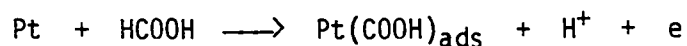
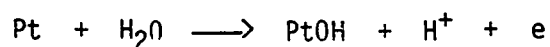
Here, Pt atoms on the surface serve as adsorption sites for CO and Sn ad-atoms act as oxygen adsorption sites. Due to the Sn ad-atoms, oxygen is introduced to the surface at a potential 390 mV negative of the potential where oxygen adsorbs on Pt, thus reducing the overpotential substantially. As little as 0.03 monolayer Sn can cause this shift in the polarization curve. The greatest overall enhancement of the oxidation occurs at 0.50 monolayer Sn. A gold substrate covered with one monolayer of Pt has the same characteristics as a solid Pt substrate. Motoo and Watanabe (231) found an identical mechanism to be operative in the oxidation of CO on Pt with As ad-atoms. In this case, the overpotential is reduced by 450 mV when the As coverage is 0.7 monolayer. This result is somewhat surprising, in that As is generally considered to be a catalyst poison.

Bilmes, de Tacconi, and Arvia (232) have observed a multiplicity of anodic peaks while oxidizing CO on polycrystalline Pt in 1 N HClO₄. If CO is allowed to adsorb at open circuit potential for a long time, only one very sharp anodic peak ($E_p \approx 0.95$ V vs. NHE) is obtained on a subsequent potential scan. With a complex potentiodynamic program, at least 3 anodic

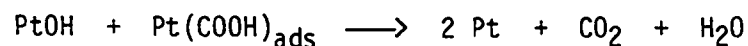
peaks can be seen. At the lower potentials, the surface reaction between adsorbed oxygen and adsorbed CO is expected to be important. The other two peaks are attributed to the direct oxidation of adsorbed CO and to the reaction of adsorbed oxygen and CO from the bulk of the solution.

Jolson (233) investigated the oxidation of CO on rotating disc electrodes made from various electrode materials. Of those tested, oxidation remained at the convective-diffusion controlled value on Pt for the longest time period. Jolson observed CO adsorption at negative potentials; this adsorbate poisons the Pt surface toward CO oxidation from the bulk solution. At very low CO concentrations and very low overpotentials, there is evidence that oxidation can proceed in the absence of surface oxides, but adsorption is a necessary prerequisite.

In 1973, Capon and Parsons (234) published an excellent paper on the anodic oxidation of HCOOH on a number of noble metals. On Pt, three anodic peaks are recorded on a positive-going potential sweep. The second peak ($E \approx 0.9$ V vs. RHE) is ascribed to the reaction sequence



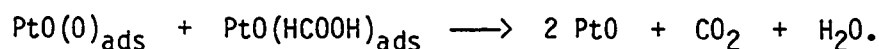
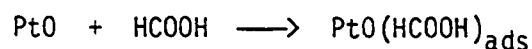
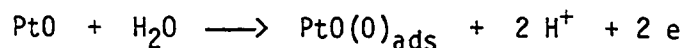
then either



or

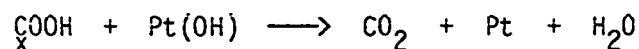
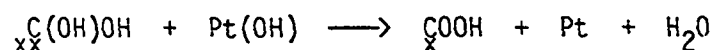


Oxidation of HCOOH by this sequence is halted by the further oxidation of the PtOH to give inactive PtO. The third anodic peak ($E = 1.4 - 1.5$ V) can be ascribed to the sequence



According to Capon and Parsons, this $\text{PtO(0)}_{\text{ads}}$ specie was a precursor of the phase oxide, PtO_2 . Although the description of oxide growth of Pt is somewhat dated, the fundamental concepts of electrocatalysis by an adsorbed hydroxyl radical and by a lower oxide/higher oxide redox couple remain sound.

Adzic and a series of co-workers have authored papers on the anodic electrochemistry of HCOOH on Pt. Adzic, Popov, and Pamic (235) found that a higher average current density for the oxidation of HCOOH on Pt and Pt + Pb ad-atom electrodes can be maintained if the potential is periodically pulsed into the oxide region. This enables the following surface reactions to take place:



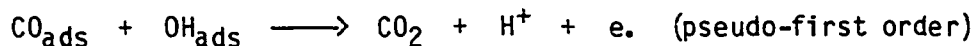
An "x" represents an adsorbate-substrate interaction. Species having

multiple interactions are more difficult to oxidize than those with single interactions, and are commonly referred to as "poisons". Removal of these "poisons" frees Pt sites that then participate in the oxidation of HCOOH from the bulk solution, thus giving a higher average current density. Adzic, O'Grady, and Srinivasan (236) oxidized HCOOH and CH₃OH on Pt electrodes modified by Pb, Bi, and Tl ad-atoms in 85% H₃PO₄. The ad-atoms greatly improved the overall rate of HCOOH oxidations, relative to Pt alone, but due to phosphate ion adsorption the rate is less than that obtained for identical electrodes in a HClO₄ electrolyte. The electrocatalytic activity is in the order Pb > Bi > Tl. These workers again identify the anodic peak at 0.9 V vs. RHE as resulting from the successive surface reactions between the strongly bound intermediates and adsorbed hydroxyl species. The electrocatalytic effects on CH₃OH oxidation are similar in nature but smaller in magnitude.

Beden, Lamy, and Leger (237) conducted cyclic voltammetric experiments on a number of noble metals in a 0.25 M K₂SO₄ + 0.1 M sodium formate solution. In the absence of the formate, Pt surface oxidation began at about -0.2 V vs. mercurous sulfate reference electrode. In the presence of formate, oxidation began at approximately -0.5 V on the forward scan, peaked at 0.0 V, and then decreased to zero as the potential was scanned to more positive potentials. A much sharper peak with $E_p = -0.2$ V was recorded on the reverse scan. The 200 mV difference in the peak potentials on the forward and reverse scans is indicative of strongly-adsorbed species that are oxidatively removed in the oxide region.

Vassiliev et al. (238) have conducted a very elegant study of HCOOH and CH₃OH oxidation on smooth and platinized Pt electrodes having Sn ad-atoms. A technique utilizing fast potentiodynamic pulses enabled them to control the surface coverages of the Sn and the organic adsorbates. The electrocatalytic effect of the Sn ad-atoms is independent of the nature of the organic and the state (roughness) of the electrode surface. Under those conditions where the rate-determining step is $R_{ads} + OH_{ads}$, the "promoting" effect of Sn is clear; if the rate-limiting step is either an electron transfer or some other surface interaction, the promoting effect is not observed. In this system, Pt is active with respect to the chemisorption of the organic substance, and the Sn ad-atoms provide a high surface concentration of OH radicals.

This same concept of a "mixed" electrocatalyst was used by de Tacconi et al. (239) in the electrooxidation of HCOOH on Pt + Rh alloys. The supporting electrolyte was 0.5 M H₂SO₄. A maximum amount of HCOOH is adsorbed on alloys with 40-50 atomic % Rh, but the maximum electrocatalytic activity occurs at 15-20 atomic % Rh. They judge their results to be consistent with the bifunctional theory of electrocatalysis, i.e.

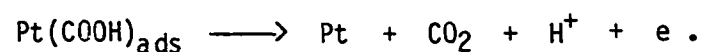
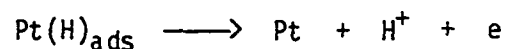
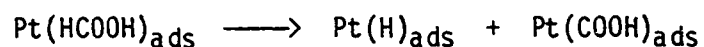
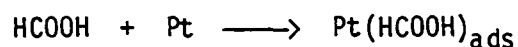


They do not give the steps in the production of CO_{ads} from HCOOH.

Although not explicitly stated by de Tacconi et al. (239), it must be assumed that Pt acts as the CO adsorption sites. It is known that oxide formation begins on Rh at a potential that is slightly less positive than

that for Pt oxide formation. de Tacconi et al. were not able to determine if CO adsorption was linear (one site) or bridged (two sites), but it was clear that total surface coverage of these species was relatively high. Incidentally, Sobkowski and Zelenay (240) found that the oxidation of HCOOH on Rh in 0.5 M H₂SO₄ was almost exactly the same as the reaction on Pt, including the oxidation of the strongly-adsorbed species by an adsorbed hydroxyl radical. They state that HCOOH adsorption on Rh requires two sites while only one site is needed on Pt.

Conway and co-workers (241) probed the anodic electrochemistry of HCOOH on Au-Pt alloy electrodes. A typical cyclic voltammogram has three anodic peaks on the forward scan and one peak on the reverse scan. The first anodic peak is due to HCOOH oxidation on Pt sites by the reactions

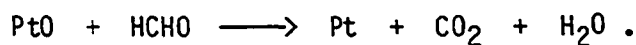


"Third-body" effects are important in this peak. The second anodic peak is associated with a surface reaction involving the initial OH species deposited in the course of Pt surface oxidation and either an adsorbed HCOOH or a self-poisoning specie "P" that is the result of a parallel side reaction. The third and most positive peak is associated with an anodic reaction on or with the more developed (i.e., higher oxidation state) surface oxide on Pt. Conway and co-workers (241) noted that CH₃OH

oxidation on Au-Pt alloys is qualitatively and quantitatively different than HCOOH oxidation, probably due to the initial formation of COH_{xxx} species in the oxidation of methanol.

Koch, Rand, and Woods (242) considered the oxidation of HCHO and CH₃OH on Pt with Sb, As, Bi, Hg, Re, Te, or Sn ad-atoms, and on a series of Pt-Rh alloys. All of these electrodes have an enhanced activity over Pt alone, which once again can be assigned to the greater ease of oxygen adsorption on the added metal. The reaction of the adsorbed organic species with adsorbed OH radicals is rate determining, according to Koch, Rand, and Woods. They also found a rough correlation between the electrocatalytic activity and the E° for the metal/lowest metal oxide couple.

Kuliev et al. (243) have investigated the adsorption and electro-oxidation of HCHO on Pt. Catalytic decomposition and oxidation of the adsorbed hydrogen produced occurs at low applied potentials. At higher potentials, the slow step of the electrooxidation process is the reaction between the surface oxide PtO and HCHO from the solution, viz.

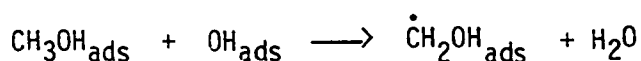


At potentials greater than 1.3 V vs. RHE, the current decreases due to a conversion of PtO to PtO₂, which is reduced by formaldehyde with greater difficulty. Kuliev et al. (243) state that the reaction given above is in addition to the oxidation of chemisorbed organic species by OH radicals.

Motoo and Shibata (244) have measured the catalytic effects of a number of ad-atoms on HCHO oxidation on Pt. The ad-atoms fall into two

groups. The first group, consisting of Cu, Ag, Tl, Hg, Pb, As, Bi, Te, and Se exert a relatively small enhancement that seems to be related to a number of Pt sites that each ad-atom occupies. The second group consists of Ge, Sn, and Sb; the enhancement factors are roughly an order of magnitude greater than those in the first group. Motoo and Shibata note that the common feature of Ge, Sn, and Sb is the ability to adsorb oxygen atoms at fairly low potentials. Motoo and Shibata (244) conclude that "these ad-atoms facilitate oxidation by accepting oxygen atoms from water molecules and donating them to a surface intermediate."

The electrochemical oxidation of CH₃OH on Pt has been extensively studied for a number of years. It is difficult to decide precisely who was the first to suggest that methanol oxidation involved the participation of adsorbed hydroxyl radicals or a surface oxide. Workers such as Frumkin, Buck, Vielstich, and Bockris all proposed a mechanism of this type in the 1950s and early 1960s. Perhaps two of the best of these earlier papers are those of Bagotzky and Vasilyev (245,246). In the first paper (245), they suggest that a reaction of the type



may be rate determining, but in the same paper they make the crucial distinction between the activity of adsorbed hydroxyl radicals and the inhibitory effects of other forms of adsorbed oxygen species. In the later paper (246), Bagotzky and Vasilyev have recognized that methanol adsorption seems to involve multiple dehydrogenation steps, and that the hydroxyl radical reacts with the chemisorbed intermediate.

Sidheswaran and Lal (247) could fit their data on the oxidation of CH_3OH and HCHO on a Pt electrode to a rate equation of the type

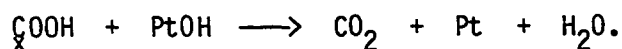
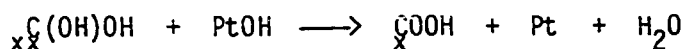
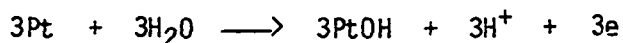
$$i = nFk \theta(1-\theta)\exp[\beta EF/RT].$$

Here, k is the heterogeneous rate constant, θ is the relative surface coverage of the adsorbed organic species, and β is the transfer coefficient, found to be ca. 1. This is consistent with a non-electrochemical rate-determining step like



The electroformation of OH_{ads} was assumed to be a fast, preceding reaction.

Capon and Parsons (248) preferred the following mechanism for the anodic peak obtained at 0.9 V vs. RHE in the oxidation of CH_3OH and HCOOH :



In their paper proposing the "bi-functional mechanism of electro-catalysis through surface reaction", Watanabe and Motoo (249) examined CH_3OH oxidation on a Pt electrode having Au ad-atoms. Both 0.5 M H_2SO_4 and 1 M NaOH supporting electrolytes were used. Watanabe and Motoo propose that $\underset{\text{xxx}}{\text{C}}\text{OH}$ intermediates react via a surface interaction with neighboring O-Au-Pt(subs) species to give $\text{CO}_2 + \text{H}^+ + \text{e} + \text{Au-Pt}(\text{subs})$. The

crucial O-Au-Pt(subs) species were formed at much more negative potentials (vs. RHE) in 1 M NaOH than in 0.5 M H₂SO₄. It must be noted that an electrocatalytic effect of this kind is usually associated with ad-atoms that adsorb oxygen at potentials negative to that of Pt; this is certainly not the case with Au ad-atoms.

Mikhailova, Osetrova, and Vasil'ev (250) also utilized the bifunctional mechanism of electrocatalysis in a study of CH₃OH and HCOOH in 1 N H₂SO₄ on Pt with Sn ad-atoms. The surface coverage of OH_{ads} on Pt in the potential region around 0.7 V vs. RHE is low, according to these workers. The addition of Sn dramatically increases the OH_{ads} coverage since Sn has a tendency for easy and reversible oxygen adsorption in this region. They postulate that Sn acts as a center for OH_{ads} and that Pt atoms act as a center for the organic reactant. The slow step in the electrooxidation is the interaction of the chemisorbed organic particle with adsorbed hydroxyl radicals. Mikhailova, Osetrova, and Vasil'ev (250) empirically related Sn coverage and the catalytic effect by the equation

$$i_{Pt + Sn}/i_{Pt} = \exp[7.2 \theta_{Sn}],$$

where $i_{Pt + Sn}$ is the anodic current in the presence of Sn, i_{Pt} the current in the absence of Sn, and θ_{Sn} is the Sn coverage.

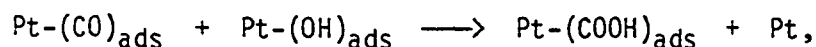
Hampson, Willars, and McNicol have used a potential-step technique to study the CH₃OH oxidation reaction on Pt (251), and have reviewed the oxidation mechanisms at Pt in acid electrolytes (252). In the potential-step technique, positive potential increments were applied to an initial potential of 0.45 V vs. RHE, a potential where the electrode was judged to

be free of adsorbed hydrogen or oxygen. However, adsorbed CH_3OH is certainly present at 0.45 V. For small potential steps, the transient current can be fitted to a mathematical model originally proposed for a general nucleation and growth process (253). This is in turn related to the formation of adsorbed hydroxyl radicals. At longer times and at higher potentials the current tails off. This is related to the formation of a strongly-bound oxide that gradually increases in coverage and finally becomes the dominant surface species, inhibiting further CH_3OH adsorption and oxidation. They conclude that in order to achieve maximum currents, there must be a delicate balance between OH adsorption and methanol adsorption. The review article (252) is an excellent source document on this specific reaction. While pointing out that there is no universally accepted theory, they do state that "the oxidation most likely proceeds via a reaction involving either an adsorbed (possibly strained and therefore reactive) water molecule, or adsorbed OH species derived from the electrosorption of water."

Katayama (254) has found that the long-term activity of 16 atom % Pt-Sn oxide is 14 times better than Pt for the electrooxidation of CH_3OH . While neither OH_{ads} nor direct oxide participation is explicitly discussed, Katayama does state that either Pt/Pt(II) or Pt(II)/Pt(IV) redox coupling takes part in the mechanism.

Beden et al. (255) have conducted an extensive investigation into methanol electrooxidation on Pt in 0.5 M KOH, both in the presence and absence of Pb, Bi, Cd, and Tl ad-atoms. The mechanism presented by Beden et al. has 9 steps, the first of which is the formation of adsorbed

hydroxyl radicals; 6 of the remaining 8 steps involve these hydroxyl radicals as one of two reactants in a surface reaction. The proposed rate-determining step is



where $\text{Pt-(CO)}_{\text{ads}}$ is the adsorbed residue resulting from 4 successive dehydrogenations of adsorbed CH_3OH . The electrocatalytic activity of the electrodes with Pb and Bi ad-atoms is greater than that of Pt only, while Cd and Tl ad-atoms have an inhibiting effect at certain potentials. The different effects of these ad-atoms can be ascribed to a bulk deposition of Cd and Tl that leads to severe blockage of CH_3OH adsorption sites, and to an increase in the hydroxyl radical coverage (but without a large decrease in CH_3OH adsorption sites) due to chemisorption on Pb and Bi.

Bagotzky, Vassilyev, and Khazova (256) have published a paper entitled "Generalized scheme of chemisorption, electrooxidation and electroreduction of simple organic compounds on platinum group metals." This paper gives a scheme for the electrochemistry of CH_4 , CH_3OH , HCHO , HCOOH , and CO_2 and all possible intermediate products (e.g., $\overset{\text{C}}{\underset{\text{X}}{\text{CH}_2\text{OH}}}$, $\overset{\text{C}}{\underset{\text{X}}{\text{OH}}}$, $\overset{\text{C}}{\underset{\text{X}}{\text{CHO}}}$). In all cases, oxidation is represented as the interaction of an adsorbed hydroxyl radical with a carbon-metal bond. The actual pathway along the scheme and the yield of products is determined by the rates of individual steps, which are in turn determined by factors such as temperature, potential, and the coverages of foreign species, adsorbed hydrogen, adsorbed hydroxyl radicals, and adsorbed organic species.

The anodic electrochemistry of organic substances having more than one carbon has been examined in some detail. In the oxidation ethanol on platinized platinum, Sidheswaran and Lal (257) were not able to unambiguously assign a rate-determining step; it was either the formation of the adsorbed OH radical, or the interaction of this radical with the adsorbed ethanolic residue.

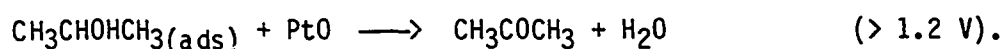
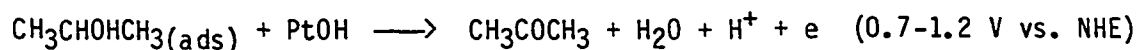
The oxidation of ethanol and acetaldehyde on smooth Pt in 0.5 M H₂SO₄ was studied by Raicheva et al. (258). Two anodic peaks were found. The first (less-positive) peak was attributed to the electrooxidation of the carbon-containing products of the dissociative chemisorption of the ethanol and acetaldehyde on the Pt surface. The second peak was attributed to the oxidation of the surface and the resulting chemical interaction of the organic substance and the surface oxide.

Snell and Keenan (259) used the competitive adsorption of Cl⁻ on Pt as a means of examining the role of adsorption in the oxidation of ethanol on Pt. Two waves are obtained on the forward scan of a cyclic voltammogram. The first wave can be assigned to a surface chemical reaction between chemisorbed CH₃CHOH and adsorbed hydroxyl radicals. The second wave is due to another surface reaction, this time involving CH₃CH₂OH_(ads) and PtO. Acetaldehyde and water are the products in both cases.

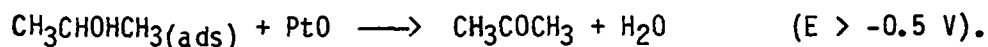
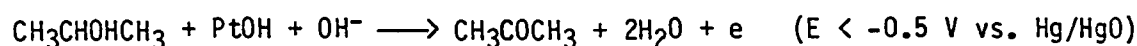
Dzhambova, Sokolova, and Raicheva (260) oxidized the primary alcohols having 1-4 carbons on Pt, 40% Au - 60% Pt, 60% Au - 40% Pt, and Au electrodes. For each oxidation, the rate-determining step is a chemical

reaction on the surface. On a given electrode material, the anodic peak potential does not change as the number of carbons is increased.

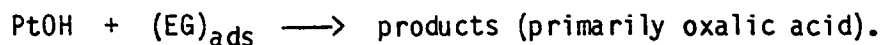
Rao and Roy (261) oxidized isopropanol to acetone on platinized platinum in 2.5 M H₂SO₄ and 2.5 M KOH. The mechanism in acid is:



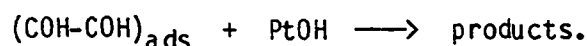
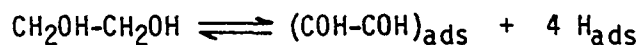
In base, the corresponding mechanism is:



Ethylene glycol (EG) is an attractive fuel for fuel cells and for that reason has been investigated in detail. Vigh (262) holds that the rate-limiting step in EG oxidation is



Soviet workers (263) have been somewhat more specific, i.e.,



Vigh (262) argues that 4 dehydrogenations do not take place prior to the surface reaction.

Sidheswaran (264) has given a very complex scheme for steady-state EG oxidation, accounting for the variety of products (CO₂, CHO-CHO, CH₂OH-CHO, CH₂OH-COOH, CHO-COOH, and COOH-COOH) that are found. As in the

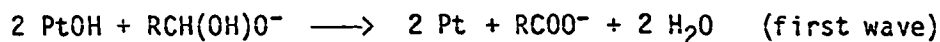
scheme of Bagotzky et al. (256), the common oxidant is the adsorbed hydroxyl radical.

Kadrikan, Beden, and Lamy (265,266) have very recently examined EG oxidation on Pt with a number of ad-atoms. For an acidic media (265), they agree with Seber, Vassiliev and Bagotsky (263) that the anodic peak at ca. 0.8 V vs. RHE is due to the reaction

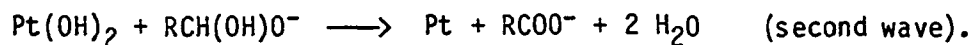
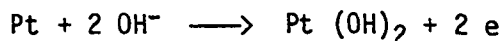


Of the ad-atoms tested, Cd and Re cause the polarization curve to shift to more negative potentials but do not change the magnitude of the current density. Ad-atoms of Pb, Cu, Bi, and Tl have no effect. In a basic media (266), however, Pb, Bi, and Tl greatly enhance the electrocatalytic activity, Cd again shifts the polarization curve to more negative potentials, and Cu, Ru, and Re have no effect. The enhanced activity of Pb, Bi, and Tl in base is explained by the anodic stripping of bulk deposits of these metals at potentials just negative of that where EG oxidation begins. This stripping frees additional Pt sites for EG adsorption, which then rapidly react via the bifunctional mechanism.

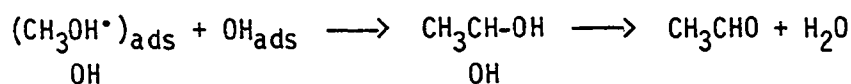
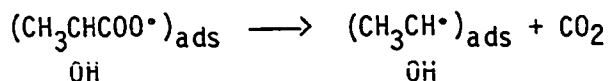
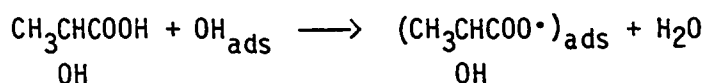
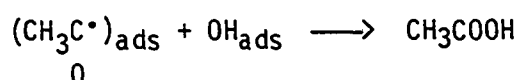
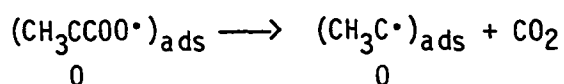
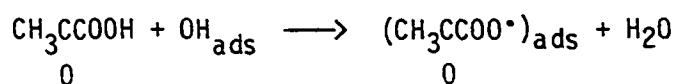
Sibille et al. (267) were interested in determining the mechanism of anodic oxidation of aldehydes in basic solution. Nine aldehydes were examined at a Pt RDE in aqueous solutions, pH 9-14. Most of the aldehydes gave only one anodic peak, but some (e.g., acetaldehyde) gave two anodic peaks on the forward scan. According to Sibille et al., the homogeneous conversion of the aldehyde into the geminal diol anion ($\text{RCH}(\text{OH})\text{O}^-$) occurs before any electrochemical step. The remainder of the mechanism is:



and

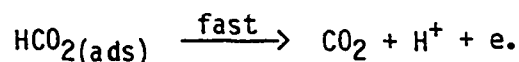
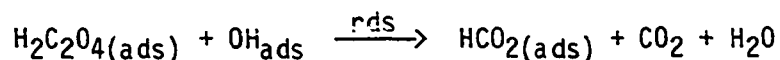
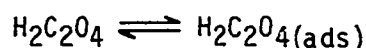


Horyani (268) has proposed the following mechanisms for the oxidation of pyruvic acid (CH_3CCOOH) and lactic acid (CH_3CHCOOH).



The formation of small amounts of acetic and pyruvic acids during lactic acid oxidation are accounted for by the abstraction of the tertiary hydrogen atom to give an adsorbed tertiary radical, following by a radical combination reaction with another hydroxyl radical. Horyani (268) relates the potential dependence of these oxidations to the rate of formation of OH_{ads} . This formation rate is in turn related to the thickness of the oxide film, which acts as a barrier to charge transfer.

The oxidation of oxalic acid on Pt in 1 M HClO₄ and in a series of phosphate buffers (pH 0.55 to 6.28) was studied by Inzelt and Szetey (269). This reaction proceeds by the mechanism



The initial adsorption is reversible and follows the Temkin isotherm.

In the anodic oxidation of ascorbic acid on Pt, Takamura and Sakamoto (270) found that Bi and Pd ad-atoms exerted a marked catalytic effect. Maximum activity is obtained when the coverage is 0.5 - 0.7. While a detailed interpretation was not given, Takamura and Sakamoto do state that the ad-atoms resulted in an increase in activated water species (such as OH_{ads}) on Pt that can act as "electron captors" in the oxidation of ascorbic acid to dehydroascorbic acid.

The oxidation of tetrahydrofuran (THF) on Pt in an acidic solution was explained by Sugawara and Sato (271). The initial step involves the discharge of THF to form a radical, which then chemically reacts with the oxide layer to give the hydroperoxide of THF.

Cyclohexene can be oxidized on platinized platinum in 1 M H₂SO₄. Alciaturi and Marschoff (272) conducted their experiments at 50°C, where the yield of CO₂ was expected to be greater than 95%. At a scan rate of 100 mV s⁻¹, a broad, irreversible peak (E_p ≈ 1.05 V vs. SCE) is obtained on the forward scan, while at 1 mV s⁻¹ a much sharper peak (E_p ≈ 0.82 V)

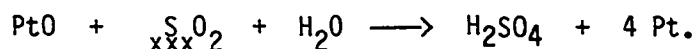
is observed. There is very little, if any, anodic current on the reverse scan on an oxide-covered electrode. Alciaturi and Marschoff conclude that hydrocarbon oxidation occurs simultaneously with platinum oxide formation. The oxidation mechanism is identical to the "reactant-pair" mechanism of Gilman (227).

Phenol oxidation at Pt in acidic media was re-examined by Levina, Kolosova, and Vasil'ev (273). They conclude, as did Ginzburg (274), that surface oxides are involved. Phenol adsorption is necessary, but is not the slow step in the process. The potential region for phenol oxidation shifts at 59 mV/pH in the range pH 0.4 to 14. This indicates to Levina, Kolosova, and Vasil'ev that the OH_{ads} produced in a fast, preceding discharge of H_2O or OH^- is one of the reactants in the slow step of the process.

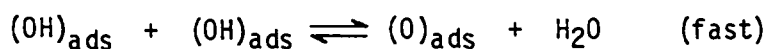
Slaidens and Actina (275) examined the oxidation of Mn(II) at a Pt RDE in 1 M H_2SO_4 . Cyclic voltammetry at 4 mV s^{-1} was utilized. They found that an oxide film on Pt effects the rate of Mn(II) oxidation in 2 ways: a thin layer, or partially covered surface, accelerates the anodic process; a thick layer decreases the rate of electrochemical oxidation.

The oxidation of SO_2 has received some attention very recently. Appleby and Pichon (276) have used cyclic voltammetry at stationary Pt electrodes and at a RDE made from 10% Pt-carbon paste. The shape of $i-\omega^{1/2}$ plots are a function of the concentration of H_2SO_4 in the supporting electrolyte; at high (62-81%) H_2SO_4 concentrations, these plots are flat, while at somewhat lower concentrations (44%) the plot is curvilinear. While Appleby and Pichon propose a very complex overall

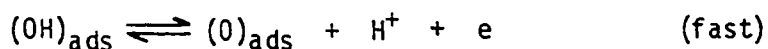
scheme, they also conclude that at high rotation speeds (i.e., high SO₂ flux), the surface reaction PtO + SO₂ → Pt + SO₃ becomes rate limiting. The involvement of PtO was earlier reported by Seo and Sawyer (277) and Comtat and Mahenc (278) in 0.5-1.0 M H₂SO₄. Audry and Voinov (279) also have conducted SO₂ oxidation on Pt in 44% H₂SO₄. According to them, SO₂ can adsorb on Pt in two different ways -- binding to either 1 Pt atom or to 3 Pt atoms. A "full" monolayer of SO₂ reportedly has 30% of the Pt sites bonding to one SO₂ molecule and the remaining sites bonded to SO₂ molecules in a 3:1 ratio. The oxidation occurring on an oxide-covered electrode is



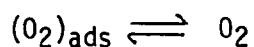
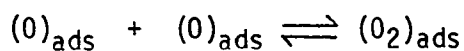
The volume of literature on the oxygen evolution reaction on Pt precludes any in-depth review in this dissertation. Fortunately, several excellent reviews are available (51, 280-283). As pointed out by Hoare (51), "an unbelievable number of reaction paths are possible if all intermediates are considered....Since many of these reaction paths are not unique in the value of the kinetic parameters, evidence other than that obtained from Tafel slopes is required to identify unambiguously the complete mechanism." In 1968, Hoare (51) favored a reaction mechanism in which the formation of adsorbed hydroxyl radicals was the rate-determining step, followed by either



or



and then



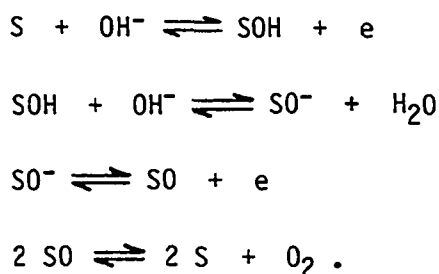
Damjanovic's review (280), which was published just after that of Hoare, is considerably less definite. Damjanovic could only offer the reader one of three possible mechanisms in acidic solutions and one of three (a different three) possible mechanisms in base. There has been some progress in elucidating the mechanism of the oxygen evolution reaction (OER) since 1968-1969, however.

Damjanovic and Ward (281), in a 1975 review, emphasized the modification of the kinetics of the OER by the continuing oxide growth. The oxide growth law operative during $O_2(g)$ evolution is very different from the growth law observed prior to $O_2(g)$ evolution. The continuing increase in oxide thickness causes a decrease in the catalytic activity, which Damjanovic and Ward attribute to a larger and larger voltage drop across the semiconducting oxide film. The following year, Damjanovic and Jovanovic (284) proposed a mechanism in which a chemical step following a charge transfer step is rate determining. In this mechanism, there is the direct participation of oxygen atoms in surface oxide film. The charge transfer step is once again the formation of adsorbed hydroxyl radicals.

Miles et al. (285) determined the transfer coefficient for the OER on number of noble metals and their alloys. The value is approximately 1 for Pt as well as Ir, RuO_2/TiO_2 , and Ru-Ir (50:50). A transfer coefficient of

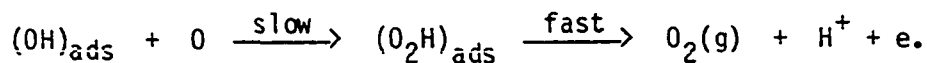
1 is consistent with a slow chemical reaction as the rate-determining step.

Iwakura, Fukuda, and Tamura (286) studied $O_2(g)$ evolution on a hydrated PtO_2 electrode in 1 N KOH. They propose the following mechanism, where S is a site on the surface:



The second step is rate determining at low overpotentials while the first step becomes rate controlling at high overpotentials.

Burke, McCarthy, and O'Meara (287) have speculated on the mechanism of the OER on Pt. The initial electron transfer is assumed to occur from one of the lone pair (sp^3) orbitals of the oxygen atom, as opposed to coming from an O-H bond. This gives an adsorbed cation radical that then loses a proton to give the adsorbed (neutral) hydroxyl radical. These workers also believe that the surface oxide film participates in the OER, possibly by way of intermediate peroxy radicals, viz.



The fact that hydrogen peroxide is not detected during $O_2(g)$ evolutions does not eliminate its possible existence as a short-lived intermediate on the electrode surface.

Huang (288) maintains that the first step in $O_2(g)$ evolution on Pt is the formation of an adsorbed hydroxyl radical. The second step is a charge transfer via electron tunneling.

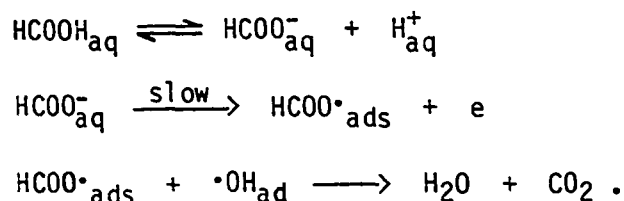
There is some direct evidence of the participation of the oxide film in the OER. In 1956, Rozenthal and Veselovskii (289) formed an O^{18} -enriched Pt oxide by polarizing an electrode in an O^{18} -enriched solution. When the electrode was transferred to a unenriched solution and oxygen gas was evolved, the initial $O_2(g)$ formed contained O^{18} . This experiment has been repeated very recently by Churchill and Hibbert (290) with identical results.

Evidence is continuing to accumulate that some anodic reactions on Au electrodes proceed by mechanisms that include the direct participation of a surface oxide. Erlikh, Anni, and Palm (291,292) have examined the oxidation of NO_2^- on a Au RDE; a variety of acid supporting electrolytes were used, including 1 N Na_2SO_4 and 1 N $NaNO_3$ solutions that were buffered with "a universal" buffer solution. A very sharp NO_2^- oxidation wave begins at a potential about 120 mV negative of the potential where surface oxidation begins in the absence of NO_2^- . A maxima is obtained at $E = 0.91-0.93$ V vs. Ag/AgCl reference electrode and a minima is obtained at 1.10 V; more positive potentials lead to O_2 evolution. The reaction rate is diffusion controlled for rotation speeds less than 950 rpm, but the reaction exhibits mixed kinetics (see Section IV) at rotation speeds greater than 950 rpm. Erlikh, Anni, and Palm (291) conclude that NO_2^- oxidation occurs via an interaction with an "active surface oxygen (AuOH)" and that passivation is due to the transformation of the oxide into a

less-active form by the oxidation to a higher (i.e., either AuO or Au₂O₃) state. The authors also suggest that the higher oxides partially block the electrode surface. In their second paper (292), Erlikh, Anni, and Palm expanded upon the idea of partial surface blockage. The equations for an inhomogeneous electrode surface developed by Landsberg and co-workers were utilized (see Section IV and references given therein). From an analysis of plots of $\log i$ vs. T^{-1} at various pH and rotation speeds, these workers conclude that surface blockage was negligible at pH 1 but was significant at pH 4.1 and 6.4. It should be noted, however, that these workers evidently used the Britton buffer at pH 4.1 and 6.4. The adsorption effects of the phosphate, borate, and acetate ions present in this buffer seem to have been ignored. Erlikh, Anni, and Palm again conclude (292) that passivation is the result of a conversion of the oxide from an active form (AuOH) to a less active form (AuO).

Capon and Parsons (234) have studied the oxidation of HCOOH on Au as well as on a number of other noble metals. In cyclic voltammetric experiments, Capon and Parsons observed an anodic current that started about 500 mV negative of the potential where "classical" gold oxide formation occurred. This current increased as the potential was scanned toward more positive values, peaked in the oxide region, and then rapidly decreased with further surface oxidation. They concluded that HCOOH oxidation on Au occurs only at a high overpotential and in the presence of an active surface oxide that they denoted as Au(O)_{ad}. More specifically, oxidation of HCOOH is the result of a reaction between a chemisorbed intermediate specie and a metal oxide specie.

Maximovitch (293) was the next investigator to suggest that HCOOH oxidation on Au proceeded through a surface reaction. He used an Au RDE in a 0.5 M Na₂SO₄ solution with pH > pK_a of formic acid. The basic shape of the i-E curve was similar to that of Capon and Parsons. Maximovitch utilized positive potential scan limits that were less positive than those used by Capon and Parsons and was able to record an anodic current on the reverse scan. This current increased following oxide reduction. When the electrode was potentiostated between 0.0 - 0.1 V vs. mercuric sulfate reference electrode, the resulting anodic current was proportional to the square root of the rotation speed for speeds up to 3600 RPM. Maximovitch proposed the following mechanism:



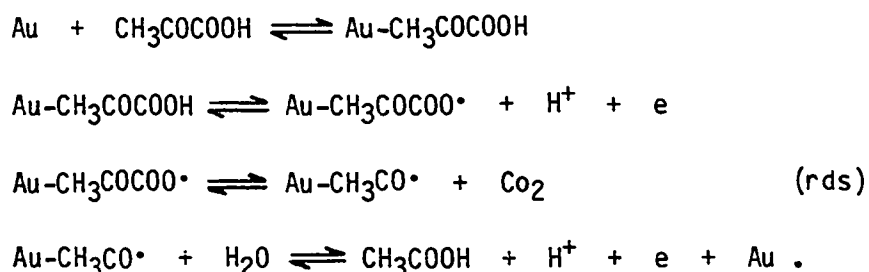
The symbol HCOO[•]_{ads} represents an adsorbed formate radical and the symbol OH_{ads} represents the adsorbed hydroxyl radical formed by the reaction OH⁻ ⇌ •OH_{ads} + e.

Beden, Lamy, and Leger (237) oxidized sodium formate on Au in 0.25 M K₂SO₄. Oxidation begins at -0.3 V vs. mercurous sulfate reference electrode and reaches a 300 mV-wide plateau at about 0.2 V. At 0.5 V, surface oxidation begins and the anodic current rapidly decreases with potential. Anodic current is restored on the reverse scan when the surface oxide is reduced.

Besenhard et al. (294) recognized that HCOOH oxidation on Au occurs by two different mechanisms in two different potential regions. At low overpotentials, the mechanism consists of a slow oxidation of adsorbed formate ions to give adsorbed HCOO, followed by a second and faster one-electron transfer. The other mechanism occurs at high overpotentials and is intimately related to the mechanism of Au oxide formation. Besenhard et al. propose that the first step in Au oxide formation is the discharge of OH⁻ or O²⁻ on the surface to form a reactive intermediate state that they denote as <Au...O>. The oxygen atoms in this reactive intermediate state are in nonequilibrium positions. While in this state, the oxygen atoms may either react with HCOOH to give CO₂ and H₂O or undergo surface rearrangements to give domains of the higher, stable oxides. The relative rates of these two competing reactions are determined by the scan rate, potential, and the time that the electrode has been polarized.

Gonzalo, Aldaz, and Vazquez (295) have investigated the oxidation of pyruvic acid (CH₃-CO-COOH) on a Au electrode in several electrolytes. Differential double-layer capacitance measurements indicates that pyruvic acid is adsorbed on Au; electron spin resonance establishes that free radicals are not present in the electrolyte to any appreciable extent. Cyclic voltammograms at a RDE have many of the same features previously described: oxidation beginning about 0.2 V negative of the potential for "classical" Au oxide formation, an anodic current peak in the oxide region, and a rapidly decreasing current as the potential is scanned to even more positive values. On the negative potential scan, anodic current is restored when the Au oxides are reduced. Large currents were obtained

in 0.5 M H₂SO₄ and 0.1 M NaOH, but smaller currents were recorded at intermediate pH values in electrolytes where the pH was adjusted with the Britton-Robinson buffer. These authors also seem to have been unconcerned with anion adsorption effects. If the electrode was potentiostated at potentials just negative of the oxide region, a time-independent and nearly mass-transport limited current was obtained. If the potential was set at potentials within the oxide region, the resulting current decayed as a function of time. The mechanism of pyruvic acid oxidation according to Gonzalo, Aldaz, and Vazquez (295) is

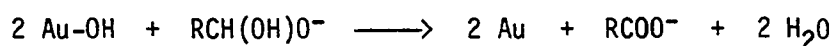
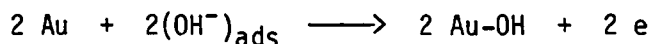


They ascribed inhibition to the electroformation of AuOH, which decreases the free surface area. It should be noted that these workers have attributed inhibition to the lowest Au oxidation state in the potential region where the higher Au oxides are certainly the predominant species.

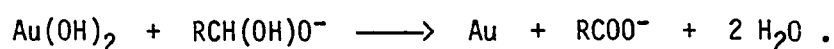
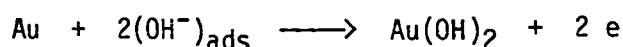
Sibille et al. (267) studied the oxidation of nine aldehydes on a Au RDE in aqueous solutions with pH 9-14. The potential of the onset of oxidation was nearly identical for all of the aldehydes. The shape of the i_d - E_d curves were similar to those for HCOOH and pyruvic acid. In a phosphate-carbonate electrolyte with pH 11.7, current plateaus on the forward and reverse scans were obtained, but $i_{\text{fwd}} \neq i_{\text{rev}}$. Sibille et al.

(267) propose that aldehyde oxidation proceeds by two slightly different mechanisms depending on the electrode potential. These mechanisms are:

1. At less positive potentials



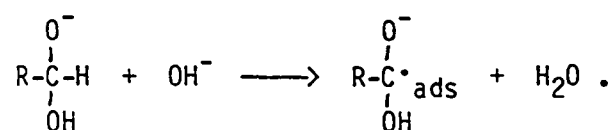
2. At more positive potentials



The specie RCH(OH)O^- represents a gem-diol anion formed in a prior chemical step.

Evans' group at the University of Wisconsin has also studied the oxidation of aldehydes at Au electrodes in base. Van Effen and Evans (296) obtained two anodic peaks, one at -0.6 V vs. SCE and a second that started at about -0.4 V and reached a current plateau before being strongly inhibited by the formation of a bulk phase oxide. The current was restored on the negative scan following oxide reduction. The currents were 75%-80% of the mass-transport limited value, the magnitude of the deviation increasing with the rotation speed. Van Effen and Evans argued against the mechanism of Sibille *et al.* (267), stating that their data establish the oxide as an oxidation inhibitor. Van Effen and Evans did not make any distinctions between the various forms of the surface oxide. Van Effen, Hui, and Evans (297) considered the oxidation of a series of halogenated benzaldehydes in 1.0 M NaOH with 10% tert-butanol. An Au RDE with a gold electrodeposit (analogous to a Pt black electrode) was used. Two oxidation waves were not observed, but rather one broad current

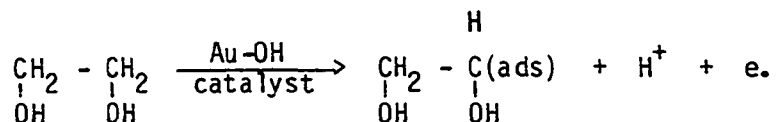
plateau that began at about -0.9 V vs. SCE. The anodic current was subject to the usual inhibitory effects of the higher surface oxide states. This particular electrode gave anodic currents that were mass-transport limited. Based on substitution effects (i.e., the number and position of the halogens on the aromatic ring) Van Effen, Hui, and Evans (297) state that their data are constant with a mechanism in which the rds is



This mechanism is identical to the one derived by Van Effen and Evans (298) from a study of the less-positive anodic wave obtained on a smooth Au electrode.

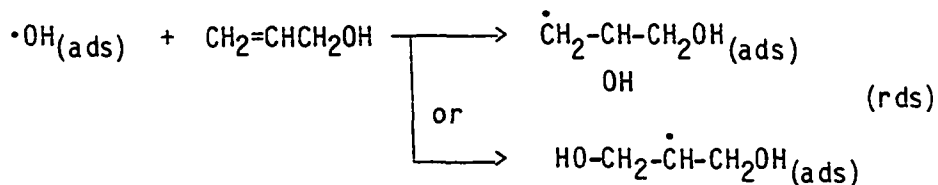
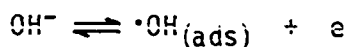
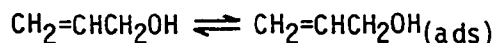
Adzic and Avramovic-Ivic (299), as part of a very extensive effort, have oxidized HCHO in alkaline solutions on Au electrodes that have been modified with Pb, Tl, and Bi ad-atoms. The ad-atoms (most likely in the form of underpotential deposits) cause an increase in the electrocatalytic activity, which Adzic and Avramovic-Ivic attribute to a modification of the properties of the AuOH layer.

The electrooxidation of ethylene glycol at Au in 1 M KOH was examined by Hauffe and Heitbaum (300). Analysis of data obtained from cyclic voltammetry, open-circuit potential decay, and RRDE experiments suggests to these workers that the rate-determining step was the one electron transfer

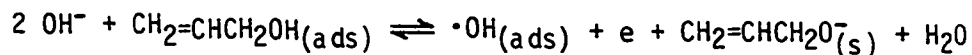
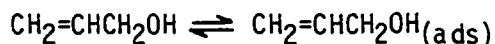


Allylic alcohol oxidation on Au has been studied by Celdran and Gonzalez-Velasco (301). The anodic currents obtained in alkaline solutions were larger and began at less positive potentials than those obtained in acidic solutions. Onset of oxidation occurred at a potential where the surface was covered by a monolayer of OH_{ads} . The Tafel slope was 100-125 mV for $E < -0.46$ V vs. SCE, and was dependent to a small extent on the solution pH. At $E > -0.46$ V, the Tafel slope was 278 mV and was not pH dependent. Celdran and Gonzalez-Velasco therefore concluded that there must be a change in reaction mechanism at -0.46 V. The proposed mechanisms are:

1. $E < -0.46$ V

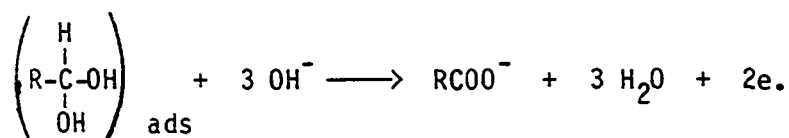
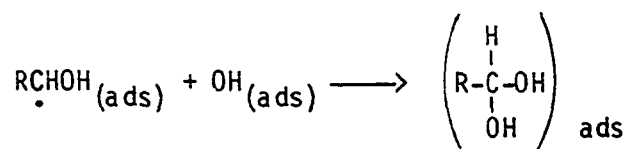
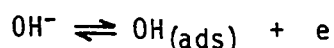
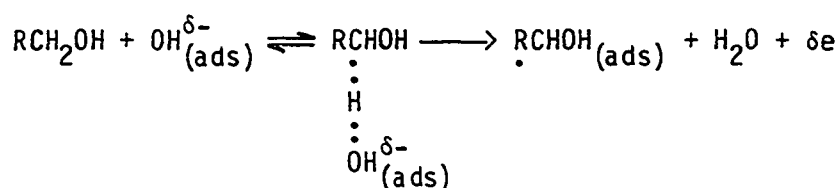
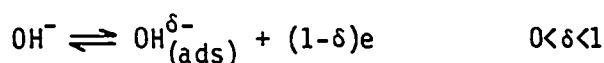


2. $E > -0.46$ V



The convoluted mechanism given for $E > -0.46$ V is an attempt to account for the very large Tafel slope that is observed. The experiments were conducted in fairly concentrated allyl alcohol solutions and it was assumed that $\theta_{\text{alcohol}} \gg \theta_{\text{OH}}$. The second step represents the displacement of an adsorbed allyl alcohol and formation of an adsorbed hydroxyl radical in a position where polymerization can be initiated.

Beltowska-Brzezinska has oxidized small aliphatic alcohols on 60% Au-40% Pt electrodes (302) and on pure Au (303) in 1 M KOH. The Au-Pt alloy is a better electrocatalyst than pure Pt. On the alloy electrode, the proposed oxidation mechanism is



The mechanism includes the participation of adsorbed hydroxyl radicals and adsorbed hydroxyl species having an electroreduction valence between -1 and 0.

French workers have investigated the anodic electrochemistry of the only amino acids that they claim are electroactive. Reynaud, Malfroy, and Canesson (304) have oxidized cysteine, cystine, and methionine on Au. All three of these amino acids can be oxidized from an adsorbed state; this oxidation begins at potentials negative of the potential where the gold surface is oxidized to the higher (Au(II) and Au(III)) states. Cystine and methionine are similar in that a single anodic peak is obtained as the potential is scanned into the oxide region, a minima occurs at about 1.25 V vs. SCE, followed by another rapid increase in anodic current. In other words, above 1.25 V the surface oxides do not inhibit the oxidation. Cysteine, however, gives a cyclic voltammogram that is more characteristic of a reaction where the gold oxides inhibit the oxidation, including the appearance of anodic current on the reverse scan following the electrochemical reduction of the oxides. Reynaud, Malfroy, and Canesson (304) conclude that electrochemical oxidation of the adsorbed amino acid occurs at the more negative potentials and is catalyzed by a labile metal oxide (see ref. 294) and that the anodic current obtained at higher potentials is due to the oxidation of the amino acid that diffuses to the electrode. X-ray photoelectron spectroscopy could identify adsorbed

$$\begin{array}{c} \text{O} \\ | \\ \text{R-S-S-R} \end{array}, \begin{array}{c} \text{O} \\ | \\ \text{R-S-S-R} \\ | \\ \text{O} \end{array}, \text{ and } \text{R-S-SO}_3^- \text{ species. Malfroy and Reynaud (305) have also}$$

oxidized tryptophan and tyrosine at Au. These amino acids are also oxidized from an adsorbed state at potentials negative of the region where phase oxides are formed, but there is relatively little current at the more positive potentials. The one exception to this observation is a tryptophan derivative at pH 8. Depending on pH, amino acid concentration, and electrode rotation speed, either a monomeric product or a polymeric product that films the electrode surface is obtained.

Frankenthal and two co-workers have examined the oxygen evolution reaction and the oxide formation reaction in the course of studies on the corrosion of gold. Frankenthal and Thompson (306) state that oxygen evolution occurs at low potentials on a gold surface partially covered with adsorbed oxygen, and at high potentials on a film of $\text{Au}(\text{OH})_3$. These results agree with earlier work of Hoare (152). From the observations that $\text{Au}(\text{OH})_3$ begins to form at the same potential as $\text{O}_2(\text{g})$ evolution, and that the Tafel slopes for $\text{Au}(\text{OH})_3$ formation and $\text{O}_2(\text{g})$ evolution are the same, Frankenthal and Thompson state that the mechanisms for the two processes must have the same rate-determining step. The most likely rate-determining step is judged to be the oxidation of water to an intermediate O or OH radical adsorbed on the film. Duncan and Frankenthal (307) later studied the effect of pH on these reactions. The Tafel slope for oxide film formation is identical for pH 0.0, 1.7, and 2.8. At a given film formation rate ($1 \times 10^{-6} \text{ A cm}^{-2}$), the potential shifts 60 mV/pH. The $\text{O}_2(\text{g})$ evolution reaction behaves in precisely the same manner, with a potential shift of 58 mV/pH. Duncan and Frankenthal maintain that these data substantiate the conclusion of Frankenthal and Thompson (306)

concerning the commonality of the rate-determining step for $\text{Au}(\text{OH})_3$ formation and $\text{O}_2(\text{g})$ evolution.

Samec and Weber (308) oxidized SO_2 on a Au RDE in 0.5 M H_2SO_4 . A limiting current plateau begins at ca. 0.65 V vs. RHE and continues up to ca. 1.4 V, where oxide formation begins. A small anodic current is recorded on the reverse scan, even for a positive potential scan limit of 1.7 V. Following oxide reduction, the anodic current returns to the same limiting value obtained on the forward scan. Although the data might indicate the participation of a chemisorbed oxygen specie, the mechanism proposed by Samec and Weber involves the direct electrochemical oxidation of SO_2 on a surface layer of "reduced SO_2 ", followed by hydrolysis to give HSO_4^- .

Zakharov (309) performed a voltammetric study of diethyl dithiocarbamate on Au in solutions with pH 4.6-8.5. A wave obtained at potentials greater than 1.0 V was characterized by a very sharp maxima. Zakharov attributed this wave to the further oxidation of tetraethylthiuram disulfide, which is produced by the oxidation of the dithiocarbamate at about 0.43 V. The products of the oxidation of the disulfide contained oxygen, e.g., HSO_4^- . Since oxygen-containing products were not obtained when a graphite electrode was used, Zakharov attributes the oxygen uptake to the direct participation of the oxygen adsorbed on Au.

Anodic oxides formed on Pd electrodes can be participants in anodic oxidations. Capon and Parsons (234) oxidized HCOOH on Pd as part of a study of several noble metals. Cyclic voltammetry established that

strongly-adsorbed intermediate products are not formed on Pd. It was this lack of adsorption of intermediate products that led Capon and Parson to predict that CH_3OH oxidation on Pd would be negligible; this was verified experimentally. There is essentially no anodic current obtained in the oxide region on Pd; this behavior is significantly different from that of Pt and Rh, which evidently have two regions of "active oxide". Formic acid oxidation on Pd becomes significant only after any previously-formed oxide is completely reduced; this is also quite different from HCOOH oxidation on Pt, where the rate of oxidation becomes large as soon as Pt oxide reduction is initiated. Capon and Parsons attribute this difference to an acceleration of Pt oxide reduction by HCOOH . Capon and Parson conclude that it is unlikely that an "active oxide" on Pd is not formed; the relative lack of reactivity is probably caused by the adsorption characteristics of HCOOH on Pd.

A slightly later work by Capon and Parsons (248) did verify that an easily-oxidized intermediate product (i.e., a weakly-adsorbed intermediate product) is formed on Pd when it is simply immersed in a HCOOH or CH_3OH solution. These results are consistent with their earlier work and with their theory that "active oxides" react via surface reactions only with strongly-adsorbed intermediate products.

Beden, Lamy, and Leger (237) also used Pd as an anode for the oxidation of formate in 0.25 M K_2SO_4 . The oxidation wave begins at -0.9 V vs. mercurous sulfate reference electrode; this is 600 mV negative on the onset of oxidation on Au. A broad peak is reached at -0.2 V, but the current quickly decreases to zero as surface oxidation occurs. As soon as

the oxide is reduced on the reverse scan, an anodic current comparable to that obtained on the forward scan is observed.

Watanabe and Motoo (249) found that the oxidation of CH_3OH on Pd in 0.5 M H_2SO_4 was catalyzed by Au ad-atoms. It is in the paper that they proposed their "bi-functional mechanism of electrocatalysis through surface reactions." In this mechanism, CH_3OH adsorption gives $\text{Pd}(\text{OCH})_{\text{ads}}$ intermediate products which are located next to $\text{O-Au-Pd}(\text{substrate})$ species. This latter specie is intended to represent a chemisorbed oxygen atom on a Au atom that has in turn been underpotential deposited on a Pd substrate. The two species cited above react in a surface reaction to give $\text{CO}_2 + \text{H}^+ + \text{e} + \text{Pd} + \text{Au-Pd}(\text{substrate})$. The initiation of the oxidation at more negative potentials in 1 M NaOH is attributed to the formation of the $\text{O-Au-Pd}(\text{substrate})$ species at more negative potentials in base.

The electrochemical and gas phase heterogeneous catalytic oxidations of CO were compared by Blurton and Stetter (310). Platinum, palladium and ruthenium were considered. The activity of Pd and Ru were much lower than the activity of Pt. Using Conway's theory for Pt electrooxidation (see Section II.B), Blurton and Stetter state that the increase in anodic current between 0.8 V and 1.1 V parallels the increase in the reversibly-bound PtOH on the surface, and that the decrease in the current at higher potentials reflects the diminished availability of PtOH due to conversion to PtO. Blurton and Stetter estimate that the surface coverage of the active metal-OH species on Pd and Ru must be several orders of magnitude lower than on Pt.

Zhirnova et al. (311) examined the effects of a large number of ad-atoms on the oxidation of CH_3OH on Pd. In 1 N H_2SO_4 , Ti and Cu had no effect, while Bi, Tl, Pb, Ag, Sn, I, and S all decreased the activity. All of the above ad-atoms decreased the activity of Pd in 1 N KOH. The slope of a Tafel plot for Pd only is the same as the slope for Pd in the presence of any of the ad-atoms listed above; Zhirnova et al. interpreted this as strong evidence that the reaction mechanism is unchanged. They state that the rds is the reaction between the carbon-containing species produced during adsorption on the electrode and OH_{ads} produced by the discharge of H_2O or OH^- . These authors recognize that this explanation is particularly troublesome when dealing with the effect of Sn ad-atoms. It is known that Sn enhances the activity of Pt towards CH_3OH oxidations (250); this was explained in terms of the more reversible adsorption of OH_{ads} on Sn than on Pt. Zhirnova et al. (311) deal with this difficulty by suggesting that Sn-Pd interactions increase the strength of the Sn- OH_{ads} interaction.

Lu and Ammon (312) have investigated the anodic oxidation of SO_2 in concentrated (50%) H_2SO_4 . Pre-anodized Rh, Ir, Re, Pt, Ru, Au, and Pd electrodes were tested; the electrocatalytic activity increases in order listed. The limiting current density for a saturated SO_2 solution was twenty times greater on Pd than on the next best electrocatalyst, which was Au. The electrochemical oxidation of SO_2 on Pd begins at an anodic potential (0.6 V vs. RHE in the same electrolyte) where the formation of adsorbed oxygen-containing species occurs. On other metals (e.g., Pt), these oxygen-containing species are converted to metal oxides at higher

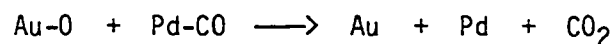
potentials, oxides that partially cover and inhibit SO_2 oxidation. This simply does not happen on Pd, and in fact, an oxide-covered Pd electrode exhibits a high and continuing electrocatalytic activity for SO_2 oxidation. Lu and Ammon (312) do not speculate on the precise electrochemical mechanism.

Breiter (313) and Gossner and Mizera (314,315) have conducted investigations of the CO oxidation reaction on Pd. Breiter (313) utilized cyclic voltammetry on a stationary Pd wire in 0.5 M H_2SO_4 . A very sharp peak is obtained on the forward scan between 1.0 V and 1.2 V vs. RHE; the sharpness of this peak decreased as the scan rate increased. At slow scan rates, an anodic current plateau is observed on the reverse scan, as well as a cathodic peak that is undoubtedly due to PdO reduction. Breiter ascribes the anodic current plateau to the oxidation of CO that diffuses to the electrode, so it is clear that oxidation can proceed on a surface that is partially covered by PdO. Breiter also concludes that CO does adsorb on Pd, but that a large portion of the adsorbed CO is oxidized in the absence of appreciable amounts of chemisorbed oxygen.

Gossner and Mizera (314,315) have examined CO oxidation on Pd-Au alloys that are 10-20% Au. The reaction on the alloy electrodes is faster than on pure Pd. Carbon monoxide adsorption occurs to a significant extent only on the Pd sites. The Au sites act as reaction centers, so it would appear that alloys with 10-20% Au give both a high coverage of adsorbed CO and a significant number of Au-Pd units. The mechanisms that Gossner and Mizera (314) propose are

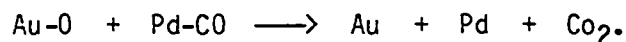


or



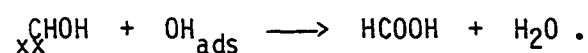
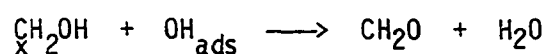
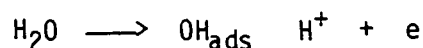
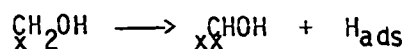
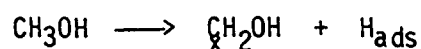
In this paper (314), they do not differentiate between a chemisorbed oxygen specie and a phase oxide.

Gossner and Mizera (315) have expanded upon their somewhat earlier work, but reached identical conclusions. In a series of experiments where an oxidized alloy electrode was open-circuited in a solution saturated with CO, there was a preferential decrease in the gold oxide coverage. This means that if a Pd-CO unit can react with either a Pd-O specie or a Au-O specie, the reaction will proceed via the reaction



The reaction with the Au-O species evidently has a lower activation energy. Gossner and Mizera recognize that this is another example of the bifunctional mechanism of electrocatalysis, a mechanism originally proposed by Watanabe and Motoo (249).

The literature dealing with Ir anodes is considerably less extensive. Vol'fkovich et al. (316) and Bagotzky et al. (317), at the Institute of Electrochemistry in Moscow, investigated the oxidation of methanol on smooth Ir and on porous Ir, respectively. The results obtained on a smooth Ir electrode are very similar to those obtained on smooth Pt, so the proposed reaction mechanism is also very similar. This mechanism is



The stepwise dehydrogenation on Ir stops following two steps, whereas three steps occur on Pt. The experiments on a porous Ir electrode (317) confirmed that CH_3OH loses 2 atoms of hydrogen during adsorption in an acid solution.

In their classic paper on the oxidation of HCOOH on noble metals, Capon and Parsons (234) noted that Ir was less active than the other noble metals tested. There did appear to be some adsorption of "intermediates". There was no large anodic peak in the oxide region on the forward potential scan, but the Ir oxide was not completely inactive, as was Pd oxide. Also, in contradiction with the other noble metals, there was no anodic current on the reverse scan until the oxide had been completely reduced. (It appears from the voltammogram that Capon and Parsons conducted their experiments on Ir before the thick oxide film described in Section II.B was formed.) Capon and Parsons could not explain what they considered the unique behavior of Ir.

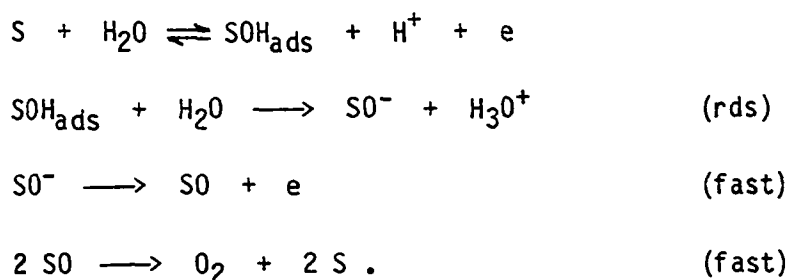
Buckley and Burke (318) have studied the evolution of $\text{O}_2(\text{g})$ on Ir in some detail. For potentials less than 1.75 V vs. RHE, the current density for the oxygen evolution reaction decayed as a function of time. In an

acidic solution, there was essentially no decrease in the current density for the $O_2(g)$ evolution reaction with time for potentials greater than 1.75 V. In basic solutions, however, the decay rate of the current density at potentials greater than 1.75 V was very similar to that of Pt. Data obtained in an acidic solution gave a Tafel plot with breaks at 1.57 V and 1.78 V. Buckley and Burke attribute these breaks to changes in the mechanism. They assume that adsorbed hydroxyl radicals produced by the reaction



are central to the $O_2(g)$ evolution reaction. The thermodynamic basis for this assumption was given by Hickling and Hill (319). At low overpotentials, the rate of $O_2(g)$ evolution is determined by the reaction of the adsorbed hydroxyl radicals with other surface species, such as chemisorbed oxygen atoms. At intermediate overpotentials, the overall rate is limited by the formation of adsorbed hydroxyl radicals according to the reaction given above. The decrease in the oxygen evolution current with time for potentials less than 1.75 V is attributed to a slow transformation of the surface oxide that either decreases the rate of formation of hydroxyl radicals or lowers electron mobility within the oxide film. At high overpotentials, Buckley and Burke (318) speculate that a higher oxidation state of iridium is produced in the outer region of the oxide film. This higher oxidation state reacts with water to form an unstable oxide, which in turn decomposes to give $O_2(g)$ and the lower oxidation state. Oxygen evolution in a basic solution occurs via a hydroxyl radical for all potentials.

Gottesfeld and Srinivasan (219) have also studied the oxygen evolution reaction (OER) on Ir. Based on combined ellipsometric and reflectometric measurements, Gottesfeld and Srinivasan conclude that the phase oxide on Ir in the OER region has a high level of bulk defects leading to a high surface concentration of active sites. These active sites S are involved in the OER thusly:



Evidently, the affinity of the Ir active sites for the adsorbed hydroxyl radicals is great enough to shift the rate-determining step to the second step of the sequence; this results in lowering the Tafel slope from $2.3 RT/\beta F$ to $2.3 RT/F$, which is typical of the better oxygen evolution electrocatalysts. The higher affinity of the active sites is correlated with an increase in the oxidation state of oxide. In summary, Gottesfeld and Srinivasan (219) describe $O_2(g)$ evolution as a process in which a metal ion in the oxide is increased to a higher oxidation state when the potential is raised to a value in the OER range. An electrosorbed hydroxyl radical is then formed, which further reacts by the sequence given above. The loss of electrode activity is ascribed to a stabilization of the higher oxide state with time.

A group of Spanish workers has recently begun to study the oxidation of simple organic molecules on Ir. Sanchez Cruz and Fernandez Otero (320) oxidized HCOOH on Ir in 1 N HClO₄. Potentiodynamic experiments gave a peak at 0.4 V vs. SCE, but at potentials greater than 0.9 V, they report that HCOOH oxidation occurs on an oxide covering and that a much larger anodic current is produced. At low scan rates, the oxide film is chemically reduced by HCOOH. Ureta Zanartu, Fernandez Otero, and Sanchez Cruz (321) compared the anodic oxidation of CH₃OH on Ir and Rh. Cyclic voltammetry gives anodic peaks that have peak potentials that coincide with the potential for surface oxidation.

III. EXPERIMENTAL

A. Electrodes and Rotators

Several electrodes manufactured by Pine Instrument Co., Grove City, PA, were utilized. These included: a Pt RDE Model DD20 (0.455 cm^2); a Au RDE Model DD20 (0.446 cm^2); a Pt-Pt RRDE Model DT6 (disc area 0.459 cm^2 , $\beta^{2/3} = 0.368$, $N = 0.178$); a Pd RDE Model DD15 (0.447 cm^2); a Pt RDE Model AFMD 18 (0.166 cm^2); and a Au RDE Model AFMD 18 (0.162 cm^2). An Ir RDE was fabricated in the chemistry shop at Iowa State University and had a geometric area of 0.496 cm^2 . The electrodes were polished using standard metallographic techniques to a $1 \mu\text{m}$ finish.

The electrode rotators were also manufactured by Pine Instrument Co. The rotator used with the Model DD20, DT6, and DD15 electrodes was the Model ASR2. This rotator had continuous speed control from 200 RPM to 10,000 RPM with better than 1% accuracy. The wobble at the end of the electrode was less than $\pm 0.005 \text{ cm}$. The rotator used with the AFMD electrodes and the IR electrode was the prototype of the Pine Instrument Co. Model MSR rotator. The speed could be set with 1% accuracy from 100 RPM to 10,000 RPM. The MSR rotator had a high-torque motor and was designed to accelerate and decelerate rapidly. For example, the rotator with electrode was determined to accelerate from 1000 RPM to 4000 RPM in 22 msec. The MSR controller had input jacks that permitted the application of any desired rotation-speed program as an analog voltage signal.

B. Potentiostats

The potential of the working electrode was controlled using either a Model RDE3 potentiostat (Pine Instrument) or a Model 173 potentiostat (Princeton Applied Research, Princeton, NJ) with a Model 176 current-to-voltage convertor. Both potentiostats could be operated as three-electrode potentiostats; in addition, the RDE3 could be operated as a four-electrode potentiostat for use in rotating ring-disc studies. Both potentiostats had input jacks which allowed the application of an external voltage program to the working electrode(s). Several useful programs were applied using a Model 175 Universal Programmer (Princeton Applied Research), which was operated in either a pulse or sweep mode and was continuously adjustable over seven orders of magnitude in each mode. The reference electrode was a saturated calomel mini-electrode (Corning Scientific Instruments, Corning, NY) and all potentials are reported versus this electrode.

C. Triple-Pulse Amperometry Apparatus

In the single experiment performed to establish the applicability of triple-pulse amperometry to the quantitative determination of As(III), the experimental apparatus used was that described in detail by Hughes (322).

D. Lock-In Amplifiers

Two commercial lock-in amplifiers were used in the sinusoidal hydrodynamic modulation voltammetry. An Ortholoc 9502 (Ortec, Inc.,

Oak Ridge, TN), with a lower frequency limit of 0.5 Hz was used in some experiments. This lock-in required an external oscillator. Other experiments utilized an Ithaco Model 391A (Ithaco Inc., Ithaca, NY). This lock-in had plug-in circuit boards that determined the frequency range of the instrument as well as the frequency of an internal oscillator. The cards used were for 0.1 to 11 Hz. An interface between the potentiostat and the lock-in amplifiers was not required.

E. Chemicals

All of the chemicals used were reagent grade or better. Specifically, As(III) solutions were made from primary standard As_2O_3 (Baker Chemical Co.). The water used to make all solutions was triply-distilled, with demineralization occurring after the first distillation, the second demineralization from alkaline permanganate (0.1 M KMnO_4 /0.1 M KOH), and the final distillation from approximately 1 M H_2SO_4 . Dissolved oxygen was removed from solution by dispersion with nitrogen that had passed over a heated bed of copper turnings.

F. Miscellaneous

Current-potential and current-time behavior was recorded using an Omnigraphic Series 100 x-y recorder (Houston Instrument, Austin, TX) with the time-base option. Potentials were measured with a Model 3466A digital multimeter (Hewlett-Packard Corp., Loveland, CO). A Model 122A oscilloscope (Hewlett-Packard) was used to monitor the 3 Hz ac signal and to set $\Delta\omega$ in the hydrodynamic modulation experiments.

IV. THEORY OF MIXED KINETICS OF ELECTROCHEMICAL
REACTIONS AT ROTATING DISC ELECTRODES

A. Introduction

If the rate of the charge transfer step and all associated chemical reactions are fast relative to the rate of mass transport, the equation that describes the current-potential response is relatively simple. The overall rate of the reaction v can be obtained by combining the definition of current with Faraday's Law:

$$i \text{ (amps)} = dQ/dt \text{ (coulombs/sec)} \quad \text{IV-1}$$

$$\frac{Q}{nF} \frac{\text{coulombs}}{\text{equiv} \cdot \text{mole}} = N \text{ (number of moles electrolyzed)} \quad \text{IV-2}$$

$$v(\text{moles/sec}) = \frac{dN}{dt} = \frac{i}{nF} \quad \text{IV-3}$$

In his diffusion layer treatment (323), Nernst assumed that there existed a stagnant layer of fluid of thickness δ where mass transfer occurs only by diffusion. Nernst also assumed that convective mass transport maintains the concentration of the electroactive specie just outside the diffusion layer at C^* , the bulk concentration value. The flux J at the electrode surface is simply

$$-J_{(x=0)}(\text{moles sec}^{-1} \text{ cm}^{-2}) = D \frac{\delta C}{\delta x} \quad x=0 \quad \text{IV-4}$$

where x represents the distance from the electrode ($x=0$ at the electrode surface) and D is the diffusion coefficient of the electroactive specie.

The concentration gradient is simply

$$\frac{\delta C}{\delta x} \Big|_{x=0} = \frac{C^* - C_S}{\delta} . \quad \text{IV-5}$$

Since the overall rate is assumed to be limited by the mass transport, the flux and the rate/unit area can be equated.

$$\frac{i}{nFA} = \frac{D(C^* - C_S)}{\delta} \quad \text{IV-6}$$

$$i = \frac{nFAD(C^* - C_S)}{\delta} \quad \text{IV-7}$$

A limiting current i_L is attained when the applied potential is such that $C_{(x=0)}$ becomes 0.

While Eq. IV-7 is extremely useful, the derivation was semiempirical. In the case of the rotating disc electrode (RDE), the hydrodynamic and convective-diffusion equations can be solved rigorously for steady-state, nonturbulent flow. The mathematical solution was first given by Levich (324) in the equation that bears his name

$$i_L = 0.620 nFAD^{2/3} \nu^{-1/6} \omega^{1/2} (C^* - C_{(x=0)}) . \quad \text{IV-8}$$

In Eq. IV-8, ω represents the angular velocity of the disc in radians/sec and ν is the kinematic viscosity in cm^2/sec . Riddiford (325) and Newman (326) have rederived the Levich equation and corrected some slight errors made by Levich. The Riddiford correction will be utilized in this work when more accurate values are required and is given by

$$i_L = \left| \frac{0.554}{0.8934 + 0.316 (D/\nu)^{0.36}} \right| nFAD^{2/3} \nu^{-1/6} \omega^{1/2} (C^* - C_S) . \quad \text{IV-9}$$

In many cases, however, the rate of the charge transfer step or any one of the associated chemical steps may not be fast relative to the rate of mass transport. In the most extreme case, the reaction is said to be "kinetically controlled". Under these circumstances, the surface concentration is approximately the bulk concentration, and the overall rate of electrochemical conversion is equal to kC^* , where k is a generalized rate constant for the slowest elementary step within the reaction mechanism. Using Eq. IV-3, one obtains

$$\frac{i}{nFA} = kC^* \quad \text{IV-10}$$

and

$$i = nFAkC^*. \quad \text{IV-11}$$

The two cases just described obviously represent the extremes of a continuous series of possible electrode processes. If the rate of the diffusional (mass transport) and kinetic steps are of comparable magnitude, the overall reaction proceeds under "mixed control" (327). The general result of mixed control of the electrode reaction is that the current is less than that predicted by the Levich equation and is not a linear function of $\omega^{1/2}$. Some of the various types of electrode processes which operate under mixed control and the physical interpretation of the associated rate constants will now be presented.

B. Heterogeneous Rate Constant of a Charge Transfer Step

The derivation of the Levich equation assumed that the rate of all steps in the overall mechanism were fast relative to the rate of mass

transport. Consider an electrode process where the rate determining step is a heterogeneous, irreversible, charge transfer reaction such as



where $k = k_0 \exp[-\alpha n_a FE/RT]$, k_0 is the rate constant at $E=E^\circ$, α is the transfer coefficient of the rate determining step and n_a is the number of electrons transferred in the rate determining step. Equation IV-12 is one of the results of the Butler-Volmer formulation of electrode kinetics (328). At steady state, the flux of material electrolyzed at the electrode surface is equal to the flux of material passing through the diffusion layer. Therefore,

$$j = kC_{Ox}(x=0) = D_{Ox} \frac{\delta C_{Ox}}{\delta x} \Big|_{x=0} = \frac{D_{Ox}(C_{Ox}^* - C_S)}{\delta} \quad IV-13$$

Solving Eq. IV-13 for $C_{Ox}(x=0)$ gives

$$C_{Ox}(x=0) = \frac{C_{Ox}^*}{1 + k\delta/D_{Ox}} \quad IV-14$$

Substituting Eq. IV-14 back into either of the equations for the steady state flux and inverting gives

$$j^{-1} = (kC_{Ox})^{-1} + (D_{Ox}C_{Ox}/\delta)^{-1} \quad IV-15$$

Note that the term D_{Ox}/δ has the same units (cm/sec) as the heterogeneous rate constant, and following Albery (329) will be given the symbol k_δ to represent a "heterogeneous rate constant describing mass transport." The equation for steady state flux, therefore, becomes

$$j^{-1} = (kC_{\text{Ox}})^{-1} + (k_D^* C_{\text{Ox}}^*)^{-1} \quad \text{IV-16}$$

This equation is consistent with the previous results obtained for either mass transport or kinetically limited processes. If k and k_D^* are commensurate, the resulting current is determined by both rate constants. For the RDE,

$$i^{-1} = (nFAk C_{\text{Ox}})^{-1} + (0.62 n FA D_{\text{Ox}}^{2/3} \nu^{-1/6} \omega^{1/2} C_{\text{Ox}}^*)^{-1} . \quad \text{IV-17}$$

An analogous derivation can be performed for the case of a heterogeneous, quasi-reversible charge transfer reaction (329)



If we assume that $D_{\text{Ox}} = D_{\text{Red}}$ and define $j_{\text{Ox}} = -k_D^* C_{\text{Red}}^*$ we obtain

$$j = \frac{j_{\text{Ox}} k_f - j_{\text{Red}} k_b}{k_D^* + k_f + k_b} \quad \text{IV-19}$$

This result can be simplified for the case where $\alpha = 1/2$ and $n_a = 1$ to

$$j = \frac{j_{\text{Ox}} \exp(-\theta) - j_{\text{Red}} \exp(\theta)}{k_D^*/k_S + \exp(-\theta) + \exp(\theta)} \quad \text{IV-20}$$

where k_S is the standard heterogeneous rate constant (328) and

$$\theta = \frac{F(E-E^0)}{2RT} . \quad \text{IV-21}$$

At large positive values of θ , $j \rightarrow -j_{\text{Red}}$ and at large negative values of θ , $j \rightarrow j_{\text{Ox}}$.

C. Heterogeneous Rate Constant of a Step
not Involving Charge Transfer

If the rate-determining step is a heterogeneous reaction that does not involve a charge transfer, the kinetic current for the electrode process at a RDE is analogous in many respects to the results obtained in the previous case, this being

$$i^{-1} = (nFAk_C^*C_{ox}^*)^{-1} + (0.62 nFAD_{ox}^{2/3} \nu^{-1/6} \omega^{1/2} C_{ox}^*)^{-1}. \quad IV-22$$

Here the heterogeneous rate constant k_C^* is not a direct function of the electrode potential; this does not mean that the rate constant is potential independent. For example, if the rate-determining step involves an adsorbed reactant and the adsorption isotherm is potential dependent, then the observed rate constant would also be potential dependent. The reaction rate would also be potential dependent if there is a potential-dependent adsorption of a nonelectroactive specie which simply acts to reduce the number of active sites. Therefore, while the value of k_C^* will not be an exponential function of electrode potential, it may nevertheless be potential dependent, and the exact relationship between k_C^* and E may be difficult to establish.

D. Homogeneous Rate Constant for a Preceding
First-Order Reaction

The case where the electrode reaction is preceded by a homogeneous first-order reaction is now considered. The elementary steps of interest

are summarized by



This type of electrode process is sometimes referred to as a chemical-electrochemical process, or CE. The convective-diffusion equations were first solved by Koutecky and Levich (330,331), who made the following assumptions: substance A is electroinactive; the charge-transfer reaction is very fast; and the electrode potential is sufficiently negative such that the surface concentration of Ox is zero. Koutecky and Levich also defined the familiar equilibrium constant K as

$$K = k_1/k_2 = C_{\text{Ox}}/C_A \quad \text{IV-24}$$

and the total analytical bulk concentration C° as

$$C^\circ = C_{\text{Ox}} + C_A \quad \text{IV-25}$$

The solution of the appropriate differential equations (328) is

$$i = \frac{nFAD_{\text{Ox}}C^\circ}{\delta + \frac{1}{K} \frac{D_{\text{Ox}}}{\ell}} \quad \text{IV-26}$$

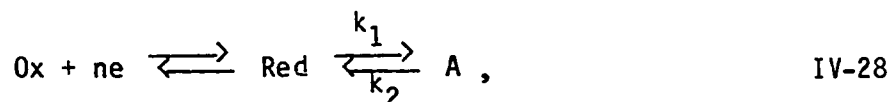
where $\ell = k_1 + k_2$. The parameter $(D_{\text{Ox}}/\ell)^{1/2}$ has the dimensions of cm for a first order reaction and may be thought of as the thickness of a "reaction layer". This thickness (usually designated by μ) represents the distance that the Ox specie can travel (by diffusion) to the electrode surface before decomposing to A. It should be noted that the concept of a

reaction layer is valid only for the case where K is small but $(D/\delta)^{1/2}$ is large (328). A "zone diagram" is often used to describe the electrochemical behavior of a CE reaction as a function of K and a dimensionless kinetic parameter (332). For a RDE, Eq. IV-26 is transformed into

$$i^{-1} = (nFAD_{\text{ox}}^{1/2}K(k_1 + k_2)^{1/2}C^0)^{-1} + (0.62 nFAD_{\text{ox}}^{2/3}v^{-1/6}\omega^{1/2}C^0)^{-1} \quad \text{IV-27}$$

E. Homogeneous Rate Constant of a Following First-Order Reaction

In the case of a following first-order homogeneous reaction



the magnitude of the limiting current is not a function of the homogeneous rate constants. However, there are now two means by which Red is removed from the vicinity of the electrode: by diffusion and by decomposition to give A. This results in a shift in the half-wave potential given by (333)

$$E_{1/2} = E^0 + \frac{RT}{nF} \ln(\delta/\mu) \coth(\delta/\mu) \quad \text{IV-29}$$

For large values of δ/μ , $\coth(\delta/\mu) \longrightarrow 1$ and Eq. IV-29 reduces to

$$E_{1/2} = E^0 + \frac{RT}{nF} \ln(1.61 D^{-1/6} v^{1/6}) + \frac{RT}{2nF} \ln\left(\frac{k_1+k_2}{\omega}\right) \quad \text{IV-30}$$

The $E_{1/2}$ is shifted toward more positive potentials by the following reaction, but an increase in the rotation speed causes a negative shift in the $E_{1/2}$ (i.e., toward the value of the $E_{1/2}$ observed if $k_1 = 0$).

E. Macroscopically Nonhomogeneous Surface

Implicit in the derivation of the Levich equation is the assumption that the disc surface is uniformly active. Accordingly, the disc is said to be "uniformly accessible", which means that the diffusional flux is equal at all points on the disc surface. While the simplest example of nonuniform disc, i.e., an "active ring" situated symmetrically about the disc, can be treated on a strictly theoretical basis (327), more physically significant cases of nonuniform discs must be modeled.

The most widely used model of a nonuniform disc was developed by Landsberg's group, as cited by References 334-340. The Landsberg model is consistent with that proposed earlier by Nagy et al. (341), but the Nagy model was based on an empirical formula derived from data obtained from an analog apparatus. In the Landsberg model, the mass transport to a single active site takes place in a "diffusion volume", illustrated in Figure IV-1.

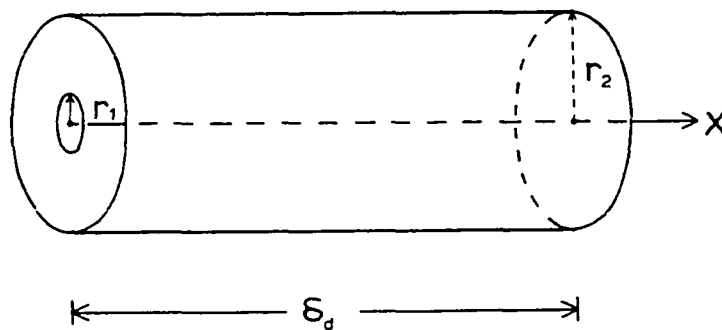


Figure IV-1. Diffusion volume of Landsberg model of a nonhomogeneous surface

The active sites on the disc surface have a radius of r_1 and are distributed on the surface with an average distance between centers of $2r_2$. Diffusion from $x = \delta_d$ to $x = 0$ is then analogous to the problem of the electrical resistance in a cylindrical conductor with a source and sink of different areas, a problem that was previously solved by Smythe (342). The result for the Landsberg model is given by

$$i^{-1} = (0.62 \text{ nFAD}^{2/3} \nu^{-1/6} \omega^{1/2} C^*)^{-1} + \left| \sum_n A_n \tanh(k_n \delta_d / r_2) \right| (\text{nFADC}^*)^{-1}, \text{IV-31}$$

where

$$A_n = -(k_n^2 r_2 J_0^2(k_n r_2))^{-1} \left| \frac{r_2}{r_1} - \left(\frac{r_1}{r_2}\right)^{2.5} \left| \sin(k_n r_1) + 2\left(\frac{r_1}{r_2}\right)^{2.5} J_1(k_n r_1) \right| \right|$$

In the expression for A_n , J_0 is the Bessel function of the first-kind order 0 and J_1 is the Bessel function of the first-kind order 1. The values of k_n are given by

$$k_n = j_{1,n} / r_2 \quad \text{II-32}$$

where $j_{1,n}$ is the n th positive zero of the J_1 Bessel function. According to Landsberg and Thiele (334), there are two limiting cases. For low rotation speeds $r_2 \ll \delta_d$, therefore, $\tanh(k_n \delta_d / r_2) \longrightarrow 1$ and Eq. IV-31 reduces to

$$i^{-1} = (0.62 \text{ nFAD}^{2/3} \nu^{-1/6} C^* \omega^{1/2})^{-1} + \left| \sum_n A_n \right| (\text{nFADC}^*)^{-1}. \quad \text{IV-33}$$

For high rotation speeds where $r_2 \gg \delta_d$, $\tanh(k_n \delta_d / r_2) \longrightarrow k_n \delta_d / r_2$ and Eq. IV-31 becomes

$$i^{-1} = (0.62 \text{ nFAD}^{2/3} \nu^{-1/6} C^* \omega^{1/2})^{-1} + \left| \sum_n A_n \frac{(x_n \delta_d)}{r_2} \right| (\text{nFADC}^*)^{-1}. \quad \text{IV-34}$$

Note that both terms on the right side of Eq. IV-34 are proportional to $\omega^{-1/2}$ while only the first term on the right side of Eq. IV-33 is proportional to $\omega^{-1/2}$. A plot of i^{-1} vs. $\omega^{-1/2}$ gives a straight line with a nonzero intercept for Eq. IV-33, while a i^{-1} vs. $\omega^{-1/2}$ plot of Eq. IV-34 gives a straight line with a different slope and with a zero intercept.

Although there have been several experimental verifications of the Landsberg model, it has been pointed out that the model is invalid for high angular velocities (327). This is principally because the distance traveled by an electroactive specie to an active site varies from point to point under these circumstances and therefore the concept of a diffusion volume is not reasonable.

A group of French workers have recently developed a theoretical treatment for the attenuation of the diffusion current density and the diffusion admittance at a partially-blocked RDE (343,344). The theoretical results have been experimentally verified (345).

G. Summary

Equations IV-17, IV-22, IV-27, and IV-33 all have the form

$$i^{-1} = B\omega^{-1/2} + Z \quad \text{IV-35}$$

In all cases, B is equal to $(0.62 nFAD^{2/3}v^{-1/6}C^*)^{-1}$ and Z is a proportional to $(nFAk_gC^*)^{-1}$, where k_g is a generalized rate constant or combination of rate constants. The only difference in the results for four different types of electrode processes is that Z is also proportional to $D^{-1/2}$ for the case of a preceding homogeneous first order reaction and

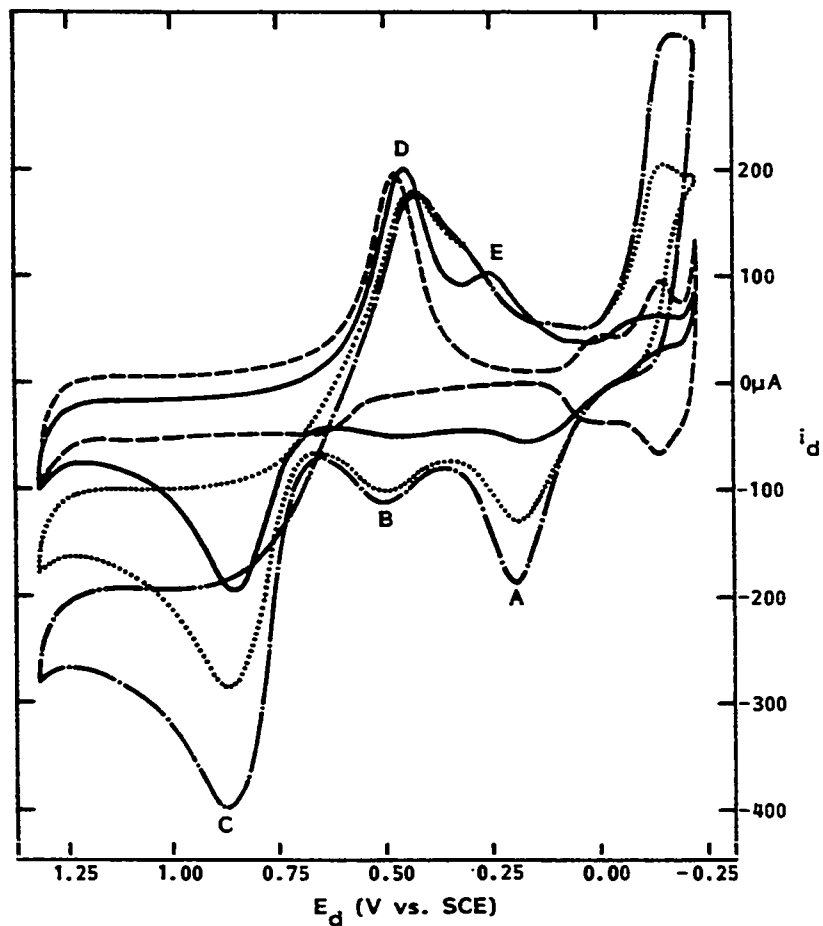
is proportional to D^{-1} for a nonhomogeneous surface. The singular observation that the experimental correspondence of i^{-1} and $\omega^{-1/2}$ is empirically fitted by an equation of the form of Eq. IV-35 cannot be taken as proof of any single type of mixed control.

V. POTENTIODYNAMIC AND RING-DISC STUDIES OF AS(III,V)

A. As(III) Electrochemistry on a Pt RDE in Acidic Media

1. The effects of changing the As(III) bulk concentration

Cyclic voltammograms at a Pt RDE as a function of As(III) concentration are shown in Figure V-1. A Pt residual curve is included as a reference. In the absence of As(III), Pt oxide begins to form at $E_d > 0.55$ V; this oxide is reduced on the negative scan (peak D) with $E_p = 0.48$ V. Faradaic formation and dissolution of adsorbed atomic hydrogen and the evolution of $H_2(g)$ occurs at $E < 0.1$ V. In the presence of As(III), an anodic peak C ($E_p = 0.87$ V) is obtained. The peak current is dependent on the As(III) bulk concentration. As the potential is scanned positive to 0.87 V, the current decreases until O_2 evolution begins (ca. 1.3 V). On scan reversal, the anodic current rapidly decreases to a value which is virtually independent of potential for 1.1 V $> E > 0.9$ V. This current is a linear function of As(III) bulk concentration at low concentrations, but deviations occur at higher concentrations. The anodic current decreases with potential for $E_d < 0.9$ V; the total current then becomes cathodic as the predominant process becomes Pt oxide reduction.. At low As(III) bulk concentrations, two reduction peaks (D and E) are observed in the potential range 0.1 V $< E_d < 0.6$ V. The reduction peak (D) at 0.47 V is again the result of Pt oxide reduction. Peak E is due to a chemisorption of As(III) involving a partial charge transfer; this will be discussed in more detail later in this dissertation. At higher bulk concentrations,



Conditions: 1000 rpm
 6.0 V min^{-1}
 0.5 M HClO_4

- Pt residual
- [As(III)] = $4.01 \times 10^{-5} \text{ M}$
- ... [As(III)] = $1.97 \times 10^{-4} \text{ M}$
- .- [As(III)] = $3.84 \times 10^{-4} \text{ M}$

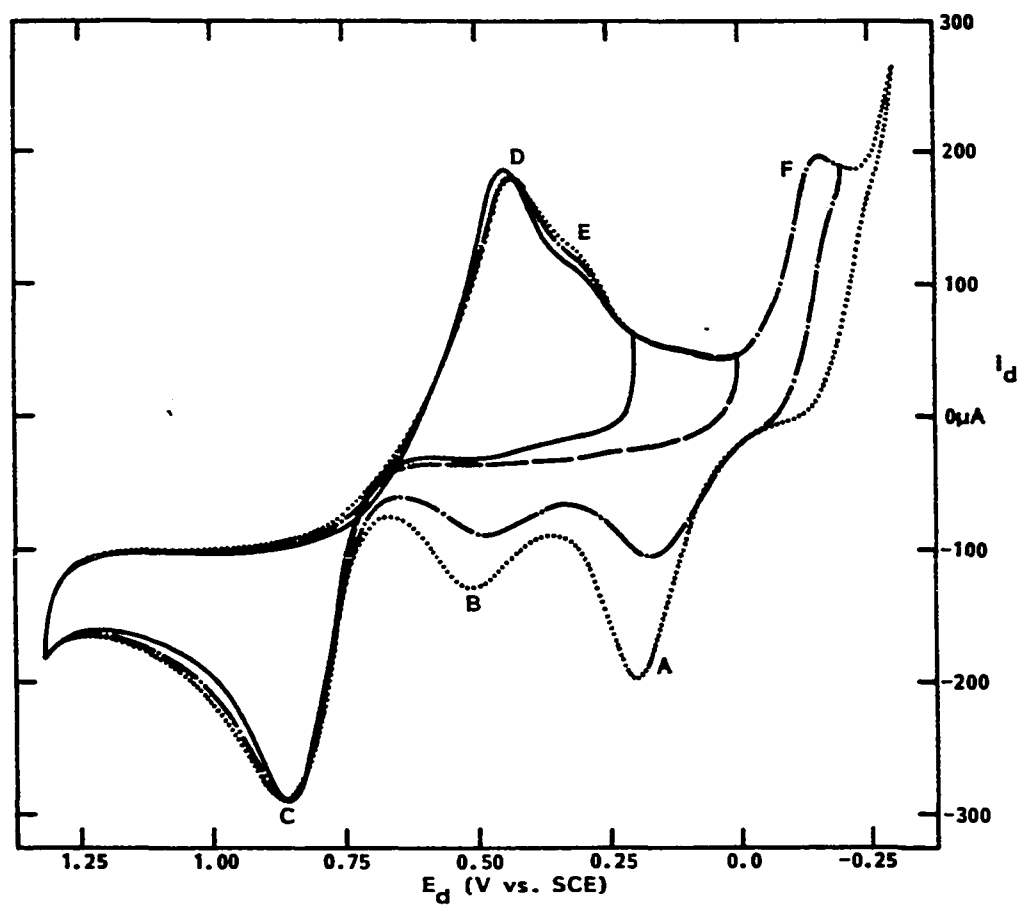
Figure V-1. Cyclic voltammograms at a Pt RDE in acidic solution as a function of [As(III)]

these peaks are not resolved. The cathodic current obtained at $E < 0.0$ V on the negative potential scan and the anodic peaks A and B at approximately 0.2 V and 0.5 V on the positive potential scan are due to the deposition and stripping of elemental arsenic, respectively.

2. The effects of changing the negative scan limit

Arsenic deposition and stripping can be more clearly observed by varying the negative scan limit, E_c , as illustrated by Figure V-2. At $E_c < 0.0$ V (Region F), a large cathodic current resulting from the electro-deposition of As(III) is obtained. This deposit is anodically stripped in the peaks A and B. If the potential is held constant at a potential where deposition of arsenic from the bulk of the solution occurs, peak A increases dramatically as the deposition time increases, while peak B increases relatively little. The stripping peak at 0.2 V is therefore due to the stripping of As in the outer As layers (i.e., As stripped from an As substrate), while the peak at 0.5 V is due to the stripping of the As in the first 1-2 monolayers. The observation of one and two stripping peaks has been reported in the determination of arsenic by anodic stripping voltammetry (19,21).

The very sharp increase in the cathodic current at $E < -0.22$ V is due to $H_2(g)$ evolution on Pt atoms not covered by arsenic atoms. It is known that the presence of As on some Pt sites does not alter the kinetics of the hydrogen evolution reaction on the remaining Pt sites, as opposed to many other irreversibly adsorbed or deposited species (346).



Conditions: 1000 rpm
 6.0 V min^{-1}
 $0.5 \text{ M HClO}_4 + 0.197 \text{ mM As(III)}$
 — 0.2 V
 --- 0.0 V
 - - - -0.2 V
 ... -0.3 V

Figure V-2. Cyclic voltammograms of As(III) at a Pt RDE in acidic solution as a function of E_c

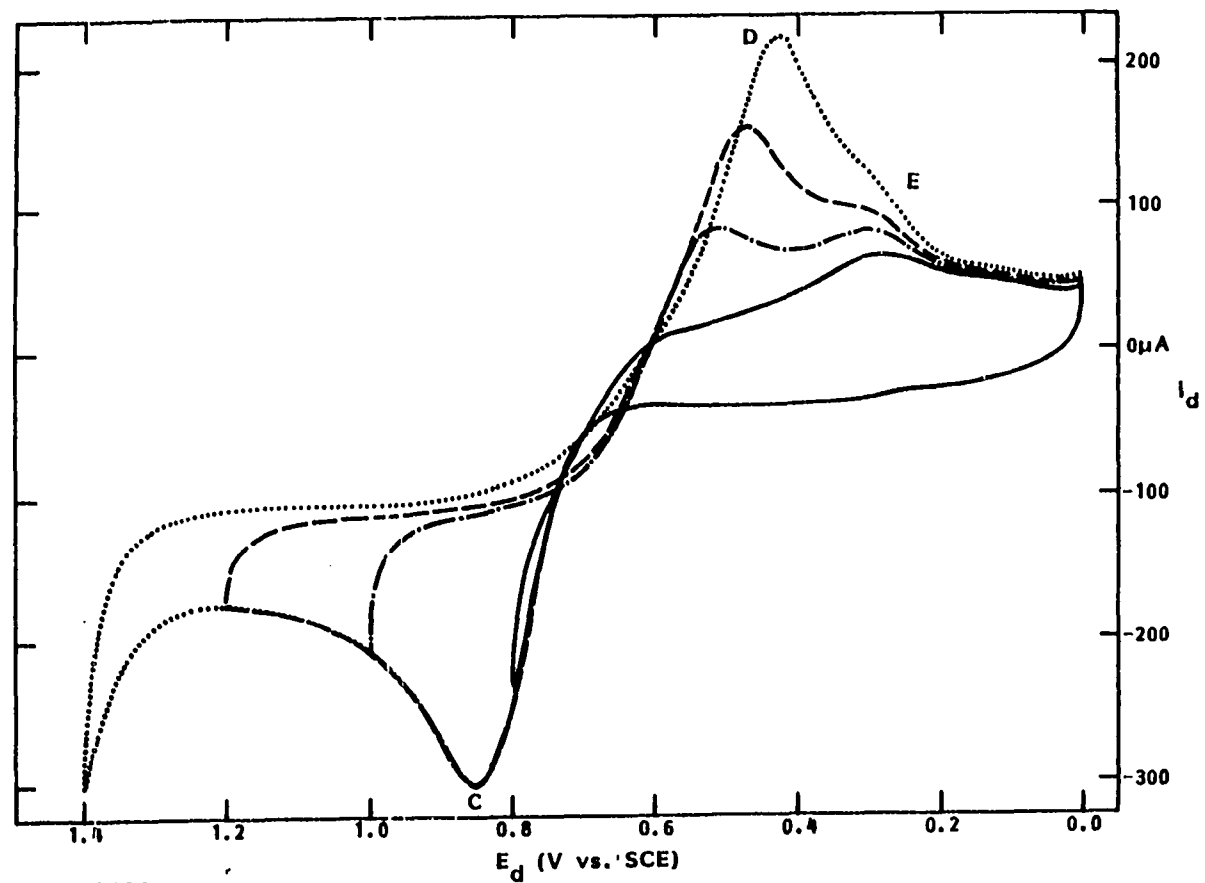
The current-potential behavior in the potential region of peak C is relatively unchanged by changes in E_c . Following deposition of very large As deposits, the anodic current on the positive scan is somewhat larger and the anodic current on the negative scan is somewhat smaller, relative to the same currents observed after deposition of small quantities of As. These effects are due to an increased amount of chemisorbed (As(III)) that is present following heavy As deposition.

3. The effects of changing the positive scan limit

Current-potential curves obtained as a function of the positive potential scan limit are shown in Figure V-3. With an E_a of 0.8 V, only a small amount of Pt oxide is formed and the chemisorption of As(III) is clearly in region E. As E_a is made more positive, the corresponding Pt oxide peak on the negative scan becomes larger and shifts to more negative potentials. These two effects cause the As(III) chemisorption peak (E) to be obscured by the Pt oxide reduction peak. More importantly, there is a continuous decrease in the anodic current on the negative scan as E_a is made more positive at this As(III) bulk concentration. At low As(III) bulk concentrations, the anodic current for As(III) is essentially independent of E_a . The As(III) faradaic current is clearly related to the quantity and nature of the Pt oxide present.

4. The effects of changing the electrode rotation speed

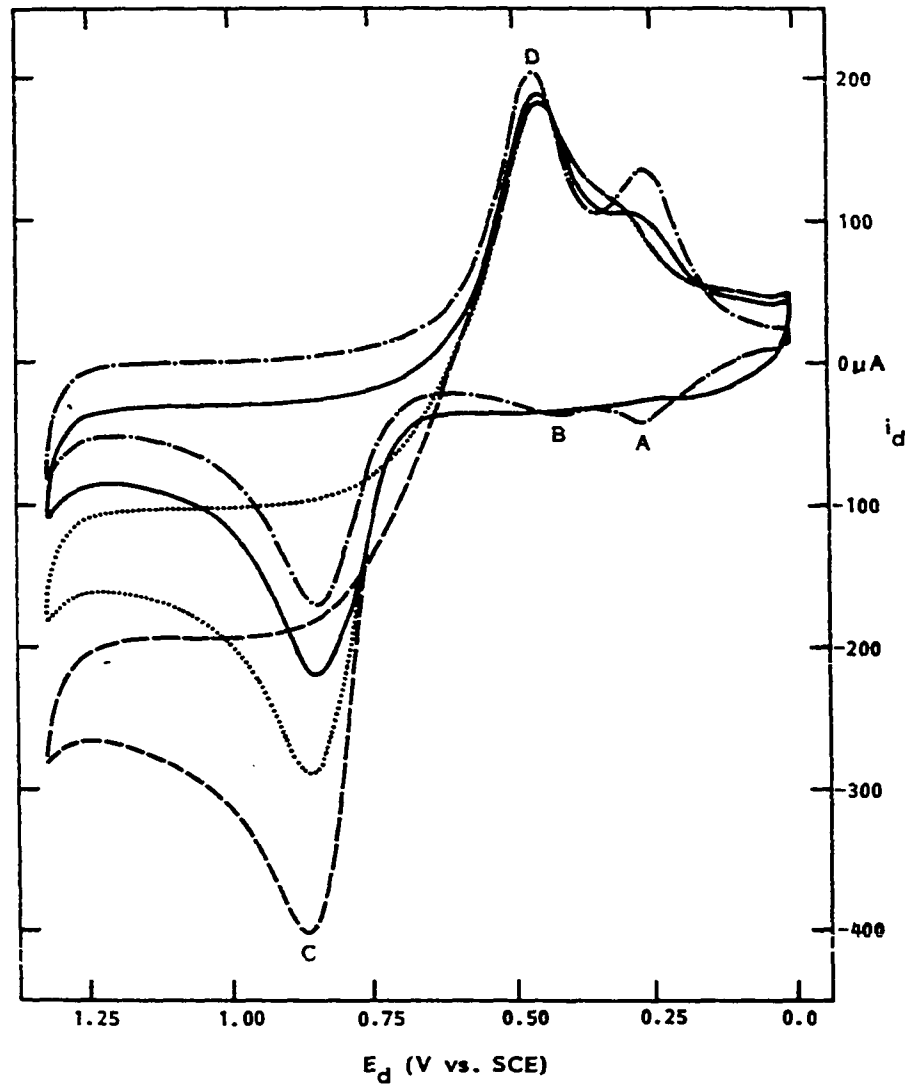
In Figure V-4, the effects of electrode rotation speed on an As(III) voltammogram are exhibited. As the rotation speed is increased, the anodic current for any $E_a > 0.7$ V is also increased. This illustrates



Conditions: 1000 rpm
 6.0 V min^{-1}
 $0.5 \text{ M HClO}_4 + 0.197 \text{ mM As(III)}$

— 0.8 V - - - 1.2 V
 - - - 1.0 V ··· 1.4 V

Figure V-3. Cyclic voltammograms of As(III) at a Pt RDE in acidic solution as a function of E_a



Conditions: 6.0 V min^{-1}
 $0.5 \text{ M HClO}_4 + 0.197 \text{ mM As(III)}$

- 0 rpm
- 100 rpm
- ... 1000 rpm
- 4000 rpm

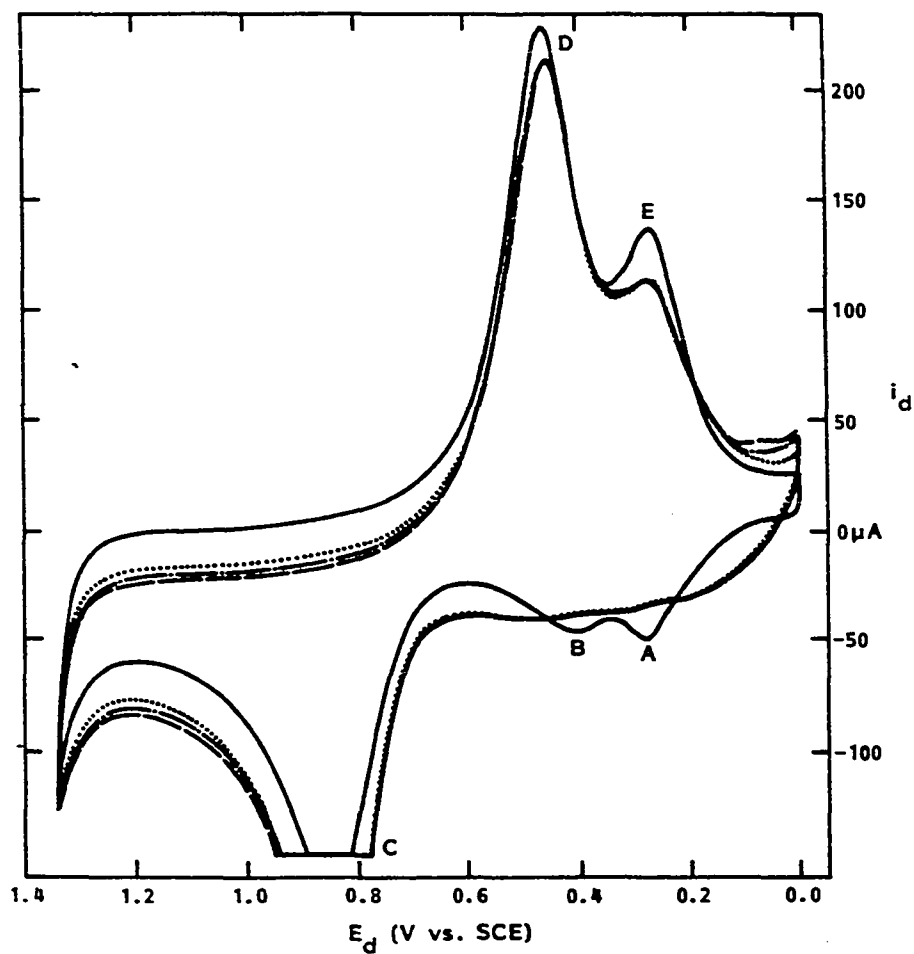
Figure V-4. Cyclic voltammograms of As(III) at a Pt RDE in acidic solution as a function of ω

that the anodic current on both the positive and negative scans is to some extent dependent on the rate of mass transfer to the electrode. If the current at a given potential (e.g., 1.0 V) on the plateau region for the negative scan is plotted versus $\omega^{1/2}$, a deviation from the theoretical Levich slope is observed at a rotation speed as low as 100 rpm. This is indicative of either a slow kinetic step or a macroscopically nonuniform surface, as described in Section IV.

At rotation speeds greater than about 500 rpm, the i - E curve for $E_d < 0.6$ V is unchanged by any further increase in rotation speed. However, at rotation speeds less than 500 rpm, this potential region exhibits some dramatic qualitative changes. These changes are shown in Figure V-5. for rotation speeds 0-100 rpm. This figure shows that the surface reactions contribute negligible currents on the negative scan and that the most dramatic increase in the size of peak E occurs when the electrode is completely stopped. There is also a significant change in the anodic current in the potential region $0.0 \text{ V} < E_d < 0.7 \text{ V}$: with rotation, the current gradually increases following scan reversal and reaches a somewhat constant value, while without rotation peaks A and B are observed to be very distinct. This behavior can be explained in terms of As(III) chemisorption and the upd of As(V), both of which will be covered in more detail.

5. The effects of changing the potential scan rate

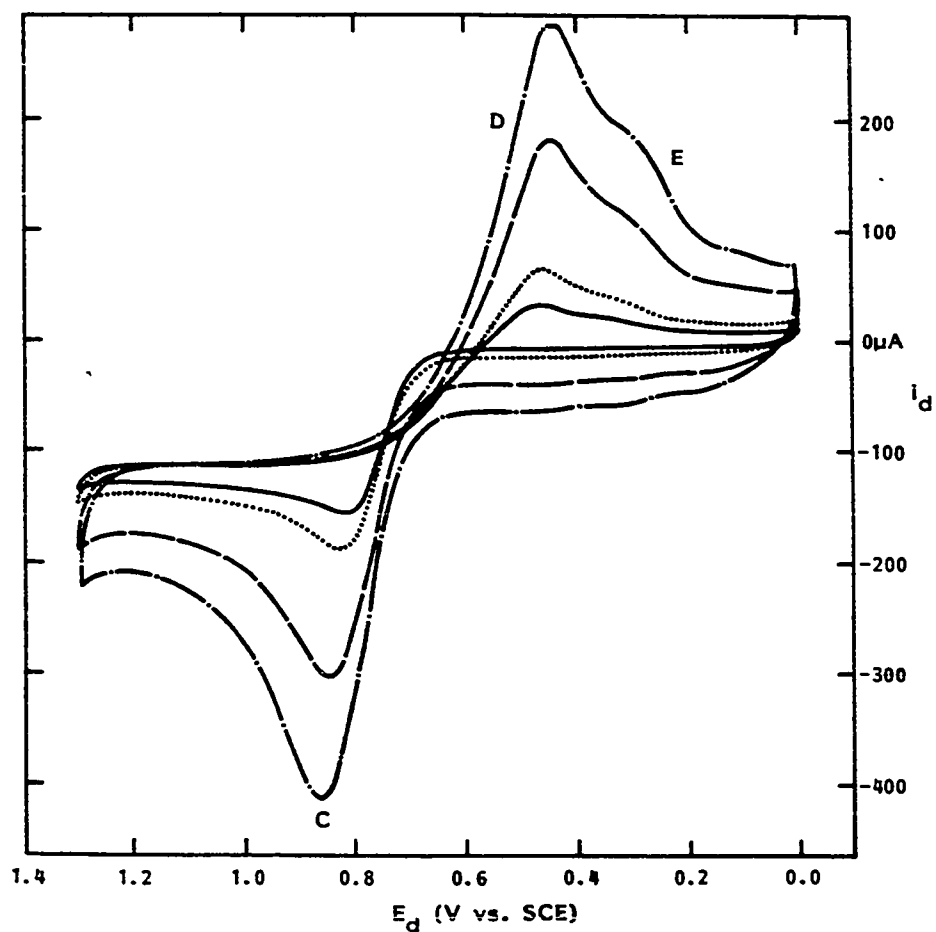
The effects of varying the potential scan rate are illustrated by Figure V-6. Anodic peak C and cathodic peaks D and E all show some scan



Conditions: 6.0 V min^{-1}
 $0.5 \text{ M HClO}_4 + 0.141 \text{ mM As(III)}$

— 0 rpm
 ... 60 rpm
 - - - 80 rpm
 - - - 100 rpm

Figure V-5. Cyclic voltammograms of As(III) at a Pt RDE in acidic solution at low ω



Conditions: 1000 rpm
 0.5 M HClO_4 + 0.198 mM As(III)

— 1.0 V min^{-1}
 ... 2.0 V min^{-1}
 --- 6.0 V min^{-1}
 -.- 10.0 V min^{-1}

Figure V-6. Cyclic voltammograms of As(III) at a Pt RDE in acidic solution as a function of scan rate

rate dependence since each is the result (partially or completely) of a surface process. The peak current for anodic peak C ($i_{p,C}$) is less dependent on scan rate than the peak currents of the cathodic processes ($i_{p,D}$ and $i_{p,E}$). For example, a factor of 10 increase in the scan rate causes $i_{p,D}$ to increase by a factor of 9.3, while $i_{p,C}$ increases by a factor of only 2.7. Angerstein-Kozłowska et al. have reported (57) that i_p for Pt oxide reduction is not linearly related to scan rate when the positive-going and negative-going sweep rates are simultaneously varied, as they were in this experiment. The much smaller increase in $i_{p,C}$ with scan rate reflects the fact that only a portion of the total current is due to a surface process. However, the anodic current obtained on the negative scan is essentially independent of scan rate; this is consistent with the earlier conclusion that faradaic reactions of the surface itself cease quickly after reversing the scan direction. The peak potentials of cathodic peaks D and E shift to more negative values as the scan rate is increased, while the anodic peak potential shifts to more positive potentials. This indicates that each peak represents an irreversible process. The source of the irreversibility of peaks C and D is undoubtedly due to the formation and reduction of Pt oxides on the electrode surface, as discussed in Section II. It is also known that adsorption of ions can increase the irreversibility of the initial stages of formation of noble-metal oxides (120). The magnitude of the anodic currents at $0.0 \text{ V} < E_d < 0.8 \text{ V}$ will be discussed later.

6. Summary

Several important conclusions can be drawn from potentiodynamic experiments performed at a Pt RDE in acidic solutions containing As(III). At sufficiently negative potentials, metallic As can be deposited on Pt from the +3 state. This deposited arsenic can be removed from the surface by anodic stripping. At sufficiently positive potentials, As(III) is oxidized at a Pt anode. The reversible reduction potential for the As(III)/As(V) couple is 0.32 V, so the reaction proceeds only at high overpotentials. Oxidation of As(III) from the bulk of the solution does not occur at a mass-transport limited rate, implying either a slow kinetic step or a macroscopically inhomogeneous surface. Initially, the anodic current in region C (see Figures V-1 through V-6) appears to be the sum of three electrochemical reactions: oxidation of the Pt surface, oxidation of adsorbed As(III), and oxidation of As(III) transported by convection from the bulk solution. (Essentially this same conclusion was drawn by Sutyagina et al. (43), except that their experiments were performed on a stationary Pt electrode and, therefore, did not have large contribution from As(III) transported by convection.) The contributions of the surface oxidation and adsorbed As(III) oxidation are highly dependent on the scan rate, scan direction, and electrode history. In addition, the current derived from the oxidation of As(III) that is transported to the electrode surface by convection is related to the quantity and nature of the Pt oxide present on the electrode surface. This is most clearly seen in the value of the anodic current on the

negative scan as a function of E_a . The surface reactions are irreversible.

B. As(III) Electrochemistry on a Pt Disc/Au Ring RRDE
in Acidic Media

1. Introduction

The rotating ring-disc electrode (RRDE) is recognized as an extremely valuable tool for the investigation of electrode reactions. Since As(V) is not electroactive unless the supporting electrolyte is 12 M HCl (13) or the As(V) is complexed with a compound such as pyrogallol (14), collection experiments (347) cannot be performed with detection of As(V) at the ring electrode. However, the RRDE has been utilized in a series of shielding and transient experiments (347) that have provided a great deal of significant information. In these experiments, the ring potential must be potentiostated at a potential where As(III) is oxidized. If the ring material is Pt, an experimental difficulty is encountered, namely the coincident growth and aging of the Pt oxide film. From Fig. V-3, it is clear that an increase in the quantity of Pt oxide on the anode surface causes a decrease in the As(III) faradaic current. Thus, potentiostating the ring electrode at a potential where As(III) is oxidized also leads to a decrease in the As(III) current with time, complicating the relationship between disc current, ring current, and electrode geometry. The ring current does become steady if the ring is potentiostated for 90 minutes or more; this would enable one to experimentally determine a factor to correct for the loss of ring activity. A more satisfactory approach is to

utilize the anodic oxidation of As(III) on a Au ring. Gold was deposited on the ring of a Pt-Pt RRDE using a current density of about 0.25 A dm^{-2} in an alkaline solution of gold cyanide. Even for very large deposition times, the potentiodynamic characteristics of the Au-plated Pt ring were not exactly those of a solid Au ring electrode. It is known that Au deposits from an alkaline cyanide solution are much more porous than deposits from other Au plating solutions (348); the differences in the potentiodynamic behaviors therefore are attributed to a very small amount of oxidation of the Pt substrate. The Au-plated ring nevertheless gave very acceptable results, and the following RRDE experiments were performed using this Pt disc/Au-plated ring electrode.

There are two important constants which relate the ring and disc currents at a RRDE. The first of these represents the ratio of the mass-transport limited ring current to the mass-transport limited disc current, the ring current measured when the disc current is zero. This ratio is given by

$$i_R/i_D \equiv \beta^{2/3} \equiv \left(\frac{r_3^3}{r_1^3} - \frac{r_2^3}{r_1^3} \right)^{2/3} \quad \text{V-1}$$

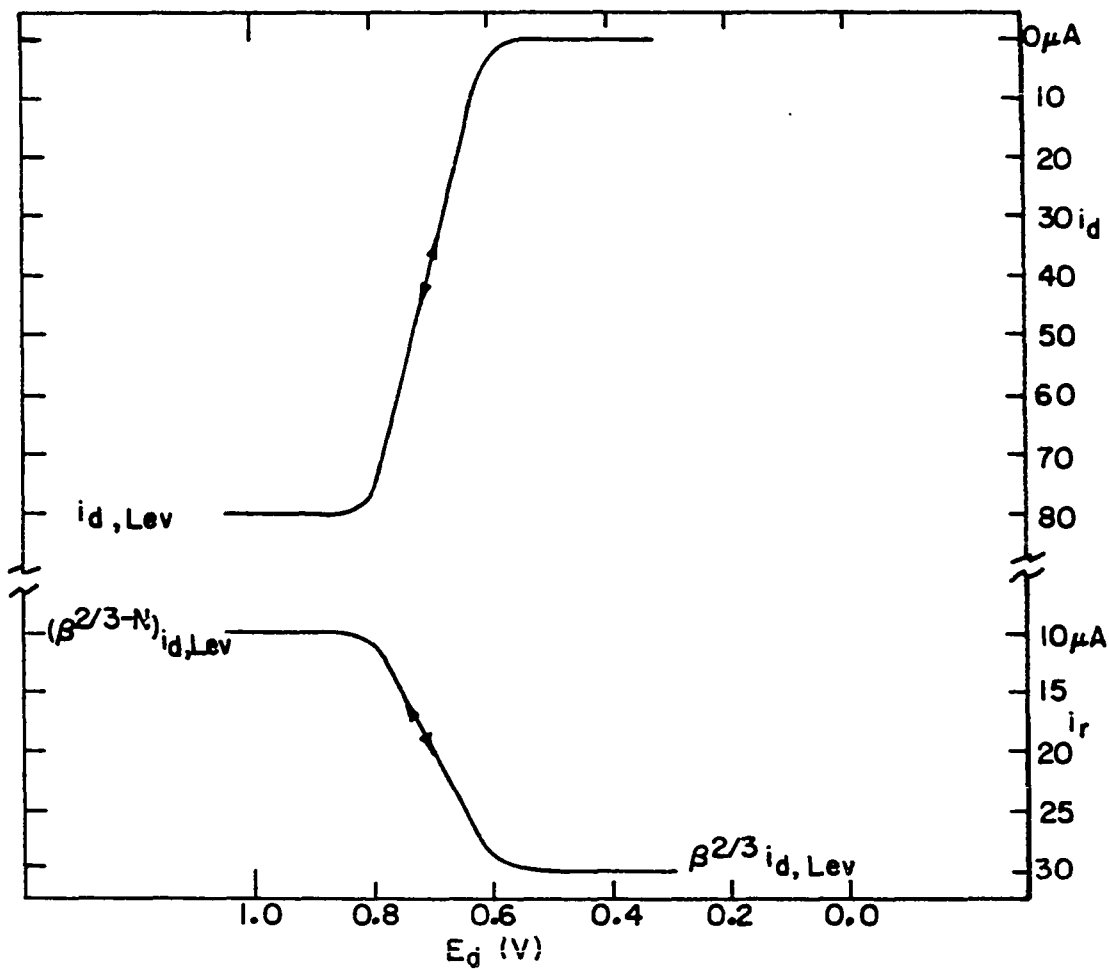
where r_1 , r_2 , and r_3 represent the disc radius, inner ring radius, and outer ring radius, respectively. The collection efficiency N also represents the ratio of ring current to disc current, but under a different set of conditions. Suppose that the disc is held at a potential where the reaction $\text{Ox} + ne \longrightarrow \text{Red}$ occurs producing a cathodic current i_d , and the ring potential is held at a potential such that the reaction $\text{Red} \longrightarrow \text{Ox} + ne$ occurs, producing an anodic ring current i_r . The ring

potential should be set positive enough to drive the surface concentration of R at the ring to zero. If the bulk concentration of R is initially zero, then

$$N = -i_R/i_D \quad \text{V-2}$$

The collection efficiency (N) can be theoretically determined (347), but it also is a function only (albeit a complicated one) of r_1 , r_2 , and r_3 . However, $\beta^{2/3}$ and N are sensitive to the values of r_1 , r_2 , and r_3 , so the accuracy of these constants is limited by the accuracy with which the radii can be determined. It is a simple process to experimentally determine $\beta^{2/3}$ and N. This was done using the I^-/I_2 couple. The limiting disc current and limiting ring current (measured with $i_d = 0$) gave a value of $\beta^{2/3} = 0.368$ on the basis of Eq. V-1. The collection efficiency was determined from the slope of a plot of $-i_r$ vs. i_d , which was obtained by potentiostating the ring at 0.0 V and varying the disc current galvanostatically. The collection efficiency was found to be 0.178.

In order to better understand the results of the particular RRDE experiments, it is useful to illustrate the theoretical i_d - E_d and i_r - E_d behavior for the reversible reaction $\text{Red} \longrightarrow \text{Ox} + ne$ that is free from side reactions such as surface oxidation or adsorption. This is illustrated by Figure V-7, where it is assumed that the bulk concentration of the oxidized specie (Ox) is zero. The disc current is zero until the potential is swept positive enough for the reaction $\text{Red} \longrightarrow \text{Ox} + ne$ to occur. The disc current reaches a maximum value when the disc potential is positive enough to drive the surface concentration of Red to zero; the



Conditions: E_r held at potential where surface concentration of R_{ed} is 0

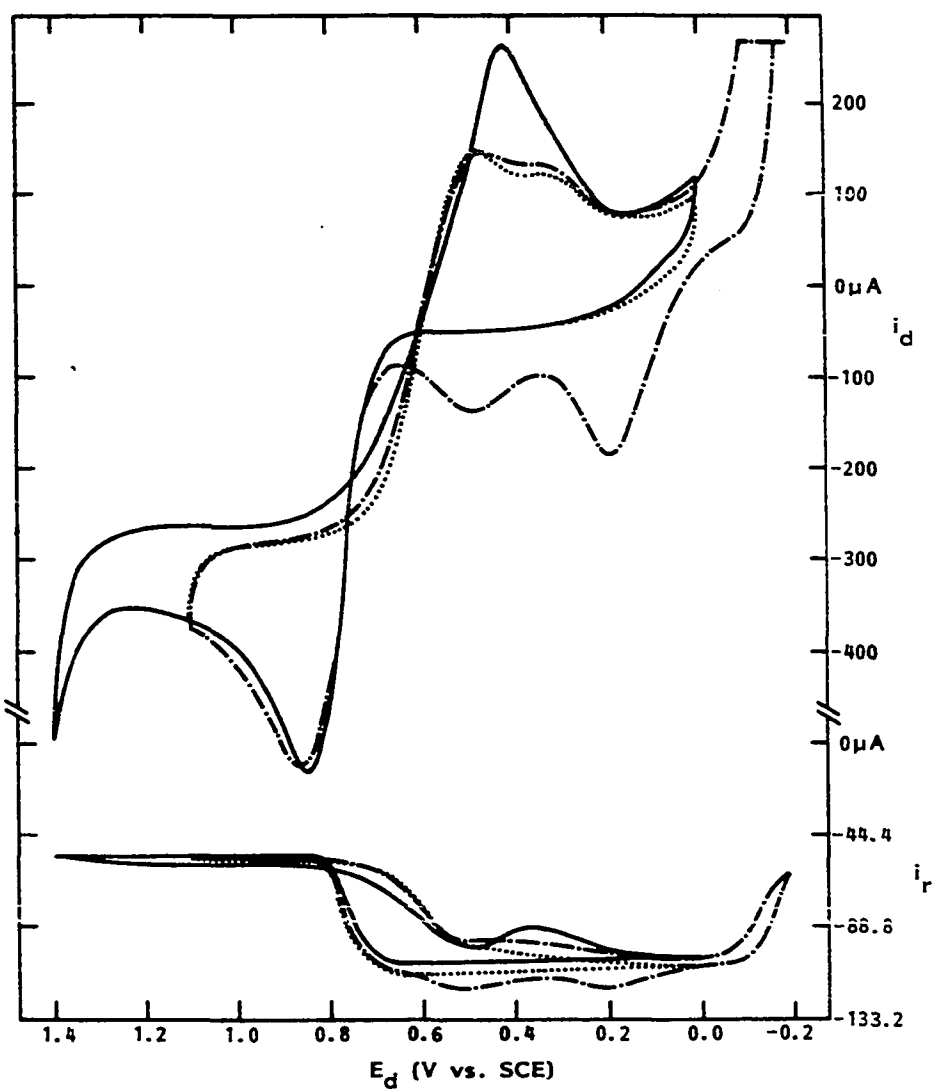
RRDE having $\beta^{2/3}$ of 0.375 and N of 0.250

Figure V-7. Theoretical $i_d - E_d$ and $i_r - E_d$ behavior

disc current is that value predicted by the Levich equation, i.e., mass-transport limited. Since the reaction is reversible and there are not surface complications, the disc current on the negative scan retraces the current obtained on the positive scan. Now consider the i_r-E_d behavior, where E_r is potentiostated at a potential where Red is also oxidized to Ox and which is sufficiently positive to ensure that the surface concentration of Red at the ring is zero. When E_d is negative of the potential required for oxidation to occur, no Red is removed from the solution by the disc, and the ring current is simply the product $\beta^{2/3} \cdot i_{d,Lev}$. In this state, the ring is often referred to as "deshielded". However, as the disc potential becomes positive enough to oxidize Red, the amount of Red that reaches the ring decreases accordingly. When $i_d = i_{d,Lev}$, the ring current has decreased by an amount $Ni_{d,Lev}$, so the ring current reaches a steady value of $\beta^{2/3} i_{d,Lev} - Ni_{d,Lev}$, or $(\beta^{2/3} - N)i_{d,Lev}$. The ring is now in the "shielded" condition. The ring current on the reverse scan also retraces the current of the forward scan.

2. Potentiodynamic experiments at the RRDE

Figure V-8 shows both i_d-E_d and i_r-E_d voltammograms for the As(III) system, with E_r held at 1.0 V. The features of the i_d-E_d curve have been previously discussed, so attention will be focused on the additional information that can be obtained from the i_r-E_d data. The ring current at $E_d = 0.0$ V is slightly less than the predicted value 113 μ A, and actually increases as E_d is scanned toward more positive potentials. This increase means that some As(III) is being liberated from the disc in the region



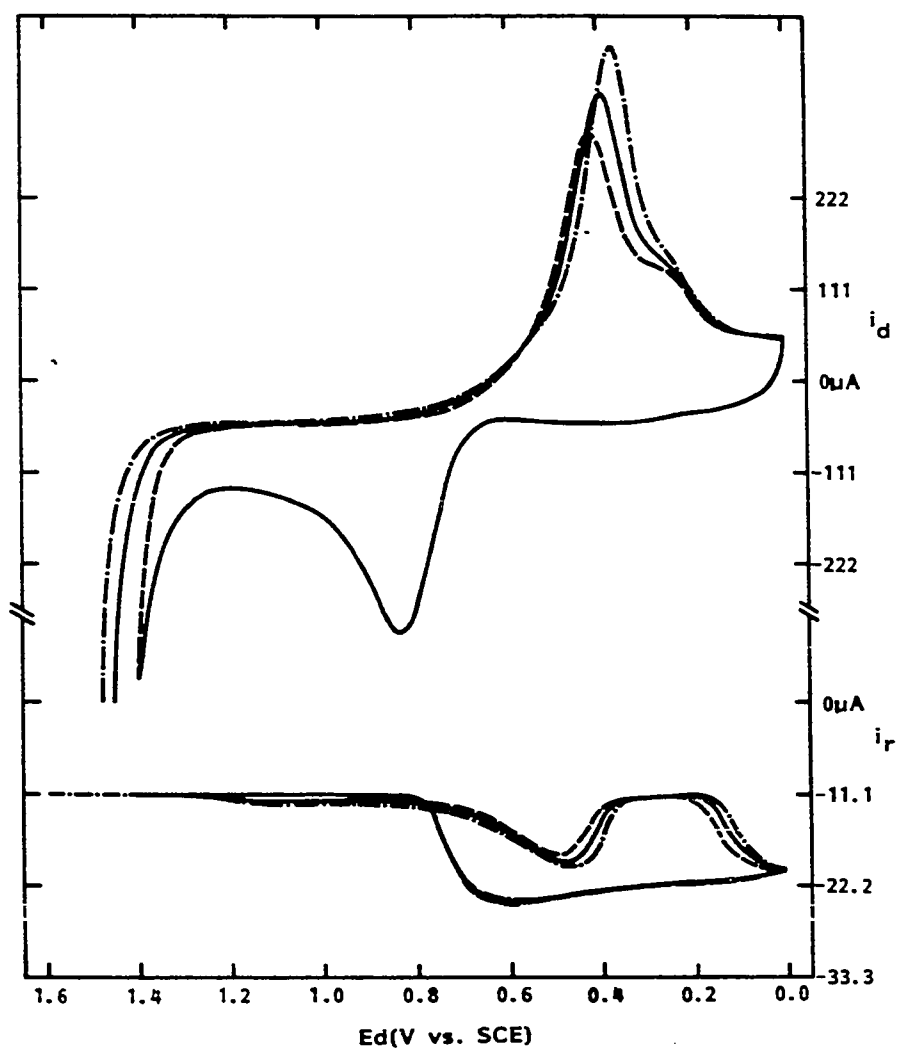
Conditions: 955 rpm
 6.0 V min⁻¹
 0.5 M HClO₄ + 0.0987 mM As(III)
 E_r 1.0 V
 - - - Scan limits + 1.1 V and -0.2 V
 ··· Scan limits + 1.1 V and 0.0 V
 — Scan limits + 1.4 V and 0.0 V

Figure V-8. RRDE cyclic voltammograms for As(III) with $E_d \leq 1.4$ V

between 0.00 V and 0.65 V. At 0.65 V, the oxidation of As(III) begins at the disc, giving the corresponding decrease in anodic ring current. The ring current attains a steady value at $E_d \approx 0.85$ V that is within about 2% of the predicted value of shielded current. If the positive scan limit is not too positive (a restriction to be discussed in further detail), the ring current on the negative scan initially retraces the current on the positive scan. At $E_d \approx 0.80$ V, the ring current does not begin to increase sharply to the deshielded value, but rather continues at the shielded value for an additional 60-70 mV. The rate of change of the ring current with disc potential on the negative scan is somewhat less than that on the positive scan. This behavior is entirely consistent with the shape of the i_d - E_d curve, but the difference in the apparent $E_{1/2}$ values between the forward and negative scans is more readily observed on the i_r - E_d curve. These results are consistent with the following explanation. Adsorbed As(III) initially inhibits the surface oxidation of Pt (see Figure V-1) in a manner similar to that of adsorbed halide ions (120). At $E > 0.7$ V, oxidation of the adsorbed As(III) begins, giving As(V) which is not adsorbed (43). Oxidation of the Pt surface then proceeds at an initially high rate until the oxide coverage attains the value for the applied potential. Oxidation of As(III) from the bulk solution proceeds on the oxide-covered anode, the rate depending on the nature of the oxide, the oxide coverage, and the applied potential. Due to the electrochemical irreversibility of the Pt oxide, oxidation on the negative scan continues at potentials negative of the potential where oxidation began on the forward scan. In other words, As(III) oxidation is catalyzed by the Pt

oxide formed during the positive scan at $E > 0.7$ V. In the sense that the $E_{1/2}$ on the negative scan is shifted toward the thermodynamic value, the reaction is "more reversible" in the presence of the oxide.

The behavior of the ring current at $E_d < 0.5$ V is dependent on the positive scan limit. If the scan limit is not too positive, the ring current continues to slowly increase as the potential is scanned negatively, but does not reach the maximum theoretical value ($\beta^{2/3} i_{d,Lev}$). As the positive scan limit is made increasingly more positive, the ring current may actually decrease as the disc potential decreases. At lower As(III) concentrations, depending on the rotation speed and positive scan limit, the ring current may either increase very little, or increase and then again decrease back to the value where As(III) is being consumed by the disc at the mass transport limited value, i.e., $i_r = (\beta^{2/3} - N) i_{d,Lev}$ (see Figure V-9). In all cases, the ring current does again increase at some potential $E_d > 0.0$ V, the precise potential depending on the positive scan limit. This is positive of the As(III)/As reduction potential. These experiments show that this additional As(III) consumption by the disc is not due to one of the familiar As(III) faradaic reactions. Similar experiments where the positive scan limit was varied from 0.80 V to 1.50 V show that the potential of the local minima in the ring current on the negative scan shifts in precisely the same manner as the Pt oxide reduction peak. This means that this As(III) consumption occurs only when an appreciable fraction of the Pt oxide has been reduced. One must conclude, therefore, that As(III) consumed by the disc in the potential range 0.0 V to 0.5 V



Conditions: 955 rpm
 6.0 V min^{-1}
 $0.5 \text{ M HClO}_4 + 0.098 \text{ mM As(III)}$
 E_r 1.0 V
 --- 1.4 V
 — 1.5 V
 -.- 1.6 V

Figure V-9. RRDE cyclic voltammograms for As(III) with $E_d \geq 1.4 \text{ V}$

following Pt oxide reduction is due to a chemisorption or adsorption of As(III) on a reduced Pt surface. (A method for quantifying this As(III) adsorption will be described shortly.) The peculiar behavior of the ring current in the potential region $0.0 \text{ V} < E_d < 0.5 \text{ V}$, therefore, is due to a combination of several factors: As(III) adsorption on a reduced Pt surface, which in turn is determined by the history of the electrode; the As(III) adsorption isotherm; the rate of mass transport of As(III) to the electrode; and the potential scan rate. In addition, the fluctuation of the ring current with disc potential is accentuated by the previous positive scan limit. A scan limit positive enough to result in the oxidation of all adsorbed As(III) to As(V) (which is not adsorbed to the electrode surface) means that all the As(III) which adsorbs following the subsequent Pt oxide reduction comes from the bulk solution.

It was previously stated that the shielded ring current was independent of scan direction if the positive scan limit was not "too positive". If the positive limit is equal to or greater than 1.2 V, the ring current at a given potential on the negative scan will be greater than that on the positive scan. This can be seen on Figures V-8 and V-9. Earlier it was stated that the As(III) faradaic current was inversely related to the quantity of Pt oxide present; this conclusion was drawn from i_d - E_d curves, examining the current on the negative scan. The RRDE data also show this conclusion to be correct, but in addition it shows that the As(III) faradaic current on the forward scan is seemingly independent of the Pt oxide coverage. For very large values of the positive scan limit, the ring current remains at the shielded value on the

reverse scan for $E_d > 1.4$ V. At potentials negative of approximately 1.4 V, the oxygen evolution reaction ceases at the disc. It is, therefore, concluded that the simultaneous evolution of oxygen in some way contributes to an increase in the rate of As(III) oxidation, since the quantity of Pt oxide is fixed immediately following scan reversal. This conclusion is confirmed by an entirely different experimental technique to be discussed in Section VII. At $E_d < 1.4$ V, it becomes apparent (see Figure V-9) that the As(III) faradaic current at the disc is indeed a function of the Pt oxide coverage when O_2 evolution is not occurring. Again, this statement is true for the case where the quantity of Pt oxide is relatively high, since the RRDE data at lower oxide coverages show almost no dependence on the scan direction.

A careful examination of Figure V-8 reveals some highly unusual behavior when the voltammograms with scan limits of 0.0 V and 1.1 V and with 0.0 V and 1.4 V are compared. The disc currents on the positive scan for $E_d > 0.25$ V are identical. The ring currents for these same disc potentials are not identical. The larger ring current for the less positive E_a means that a lesser amount of As(III) is being removed by the disc at these potentials relative to the amount removed for the more positive E_a . This is related to the incomplete oxidation and removal of adsorbed As(III) for $E_a = 1.11$ V, which in turn reduces the amount of As(III) that must be consumed from the bulk solution in order to attain the equilibrium coverage determined by the adsorption isotherm. This difference in the rate at which As(III) is removed from the bulk implies that the instantaneous As(III) surface coverage in the two cases is not

identical, yet the total disc current is identical. This apparent anomaly stimulated more experiments as well as a search for a theory which would account for equal disc currents for obviously unequal surface coverages.

In one set of RRDE experiments, the ring current obtained at $E_d = 0.0$ V on the forward scan following many cycles of the disc potential between 0.0 V and +1.1 V was compared with the ring current obtained following a three minute holding period at 0.0 V. The ring current at 0.0 V following the three minute hold was exactly $\beta^{2/3} i_{d,Lev}$, indicating that the As(III) surface coverage had attained an equilibrium value and that further As(III) chemisorption had stopped. The ring current at 0.0 V obtained when the disc was scanned continuously was about $0.976 \beta^{2/3} i_{d,Lev}$. In both cases the ring current increased as the disc potential was scanned toward more positive values. For example, at $E_d = 0.6$ V, the ring current was $1.047 \beta^{2/3} i_{d,Lev}$ when E_d had been held at 0.0 V, and $1.032 \beta^{2/3} i_{d,Lev}$ when E_d was continuously cycled. A ring current greater than $\beta^{2/3} i_{d,Lev}$ indicates that As(III) is being desorbed by the disc and leads one to the conclusion that the adsorption isotherm is potential dependent.

Experiments where the rotation speed was varied show how a given quantity and state of Pt oxide can effect the voltammetric characteristics. The ring current remains at the shielded value for a greater range of disc potentials at low rotation speeds, and the ring current shows a greater scan direction dependency at the higher rotation speeds. Higher rotation speeds do not give ring currents that attain the deshielded value at more positive potentials, since the shape of i_r-E_d

curve in the adsorption region can only be interpreted that the final stages of the adsorption are rate limited and not mass-transport limited. This is not to say that the adsorption is never mass transport limited; in fact, Figure V-9 gives an example where just such a limit is reached. This condition arises when the As(III) flux is small and the positive scan limit was positive enough to remove all the previously adsorbed As(III). It appears that the chemisorption proceeds at a mass transport limited rate until some intermediate coverage is attained and then gradually becomes more and more kinetically limited.

The RRDE can be used to give an estimate of the amount of soluble As(III) produced in the anodic stripping peaks. Figure V-8 shows ring-current peaks at those disc potentials where anodic stripping of bulk and up As is occurring. In experiments where a large amount of bulk As was deposited, the magnitudes of the corresponding ring and disc currents were compared. The theoretical peak ring current for a disc stripping peak should be $\frac{2}{3}nF_{d,peak}$; assuming that the As stripped from the disc is oxidized to the +3 state. The factor of $\frac{2}{3}$ is introduced because ring oxidation is from the +3 to +5 state. The actual ring current was 71.1% of the theoretical ring current for the stripping peak at 0.2 V, and was 92.8% of the theoretical value for the stripping peak at 0.5 V. The value obtained for the peak at 0.5 V is probably within the experimental error for this technique; however, the result obtained for the peak at 0.2 V is significantly different from the predicted value. The most straightforward interpretation of this difference is that not all of the As oxidized goes into solution, but rather that some remains adsorbed to the

electrode. This is reasonable in light of the previous evidence establishing that As(III) does adsorb on Pt. Another explanation of this discrepancy is that some fraction of the As stripped from the disc is oxidized to a higher oxidation state, presumably the +5 state. This latter explanation seems unlikely, given the standard reduction potential for the As(V)-As couple of +0.132 V vs. SCE, which is 0.125 V positive of the standard reduction potential for the As(III)-As couple. Since the oxidation state of the arsenic stripped in the peak at 0.5 V would appear to be the +3 state, it is reasonable to conclude that arsenic stripped in the peak at 0.2 V would not contain As(V). These results are difficult to interpret in light of the fact that a greater percentage of As is stripped as soluble As(III) in the peak where the interaction forces with the substrate metal would be expected to be strongest.

The presence of bulk As(V) in the same solution as the As(III) does not cause any change in the voltammetric characteristics.

3. Transient RRDE experiments: evidence for As(III) adsorption

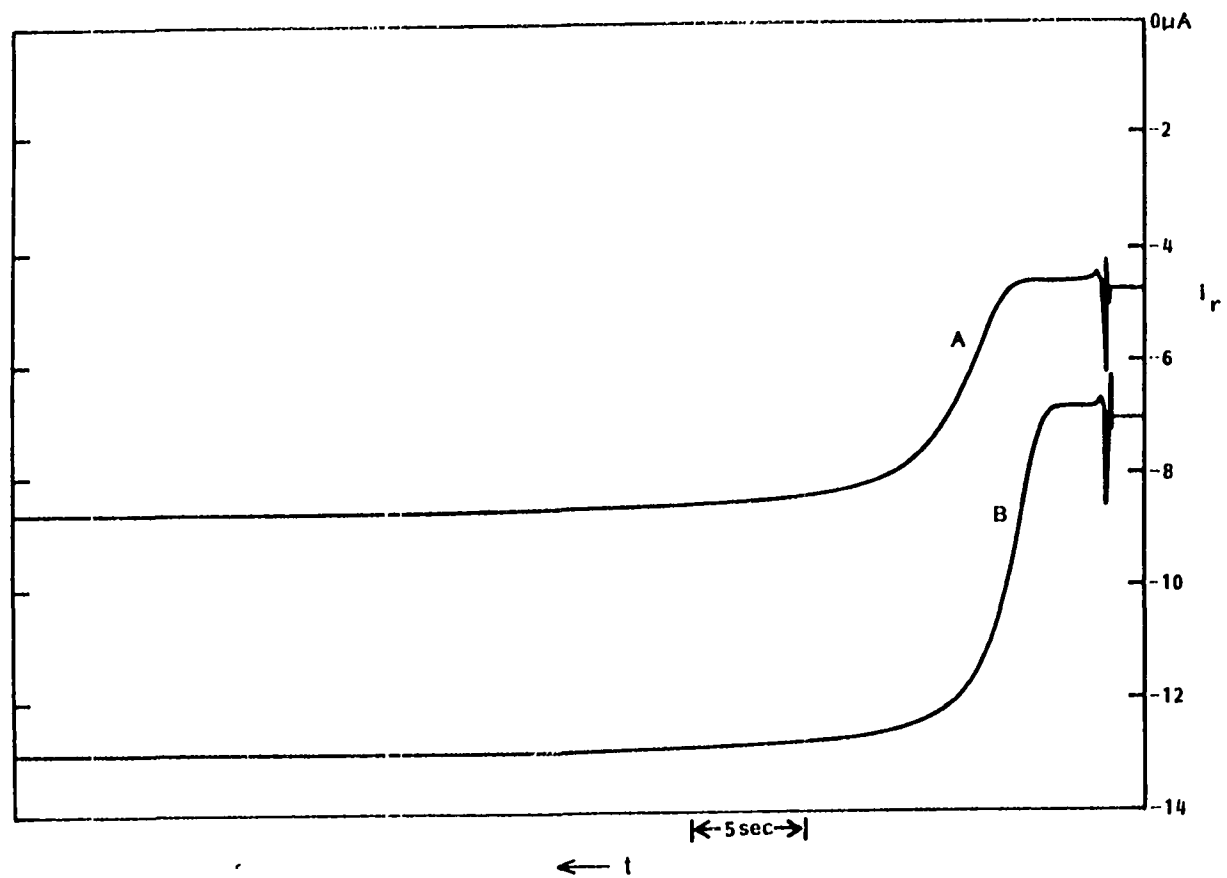
It was stated earlier in this section that the amount of As(III) that adsorbs on a reduced Pt surface can be quantified. This can be done using a transient RRDE technique. The theoretical treatment involves the solution of the basic differential equation for the transport of a species of concentration C from the bulk of the solution to the electrode surface, including the $\delta C/\delta t$ term. (In the Levich treatment, it is assumed that a steady-state condition exists and therefore the $\delta C/\delta t$ term is set equal to 0.) Two approximate solutions have been given (347,349). The first use

of a transient RRDE technique to study an adsorption process was conducted by Bruckenstein and Napp (350) on the Cu(I)-Pt system. The basic idea is that an adsorption process that occurs at the disc causes a delay in the appearance of that substance at the ring. The delay caused by adsorption is of much longer duration than the expected transit time t' , which is the time for the substance to transit the distance from the outside edge of the disc to the inside edge of the ring. An approximate value for the transit time was derived by Bruckenstein and Feldman (351) and is given by

$$\omega t' = 3.58(\nu/D)^{1/3} [\log(r_2/r_1)]^{2/3} \quad \text{V-3}$$

Substituting typical values for the constants into Eq. V-3 gives a transit time of about 29 msec for an ω of 100 sec^{-1} (955 rpm).

Figure V-10 shows the results of RRDE transient experiments carried out at two different values for [As(III)]. The disc electrode potential was held at 1.4 V prior to the transient and was then stepped to 0.2 V. Some experiments were also performed in which the disc potential was stepped from 1.1 V to 0.0 V; these results were identical with those obtained for the potential step from 1.4 V to 0.2 V at the lower As(III) concentrations, but did seem to give a greater data scatter at the higher concentrations. Since the transit time was very short relative to the time scale of the experiment, the charge associated with the adsorption of As(III) on the disc was approximated as the area under the i_r - t curve from $t=0$, i.e., the time when E_d was stepped from 1.4 to 0.2 V, until the ring current stabilized at the higher (desheilded) value. This charge (Q_R) was



Conditions: 955 rpm
 0.5 M HClO_4
 E_r 1.0 V

A 0.0416 mM As(III)
 B 0.0619 mM As(III)

Figure V-10. Transient ring current response for As(III) oxidation following potential step at the disc

measured by using a Keuffel and Esser compensating planimeter. The number of moles of As(III) that adsorb on the disc is related to this charge by

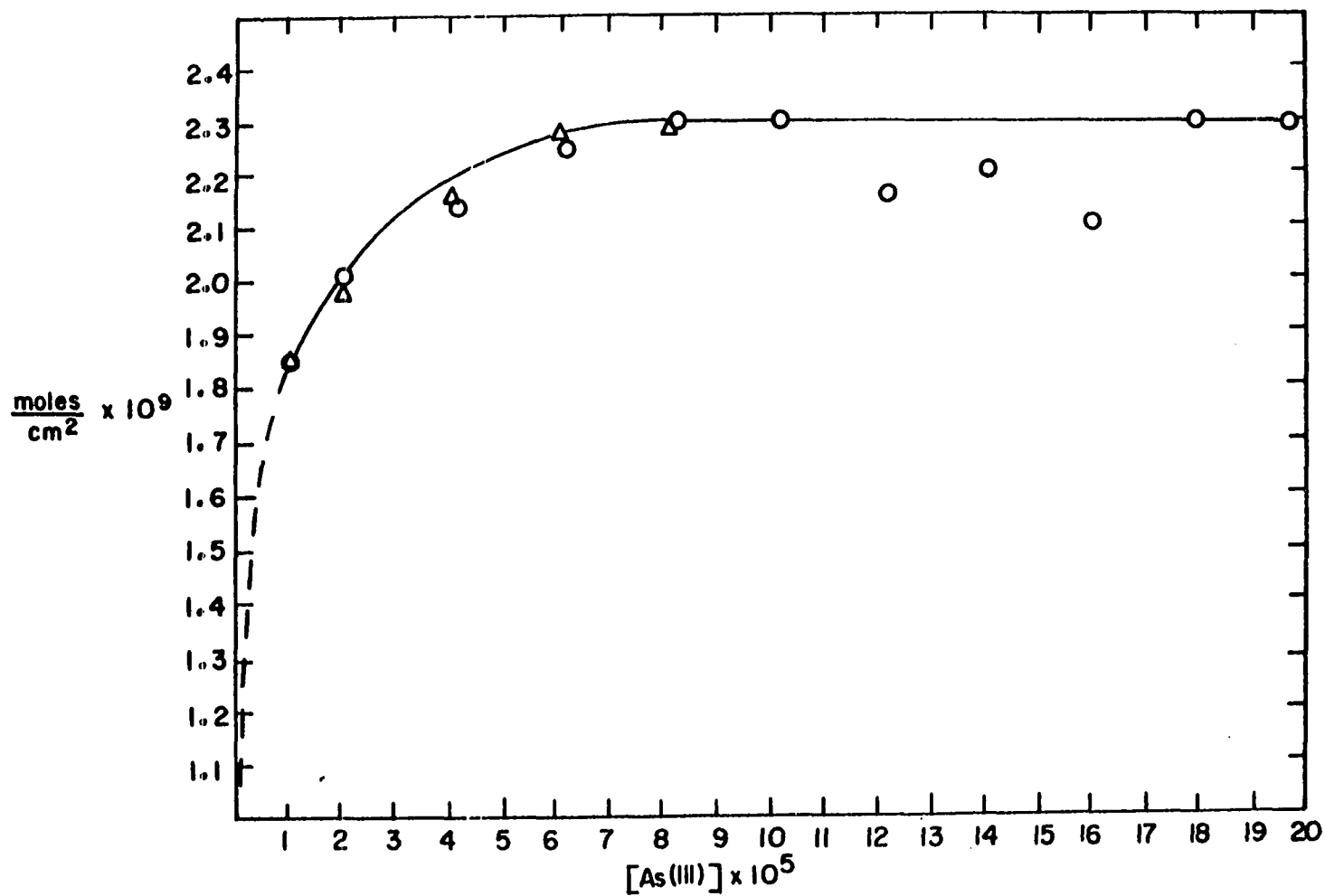
$$\text{moles cm}^{-2} = Q_R/nNFA_{\text{disc}} \quad \text{V-4}$$

For example at $[\text{As(III)}] = 4.16 \times 10^{-5} \text{ M}$, the charge under the i_p -t curve was found to be $33.9 \mu\text{C}$. This charge corresponds to 2.14×10^{-9} moles cm^{-2} of As(III) adsorbed to the disc. Similar calculations at other values of $[\text{As(III)}]$ give the adsorption isotherm as shown in Figure V-11. The maximum surface coverage is 2.30×10^{-9} moles cm^{-2} , or 1.38×10^{15} atoms As(III) cm^{-2} . A rough calculation for the number of Pt atoms per unit area for polycrystalline Pt gives 1.35×10^{15} atoms/ cm^2 , so it is concluded that As(III) adsorbs on Pt in a 1:1 ratio.

The RRDE and transient RRDE experiments have clearly demonstrated that As(III) adsorption does occur on a reduced Pt surface and occurs to a significant extent. This knowledge enables one to interpret further the data obtained from cyclic voltammetry at the RDE.

4. Adsorption pseudocapacitance in the As(III)-Pt system

In the previous discussion on the effect of scan rate (see Figure V-6), the treatment of the anodic currents in the potential region $0.2 \text{ V} < E_a < 0.8 \text{ V}$ was deferred. For scan rates of 1, 2, 6, and 10 V min^{-1} , the anodic current at 0.5 V is 8, 15, 41, and $65 \mu\text{A}$, respectively. While the anodic current does not increase linearly with scan rate there is, nevertheless, a significant relationship. Given this scan rate dependence and the relatively constant current over the potential $0.2 \text{ V} < E_a < 0.8 \text{ V}$ at a given scan rate, one might be led to conclude that these currents are

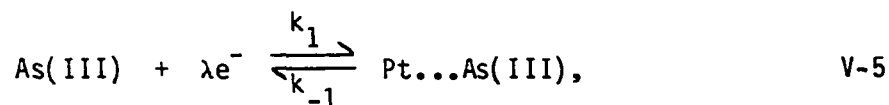


o Disc transient 1.1 V/0.0 V
 Δ Disc transient 1.4 V/0.2 V

Figure V-11. As(III) adsorption isotherm on Pt

simple charging currents, i.e., associated with the rearrangement of the electrical double-layer. A rough estimate of the double-layer capacitance can be obtained by dividing the charging current by the scan rate; a typical value for a Pt electrode in a pure acidic electrolyte is about $100 \mu\text{F cm}^{-2}$ (see Figure V-1). Using the scan rates and anodic currents of Figure V-6 gives values for the "capacitance" of 1050, 991, 902, and $856 \mu\text{F/cm}^2$. These values are almost an order of magnitude greater than those expected for a simple double-layer capacitance. A value of this size is more properly referred to as a "pseudocapacitance", a term which was first suggested by Grahame (352) to distinguish the capacitance-like behavior observed when a faradaic reaction occurs that leads to a significant surface coverage of an adsorbed intermediate from the true capacitance of the double layer. The theory of adsorption pseudocapacitance was initially developed for application to the hydrogen evolution reaction, but was later applied to a number of other electrode processes (353). The brief derivation that follows is adapted from that of Conway (354).

The faradaic adsorption reaction is denoted by



where λ represents the number of electrons transferred in the reaction. It will be assumed that follow-on reactions do not occur to an appreciable extent in the potential range of interest so that the adsorption can be treated as a quasi-equilibrium condition.

Frequently, the partial surface coverage θ for the adsorbed product is potential dependent. To attain each value of θ , it is required that a charge q be passed in order to attain that coverage from a previously uncovered state ($\theta=0$). Therefore, $q = k'\theta$, where k' is constant. The variation of θ with potential gives rise to the pseudocapacity C defined by

$$C = \frac{dq}{d\phi_M} = k' \frac{d\theta}{d\phi_M} \quad \text{V-6}$$

In this derivation, the potential of the metal electrode is denoted by ϕ_M . Again, θ can only be changed by a charge transfer across the double layer.

For a Langmuir isotherm, the forward and reverse rates of Eq. V-5 are given by

$$v_1 = k_1 [\text{As(III)}](1-\theta) \exp[-\alpha nF/RT] \quad \text{V-7}$$

$$v_{-1} = k_{-1} \theta \exp[(1-\alpha)nF/RT], \quad \text{V-8}$$

where $C_{\text{As(III)}}$ is the bulk As(III) concentration and η is the overpotential. At equilibrium, $d\theta/dt = 0$ and, therefore, $v_1 = v_{-1}$. Assuming that $\alpha = 1/2$, and combining Equations V-6 and V-8 gives

$$\frac{k'}{C} = \frac{-d\phi_M}{d\theta} = \frac{RT}{F} \frac{d}{d\theta} \left(\ln \frac{\theta}{1-\theta} \right) \quad \text{V-9}$$

and

$$C = \frac{k'F}{RT} \theta(1-\theta) \quad \text{V-10}$$

The pseudocapacitance has a maximum at $\theta = 0.5$ and it is symmetrical

with respect to θ . Expressing the partial surface coverage in terms of potential gives

$$C = \frac{k'F}{RT} \frac{K_1 \exp[-\phi_M F/RT]}{(1 + K_1 \exp[-\phi_M F/RT])^2} \quad V-11$$

where $K_1 = k_1/k_{-1}$. The pseudocapacitance also exhibits a very sharp maximum and is symmetrical when plotted versus potential.

For a Temkin isotherm, the velocity equations must be altered to

$$v_1 = k_1 [As(III)] \exp[-\alpha n F/RT] \exp[-\gamma g \theta] \quad V-12$$

$$v_{-1} = k_{-1} \theta \exp[(1-\alpha) n F/RT] \exp[(1-\gamma) g \theta] \quad V-13$$

In Equations V-12 and V-13, g is the interaction parameter defined by

$$g = 1/RT \frac{d(\Delta G_\theta^0)}{d\theta}, \quad V-14$$

and γ is a proportionality constant ($0 < \gamma < 1$), the magnitude of which depends on the form of the energy barrier for the activation-controlled adsorption/desorption process. The significance of γ is that of a symmetry factor, and in fact γ is usually equal to $1-\alpha$. Using the same assumptions as for the Langmuir isotherm gives

$$\frac{k'}{C} = \frac{-d\phi_M}{d\theta} = \frac{RT}{F} \frac{d}{d\theta} \left(\ln \left(\frac{\theta}{1-\theta} \right) \right) + \frac{gRT}{F} \quad V-15$$

Equation V-15 cannot be solved explicitly for C as a function of potential, but may be numerically evaluated. Figure 25 of reference 354 and Figures 1, 2, and 4 of reference 355 show plots of C vs θ , C vs. ϕ_M , and θ vs. ϕ_M for the Langmuir ($g = 0$) and Temkin ($g = 5, 10, 20$)

isotherms for the adsorption of H^+ on Pt. The plot of C vs. θ is symmetric about $\theta = 0.5$ and $C = 0$ at $\theta = 0.0$ and 1.0 . The maximum for the C - θ curve with $g = 0$ occurs at $1600 \mu F cm^{-2}$, while the curves for $g = 5, 10, 20$ are essentially flat with considerably smaller pseudocapacitances. For example, for $g = 5$, the maximum is $\sim 530 \mu F cm^{-2}$. Likewise, the plot of C vs. ϕ_M shows that the maximum decreases as g increases and that C becomes a flatter function of ϕ_M over a larger potential range as g increases. The slope of a plot of θ vs. ϕ_M decreases dramatically as g increases.

The Temkin isotherm is considered to be superior to the Langmuir isotherm when electrochemical processes are involved (353). The fact that the pseudocapacitance observed in the As(III)/Pt system is about $900 \mu F/cm^2$ and exhibits a fairly constant value over a range of approximately 200-300 mV indicates that a Temkin isotherm with an average g factor of about 4 may be applicable. A rough calculation of the expected current for $g = 5$ can be performed using Conway's figures.

The anodic current for the desorption of As(III) will be given by

$$i = nFA d\Gamma/dt, \quad V-16$$

where Γ is the coverage in moles/cm². But, $\Gamma = \Gamma_{max} \theta$, so

$$i = nFA \frac{d(\Gamma_{max} \theta)}{dt} = nFA \Gamma_{max} \frac{d\theta}{dt} \quad V-17$$

$$i = nFA \Gamma_{max} \left(\frac{d\theta}{dE} \right) \frac{dE}{dt}. \quad V-18$$

The term dE/dt is simply the scan rate, Γ_{max} is the maximum surface coverage obtained from the transient RRDE experiments, and $d\theta/dE$ from

Conway's figure is 1/0.32 V. For $n = 1$ and a scan rate of 0.1 V s^{-1} , Eq. V-18 predicts a current of $32 \text{ } \mu\text{A}$, compared with an experimental value of $41 \text{ } \mu\text{A}$. If the value of g was actually smaller than 5.0 as the pseudocapacitance values would suggest, then $d\theta/dE$ would be somewhat larger and the predicted current would possibly be even closer to the experimental value. However, there is no a priori reason to assume that $n = 1$ or, in fact, that n is an integral value. The topic of partial charge transfer in specific adsorption was examined in a recent treatise (356). Acknowledging that there are "indications of the reality of partial charge transfer", Habib and Bockris are forced by other evidence, such as the lack of a correlation between adsorbilities and standard free energies or covalent bond energies, to conclude that "with the concept of partial charge transfer, we are at an uncertain frontier of a developing field."

The theory of adsorption pseudocapacity also permits an explanation of the curious behavior illustrated by Figure V-8. Note that the disc current for $0.25 \text{ V} < E_d < 0.65 \text{ V}$ is identical for the voltammograms having scan limits of 0.0 V to 1.1 V and 0.0 V to 1.4 V , but that the ring currents in the same potential range are not identical. This can only mean that the anodic disc current is unrelated to the flux of As(III) at the disc. As was stated earlier, the coverage θ is a complex combination of factors which include the As(III) flux, scan rate, and positive potential scan limit. The fact that the anodic disc currents are the same is due to the constancy of $d\theta/dE_d$ over a wide range of θ .

While As(III) adsorption with (partial) charge transfer may at first appear to be improbable, it can be rationalized in terms of π bonding. It is known, for example, in compounds containing arsenic that if the atom to which arsenic has donated electrons also has an orbital of the same symmetry as the empty d-orbitals of arsenic, back-donation resulting in overall multiple-bond character can occur (357). While it may be meaningless to discuss Pt d-orbitals on the surface of a polycrystalline metal, there is solid evidence of Pt contributing to $d\pi-d\pi$ back-bonding in CO adsorption (358). This back-donation implies a specific orientation of the As(III) on the surface; this "steric factor" may contribute to the apparent decrease in the rate of adsorption that occurs at the higher relative surface coverages. Another probable cause for the decrease in the adsorption rate with coverage is a decrease in the heat of adsorption as a function of the adsorbed As(III) coverage. This would be consistent with the results of H_2 adsorption on Pt, Rh, and Ir, which show a sharp decrease in the heat of adsorption as the surface coverage increased (354).

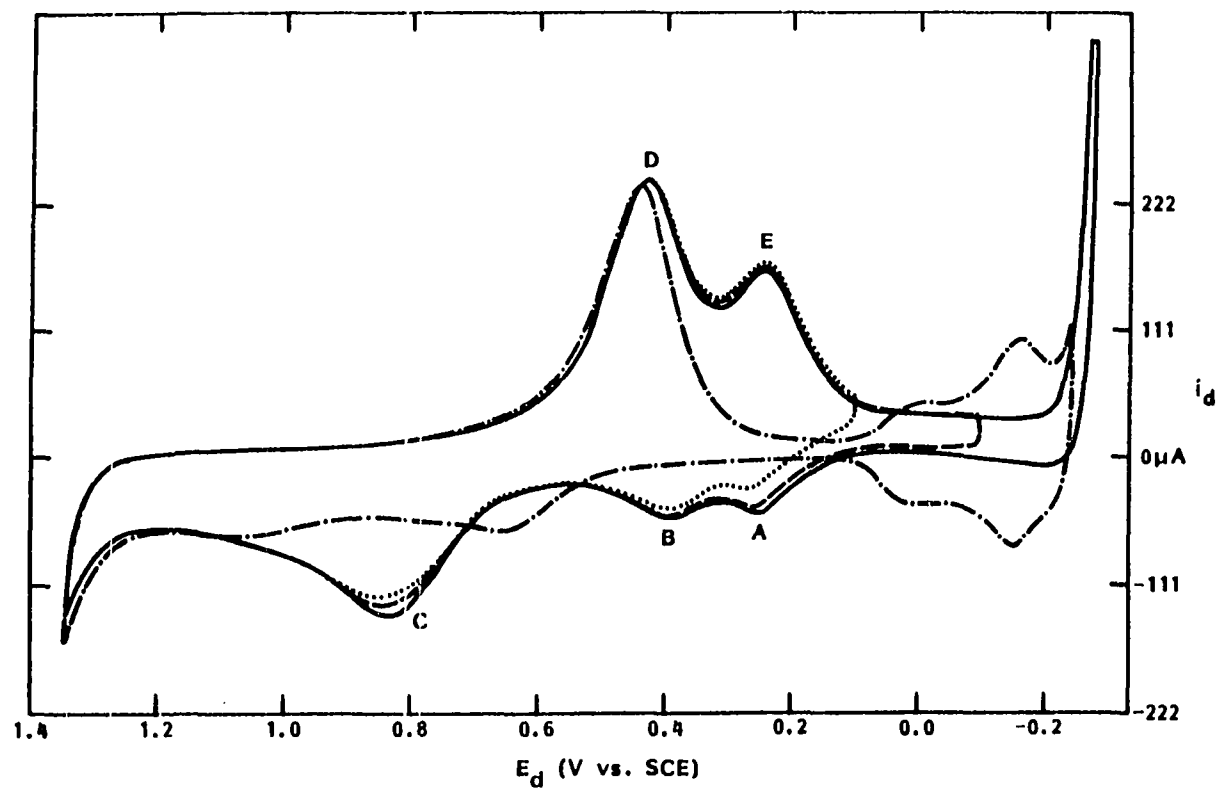
C. As(V) Electrochemistry on Pt in Acidic Media

1. Potentiodynamic studies at a Pt RDE

The anodic oxidation of As(III) gives As(V) as a product. While the electrochemistry of As(V) is not of primary interest in this dissertation, it is informative to consider the behavior of As(V) at a Pt anode as a means of understanding the As(III)-As(V) electrode reaction. As was stated earlier, As(V) is generally considered to be electroinactive

unless complexed with pyrogallol (1,2,3-trihydroxybenzene) or Cl^- in very concentrated HCl solutions. This statement is true, however, only if electroactivity is defined as a continuing oxidation or reduction of the bulk specie. As the following discussion shows, As(V) is electrochemically active when the definition is expanded to include electrochemical surface reactions.

A series of i_d - E_d curves are shown in Figure V-12 for a solution of As(V) recorded for various values of the negative limit of the cyclic potential scan. Again, a Pt residual curve is included. The predominant features of this As(V) voltammogram are: 1) a very prominent cathodic peak E at ca. 0.25 V on the negative scan; 2) two well-defined anodic peaks at 0.25 V (A) and 0.40 V (B); and 3) an anodic peak C at 0.84 V. A comparison of Figure V-12 with an As(III) voltammogram recorded at 0 rpm (Figure V-4 or V-5) reveals that the same features occur in both cases. This is reasonable if one realized that the As(V) produced in the diffusion layer by oxidation of As(III) remains in the immediate vicinity of the electrode surface in the absence of stirring. In the quiescent solution, any loss of As(V) due to diffusion away from the electrode should be replaced by As(V) formed as a result of the oxidation of As(III) (on the subsequent forward scan) that continues to diffuse to the electrode. The prominence with which cathodic peak E appears in both cases indicates that it is due to the reduction of an As(V) specie, even though As(V) is generally considered to be nonreducible. Anodic peaks A, B, and C can be explained as successive oxidations of the product of the As(V) reduction. The most likely explanation is that As(V) is reduced to



Conditions: 955 rpm
 6.0 V min⁻¹
 0.5 M HClO₄ + 0.141 mM As(V)

--- Pt residual
 ... 0.1 V
 -.- -0.1 V
 — -0.28 V

Figure V-12. Cyclic voltammograms of As(V) at a Pt RDE in acidic solution as a function of E_c

two approximately zero states by underpotential deposition processes. Anodic peaks A and B represent the oxidation of the slightly different As(0) states to adsorbed As(III) and peak C (which occurs at the same potential as the analogous peak in an As(III) solution) represents the combined oxidation of the adsorbed As(III) and the Pt surface. Anodic peak B, occurring at the more positive potential, corresponds to the oxidation of the more stable of the two As(0) states. Anodic peak A can be increased by allowing the potential to scan to more negative values, but approaches a maximum value. This increase in the amount of As(V) deposited as the potential is scanned to more negative values can also be observed in the increase in the size of peak C, due to the oxidation of a greater amount of adsorbed As(III).

Initial scan-rate studies performed in an As(V) solution seemed to indicate that the entire cyclic voltammogram was the result of surface reactions. This in turn led to the conclusion that cathodic peak E was the result of the reduction of adsorbed As(V). Later, this conclusion was shown to be in error (see the next section). It is instructive to note here that a whole range of fluxes must be examined before concluding, on the basis of scan rate data, that only surface reactions are occurring.

The shape of cathodic peak E varies as a function of scan rate. Assuming that: 1) the PtO reduction peak is symmetrical; 2) the charging currents are negligible; and 3) the $H_2(g)$ evolution current can be extrapolated to zero, the charge passed in peak E can be determined. The charge passed at 6.0 V min^{-1} is 88% of the charge passed at 1.0 V min^{-1} . This is excellent agreement given the assumptions listed above. However,

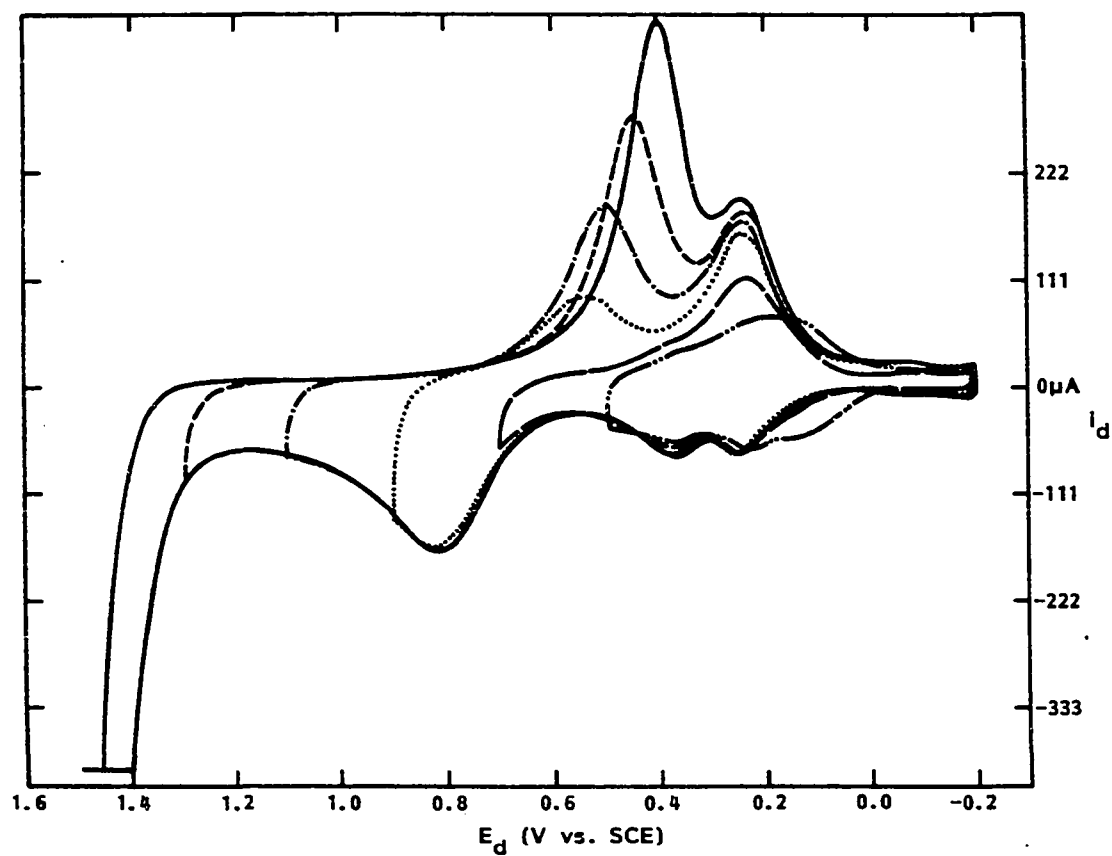
it is also reasonable to expect that slightly more arsenic would deposit at the slower scan rate. As was the case with As(III) adsorption, the deposition rate of As(V) probably decreases as the coverage increases. The slower scan rate allows the electrode potential to remain in the region where deposition occurs for a greater length of time.

2. As(V) underpotential deposition and isopotential points

The term "underpotential deposition" has been used and should be defined. Deposition that occurs at potentials positive of the value predicted by the Nernst equation for a product with an activity of 1 is called "underpotential deposition." The underpotential deposition (upd) phenomenon is complex and widespread; a recent review (359) giving 255 references is recommended.

The value predicted by the Nernst equation for the deposition of arsenic metal from a 10^{-4} M As(V) solution is 0.085 V vs. SCE.

In Figure V-13, the negative scan limit is fixed at a potential where the As(V) upd process produces the limiting As coverage and the positive scan limit is varied. The i_d - E_d curve obtained with a positive limit of 0.5 V is very different from those obtained with $E_a > 0.7$ V. In the former case, the cathodic deposition peak and the 0 to +3 oxidation peaks are not well defined. However, for $E_a > 0.7$ V, where Pt oxide formation and reduction occurs during each potential cycle, these three peaks are well defined. These results can be understood in the following way. The As(V) species in solution are considered to be electroinactive (in the more general sense) because of the filled 4p orbitals and the extended



Conditions: 955 rpm
 6.0 V min⁻¹
 0.5 M HClO₄ + 0.141 mM As(V)

— · — 0.5 V
 — — — 0.7 V
 · · · · · 0.9 V
 - - - - - 1.1 V
 - - - - - 1.3 V
 — — — — — 1.5 V

Figure V-13. Cyclic voltammograms of As(V) at a Pt RDE in acidic solution as a function of E_a

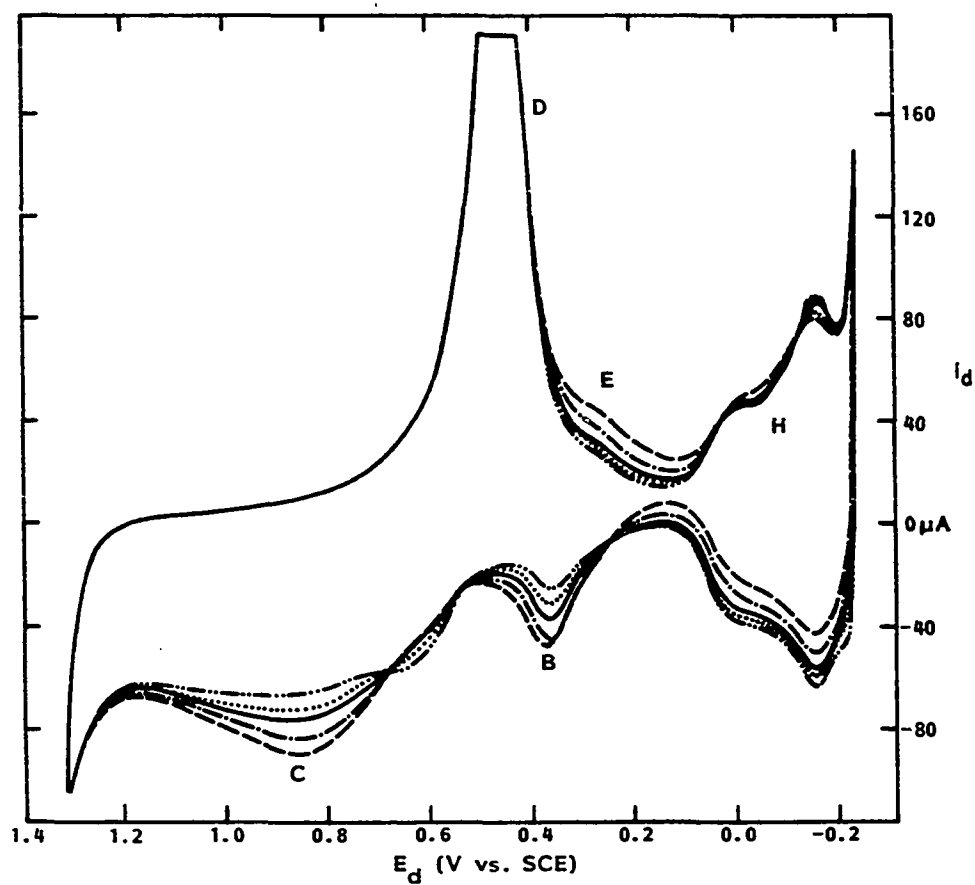
degree of hydration. It is reasonable, therefore, to assume that the free energy of deposition would have to be quite large, and in fact the process of underpotential deposition is considered to arise precisely because of a strong interaction between the deposit and the substrate. The upd process for As(V) appears to require the formation and reduction of PtO in order to generate a suitable state of the Pt surface. The generation of a suitable Pt state could, in turn, be related to the prior desorption of As(III) which acts to inhibit the deposition, or to the formation of a transient site geometry (for example, PtO-Pt pairs) which facilitates the deposition. The necessity of PtO formation and reduction for As(V) upd is established by experiments where the positive potential scan limit is set at ca. +0.6 V and the negative scan limit is set at +0.1 V. In this case, the positive limit is positive enough to oxidize the surface arsenic to the +3 state, but not positive enough for PtO formation. The negative limit (0.1 V) is negative enough to permit some As(V) underpotential deposition to occur, but is not negative enough for the limiting coverage to be attained. After a large number of cycles with these particular potential scan limits, an electrode state is achieved in which the currents are roughly 1/3 the value of those shown on Figure V-12. If the electrode is in this state and the negative scan limit is then changed to -0.2 V, a very large cathodic current is recorded on the first negative scan, and the anodic and cathodic currents throughout the potential range return to their earlier (i.e., 3 times larger) values. Similarly, if the electrode is again allowed to repeatedly scan between +0.6 V and +0.1 V, and then the positive limit is increased to a potential in the oxide

region, a large upd peak is observed on the first negative scan. These experiments establish that PtO reduction is necessary for As(V) upd and that surface contamination is not responsible for lack of As(V) upd. The cause of the current decay with the number of potential scans when the scan limits are 0.6 V and 0.1 V is attributed to a very slight desorption of the As(III) formed on each forward scan. This leads to a small but continuous decrease in the amount of arsenic on the electrode surface, because As(III) re-adsorption is negligible and the conditions for As(V) underpotential deposition are not present.

The explanations that have been advanced to explain the As(V) *i*-E curve can be tested by adding a substance to the solution that competitively adsorbs on the electrode surface, thereby preventing the As(V) upd process and subsequent oxidations and reductions from occurring. Iodide is known to strongly adsorb on Pt (360). When a solution containing 1.9×10^{-4} M As(V) was made $9.76 \mu\text{M}$ in I^- (a concentration known to exceed that necessary for monolayer I coverage), the As(V) reduction peak at 0.27 V, the cathodic current at $E_d < 0.1$ V, and all of the anodic peaks on the forward scan were either completely eliminated or greatly reduced in size. The I^- flux was evidently sufficient to occupy the Pt sites formed as the PtO was potentiodynamically reduced. This, in turn, prevented the As(V) upd process and subsequent anodic peaks for 0 to +3 and +3 to +5 oxidations.

The effects of varying the As(V) bulk concentration and/or the electrode rotation speed are dependent on the initial value of the concentration. At high [As(V)] ($> \text{ca. } 2 \times 10^{-4}$ M), the *i*-E curve does not

change with either a change in the concentration or a change in the rotation speed. These observations initially led to the conclusion that As(V) underwent underpotential deposition from an adsorbed state (also see Section V.C.1). When it was realized the As(V) was surely not adsorbed on PtO, based on a number of experimental and theoretical considerations, it became necessary to re-examine the concentration and rotation speed dependence. It was then found that the voltammogram of an As(V) solution is both concentration and rotation-speed dependent at low ($< 10^{-4}$ M) bulk concentrations. In these experiments, a positive limit of 1.32 V was used; this is sufficient to oxidize all of the surface arsenic to the +5 state which is desorbed. For example, a 10 μ M As(V) solution at a rotation speed of 240 RPM gives a slight broadening of the PtO reduction peak in the region $0.07 < E_d < 0.35$ V; the hydrogen adsorption and desorption peaks and the Pt oxidation wave are all essentially unchanged from the voltammogram obtained in pure supporting electrolyte. However, a very small anodic wave at 0.36 V does appear under these conditions. If the rotation speed is increased, the PtO reduction peak continues to broaden, there is a continuous decrease in the size of the hydrogen peaks, and the onset of Pt oxidation becomes less and less distinct. However, the most obvious feature continues to be the anodic peak at 0.36 V, the peak current increasing with rotation speed and the peak potential shifting to more positive potentials. Decreasing the rotation speed to the original value results in retracing the original voltammogram; this shows that all of the surface arsenic is oxidized and desorbed during the forward scan. Figure V-14 illustrates this behavior at a somewhat higher



Conditions: 6.0 V min^{-1}

$0.5 \text{ M HClO}_4 + 0.0456 \text{ mM As(V)}$

- - - - - 240 rpm
 ······ 540 rpm
 ————— 955 rpm
 - - - - - 2150 rpm
 - - - - - 3820 rpm

Figure V-14. Cyclic voltammograms of As(V) at a Pt RDE in acidic solution as a function of ω

[As(V)] and at five different rotation speeds. At the higher rotation speeds it becomes apparent that a cathodic peak is forming in region E. Note the "isopotential points" at 0.24 V, 0.53 V, and 0.68 V. The theory of isopotential points has been developed by Untereker and Bruckenstein (361), who also presented some examples of systems which give isopotential points. Reference 361 also gives five additional references where isopotential points were obtained; reference 362 is a more recent paper that illustrates this behavior. Basically, an isopotential point is a common intersection in a family of i - E curves that occurs when: 1) the potential scanning program is the same for all curves; 2) the electrode surface is covered with at least one adsorbed or deposited species at the start of the potential program; 3) the initial amount of adsorbed or deposited species is different for each curve; and 4) the electrode surface behaves as if it consists of independent electrochemical regions, the sum of whose areas is constant at all times for all of the i - E curves. The simplest (and most common) case that gives isopotential points involves a faradaic reaction involving an adsorbed or deposited specie on the covered portion of the electrode and the metal/metal oxide reaction occurring on the uncovered portion of the electrode. If the initial amount of the adsorbed or deposited specie is the only variable, then the condition for an isopotential point is

$$i_1^0 + C_1 E' = i_2^0 + C_2 E' \quad \text{V-20}$$

where i_1^0 and i_2^0 are the current densities for the two faradaic reactions, C_1 and C_2 are the differential double-layer capacitances of the two

regions, and E' is the potential scan rate (i.e., dE/dt). From Eq. V-20, three cases can arise. If both of the faradaic processes give currents much larger than the charging currents, then Eq. V-20 simplifies to $i_1^0 = i_2^0$. If one of the electrochemical reactions does not occur in a potential region where charging currents are important, then an isopotential point can result with

$$i_{ip} = C_i A_i E', \quad \text{V-21}$$

where i_{ip} is the current at the isopotential point, and C_i and A_i are the differential double-layer capacitance and area, respectively, associated with the inert couple. Finally, if neither faradaic process occurs in a potential region, an isopotential point can arise if $C_1=C_2$.

In the case of the As(V)-Pt system, the combination of oxidatively removing all of the surface arsenic as As(V) on the positive potential scan and the variable amount of As(V) that can be transported to and deposited at the electrode by changing the electrode rotation speeds gives precisely those conditions which lead to isopotential points. Platinum oxide formation does not occur at potentials as negative as 0.24 V; therefore, the isopotential point at 0.24 V is due to a combination of the charging current on the uncovered Pt region and the oxidation of the underpotential deposited As to the +3 state. The charging current contributions are probably negligible at the isopotential points at 0.53 V and 0.68 V, so these points are due to the oxidation of the Pt surface and As(III). Two isopotential points are obtained because the current density for the oxidation of the adsorbed As(III) would be expected to increase

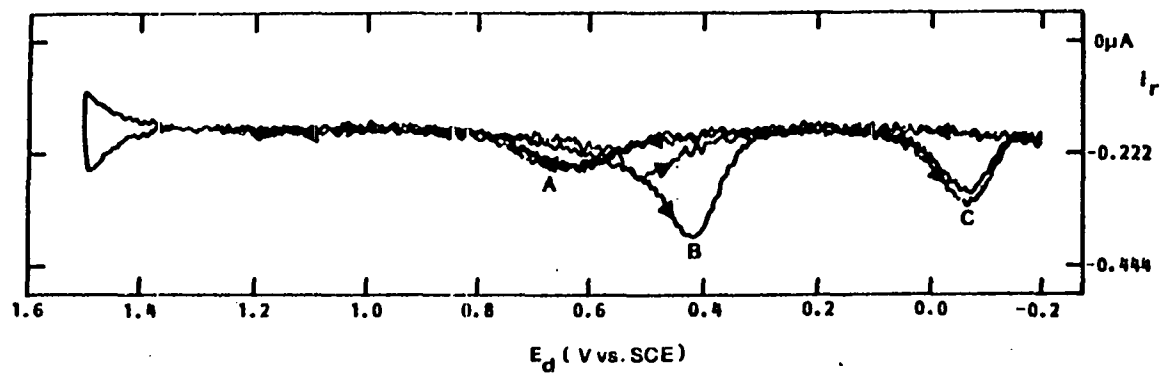
and then decrease (since there is only a finite amount of As(III) on the disc) and thus would be expected to be equal to the current density for Pt oxide formation at two different potentials.

Isopotential points can also be observed in As(III) solutions when the concentration and rotation speed are low. For the As(III) solution, the isopotential points appear at 0.16 V, 0.60 V, and 0.72 V, and are attributed to the same process as occur in the As(V) solution. The As surface coverage can be incremented by either changing the rotation speed or by decreasing the negative scan limit. At low [As(III)], an underpotential deposition of As(III) is clearly observed in a cathodic peak at 0.26 V, which is the same potential as the upd peak in the As(V) solution. This As(III) cathodic reaction, which occurs about 250 mV positive of the standard reduction potential, is also seen on Figure V-13, where adsorbed As(III) (that which was produced by the oxidation of an As(V) underpotential deposit) is reduced at about 0.2 V. This phenomenon evidently occurs in addition to the adsorption process that gives rise to the adsorption pseudocapacitance described earlier.

The O_2 reduction reaction does not appear to be effected by an As(V) underpotential deposit. It is not known whether this unusual phenomenon is due to a mechanism whereby the reduction reaction occurs on As-covered sites, or if it simply occurs on those Pt sites not occupied by As atoms. It should be noted that the theory of macroscopically inhomogeneous surfaces (see Section IV) predicts that the mass-transport limited current can be attained even when the area of the active sites represents a very small fraction of the total area.

3. RRDE studies

The Pt disc/Au ring RRDE can be utilized to study the electrochemistry of As(V). A ring current-disc potential curve is illustrated in Figure V-15. The ring was once again potentiostated at 1.0 V, a potential where As(III) is oxidized to As(V). Figure V-15 illustrates two voltammograms, one having scan limits of +1.2 V and -0.2 V, the other having scan limits of +1.5 V and -0.2 V. The ring current appears to be "offset" by an approximately 170 nA anodic current; it is believed that this is due to a combination of oxidizable impurities (possibly As(III) in the As₂O₅ used to prepare the stock As(V) solution) and very small electronic offsets in the potentiostat that become apparent only at the very high ring current sensitivity used in this experiment. It is clear from the magnitudes of the ring currents that only very minute amounts of As(III) are released by the disc. The anodic current at A on Figure V-15 occurs where As(III) adsorbed on the disc (i.e., that produced by the oxidation of the As(V) underpotential deposit) is oxidized to As(V). The anodic current at C occurs at potentials on the negative scan where some As(V) upd is occurring, so it appears that a small amount of the arsenic undergoing this process "escapes" as As(III). This indicates that an "As(III)-like" specie is an intermediate in the upd of As(V) on Pt. The anodic current at B on Figure V-15 is due the oxidation of Pt(II) produced when the PtO on the disc is reduced (363). This was deduced from the increase in this current for the more positive potential scan limit.



Conditions: 3820 rpm
 6.0 V min⁻¹
 0.5 M HClO₄ + 0.141 mM As(V)
 E_r 1.0 V

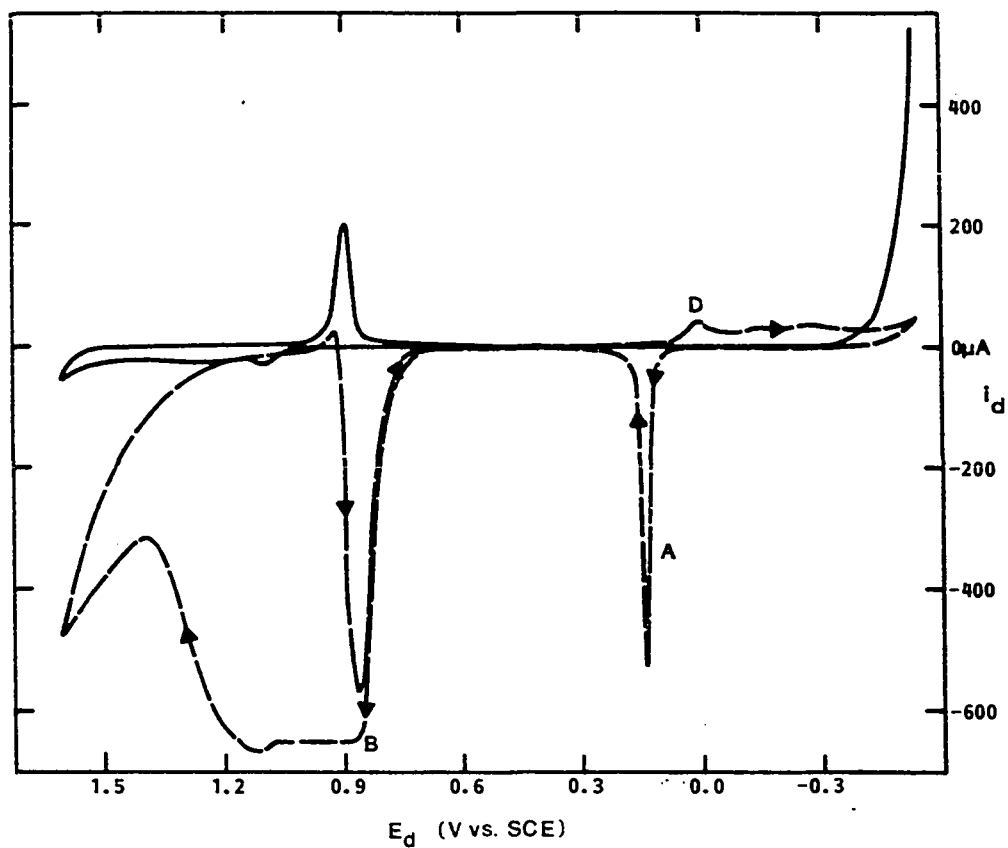
--- 1.2 V
 — 1.5 V

Figure V-15. Ring current-disc potential response in As(V) solution as a function of E_a

D. As(III) Electrochemistry on a Au RDE in Acidic Media

It has been concluded from the studies of As(III) oxidation on Pt electrodes that the thin film of PtO that is anodically formed on the electrode surface effects the electrode reaction in a number of ways. There are several other noble metals that might be used as electrocatalysts, each of which exhibits significant differences from Pt and from each other with respect to anodically-formed oxides. While it was known that As(III) could be oxidized at a Au electrode (44,45,364), it was recognized that additional experiments might provide information that could be used in developing a more complete and general reaction mechanism.

A Au residual curve and an As(III) voltammogram on a Au RDE are illustrated on Figure V-16. The Au residual curve will be discussed first. Starting at 0.0 V on the forward scan, one observes only the very small double-layer charging currents for E_d up to about 1.01 V, where the oxidation of the Au surface to a phase oxide occurs. The potential where oxide growth begins is more clearly seen at higher scan rates. Gold oxide growth continues as E_d increases up to about 1.5 V, where $O_2(g)$ evolution begins. Surface oxidation ceases quickly on scan reversal, leaving only a small charging current on the negative scan. The reduction of the surface oxide occurs in a sharp peak C with E_p at 0.90 V, whereupon the current returns to charging-current levels. There is no appreciable adsorption of molecular hydrogen on Au, and at $E_d < -0.3$ V there is a sharp increase in cathodic current, corresponding to the reduction of H^+ to $H_2(g)$.



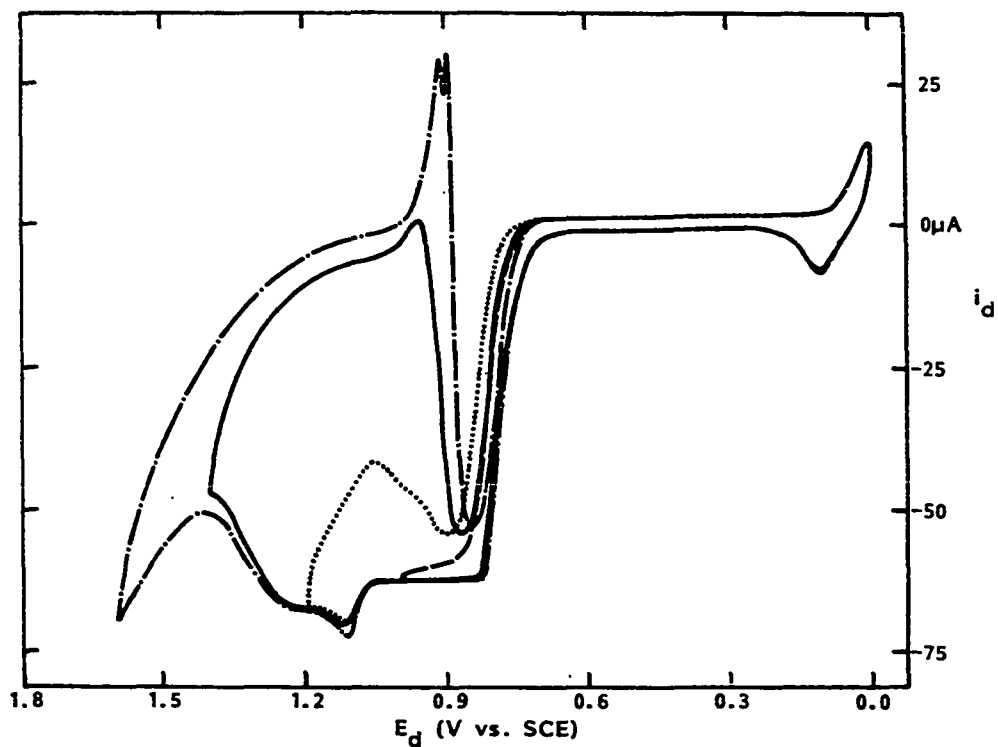
Conditions: 1000 rpm
1.0 V min⁻¹
0.5 M HClO₄

— Au residual curve
--- 1.11 mM As(III)

Figure V-16. Cyclic voltammogram of As(III) at a Au RDE in acidic solution

The addition of As(III) results in an anodic wave B that has an $E_{1/2}$ of 0.82 V. The anodic current reaches a plateau between 0.88 V and 1.02 V, implying a mass-transport limited process. At $E_D > 1.02$ V, oxidation of the Au surface causes the current to decrease rapidly. Oxygen evolution and possibly electrode re-activation causes the current to increase at $E_d > 1.4$ V. When the scan direction is reversed, essentially no anodic current is observed, as opposed to the oxidation of As(III) on Pt. At $E_d = 0.96$ V reduction of the gold oxide begins and the total current momentarily becomes cathodic. As the potential becomes slightly more negative, however, the current then becomes anodic once again, peaking at 0.86 V. The current then essentially retraces the current obtained on the forward scan. The current is negligible until $E_d = 0.08$ V, where a cathodic wave D is observed. This continues into the potential region where $H_2(g)$ evolution occurred in the absence of As(III). Following scan reversal at the negative limit, a very sharp anodic peak A is obtained with $E_p = 0.14$ V. The cathodic wave D and the anodic peak A correspond to the deposition of As(III) and anodic stripping of that deposit, respectively. This stripping peak is much sharper than the stripping peaks(s) obtained on a Pt electrode, and in fact Au was found to be superior to Pt for the determination of As(III) by anodic stripping voltammetry (21).

The role that the gold oxide plays in the oxidation mechanism was examined by varying the positive scan limit E_a , Figure V-17. When $E_a = 1.0$ V, no gold oxide is formed and the current on the corresponding negative scan is only slightly less than that of the forward scan. When



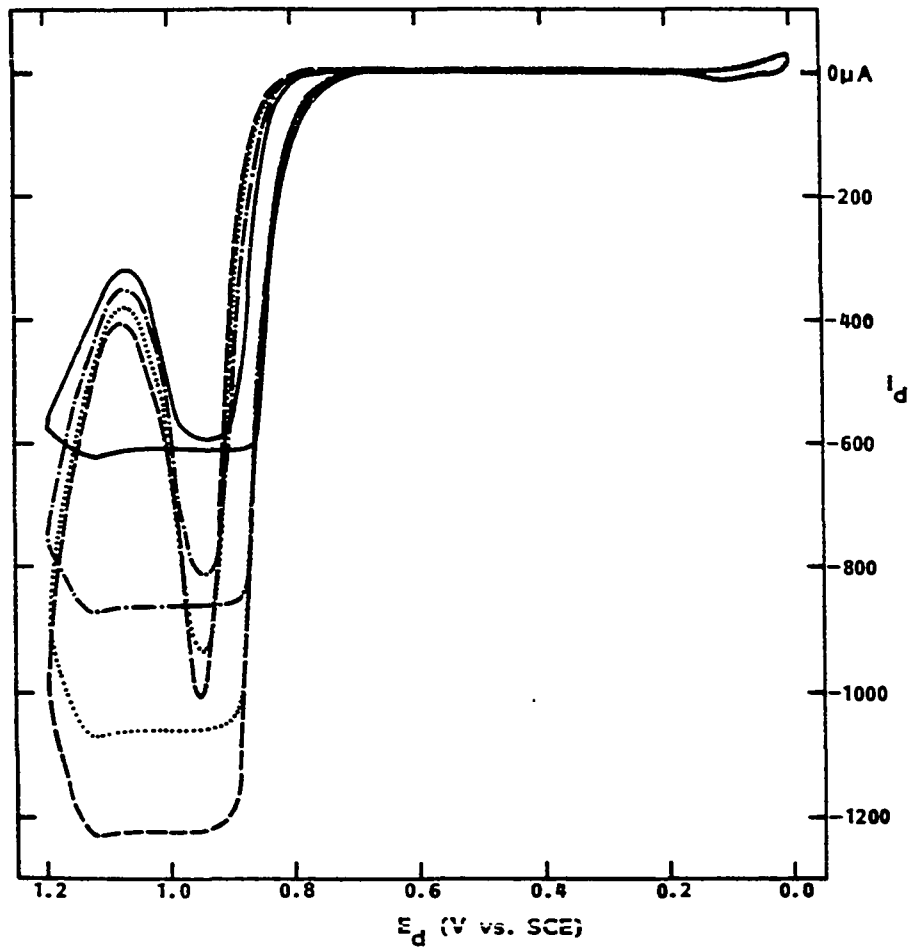
Conditions: 1000 rpm
1.0 V min^{-1}
0.5 M HClO_4 + 0.200 mM As(III)

----- 1.0 V
..... 1.2 V
———— 1.4 V
- · - · - 1.6 V

Figure V-17. Cyclic voltammograms of As(III) at a Au RDE in acidic solution as a function of E_a

$E_a = 1.2$ V, a small amount of gold oxide is formed, leading to a significantly smaller current on the negative scan. It appears that the oxide reduction current is small relative to the As(III) anodic current and that the removal of even this small quantity of oxide results in an increase in the As(III) current. Positive scan limits of 1.4 V and 1.6 V illustrate even more dramatically the effect that gold oxide has on this reaction. It is clear that the anodic oxide acts as a very powerful oxidation inhibitor, the degree of inhibition being directly related to the oxide coverage. The behavior at $E_d \approx 0.9$ V on the negative scan is due to a dynamic combination of the gold oxide reduction current and the As(III) oxidation current made possible by the appearance of oxide-free surface sites. The magnitudes of these "opposing" currents depends on the gold oxide coverage, which is itself changing as a function of potential.

The rotation-speed dependence of the anodic current was investigated in experiments illustrated by Figure V-18. For a scan rate of 1.0 V min^{-1} , a correction of $2 \text{ } \mu\text{A}$ (anodic) was applied to the net current to correct for double-layer charging. Fitting the $i_d - \omega^{1/2}$ data from Figure V-18 (plus the data for four other rotation speeds not illustrated on Figure V-18) to a linear least-squares program gives an intercept of $-1.04 \text{ } \mu\text{A}$ and a slope of $59.69 \text{ } \mu\text{A sec}^{1/2}$ with a correlation coefficient of 0.99998. This firmly establishes that the oxidation of As(III) on Au is mass-transport limited in the potential region between 0.88 V and 1.02 V on the forward scan. In other words, the Levich equation gives the precise relationship between the current, the rotation speed, and the various physical constants given by Eq. IV-9. This is significant for



Conditions: 1.0 V min^{-1}
 $0.5 \text{ M HClO}_4 + 1.026 \text{ mM As(III)}$

— 1000 rpm
- · - · 2000 rpm
· · · · 3000 rpm
- - - - 4000 rpm

Figure V-18. Cyclic voltammograms of As(III) at a Au RDE in acidic solution as a function of ω

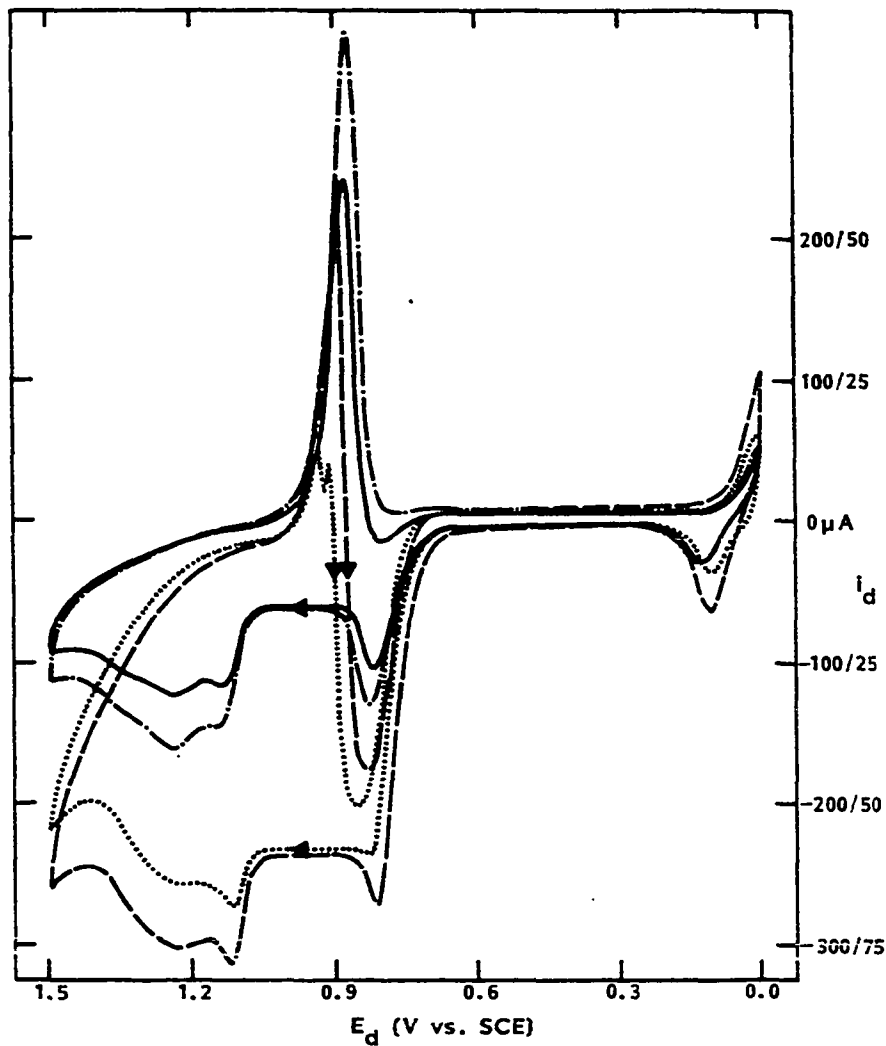
two different reasons. Use of rotation speed data and the Levich equation enables one to determine the value of the one physical constant that cannot be determined by any other relatively straightforward technique, i.e., the diffusion coefficient of the reactant. The ease with which a diffusion coefficient can be determined using a RDE makes it possible to determine this constant in a large number of supporting electrolytes. From a mechanistic viewpoint, it is clear that the oxides of Au and Pt differ radically in their ability to act as electrocatalysts for the oxidation of As(III).

Results of scan-rate studies (Figure V-19) are consistent with the conclusion drawn from the rotation-speed studies concerning the anodic current in the potential region $0.88 \text{ V} < E_d < 1.02 \text{ V}$. When the current is corrected for double-layer charging, it is found that the remaining current in this region is independent of the scan rate. This indicates that any contribution from surface reactions is negligible.

E. As(III) Electrochemistry on Ir and Pd RDEs in Acidic Media

The anodic electrochemistry of As(III) on Ir and Pd rotating disc electrodes was examined very briefly. The anodic behavior of As(III) on these metals is somewhat more difficult to discern, given the less predictable nature of the anodic oxides formed on these metals, as described in Section II.B.

The experiments on the Ir electrode were performed in 5.0 M HClO_4 in order to minimize the continuous buildup of oxide with repetitive



Conditions: 1000 rpm

0.5 M HClO_4 + 0.200 mM As(III)

- 1 V min^{-1} at $25 \mu\text{A/division}$
- 2 V min^{-1} at $25 \mu\text{A/division}$
- 6 V min^{-1} at $100 \mu\text{A/division}$
- 10 V min^{-1} at $100 \mu\text{A/division}$

Figure V-19. Cyclic voltammograms of As(III) at a Au RDE in acidic solution as a function of scan rate

potential cycling that is observed in less-concentrated acidic electrolytes. Even in 5.0 M HClO_4 there does appear to be a slight increase in the oxide current with each subsequent potential cycle. Consequently, the i_d - E_d curves do not become reproducible following 2-3 potential cycles, as is the case on Pt or Au. An anodic wave ($E_{1/2} \approx 0.8$ V) that is a combination of As(III) oxidation and Ir oxide formation and/or oxide stoichiometry changes is obtained on the forward potential scan. The anodic current for $E_d > 0.7$ V is a function of both the positive and negative scan limits. This phenomenon is evidently related to the extent that the oxide stoichiometry is changed on the forward and reverse scans.

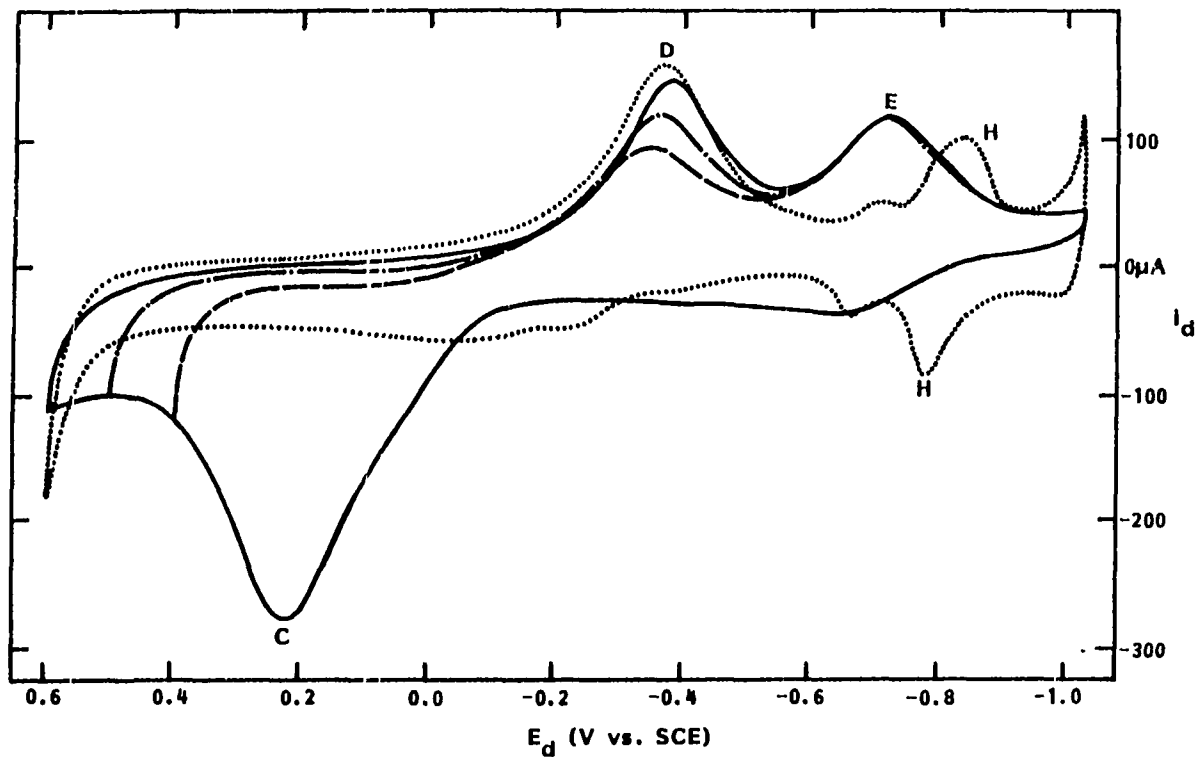
The residual current on an Ir electrode having an appreciable oxide coverage is, of course, large. This makes the collection of precise rotation-speed data difficult. The difference in the anodic current obtained at a low rotation speed (e.g., 240 rpm) and the anodic current obtained at 0 rpm is roughly equal to the value predicted by the Levich equation. At higher rotation speeds, there is a negative deviation from the Levich equation, as was the case with Pt. For $E_a < 1.3$ V, no current plateau is obtained on the reverse scan, the current simply decreasing as the potential scans to more negative values. The current on the reverse scan is rotation-speed dependent to the same extent that it is on the forward scan. With $E_a = 1.4$ V, a small current plateau on the reverse scan is obtained for 1.10 V $< E_a < 1.25$ V, but the current is only about 20% of the Levich value. The oxidation of As(III) on Ir was investigated

using the hydrodynamic modulation technique; these results are discussed in Section VII.

The electrochemistry of As(III) on Pd is not straightforward. Oxidation of arsenic that has either adsorbed or deposited on the surface occurs over a very wide range of potentials and the presence of arsenic on the surface appears to dramatically alter the formation of Pd oxide. These surface reactions introduce severe difficulties in determining the anodic current resulting from the oxidation of As(III) transported from the bulk solution to the electrode. There may be oxidation of soluble As(III) occurring between 1.00 V and 1.25 V, but it is surely a small fraction of the total As(III) flux. There is no anodic current on the reverse scan for $E_d < 1.1$ V, even though PdO reduction does not begin until $E_d = 0.5$ V. In this respect, PdO has effects similar to the Au(II) oxide, but is quite different from that of PtO. A slight rotation-speed dependence is obtained between 1.30 V and 1.42 V on the forward scan and 1.40 V and 1.20 V on the reverse scan. Neither the current on the forward scan nor the current on the reverse scan is a linear function of $\omega^{1/2}$. Evidently, the kinetics of the oxidation of As(III) on Pd are very slow, because even at relatively low rates of mass transfer to the electrode, the voltammogram appears to be highly irreversible. It was unfortunate that a Pd electrode compatible with the rotator used in the hydrodynamic modulation experiments was not available.

F. As(III) Electrochemistry on a Pt RDE in
Basic Media

The electrochemical behavior of As(III) in basic solutions is significantly different from that in acidic solutions. Figure V-20 is an illustration of an As(III) cyclic voltammogram on Pt in 0.5 M NaOH. A Pt residual curve is also included on this figure; note that in strong base the oxide formation wave is less distinct, the PtO reduction peak D is broader, and the sizes and shapes of the hydrogen adsorption and desorption peaks are altered, relative to the corresponding phenomena in acidic solutions. The addition of As(III) again gives an anodic peak C with $E_p = 0.23$ V; note that this potential is about 600 mV positive of the PtO reduction peak, whereas in an acidic solution, the corresponding anodic peak is only 400 mV positive of the oxide reduction peak. A relatively small anodic current is observed on the negative scan provided that the oxide coverage is small. Increasing the positive scan limit and thereby the oxide coverage causes the As(III) oxidation current to rapidly return to zero on the negative scan. The cathodic peak E at -0.67 V would, by analogy, be due to As(III) adsorption pseudocapacitance. A rough calculation of the "capacitance" at -0.4 V for 1, 6, and 10 V min⁻¹ gives values that range from 667 to 756 $\mu\text{F cm}^{-2}$; these values are clearly in the range of a pseudocapacitance. Note that peak E occurs 300 mV negative of the PtO reduction peak, while the analogous peaks in acid were not "resolved". Decreasing the negative potential scan limit to values less than -1.0 V does not lead to a large anodic stripping peak. This



Conditions: 1000 rpm
 6.0 V min⁻¹
 0.5 M NaOH + 0.20 mM As(III)

..... Pt residual
 ----- 0.4 V
 -.-.-.- 0.5 V
 ——— 0.6 V

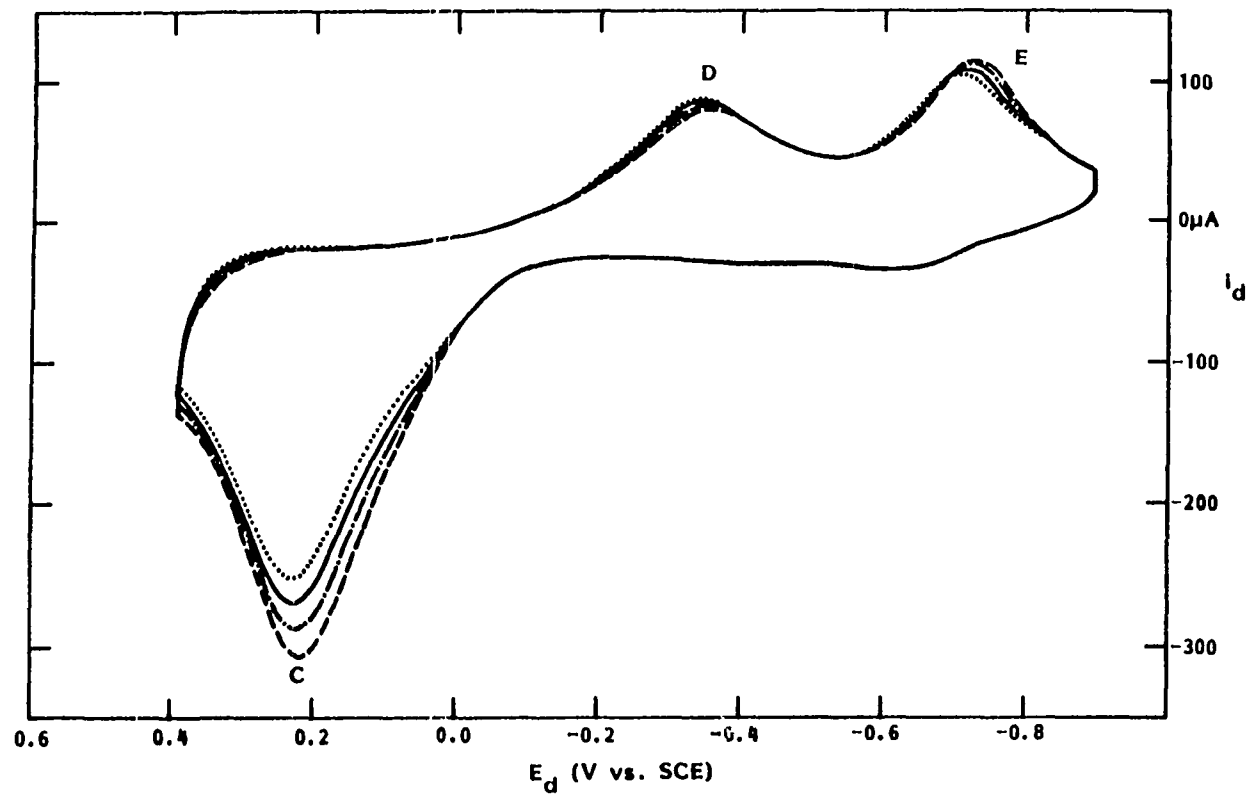
Figure V-20. Cyclic voltammograms of As(III) at a Pt RDE in basic solution as a function of E_a

means that appreciable bulk deposition of As does not occur in basic solutions on Pt.

A rotation-speed study (Figure V-21) established that the peak current of anodic wave C exhibits a small rotation-speed dependence, but that the anodic current on the negative scan is independent of rotation speed. This behavior is dramatically different from that in acidic solutions. The very slight increase in the adsorption pseudocapacity peak E with rotation speed is consistent with the concept of limiting, monolayer coverage of adsorbed As(III).

Examination of the peak currents as a function of scan rate leads to the conclusion that the anodic peak C and the cathodic peak E are the result of both surface and mass-transport controlled processes. For a given change in the scan rate, the shift in the anodic peak C is more pronounced in a basic solution than in an acidic solution. For example, a change in the scan rate from 1.0 V min^{-1} to 10.0 V min^{-1} causes a 145 mV positive shift in 0.5 M NaOH, but the same change in the scan rate in 0.5 M HClO₄ produces only a 50 mV shift.

The major differences in As(III) behavior in acidic and strongly basic solutions are these: a separation of the PtO reduction and pseudocapacity peaks; the different rates at which the anodic peak shifts as a function of scan rate; and the very limited anodic current obtained on the negative scan in base. Given the pK_a values for As(III) in solution (pK_1 8.62, pK_2 12.13, pK_3 13.40), it is clear that As(III) in 0.5 M NaOH would consist of HAsO_3^{2-} and AsO_3^{3-} . This has also been verified directly by Raman spectroscopy (4). On the basis of electrostatics, one



Conditions: 6.0 V min^{-1}

$0.5 \text{ M NaOH} + 0.200 \text{ mM As(III)}$

..... $\omega = 500 \text{ rpm}$

———— $\omega = 1000 \text{ rpm}$

- · - · - $\omega = 2000 \text{ rpm}$

----- $\omega = 4000 \text{ rpm}$

Figure V-21. Cyclic voltammograms of As(III) at a Pt RDE in basic solution as a function of ω

would expect that the oxidation would be even more favorable in base. It would, therefore, appear that changes in the electrode surface, specifically the nature of and coverage by PtO, are the predominant factors. As discussed in Section II.B, the exchange current density for oxide growth in a pH 14 solution is 10^3 times that in an acidic solution. It, therefore, follows that at any given overpotential, a greater oxide coverage would be formed on a Pt anode in base than in acid. This explains why positive scan limits that are only 100-200 mV positive of the anodic peak potential give very small anodic currents on the reverse scan (e.g., $i/i_{Lev} = 0.13$ for $E_a = 0.4$ V) and why further increments in E_a lead to even smaller currents. The slight rotation-speed dependence on the forward scan indicates that low oxide coverages in base can act as an oxidation catalyst. The lack of any rotation-speed dependence on the negative scan indicates that the oxide growth rate quickly leads to an anodic film that gives an apparent rate constant that is small relative to the rate of mass transfer, even at low rotation speeds.

As a function of scan rate, the peak potential of anodic peak C shifts about three times faster in a basic solution than it does in an acidic one. The peak in base also consists of a combination of Pt oxide formation, adsorbed As(III) oxidation, and oxidation of As(III) from the bulk. It is unlikely that oxidation of the adsorbed As(III) would differ in any significant way in the two media. Once again, however, the faster rate of oxide growth in base suggests why the anodic wave appears to be more irreversible in base. Conway's theory of Pt oxide growth (see

Section II.B) basically states that the initial oxide that is formed is reversible, but that irreversibility is introduced by both further oxidation and place-exchange when the potential is swept about 350 mV positive of onset of oxide formation. In base, where the overall rate is known to be 10^3 higher than in acid, it is reasonable to assume that the oxide formation would become irreversible at a somewhat smaller overpotential. In addition, the As(III) oxidation reaction itself appears to be most reversible, in a kinetic sense, on the thermodynamically reversible oxide. Therefore, in a basic solution, the introduction of thermodynamic irreversibility into the oxide formation at a lower overpotential and the kinetic irreversibility of As(III) oxidation on the thermodynamically irreversible PtO combine to give an overall oxidation wave that is somewhat more irreversible than the corresponding wave in an acidic solution. This, in turn, accounts for much larger shift in the peak potential with scan rate.

Given the large differences in the electrochemistry of As(III) in 0.5 M HClO₄ and in 0.5 M NaOH, it was of some interest to investigate the behavior at intermediate pH values. It was observed that the behavior in less-concentrated acidic solutions was essentially the same as that in 0.5 M HClO₄. The results presented here deal with several neutral and moderately basic solutions.

Significant pH gradients can exist in the vicinity of the double layer in unbuffered solutions; therefore, it was necessary that the experiments be performed in buffered solutions. This unfortunately led to the introduction of another supporting electrolyte, which in turn makes

exact comparisons impossible. The major concern here is the slight modifications of the oxide growth characteristics caused by the different adsorption properties of the anions in the supporting electrolyte. In order to minimize the effects of anion adsorption as much as possible, a 0.05 M sodium phosphate buffer was used; the pH was adjusted using concentrated HClO_4 and NaOH . Fortunately, as the pH of the buffer was changed, clear and unambiguous trends were observed which were large compared to the electrolyte effects.

Increases in pH caused all of the peaks observed in the i_d - E_d curves, i.e., the major anodic peak, the PtO reduction peak, and the As(III) adsorption peak to shift to more negative potentials vs. SCE. The major anodic peak shifted at a rate slightly less than the "normal" value of 59 mV/pH unit, averaging 53 mV/pH unit over a 4.18 pH unit change. The oxide reduction peak shifted at the slightly higher than normal rate of 67 mV/pH unit over the same range. The As(III) adsorption peak appeared to shift at a considerably higher rate, 87 mV/pH unit, but this value is based on only three values over a 2.60 pH unit range.

Experiments were performed where a constant overpotential was applied at each pH. This overpotential was attained by adjusting the positive scan limit to a value 200 mV positive of the anodic peak potential at each pH. Table V-1 gives the anodic current obtained on the negative scan as a function of pH. Assuming a value for the As(III) diffusion coefficient of $9.4 \times 10^{-6} \text{ cm}^2 \text{ sec}^{-1}$ (a value obtained in a 0.05 M borate buffer at pH 8.67, but total ionic strength of 0.5 M (365)) gives a mass-transport limited current at 108 μA . The observed current varies from 77% of the

Table V-1. Anodic current for As(III) oxidation on Pt as a function of pH

pH	i (anodic, μA)
6.90	83
8.10	57
9.11	40
10.02	37
11.08	32

Levich current at pH 6.90 to 30% at pH 11.08. In 0.5 M NaOH, the current was 10-12% of the Levich current for an equivalent overpotential, while in 0.5 M HClO₄ the corresponding value was at least 90%. There is a clear trend of a smaller apparent rate constant and, therefore, a smaller anodic current as the pH increases for a given overpotential. These results can also be rationalized in terms of the results of Damjanovic *et al.* (124) for the exchange-current density for oxide formation as a function of pH in basic solutions. Given the increase in exchange-current density with pH, a fixed overpotential would, of course, lead to a greater oxide coverage with pH. The effect of the exchange-current density also is seen in experiments where the positive scan limit was incremented at each pH; as the pH increases, a given increment (typically 0.1 V) has a larger effect on the anodic current. At the lower pH values, the anodic current was rotation-speed dependent on the forward scan and to a lesser extent on the negative scan. The anodic current on the negative scan formed a current plateau for pH up to and including pH 9.11. At pH < 10.02, a well-shaped plateau was not observed.

G. As(III) Electrochemistry on a Au RDE in
Basic Media

The oxidation of As(III) on Au in basic solutions was examined briefly. In general, the results were analogous to those obtained on Pt: the oxidation is kinetically limited to a significantly greater extent in the basic solutions than in the acidic solutions. Recall that in a 0.5 M HClO₄ solution, mass-transport limited currents were obtained on a Au anode over a range of potentials where a phase gold oxide was not present. This behavior is not observed in basic solutions. In 0.5 M NaOH, the As(III) anodic wave begins at -0.05 V, or only about 150 mV negative of the potential where an appreciable (i.e., bulk) oxidation of the Au surface occurs in the absence of As(III). The anodic wave is not as "sharp" as the reversible wave observed on Au in an acidic solution, and the wave has an inflection point at 0.14 V. The current reaches a peak at 0.34 V and then decreases rapidly as the disc potential is scanned to more positive potentials. This behavior in the oxide region is identical to that observed in acidic solutions: a rapid decrease in the current when an appreciable amount of gold phase oxide is formed. However, in a 0.5 M NaOH solution, there is no potential range where the As(III) current reaches the mass-transport limited value before phase oxide begins to inhibit the reaction. Scan reversal at 0.4 V does give a small current plateau (ca. 60 mV), but the current is estimated to be less than half of the mass-transport limited value and is not a linear function of $\omega^{1/2}$. Scan reversal at more positive potentials gives little or no

current on the negative scan until the gold oxide is electrochemically reduced.

The electrochemistry of As(III) on Au in a Bates and Bower borax buffer (HClO_4 was used instead of HCl) at pH 8.00 was, as expected, intermediate between that in strong acid and strong base. Gold phase oxide formation begins at 0.50 V in this buffer; addition of As(III) gives an anodic wave that begins at 0.21 V. A very sharp peak is obtained at 0.50 V; if the scan is reversed at this potential, the current on the reverse scan essentially retraces the current recorded on the forward scan. If the potential is allowed to scan positive of 0.50V, a local minimum is obtained at 0.61 V, followed by another, broader peak with $E_p = 0.83$ V. At $E_d > 0.83$ V, the current again decreases with potential until $\text{O}_2(\text{g})$ evolution begins at about 1.10 V. Reversing the scan direction at $E_d < 0.9$ V gives a small plateau on the reverse scan, the magnitude of which is a function of the positive limit. The currents on the forward scan and the reverse scan (provided that $E_d < 0.9$ V) are rotation-speed dependent. For a positive limit of 0.6 V, the plateau current is within about 5% of the Levich current if the rotation speed is low, again assuming that the diffusion coefficient is $9.4 \times 10^{-6} \text{ cm}^2 \text{ sec}^{-1}$. As $\omega^{1/2}$ is increased, the negative deviation from the Levich current becomes greater and greater. A scan-rate study shows that there is a surface process that contributes to the peak current at 0.50 V, but that the current on the negative scan is free of contributions from surface reactions.

To date, there has been no study of the exchange-current density for gold oxide formation over a wide range of electrolyte pH. Cyclic voltammograms of Au in the Bates and Bower buffer obtained at 24 V min^{-1} indicate that incipient oxidation may begin at potentials as negative as -0.075 V vs. SCE . As is the case in acidic solutions, the As(III) oxidation appears to be electrocatalyzed by the gold oxide precursor and inhibited by the phase gold oxide.

VI. POTENTIOSTATIC STUDIES OF As(III) OXIDATION

It was observed in experiments for which the electrode rotation speed was varied that the anodic current resulting from the oxidation of As(III) in solution was not a linear function of the square root of rotation speed. Recall that the Levich equation predicts just such a relationship, viz.

$$i = 0.62 nFAD^{2/3} \nu^{-1/6} (C^* - C_s) \omega^{1/2} . \quad \text{VI-1}$$

In Eq. VI-1, A is the geometric area of electrode, D is the diffusion coefficient, ν is the kinematic viscosity, C^* is the bulk concentration of the electroactive species, C_s is the concentration at the electrode surface and n and F have their usual electrochemical significance. For discussion purposes, the rotation speed ω will have units of revolutions per minute (rpm); however, the rotation speed must be converted to radians per second when Eq. VI-1 is used. A deviation from the Levich equation is indicative of "mixed kinetics", as discussed in Section IV. More precisely, this deviation can be caused by either a relatively slow chemical step (heterogeneous or homogeneous) or by a macroscopically inhomogeneous electrode surface. As derived in Section IV, the general form of the equation for the current is

$$i = \frac{nFADC^*}{\delta + K} , \quad \text{VI-2}$$

where δ represents the diffusion layer thickness at a homogeneously accessible electrode and K is a constant. For the case where a slow chemical step is involved, K is of the form D/k , where k is the

heterogeneous or homogeneous rate constant. For the case where an inhomogeneous electrode surface is involved, K is a complex function of the radius of the "active sites" and their distribution on the surface (see Section IV). For the rotating disc electrode, the diffusion layer thickness is equal to $1.61 D^{1/3} \nu^{1/6} \omega^{-1/2}$ (324). Substituting for δ in Eq. VI-2 gives

$$i = \frac{nFADC^*}{1.61 D^{1/2} \nu^{1/6} \omega^{-1/2} + K} \quad \text{VI-3}$$

Equation VI-3 can be algebraically transformed in two different ways to facilitate the evaluation of K . A plot of $i/\omega^{1/2}$ vs. i gives an intercept of $0.62 nFAD^{2/3} \nu^{-1/6} C^*$ (the slope of a "Levich plot") and a slope that is proportional to K . A plot of i^{-1} vs. $\omega^{-1/2}$ gives a slope that is the reciprocal of the "Levich slope" and an intercept that is $K/nFADC^*$. In the case of a heterogeneous reaction, the intercept becomes i_K^{-1} , where

$$i_K = knFAC^* \quad \text{VI-4}$$

Here, i_K represents the kinetic current that would be obtained in the absence of any mass-transfer effects, the so-called "true kinetic current." Both of these transformations of Eq. VI-3 have been used in the analysis of data obtained from potentiostatic experiments performed at rotating disc electrodes.

As Scheller, Landsberg, and Wolf (338) have pointed out, the product of D and the intercept of a plot of i^{-1} vs. $\omega^{-1/2}$ is a constant in the case of a partially-blocked (inhomogeneous) electrode. This was

verified by Scheller, Landsberg, and Wolf in experiments conducted on two completely different systems. In the first system, $\text{Fe}(\text{CN})_6^{3-}$ was reduced on a specially prepared model electrode. The model electrode was made by applying a photoresist to the surface of a Pt RDE and then exposing and developing the photoresist to generate a known number of active sites and a known degree of blockage. The diffusion coefficient and the kinematic viscosity were varied by the addition of glycerin; the value of the diffusion coefficient was calculated from the slope of the i^{-1} vs. $\omega^{-1/2}$ plot. The product was constant to within about 1%. In the second system, Scheller, Landsberg, and Wolf (338) conducted experiments on the reduction of ClO^- on a macroscopically inhomogeneous graphite electrode. In this case, the diffusion coefficient was varied by increasing the concentration of the KOH supporting electrolyte. Again, the product of D and the intercept of the i^{-1} vs. $\omega^{-1/2}$ plot was constant.

The Landsberg theory for mixed kinetics was tested for As(III) oxidation on a Pt RDE by varying the ionic strength of supporting electrolyte at a constant pH. The supporting electrolytes used were 0.5 M HClO_4 , 0.5 M HClO_4 + 2.25 M NaClO_4 , and 0.5 M HClO_4 + 4.50 M NaClO_4 . The NaClO_4 used to adjust the ionic strength was "analytical reagent" grade that was twice recrystallized from water in order to minimize Cl^- contamination. While it is possible to determine the value of the diffusion coefficient from the slope of a plot of i^{-1} vs. $\omega^{-1/2}$, the diffusion coefficient was independently determined. This was done by determining the slope of a plot of i vs. $\omega^{1/2}$ on a Au RDE, where Levich

behavior is observed (see Section V.C). Conventional cyclic voltammetry can, of course, be used for 0.5 M HClO₄, but in the case of 0.5 M HClO₄ + 2.25 M NaClO₄ and 0.5 M HClO₄ + 4.5 M NaClO₄ supporting electrolytes, a slightly different technique was required. As little as 0.01 ppm Cl⁻ can cause a shift in the As(III) oxidation wave observed at a Au RDE, and 0.13 ppm Cl⁻ causes the complete elimination of a limiting current plateau. Even using recrystallized NaClO₄, it is apparent that Cl⁻ contamination in excess of 0.13 ppm occurs in solutions with NaClO₄ concentrations greater than about 2 M. If, however, the potential is stepped from -0.100 V to +1.000 V, a limiting anodic current is obtained that lasts for several seconds, depending on the rotation speed. This is because Cl⁻ is desorbed from the electrode at -0.100 V and it takes a finite period of time, depending on the Cl⁻ flux, for a sufficient amount of Cl⁻ to accumulate on the disc to inhibit As(III) oxidation. Fitting the $i - \omega^{1/2}$ data with a least-squares program gave very small intercepts (relative to the measured limiting currents) and correlation coefficients greater than 0.9999, again establishing the Levich behavior of As(III) oxidation on a Au RDE.

The raw data for the i^{-1} vs. $\omega^{-1/2}$ plots was obtained in the following manner. At $t = 0$, the potential was stepped to 1.10 V. The electrode rotation speed was 300 rpm. At $t = 12, 18, 24, 30,$ and 60 minutes, the electrode rotation speed was linearly ramped from 300 rpm to 5000 rpm at 6000 rpm min⁻¹ and the current recorded as a function of the rotation speed. As soon as the rotation speed reached 5000 rpm, it was immediately reduced back to 300 rpm. Linear regressions were then

performed on the $i^{-1} - \omega^{-1/2}$ data for 12 rotation speeds. The correlation coefficients of these linear regressions were excellent, ranging from $r = 0.9981$ to $r = 0.9998$. According to theory, the slope of a plot of i^{-1} vs. $\omega^{-1/2}$ is the reciprocal of the Levich slope. Table VI-1 is a summary of the results obtained in the three supporting electrolytes of different ionic strengths.

The agreement between the theoretical slope and the experimentally determined slope is excellent for $I = 0.5$ M, very good for $I = 5.00$ M, and satisfactory for $I = 2.75$ M. While the average slope for $I = 2.75$ M is 6.7% less than the theoretical slope, this is not excessive given the uncertainties in A , D , ν , and C^* . Such agreement indicates that if potential, time, and $As(III)$ bulk concentration are fixed, Eq. VI-2 adequately describes the current resulting from the oxidation of $As(III)$ under mixed kinetic control at a Pt RDE. It is also quite clear that the product of D and the intercept of the i^{-1} vs. $\omega^{-1/2}$ plot is not a constant. These data can be compared qualitatively with that of Scheller, Landsberg, and Wolf (338), who obtained values of 2.20, 2.21, and $2.22 \times 10^{-8} \text{ cm}^2 \mu\text{A}^{-1} \text{ s}^{-1}$ for the analogous product in the $Fe(CN)_6^{4-}/Pt$ system. The conclusion to be drawn is that the condition of mixed kinetics that arises in the oxidation of $As(III)$ on Pt does not arise solely from the nonlinear diffusion of $As(III)$ to isolated active sites on the electrode surface. This does not preclude, however, the possibility that mechanism involves both nonlinear diffusion and a relatively slow chemical step. However, for purposes of discussion, the constant K in Eq. VI-3 will be equated with D/k ; subsequent analysis

Table VI-1. Summary of data collected to test the theory developed for a macroscopically inhomogeneous electrode surface

Time (min)	I ^a = 0.5 M		I = 2.75 M		I = 5.00 M	
	Slope ^b	D·int·10 ⁸ cm ² μA ⁻¹ s ⁻¹ ^c	Slope	D·int·10 ⁸ cm ² μA ⁻¹ s ⁻¹ ^d	Slope	D·int·10 ⁸ cm ² μA ⁻¹ s ⁻¹ ^e
12	+0.7	2.99	-4.8	3.36	-2.4	4.96
18	+0.4	3.56	-5.8	4.12	-3.3	5.98
24	+0.7	4.02	-5.8	4.72	-2.9	6.80
30	+0.0	4.48	-7.4	5.34	-4.2	7.66
60	-2.1	6.32	-9.9	7.65	-5.4	11.0

^a I = ionic strength.

^b Expressed as a % difference from the theoretical slope.

^c Product of the diffusion coefficient and the intercept of i^{-1} vs. $\omega^{-1/2}$ plot;
 $D = 1.15 \times 10^{-5} \text{cm}^2 \text{s}^{-1}$.

^d $D = 9.30 \times 10^{-6} \text{cm}^2 \text{s}^{-1}$.

^e $D = 6.60 \times 10^{-6} \text{cm}^2 \text{s}^{-1}$.

will be reported in terms of k , a chemical rate constant with dimensions of cm s^{-1} .

The numerical value of k has been determined under a number of conditions. Two different potentiostatic techniques were utilized to measure k at relatively short times. The first of these techniques was to record the i - t response following a potential step at 5 steady-state rotation speeds. These data were analyzed using the plot of $i/\omega^{1/2}$ vs. i and is summarized in Table VI-2. The theoretical intercept is $53.6 \mu\text{A s}^{1/2}$; the average value of intercepts of the linear regressions is $54.3 \mu\text{A s}^{1/2}$, which is only 1.3% high. There is no clear trend in k as a function of potential, but at a given potential, k decreases with increasing time. The second method of determining k at relatively short times is to simply apply Eq. VI-3 (with $K = D/k$) to the i - t response for a fixed potential and a fixed rotation speed. Typical data, obtained at potentials between 0.9 V and 1.2 V and at a rotation speed of 2000 rpm, is given in Table VI-3. At a given potential, k decreases monotonically with time. For a fixed time, k decreases monotonically as the potential increases. There does not appear to be any simple relationship between k and t for times between 20 s and 140 s that is applicable to all four values of potential. The values of k calculated from i - t data at a fixed rotation speed are quite comparable to the values given in Table VI-2.

Table VI-2. Summary of the parameters from linear regression analysis performed on data from potentiostatic experiments at steady-state rotation speeds

Potential (V vs. SCE)	t = 30s			t = 60s		
	$i\omega^{-1/2}(\mu\text{A s}^{1/2})^a$	$k(\text{cm s}^{-1})^b$	r	$i\omega^{-1/2}(\mu\text{A s}^{1/2})$	$k(\text{cm s}^{-1})$	r
0.8	57.2	0.021	0.9908	57.4	0.021	0.9930
0.9	49.4	0.011	0.9972	49.0	0.0075	0.9871
1.0	50.5	0.068	0.9977	51.3	0.047	0.9946
1.1	52.9	0.030	0.9937	55.4	0.020	0.9959
1.2	55.8	0.013	0.9853	62.8	0.0076	0.9874

^aTheoretical intercept = 53.6 $\mu\text{A s}^{1/2}$.

^bCalculated from $k = \frac{(0.6005)D^{2/3}\nu^{-1/6}}{\text{slope}}$.

Table VI-3. Calculated^a values for $k(\text{cm s}^{-1})$ at various times after a potential step at $t=0$

E (V vs, SCE)	+20 s	+30 s	+60 s	+120 s
0.9	0.0483	0.0474	0.0449	0.0429
1.0	0.0345	0.0335	0.0321	0.0306
1.10	0.0298	0.280	0.0264	0.0246
1.2	0.0242	0.227	0.0200	0.0175

^aCalculated from $i = nFADC*/(\delta+D/k) = 8.52 \times 10^{-2}/(1.14 \times 10^{-3} + 1.15 \times 10^{-5}/k)$.

The raw data used to determine k at longer polarization times were obtained using the technique described earlier, in which the rotation speed was linearly ramped from low speeds to high speeds. Initially, it was felt that it would be useful to compare the kinetic parameters for As(III) oxidation with those of a reaction known to be reversible. There have been numerous studies that have shown that Br^- oxidation on Pt is reversible (see ref. 366 and the citations therein). Unfortunately, as these studies will show, the kinetics of Br^- oxidation on Pt electrodes having a significant oxide coverage are not as straightforward as one might assume. Nevertheless, some results from Br^- oxidation will be included for comparison purposes.

One series of experiments performed to determine k used the Model ASR rotator. This rotator uses a rather large RDE. This, in turn, limits the rate at which the rotation speed can be scanned. The maximum rate was determined by ramping the rotation speed from low speeds to high speeds and then back to low speeds. Any differences in current at a given rotation speed can be attributed to slow response of the rotator. No differences in current were observed at $\omega > 600$ rpm when the rotation speed was scanned at $5000 \text{ rpm min}^{-1}$. At $100 \text{ rpm} < \omega < 600 \text{ rpm}$, the effects of rotator response could be observed at $5000 \text{ rpm min}^{-1}$; in this range of rotation speeds, the rate of change was limited to $2000 \text{ rpm min}^{-1}$. A similar kind of response was observed by Miller, Bellavance, and Bruckenstein (367).

The electrode was potentiostated at $0.9 \text{ V} - 1.2 \text{ V}$ for As(III) oxidation and was potentiostated at $1.1 - 1.3 \text{ V}$ for Br^- oxidation. Following a polarization time of 15 min, the $i - \omega^{1/2}$ data were taken as described above. These data are summarized in Table VI-4 for As(III) oxidation and Table VI-5 for Br^- oxidation. Sixteen rotation speeds between 350 rpm and 4075 rpm were used in the linear regressions for As(III). The theoretical intercept for the As(III) reaction is $6.05 \mu\text{A s}^{1/2}$; the average of the four values from the linear regressions is $5.58 \mu\text{A s}^{1/2}$, which is 7.8% low. The values of k decrease as the potential increases. The values for k are somewhat higher than might be expected, given the longer polarization time. For the linear regressions of the Br^- data, 14 rotation speeds between 850 rpm and 4075 rpm were

used. A value of $1.58 \times 10^{-5} \text{cm}^2 \text{s}^{-1}$ (368) was used for the diffusion coefficient of Br^- .

Table VI-4. Summary of parameters from linear regressions on As(III) data obtained by linearly ramping the rotation speed. ASR rotator

Potential (V vs. SCE)	$i\omega^{-1/2} (\mu\text{A s}^{1/2})^a$	$k (\text{cm s}^{-1})^b$	r
0.9	5.53	0.0892	0.9976
1.0	5.61	0.0516	0.9989
1.1	5.47	0.0249	0.9953
1.2	5.71	0.0108	0.9988

^aTheoretical intercept = $6.05 \mu\text{A s}^{1/2}$.

^bCalculated from $k = \frac{(0.6005)D^{2/3}v^{-1/6}}{\text{slope}}$.

Table VI-5. Summary of parameters from linear regressions on Br^- data obtained by linearly ramping the rotation speed. ASR rotator

Potential (V vs. SCE)	$i\omega^{-1/2} (\mu\text{A s}^{1/2})^a$	$k (\text{cm s}^{-1})^b$	r
1.1	38.7	0.225	0.9727
1.2	38.4	0.215	0.9813
1.3	37.7	0.184	0.9898

^aTheoretical intercept = $39.0 \mu\text{A s}^{1/2}$.

^bCalculated from $k = \frac{(0.62)D^{2/3}v^{-1/6}}{\text{slope}}$.

The average of the experimental intercepts is $38.2 \mu\text{A s}^{1/2}$, just 2% less than the theoretical intercept. The values of k are significantly greater than those for As(III) oxidation and are in the range where the reaction is usually considered to be reversible. It should be noted, however, that these values are 2-4 orders of magnitude smaller than the corresponding heterogeneous rate constants for the electron transfer reactions, as calculated from the values of the transfer coefficient and the exchange current density given by Rubinstein (366) and the applied overpotentials. In other words, at these overpotentials, another slow chemical process, characterized by the k values given in Table VI-5, is rate limiting.

The acquisition of data using the technique of linearly ramping the rotation speed was later modified by using the MSR rotator. The high-torque motor and the less-massive electrode permitted the use of somewhat higher rates of change of rotation speed. These results are given in Table VI-6 for As(III) and Table VI-7 for Br^- . At least 14 rotation speeds were used in the As(III) linear regressions and at least 12 rotation speeds were used in the Br^- linear regressions. The average of the intercepts from the linear regressions of the As(III) data is the same as the theoretical value. The values for k obtained with the MSR rotator are 15-50% smaller than those obtained with the ASR rotator. The reason for this difference is not known. For Br^- , the average of the intercepts of the linear regressions is 3.8% less than the theoretical intercept. The values for k at 1.1 V and 1.3 V are in excellent agreement with the values given in

Table VI-6. Summary of parameters from linear regressions on As(III) data obtained by linearly ramping the rotation speed. MSR rotator

Potential (V vs. SCE)	$i\omega^{-1/2} (\mu\text{A s}^{1/2})^a$	$k (\text{cm s}^{-1})^b$	r
0.9	2.72	0.0630	0.9837
1.0	2.71	0.0436	0.9868
1.1	2.90	0.0207	0.9941
1.2	3.35	0.00532	0.9954

^aTheoretical intercept = $2.92 \mu\text{A s}^{1/2}$.

^bCalculated from $k = \frac{(0.6005)D^{2/3}v^{-1/6}}{\text{slope}}$.

Table VI-7. Summary of parameters from linear regressions on Br⁻ data obtained by linearly ramping the rotation speed. MSR rotator

Potential (V vs. SCE)	$i\omega^{-1/2} (\mu\text{A s}^{1/2})^a$	$k (\text{cm s}^{-1})^b$	r
1.1	16.78	0.233	0.9767
1.2	17.23	0.176	0.9749
1.3	16.66	0.173	0.9810

^aTheoretical intercept = $17.54 \mu\text{A s}^{1/2}$.

^bCalculated from $k = \frac{(0.62)D^{2/3}v^{-1/6}}{\text{slope}}$.

Table VI-5, but the value obtained as 1.2 V is 18% less than the corresponding value in Table VI-5.

The same data that were used to test the Landsberg theory of macroscopic inhomogeneity (see Table VI-1) can be used to give values of k as a function of time and ionic strength. These data are collected in Table VI-8. It is clear that k is dependent on the ionic strength. The values at $I = 2.75$ M are $50 \pm 2\%$ of the values at $I = 0.5$ M, and the values at $I = 5.00$ M are $24 \pm 2\%$ of the values at $I = 0.5$ M. The best linear correlation between k and polarization time for all three ionic strengths came from plots of k vs. $\log t$. Linear regressions of k on $\log t$ gave the results below:

$$\begin{aligned} I = 0.50 \text{ M: } k(\text{cm s}^{-1}) &= 0.0415 - 0.0166 \log t(\text{min}); r = 0.9955, \\ I = 2.75 \text{ M: } k(\text{cm s}^{-1}) &= 0.0230 - 0.0100 \log t(\text{min}); r = 0.9927, \\ I = 5.00 \text{ M: } k(\text{cm s}^{-1}) &= 0.0118 - 0.00526 \log t(\text{min}); r = 0.9936. \end{aligned}$$

Table VI-8. Values of $k(\text{cm s}^{-1})$ as a function of time and the ionic strength I at a constant pH. Applied potential 1.10 V vs. SCE

Time (min)	$I = 0.5$ M	$I = 2.75$ M	$I = 5.00$ M
6	0.0355	0.0174	0.00797
12	0.0245	0.0126	0.00607
18	0.0205	0.0103	0.00503
24	0.0182	0.00898	0.00443
30	0.0163	0.00795	0.00393
60	0.0116	0.00554	0.00275
90	0.00910	---	---
120	0.00767	---	---

The regressions for $I = 0.5 \text{ M}$ and $I = 2.75 \text{ M}$ do not include the data taken at $t = 6 \text{ min}$. For $I = 0.5 \text{ M}$, the fitted value for $t = 1 \text{ min}$ is within a factor of about 2 of the values given in Tables VI-2 and VI-3.

Another series of experiments were performed in order to evaluate the effect of pH on k in acidic solutions. These experiments were performed in solutions with a constant ionic strength of 1.00 M , adjustments again made with recrystallized NaClO_4 . The data are collected in Table VI-9.

The linear regressions of k on $\log t$ are given below:

$$\begin{aligned} \text{pH} = 0.0: & \quad k(\text{cm s}^{-1}) = 0.0294 - 0.0115 \log t(\text{min}); \quad r = 0.9997, \\ \text{pH} = 0.4: & \quad k(\text{cm s}^{-1}) = 0.0325 - 0.0136 \log t(\text{min}); \quad r = 0.9956, \\ \text{pH} = 1.0: & \quad k(\text{cm s}^{-1}) = 0.0144 - 0.00617 \log t(\text{min}); \quad r = 0.9914, \\ \text{pH} = 2.0: & \quad k(\text{cm s}^{-1}) = 0.0132 - 0.00586 \log t(\text{min}); \quad r = 0.9914. \end{aligned}$$

Table VI-9. Values of $k(\text{cm s}^{-1})$ as a function of time and pH at a constant ionic strength and a constant overpotential

Time(min)	pH = 0.0	pH = 0.5	pH = 1.0	pH = 2.0
6	0.0227	0.0207	---	0.00998
12	0.0170	0.0182	0.00805	0.00707
18	0.0150	0.0153	0.00661	0.00571
24	0.0136	0.0134	0.00576	0.00490
30	0.0123	0.0121	0.00516	0.00432
60	0.00900	0.00861	0.00369	0.00293

For any given time, the value of k for pH 0.0 and 0.5 are very similar. At pH 1.0 and 2.0, two effects are observed. While the values of k_1 (i.e., k at $t=1$ min) are very similar for pH 1.0 and 2.0, they are roughly half of the values obtained at pH 0.0 and 0.5. Similarly, the rate of decrease of k with time about the same for pH 1.0 and 2.0, but this rate of decrease is about half the rate of decrease at pH 0.0 and 0.5.

While the mechanism of As(III) oxidation on noble metal electrodes will be discussed in detail in Section VIII, it can be pointed out here that the relationship between k and $\log t$ strongly implies that the Pt oxide coverage is a key factor in determining the numerical value of k . It is well-known that under potentiostatic conditions, Q_{oxide} is a linear function of $\log t$.

There are, however, some additional complexities present in the kinetics of the oxidation of As(III) on Pt. One simple way to illustrate this complexity is to generate i - t curves at a series of values for the As(III) flux. The Levich equation (Eq. VI-1) predicts that the limiting current is a linear function of both C^* and $\omega^{1/2}$. In Figure VI-1, the current-time response is shown for the oxidation of As(III) at a Pt RDE following a potential step to 1.10 V at a fixed rotation speed. The quotient of the current sensitivity (i.e., $\mu\text{A}/\text{inch}$) divided by the bulk concentration was maintained constant for 4 bulk concentrations. In Figure VI-2, the current-time response following the same potential step is recorded, but the bulk concentration of As(III) was a constant and the quotient of the current sensitivity divided by $\omega^{1/2}$ ($\text{radians}^{1/2}\text{sec}^{-1/2}$) was maintained a constant over 5 different $\omega^{1/2}$. If the relationship

Figure VI-1. Potentiostatic $i-t$ response as a function of $[\text{As(III)}]$

Conditions: 955 rpm

0.5 M HClO_4

E_d 2.2 V

----- $[\text{As(III)}] = 0.515 \text{ mM}; 50 \text{ } \mu\text{A/in}$

-·-·-· $[\text{As(III)}] = 1.026 \text{ mM}; 100 \text{ } \mu\text{A/in}$

-·-·-· $[\text{As(III)}] = 1.534 \text{ mM}; 149.6 \text{ } \mu\text{A/in}$

———— $[\text{As(III)}] = 2.039 \text{ mM}; 198.8 \text{ } \mu\text{A/in}$

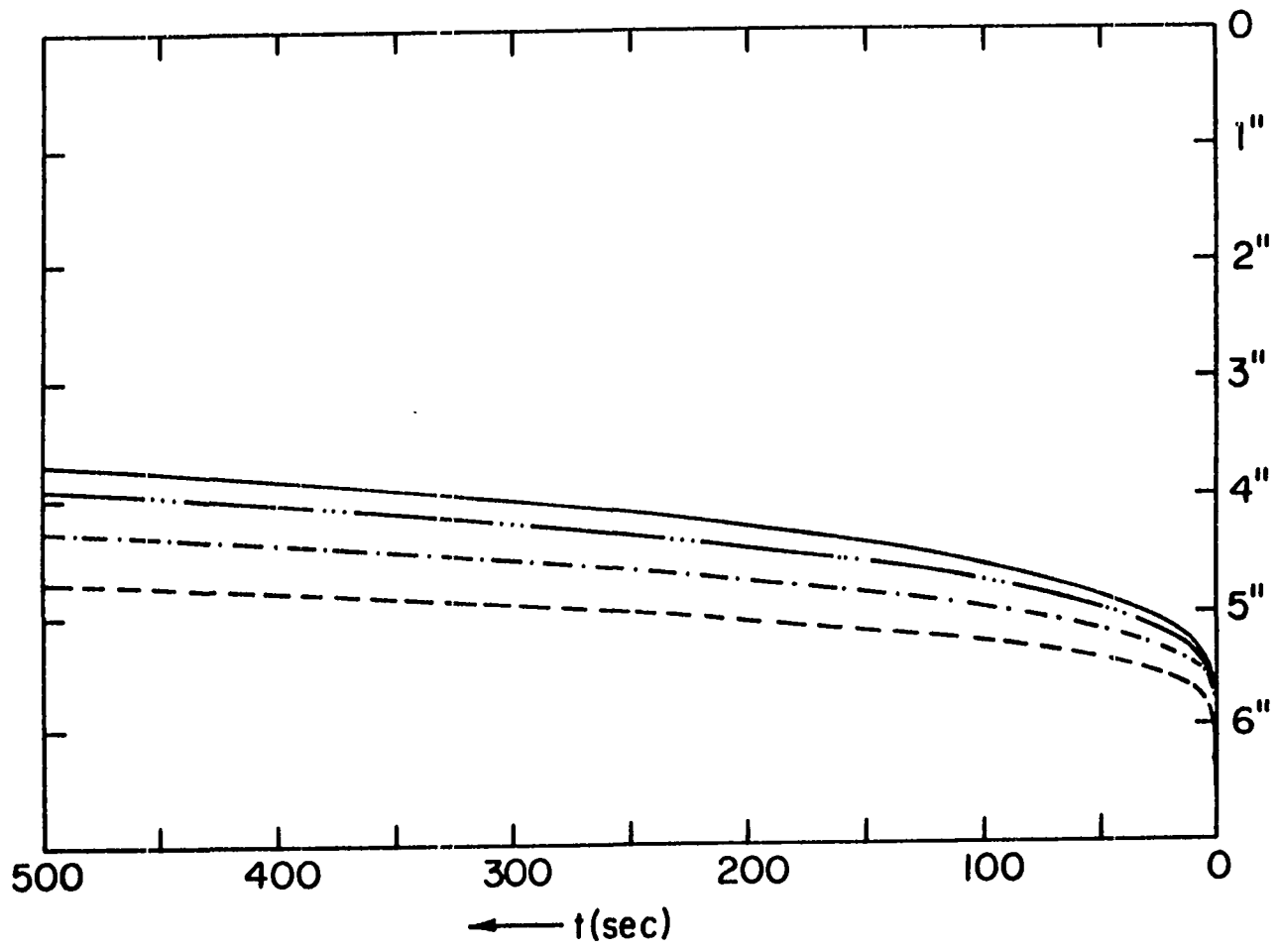


Figure IV-2. Potentiostatic i - t response as a function of $\omega^{1/2}$

Conditions: 0.5 M HClO_4 + 2.039 mM As(III)

E_d 1.1 V

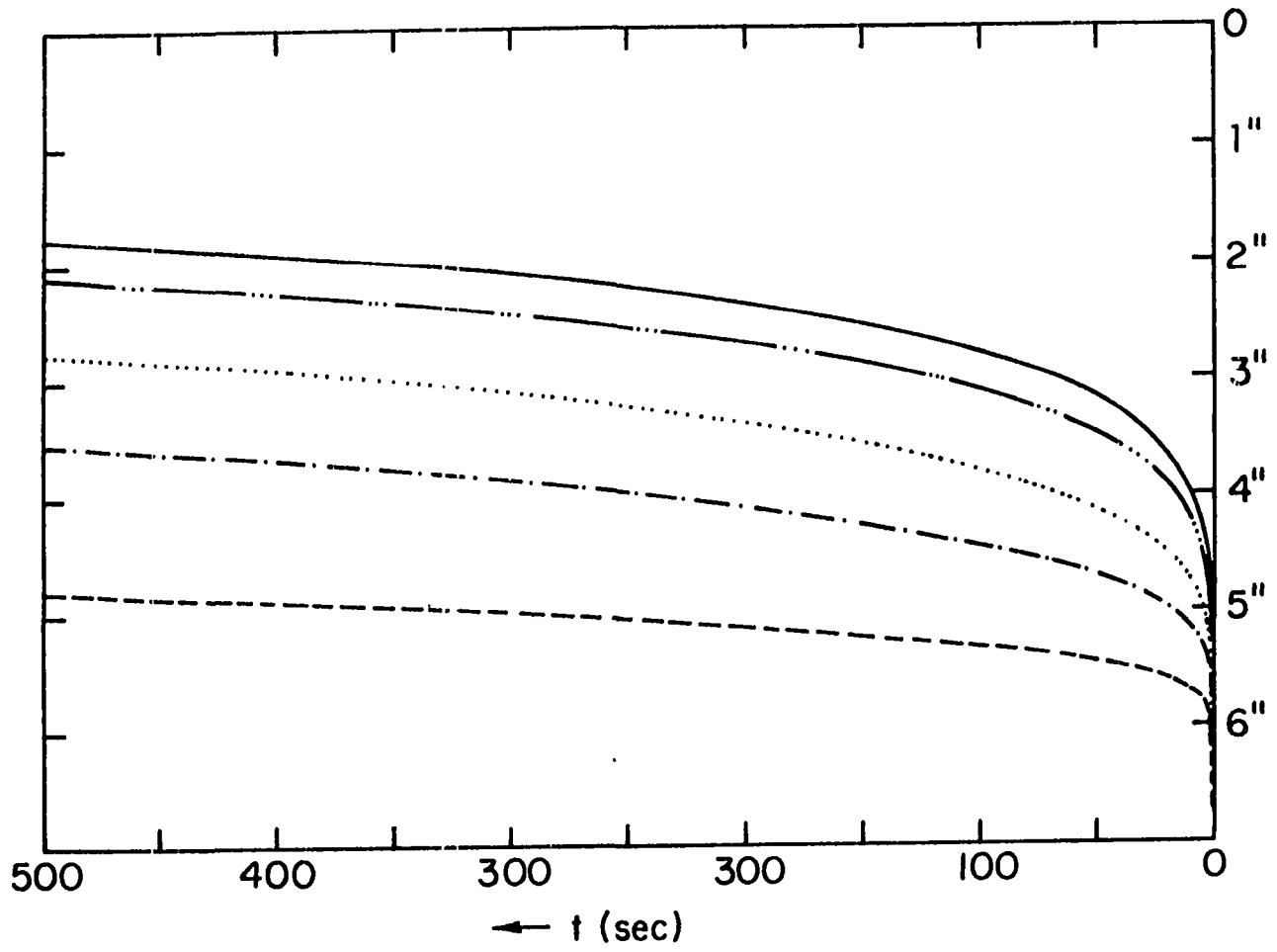
----- $\omega^{1/2} = 5.00 \text{ rad}^{1/2} \text{ s}^{-1/2}$; 100 $\mu\text{A/in}$

-.-.-.- $\omega^{1/2} = 10.00 \text{ rad}^{1/2} \text{ s}^{-1/2}$; 200 $\mu\text{A/in}$

..... $\omega^{1/2} = 15.00 \text{ rad}^{1/2} \text{ s}^{-1/2}$; 300 $\mu\text{A/in}$

-.-.-.- $\omega^{1/2} = 20.00 \text{ rad}^{1/2} \text{ s}^{-1/2}$; 400 $\mu\text{A/in}$

_____ $\omega^{1/2} = 25.00 \text{ rad}^{1/2} \text{ s}^{-1/2}$; 500 $\mu\text{A/in}$



between i and C^* was that of the Levich equation, then the four i - t curves of Figure VI-1 would be superimposed. The fact that they are not superimposed is indicative of mixed kinetics. The same conclusion can be drawn from Figure VI-2. Figures VI-1 and VI-2 are convenient ways of illustrating the effects of significant changes in the rate of mass transfer on a reaction proceeding under mixed kinetic control.

The basic equation of mixed kinetics at a rotating disc electrode is

$$i = \frac{nFADC^*}{1.61 D^{1/3} \nu^{1/6} \omega^{-1/2} + K} \quad \text{VI-3}$$

This equation predicts that for a fixed rotation speed and a fixed value of K , a plot of i vs. C^* should be linear and have a zero intercept. Earlier in this section, K was tentatively identified with D/k , where k is a chemical rate constant. It has been shown that k is a function of several parameters. It was expected that if polarization time, applied potential, ionic strength, and pH were either held constant or fixed, then some reproducible value of k also would be fixed. These conditions are met in Figure VI-1 by selecting a time t and simply determining i at each C^* using the deflection of the recorder and the current sensitivity. A different value of t would give different value of k and would, therefore, product a different slope for a plot of i vs. C^* .

Earlier work (364) at Iowa State University stated that a plot of i vs. C^* was linear, but that the intercept was not zero. These data were obtained from cyclic voltammograms; the nonzero intercept was attributed to inadequate correction for the background current. Replotting the original data has confirmed that the intercept is not zero. Similar

cyclic voltammograms obtained in this study (see Figure V-1) also give anodic currents that are a linear function of concentration, but also give nonzero intercepts. Potentiostatic experiments, especially at the As(III) concentrations that were used and at times greater than a few seconds, should not be subject to any appreciable error due to background current. When the currents given in Figure VI-1 are plotted versus C^* at a number of given times, a family of linear plots all having a zero intercept is not obtained. At short times, a "best fit" of these data is linear but has an intercept of $+30 \mu\text{A}$. If the plot is constrained to a $0 \mu\text{A}$ intercept, the point at $C^* = 2.04 \text{ mM}$ falls beneath the line. As the polarization time increases, a plot of i vs. C^* becomes increasingly more curvilinear. A more sensitive measure of linearity is the ratio i/C^* . If i and C^* truly are related by a linear function, then i/C^* should be a constant. In fact, i/C^* is not a constant for any given time, and, furthermore, the relative deviation in i/C^* increases with the polarization time. For example, for $t = 12.5\text{s}$, i/C^* for $C^* = 0.515 \text{ mM}$ is $548 \mu\text{A mM}^{-1}$ and i/C^* for $C^* = 2.039 \text{ mM}$ is $510 \mu\text{A mM}^{-1}$; the relative decrease is 7%. At $t = 500 \text{ s}$, the analogous relative decrease is 21%. It should be pointed out that i/C^* for various C^* is, in fact, constant for both the oxidation of As(III) on Au (a reaction that exhibits Levich behavior) and the reduction of ferricyanide on special Pt electrodes (336,337) -- a system where the basic equation for mixed kinetics (Eq. VI-3) is applicable. This nonlinearity means that the rate constant k is not simply a function of potential, time, ionic strength, and pH, but is somehow determined to some extent by the As(III) flux itself. In other

words, for a fixed potential, time, ionic strength, and pH, different values of k will be obtained at different levels of As(III) flux. The fact that k is influenced by the As(III) flux and not simply by the As(III) bulk concentration is discerned from an analysis of the data on Figure VI-2, where the concentration was held constant and the flux was varied by changing the rotation speed. From Equation VI-3

$$i/\omega^{1/2} = \frac{nFADC^*}{1.61 D^{1/3} \nu^{1/6} + (D/k)\omega^{1/2}} \quad \text{VI-5}$$

The ratio $i/\omega^{1/2}$ is a function of $\omega^{1/2}$; therefore, a plot of $i/\omega^{1/2}$ vs. $\omega^{1/2}$ is expected to be curvilinear, $i/\omega^{1/2}$ decreasing as $\omega^{1/2}$ increases. However, Eq. VI-5 can be solved for k for various values of $\omega^{1/2}$ at a fixed time. For example, at $t = 100$ s, $i/\omega^{1/2} = 106 \mu\text{A s}^{1/2}$ for $\omega^{1/2} = 5.01 \text{ s}^{-1/2}$; solving Eq. VI-5 gives $k = 0.0233 \text{ cm s}^{-1}$. For the same time, $i/\omega^{1/2} = 55.8 \mu\text{A s}^{1/2}$ for $\omega^{1/2} = 25.00 \text{ s}^{-1/2}$; solving Eq. VI-5 gives $k = 0.0144 \text{ cm s}^{-1}$.

As was the case with the data at different ionic strengths and different pH, the best correlation found between k and t for all of the various values as As(III) flux is k vs. $\log t$. However, good correlations between k and $\log t$ were obtained only for $t > 100$ s; the relationship between k and t for $t < 100$ s will be discussed in Section VIII. These correlations are summarized in Table VI-10 for the data from Figure VI-1, and in Table VI-11 for the data from Figure VI-2. The values of k_1 are large because in this case the time scale was in seconds. The general trend is toward smaller values of k_1 and toward greater rates of decay as the flux increases. These results indicate quite clearly that

Table VI-10. Summary of parameters of linear regressions of k vs. $\log t$ (s). $\omega^{1/2} = 10.00 \text{ rad}^{1/2} \text{ s}^{-1/2}$

$C^*(\text{mM})$	$k_1(\text{cm s}^{-1})^a$	Slope	r
0.515	0.0937	-0.0265	0.9976
1.026	0.0690	-0.0199	0.9989
1.534	0.0579	-0.0171	0.9966
2.039	0.0496	-0.0147	0.9976

^aValue of k at $t = 1 \text{ s}$.

Table VI-11. Summary of parameters of linear regressions of k vs. $\log t$ (s). $C^* = 2.039 \text{ mM}$

$\omega^{1/2} (\text{rad}^{1/2} \text{ s}^{-1/2})$	$k_1 (\text{cm s}^{-1})^a$	Slope	r
5.01	0.0526	-0.0149	0.9988
10.00	0.0430	-0.0124	0.9990
15.00	0.0408	-0.0120	0.9988
20.00	0.0340	-0.00994	0.9985
25.00	0.0353	-0.0106	0.9974

^aValue of k at $t = 1 \text{ s}$.

the rate constant of the rate-determining step is in part fixed by the flux of As(III) at the electrode. While this conclusion is undoubtedly unusual, perhaps the most plausible explanation is that the nature of the oxide film is affected by the occurrence of a simultaneous faradaic reaction on the electrode. This point will be discussed in more detail in Section VIII.

Not only is the As(III) flux an important factor, but the length of time that the electrode is polarized at that flux also is important. For example, an electrode was polarized at 1.10 V in a 2.54 mM As(III) solution. After 1000 s, the current was 48.0% of the Levich (mass transport limited) value. Then the same electrode was polarized at the same potential and at the same rotation speed, but in a 0.258 mM As(III) solution. After about 500 s, additional As(III) was added to bring the total concentration to 2.54 mM. In this case, the current after a total of 1000 s was 57.2% of the Levich value. A somewhat similar experiment was conducted at longer polarization times. In this experiment, the electrode was first polarized at 1.10 V for 35 min in the supporting electrolyte only. After this 35 min of oxide growth, As(III) was added to give a 5.00 mM solution. At $t = 35 \text{ min} + 500 \text{ s}$, the anodic current was 55.6% of the calculated Levich current. If the electrode was polarized from $t=0$ in the 5.00 mM As(III) solution, the current at $35 \text{ min} + 500 \text{ s}$ was 26.4% of the Levich current. Depletion of As(III) under these conditions is estimated to be less than 1%. Interestingly, when the electrode was polarized for 35 min at the same potential and at the same rotation speed, but in a solution of supporting electrolyte that was 4.88 mM in As(V), the addition

of As(III) to make the solution 5.00 mM in As(III) gave a current at $t = 35 \text{ min} + 500 \text{ s}$ that was 41.8% of the Levich current. Since As(V) does not undergo any anodic reactions, no effect was expected.

The importance of oxide coverage as well as applied potential can be demonstrated by potentiostatic experiments. At a fixed bulk concentration and a fixed rotation speed, the i - t behavior was recorded for 30 minutes following 3 different potential-step sequences. In the first, the potential was stepped from 0.00 V to 1.100 V. In the second, the potential was stepped to 1.200 V for 5 minutes and was then stepped to 1.100 V for the remaining 25 minutes. In the third sequence, the potential was stepped from 0.00 V to 1.400 V and held for 5 minutes and then stepped to 1.100 V for the remaining 25 minutes. The current-time behavior for the first sequence was the usual slow decay with time (e.g., Figure VI-1 or Figure VI-2). The current after 30 minutes was 58.4% of the Levich current. In the second sequence, the current decayed at a somewhat higher rate during the first 5 minutes; following the potential step to 1.100 V, there was a very small ($< 1 \mu\text{A}$) decrease in current, but the decay rate (di/dt) decreased to a value that was identical with the first potential sequence. For this sequence, the current at $t = 30 \text{ min}$ was 53.5% of the Levich current. In the third sequence, the current decreased by ca. $30 \mu\text{A}$ following the potential step from 1.400 V to 1.100 V, but the decay rate for $t > 5 \text{ min}$ was the same as that for the other two sequences. In this case, the current at $t = 30 \text{ min}$ was only 34.8% of the Levich current. Evidently, the total quantity of oxide is important in fixing the value of k , and the phenomenon that is responsible for the

decrease in k with time at a given potential (possibly oxide aging) is independent of the oxide coverage.

A few potentiostatic experiments have been performed on anode materials other than Pt. A potentiostatic experiment at long (35 min) polarization times was performed on an Ir RDE. The electrode was polarized at 1.10 V for 35 min in the supporting electrolyte alone, then sufficient As(III) was added to make the solution 5.00 mM. At $t = 35 \text{ min} + 500 \text{ s}$, the anodic current was 79.2% of the mass transport limited current. This can be compared with the 55.6% obtained under identical conditions on Pt. When the solution contained As(III) during the entire polarization time, the current at $t = 35 \text{ min} + 500 \text{ s}$ was 72.5% of the Levich current. The corresponding value using a Pt electrode was 26.4%. When polarization occurred in the presence of As(V), the As(III) anodic current obtained at $t = 35 \text{ min} + 500 \text{ s}$ was only 51.4% of the Levich current. Recall that under identical conditions on Pt, the effects of polarization in the presence of As(V) were intermediate between those of supporting electrolyte only and those of supporting electrolyte plus As(III). Nevertheless, it is clear that the Ir electrode does give significantly greater currents for As(III) oxidation than does Pt, especially in the case where electrode polarization occurs in the presence of As(III).

Two potentiostatic experiments on Au were performed. In an experiment where a 0.5 M HClO_4 + 0.515 mM As(III) solution was potentiostated at 0.900 V, a very unusual i - t behavior resulted. Based on a cyclic voltammogram of the same solution, it was expected that current

would not change as a function of time. Instead, the current slowly decreased for the first two minutes, rapidly decreased for about the next four minutes to a value about 35% of the mass-transport limited value, and then resumed a relatively slow rate of decrease.

The cause of the abnormal behavior exhibited in these separate techniques was found to be trace Cl^- in the HClO_4 reagent. A spectrophotometric determination of Cl^- in 5.0 M HClO_4 using the mercury(II) thiocyanate method (369) showed that the concentration was $< 10^{-6}$ M. This meant that the $[\text{Cl}^-]$ in the concentrated reagent was in fact considerably less than the label value. Nevertheless, even this very small concentration can lead to "fouling" the electrode in potentiostatic experiments at a RDE or in SHMV experiments (Section VII), where the scan rate is limited to 0.1 - 0.3 V min^{-1} . The adsorption of Cl^- on Au is well known (370), and the effect of somewhat larger chloride concentrations on the As(III) oxidation on Au was previously observed by Lown (364). As little as 0.017 ppm Cl^- causes a positive shift in the $E_{1/2}$ of the As(III) oxidation wave. The limiting current plateau is eliminated by the addition of about 0.1 ppm in cyclic voltammetry experiments at 1.0 V min^{-1} and 955 rpm. However, when standard additions of Cl^- were made to a 5.0 M HClO_4 solution to give Cl^- concentrations of 0.02 ppm, 0.04 ppm, etc., the $E_{1/2}$ for bulk oxide formation (1.16 V) did not shift from the value obtained in the absence of added Cl^- . Since Cl^- causes a positive shift in the As(III) oxidation wave on Au at disc potentials in the range 0.85 V to 1.02 V and Cl^- does not cause any shift in Au oxidation wave obtained in the absence of As(III), it can be concluded that Cl^- does not inhibit

the As(III) reaction by altering the bulk phase oxide. Rather, Cl^- appears to poison the electrocatalyst by blocking the formation of an active surface moiety, possibly the gold oxide precursor. This explanation is preferred over one which attributes these Cl^- effects to a simple surface fouling. The $E_{1/2}$ for this reaction is over 500 mV positive of the thermodynamic potential for the As(III,V) couple, yet the shape of the wave is characteristic of a reversible reaction. These two facts lead to the conclusion that the reaction occurs when a potential-dependent surface specie is formed on the electrode surface.

When the potential of a Au RDE was set a 0.600 V in a Bates and Bower borax buffer (see Section V.C) at pH 8.00, the resulting anodic current was initially within 2-3% of the Levich current, but the current decayed at a steady rate of $2.5 \mu\text{A min}^{-1}$, or about 1.1% of the Levich current per minute. This decrease is attributed to a very slow formation of the Au(III) oxide at 0.600 V. Oxide growth is not apparent at this potential in this electrolyte unless a fairly high potential scan rate is used. A cyclic voltammogram of Au obtained in the supporting electrolyte alone, at a potential scan rate of 24 V min^{-1} and with $E_a = 0.6 \text{ V}$ gives a reduction peak for a quasi-reversible oxide 0.54 V and a second reduction peak at 0.27 V, indicating the presence of an irreversible oxide as well.

While it is not the expressed purpose of this dissertation to develop another analytical technique for the determination of As(III), it should be noted that the technique of triple-pulse amperometry (TPA) developed by Hughes (322) can be applied to determination of As(III) in flowing streams. The optimum TPA parameters found were: $E_1 = 1.000 \text{ V}$; $t_{E_1} = 60$

msec; $E_2 = 0.900$ V; delay time = 15 msec; and $E_3 = 0.200$ V. The analytical signal in this application of TPA is the current sampled 15 msec after the potential step to 0.900 V. In a TPA experiment performed at a Pt RDE, a plot of sampled current vs. $\omega^{1/2}$ was linear for rotation speeds up to at least 6000 rpm. The application of TPA to the determination of As(III) by flow injection analysis would be superior in many respects to the potentiostatic method given by Lown and Johnson (371).

VII. STUDIES USING HYDRODYNAMIC MODULATION OF A ROTATING DISC ELECTRODE

A. Theory

Rotating disc electrodes operating at a steady rotation speed have been in use since the 1930s. About 1970, applications of hydrodynamic voltammetry began to appear in which the electrode rotation speed was changed in some programmed manner simultaneously with the linear scan of the electrode potential. The earliest of these applications involved the variation of the rotation speed ω as a function of time in order to generate "automated Levich plots" (i.e., i_d vs. $\omega^{1/2}$). While this kind of technique can be useful, an even more useful technique can be obtained by modulating the electrode rotation speed about a fixed center speed. Miller, Bruckenstein, and co-workers have been primarily responsible for the development of the theory and the practice of "sinusoidal hydrodynamic modulation at the rotating disc electrode (SHMRDE)." A brief overview of the theory of SHMRDE, as it was historically developed, is presented here.

Miller, Bellavance, and Bruckenstein (367), in a general study of the feasibility of programmed speed control at rotating disc electrodes, made the assumption that the Levich equation adequately describes the relationship between the current i and the electrode rotation speed ω during changes in ω . The Levich equation is given by

$$i = 0.62 nFA D^{2/3} \nu^{-1/6} (C^* - C_s) \omega^{1/2} \quad \text{VII-1}$$

where C^* is the bulk concentration of the electroactive species, C_s is the

concentration at the electrode surface, and all other terms have their usual electrochemical meaning. Suppose that the rotation speed is sinusoidally modulated between ω_1 and ω_2 about the center rotation speed $\omega_0 = (\omega_1 + \omega_2)/2$. The current will modulate about a dc component proportional to $\omega_0^{1/2}$ and will have an ac component with a peak-to-peak Δi of

$$\Delta i = 0.62 n F A D^{2/3} \nu^{-1/6} (C^* - C_s) \Delta \omega^{1/2}, \quad \text{VII-2}$$

where $\Delta \omega = \omega_2 - \omega_1$. Equations VII-1 and VII-2 can be combined to give

$$\Delta i = \frac{i_0}{\omega_0^{1/2}} \Delta \omega^{1/2}. \quad \text{VII-3}$$

With proper signal processing, the modulating component can be recorded. This permits effective discrimination between convective-diffusion processes that obey the Levich equation and nonconvective-diffusion processes, such as oxide growth or solvent decomposition, that are independent of ω . In this same paper (367), they observed that following a step change in ω , the corresponding change in the convective-diffusion current took more time than could be accounted for on the basis of rotator performance. The additional delay was attributed to what Miller, Bellavance, and Bruckenstein called a "hydrodynamic relaxation process". The modulated signal showed no discernable response when oxygen and hydrogen were evolved on a Au electrode.

In 1974, Miller and Bruckenstein (372) reported several applications of SHMRDE to trace analysis. They state without proof that at low modulation frequencies (i.e., a few Hz) and small amplitudes

($\Delta\omega^{1/2}/\omega_0^{1/2} < 0.1$) there is no serious deviation from the hydrodynamic steady state.

A slightly more sophisticated theoretical treatment was presented and experimentally verified by Miller and Bruckenstein (373) in 1974 as well. In this treatment, they begin with the Butler-Volmer equation of electrode kinetics for the process $Ox + Ne \rightleftharpoons Red$

$$i = nFAk_0 \{C_{red}^0 \exp(\alpha_a F(E-E^0)/RT) - C_{ox}^0 \exp(-\alpha_c F(E-E^0)/RT)\} \quad VII-4$$

Here, k_0 is the standard heterogeneous rate constant, α_a is the transfer coefficient for the anodic reaction, and α_c is the transfer coefficient for the cathodic reaction. Anodic currents and overpotentials are positive. From Eq. VII-1

$$C_{s,ox} = C_{ox}^* + i/B_{ox}\omega^{1/2} \quad VII-5$$

and

$$C_{s,red} = C_{red}^* - i/B_{red}\omega^{1/2}, \quad VII-6$$

where $B = 0.62 nFAD^{2/3}\nu^{-1/6}$.

Substituting Eq. VII-5 and VII-6 into Eq. VII-4 and solving for i gives Eq. VII-7:

$$i = \frac{nFAk_0 \{C_{red}^* \exp(\alpha_a F(E-E^0)/RT) - C_{ox}^* \exp(-\alpha_c F(E-E^0)/RT)\}}{1 + \frac{nFAk_0}{\omega^{1/2}} \left[\frac{\exp(-\alpha_c F(E-E^0)/RT)}{B_{ox}} + \frac{\exp(\alpha_a F(E-E^0)/RT)}{B_{red}} \right]} \quad VII-6$$

Differentiating i in Eq. VII-7 with respect to $\omega^{1/2}$ and defining

$$k_E = nFAk_0 \left[\frac{\exp(-\alpha_c F(E-E^0)/RT)}{B_{ox}} + \frac{\exp(\alpha_a F(E-E^0)/RT)}{B_{red}} \right], \quad \text{VII-8}$$

it can be shown that

$$di/i = (d\omega^{1/2}/\omega^{1/2}) \{k_E/(k_E + \omega^{1/2})\}. \quad \text{VII-9}$$

For small modulations about a center rotation speed ω_0

$$d\omega^{1/2}/\omega^{1/2} \approx \Delta\omega^{1/2}/\omega_0^{1/2} \quad \text{VII-10}$$

and

$$di/i \approx \Delta i/\bar{i}, \quad \text{VII-11}$$

where \bar{i} is the current at ω_0 . Hence,

$$\Delta i/\bar{i} = (\Delta\omega^{1/2}/\omega_0^{1/2}) \{k_E/k_E + \omega_0^{1/2}\} \quad \text{VII-12}$$

Having arrived at Eq. VII-12, Miller and Bruckenstein (373) then considered three limiting cases. At either the anodic or cathodic limiting current, the term $k_E/k_E + \omega_0^{1/2} \longrightarrow 1$, so Eq. VII-12 reduces to

$$\Delta i_{lim}/\bar{i}_{lim} = \Delta\omega^{1/2}/\omega_0^{1/2}, \quad \text{VII-13}$$

where the subscript "lim" designates the limiting convective-diffusion condition. This is, of course, the same result obtained earlier. Now consider the case of a reversible reaction at a potential where the

limiting convective-diffusion current is not obtained. Since k_0 is large for a reversible reaction, $k_E \gg \omega^{1/2}$, and Eq. VII-12 then becomes

$$\Delta i / \bar{i} = \Delta \omega^{1/2} / \omega_0^{1/2}. \quad \text{VII-14}$$

In other words, normalized plots of \bar{i} / \bar{i}_{lim} vs. E and $\Delta i / \Delta i_{lim}$ vs. E should superimpose for all values of E for a reversible reaction. For a totally irreversible reaction, Miller and Bruckenstein obtain the result

$$\bar{i}_{lim} / \bar{i} = \sqrt{\Delta i_{lim} / \Delta i}. \quad \text{VII-15}$$

Equation VII-15 is derived by recognizing that k_E approaches either a cathodic or an anodic limit, substituting either limited form of k_E into equation VII-14, and eliminating the B_{Ox} or B_{Red} term using Eq. VII-5 or VII-6. Substituting this result and Eq. VII-13 into VII-12 gives Eq. VII-15. It should be pointed out that the value of the convective-diffusion current for an irreversible reaction may or may not be known.

Nevertheless, Eq. VII-15 indicates that normalized plots of \bar{i} / \bar{i}_{lim} and $\Delta i / \Delta i_{lim}$ would not superimpose for an irreversible reaction, as they do for a reversible reaction. Miller and Bruckenstein (373) then went on to experimentally verify this theory using the reduction of Pd(II) as an example of a totally irreversible reaction, the Fe(III)/Fe(II) couple at Au in 1M HCl as an example of mixed kinetic and convective-diffusion control, and the $\text{Fe}(\text{CN})_6^{3-} / \text{Fe}(\text{CN})_6^{4-}$ couple at Au in 1 M KCl as an example of convective-diffusion control. Good agreement between Equations VII-13, VII-14, and VII-15 and the experimental results was obtained.

Tokuda, Bruckenstein, and Miller (374) considered the response of the modulated current as a function of the modulation frequency. This is of importance because higher modulation frequencies permit the use of higher potential scan rates without distortion of the Δi -E curves. The response is reported in terms of a dimensionless parameter A, which is equal to 1 at hydrodynamic steady state. The response parameter A can be calculated by solving a complex set of ordinary differential equations obtained from physicochemical hydrodynamics. Response parameter A is tabulated as a function of two general parameters: 1) the relative modulation frequency $p = \sigma/\omega_0$, where σ is the modulation frequency in radians s^{-1} and ω_0 is the center rotation speed, also in radians s^{-1} ; and 2) the Schmidt number $Sc = \nu/D$. As expected, A decreases as p and Sc increase. The theory predicts that, within a range of conditions defined by p and the quantity $\epsilon = \Delta\omega_0^{1/2}/\omega_0^{1/2}$, the total current will be determined by convective-diffusion processes only; outside of this range of conditions, the current is determined by a coupling of convective-diffusion and a deviation from a hydrodynamic quase-steady state. The theory was verified over a wide range of p and for Schmidt numbers from 230-2100 for the reduction of Fe(III) on Pt.

Tokuda and Bruckenstein (375) extended the complexity of SHMRDE theory. Normalized current functions were calculated as a function of potential and as a function of λ , the rate of electron transfer relative to the rate of mass transfer, for a wide variety of p, Sc, and k_0 . Reversible, quasi-reversible, and irreversible reactions were considered. Kanzaki and Bruckenstein (376) experimentally verified the theory of

Tokuda and Bruckenstein (375), again using the reduction of $\text{Fe}(\text{CN})_6^{3-}$ and $\text{Fe}(\text{III})$ on Pt as examples of reversible and quasi-reversible processes, respectively. The reduction of $\text{Tl}(\text{III})$ in 0.1 M HCl + 1.0 M HClO_4 was used as an example of an irreversible electrode reaction. At $p = 0.05$, the normalized current-potential curve and the $(\Delta i/\Delta i_L)^{1/2}$ -potential curve for $\text{Tl}(\text{III})$ reduction could be superimposed, in accordance with theory. At $p = 0.24$, these two curves could not be superimposed, demonstrating that superposition is a limiting law for $p \rightarrow 0$.

Albery, Hillman, and Bruckenstein (377) refined the theoretical treatment of the hydrodynamics and considered galvanostatic experiments conducted under hydrodynamic modulation conditions.

B. Studies of $\text{As}(\text{III})$ Oxidation on Pt

Utilizing SHMRDE

The experimental parameters used in the following experiments are as follows. The mean (center) rotation speed ω_0 was 2000 rpm (209.4 radians s^{-1}); $\omega_0^{1/2}$ was therefore 44.72 $\text{rpm}^{1/2}$ (14.47 $\text{radians}^{1/2} \text{sec}^{-1/2}$). The modulation amplitude $\Delta\omega$ was 40 rpm (4.2 radians s^{-1}) peak-to-peak, giving a $\Delta\omega^{1/2}$ of 6.3 $\text{rpm}^{1/2}$ (2.0 $\text{radians s}^{-1/2}$). The relative modulation parameter $\varepsilon = \Delta\omega^{1/2}/\omega_0^{1/2}$ defined by Tokuda, Bruckenstein, and Miller (374) was equal to 0.14. The modulation frequency was 3 Hz (19 radians s^{-1}). The constant p , also defined by Tokuda, Bruckenstein, and Miller as the ratio of the modulation frequency to the mean rotation frequency was 0.09. From Table III of reference 374, it can be concluded that the modulation current is determined solely by convective-diffusion processes.

In other words, deviations from hydrodynamic quasi-steady state are negligible. The lock-in amplifiers were usually operated with a 12 db/octave roll-off and with a time constant of 3-4 seconds, although time constants as small as 1 second and as large as 10 seconds were occasionally used. The potential scan rate was usually 100 mV min^{-1} , but again, scan rates as low as 60 mV min^{-1} and as high as 300 mV min^{-1} was used, depending on the electrode material and the time constants in use.

Oxygen evolution on Pt begins at about 1.35 V in 0.5 M HClO_4 . The "concentration" of H_2O at the electrode surface is obviously not a function of the electrode rotation speed; therefore, the Δi for oxygen evolution should be zero. This was tested for the supporting electrolyte alone, using the same experimental conditions as were used in recording the Δi - E_d curves in the presence of As(III). These conditions included compensation for a small phase shift that was observed between the modulation signal applied to the rotator and the modulated current. The phase shift was compensated for by simply nulling the lock-in amplifier output that was in quadrature (90° out of phase) with the modulated current. There was no modulated signal observed on the forward scan for potentials up to 1.7 V, although there was a very small amount of noise at potentials greater than 1.5 V. There was a significant amount of "ringing" that occurred on the negative potential immediately following scan reversal at positive scan limits of 1.6 V or greater. This "ringing" consisted of large (approximately 6-8 times the peak-to-peak noise) anodic and cathodic oscillations that were damped as the potential scanned toward

more negative values. At a potential of 1.45 V on the negative scan, this experimental artifact was no longer evident. This "ringing", though significant, did not severely limit the experiments, since the maximum oscillations were still 8-10 times smaller than the Δi observed in the presence of As(III).

Figure VII-1 illustrates the results of a series of SHMRDE experiments; the only parameter varied was the positive potential scan limit. The potential scan rate in these experiments was 300 mV min^{-1} . Between 0.0 V and about 0.7 V on the forward scan, the Δi is zero. This is entirely consistent with the conclusions drawn earlier, i.e., that only surface-controlled processes are occurring in this potential region on the forward scan. At about 0.72 V, a very sharp anodic Δi wave begins, having an $E_{1/2}$ of 0.78 V. Using the general voltammetric current-potential equation for a reversible wave, the equation

$$E_{2/3} - E_{1/3} = \frac{0.0356 \text{ V}}{n} \quad \text{VII-16}$$

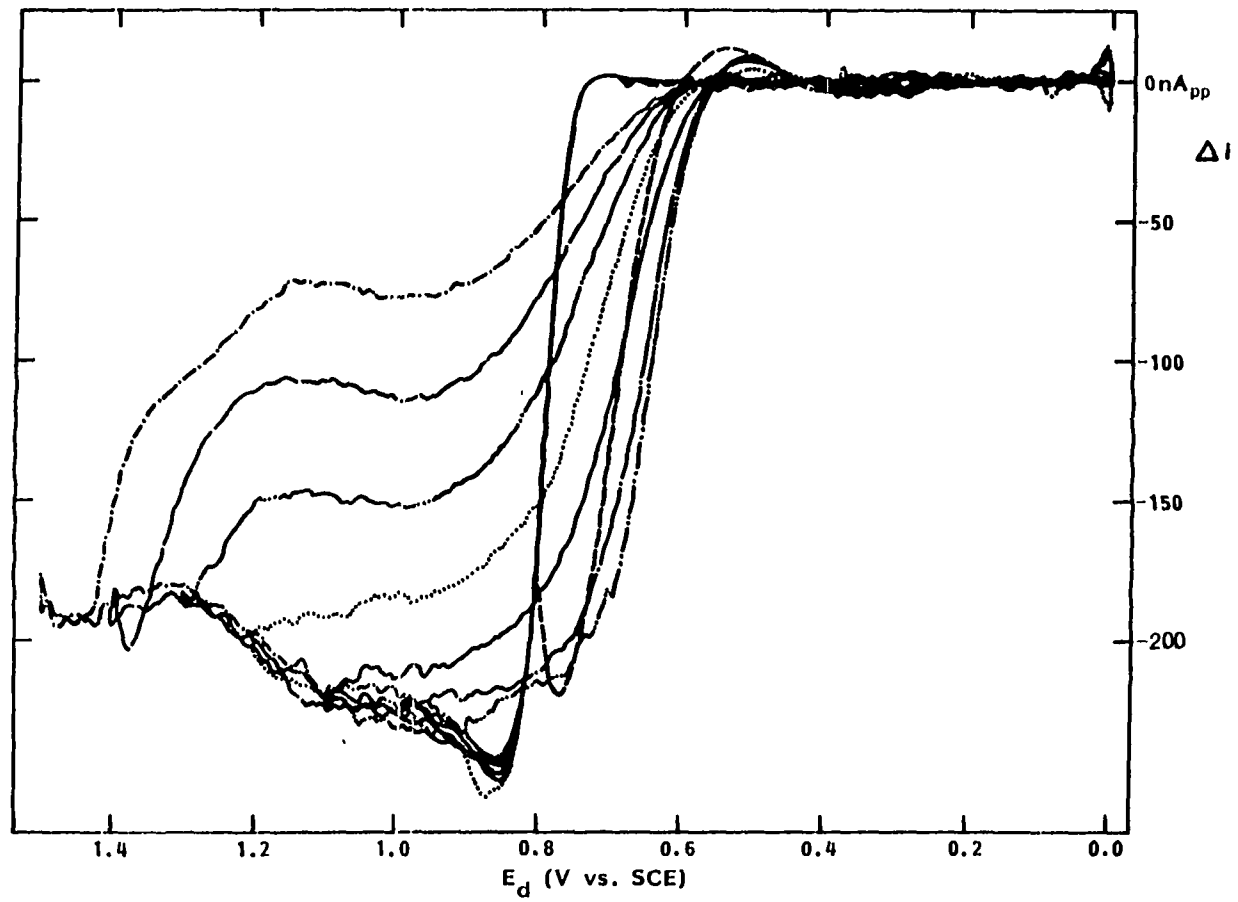
can be derived. For $n = 2$, $E_{2/3} - E_{1/3}$ should be 17.8 mV. For this $\Delta i - E_d$ wave, $E_{2/3} - E_{1/3}$ is 20 mV. It would appear that the oxidation of As(III) to As(V) is reversible, at least in the vicinity of 0.8 V. However, the thermodynamic reduction potential for the As(V)/As(III) couple is 0.32 V, so the overpotential at the onset of As(III) oxidation is 400 mV. This logical contradiction will be discussed in greater detail later on.

The onset of As(III) oxidation on the forward scan is highly reproducible and is independent of electrode history, provided that surface oxides are not present. The remainder of the $\Delta i - E_d$ curve is

Figure VII-1. SHMRDE voltammogram of As(III) at Pt as a function of E_a

Conditions: 0.3 V min^{-1}
 $0.5 \text{ M HClO}_4 + 0.200 \text{ mM As(III)}$

----- 0.8 V
-.....- 0.9 V
-.-.-.- 1.0 V
————— 1.1 V
..... 1.2 V
-.-.-.- 1.3 V
- - - - 1.4 V
-.....- 1.5 V

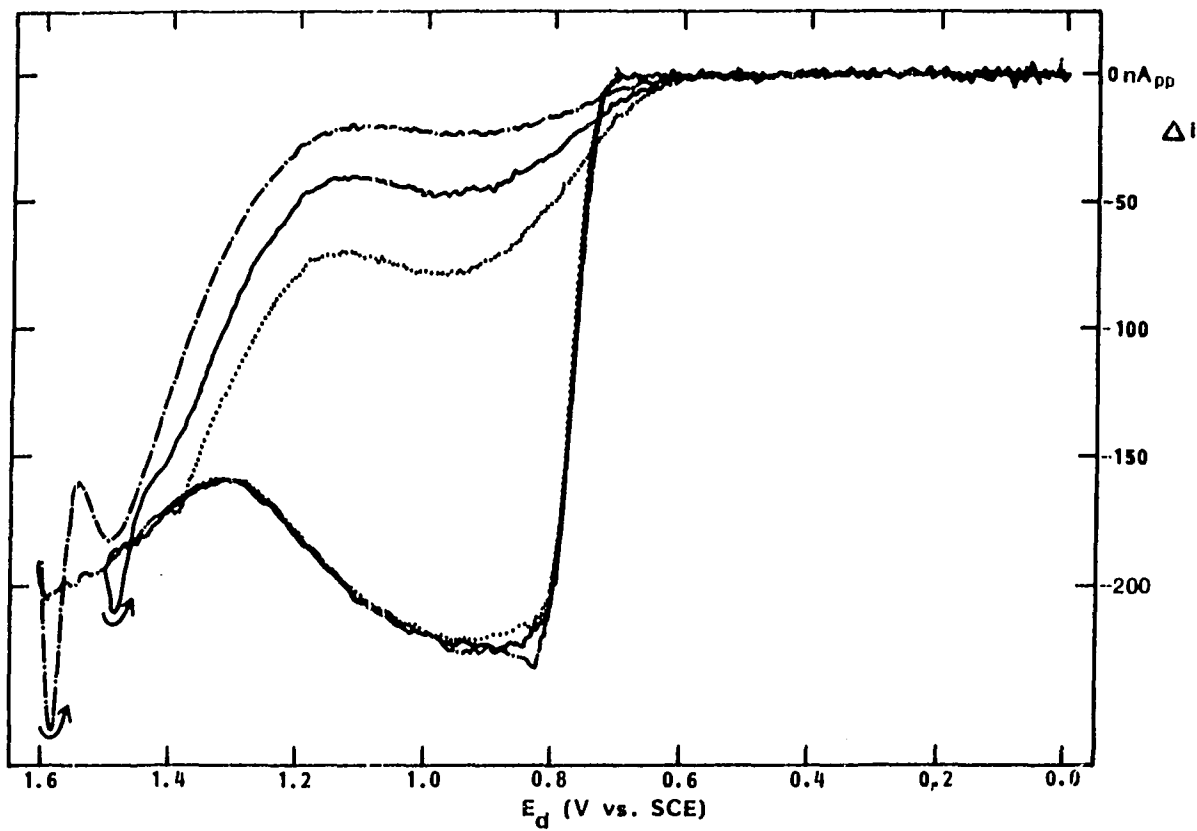


highly dependent on the positive potential scan limit. If the scan direction is reversed at 0.8 V, on the rising portion of the wave, the Δi continues to increase, peaks at 0.77 V, and then decreases to zero as the potential becomes less positive. The $E_{1/2,rs}$ (the half-wave potential on the reverse scan) is ca. 100 mV negative of the $E_{1/2,fs}$ (the half-wave potential on the forward scan). The oxidation is, in a thermodynamic sense, more reversible in the presence of the small amount of surface oxide formed under these conditions.

A limiting value of Δi is attained at 0.85 V on the forward scan. Given the results of the RRDE studies and SHMRDE results obtained at a slower scan rate, there probably is a small amount of overshoot in Δi at this potential. The value of Δi should be relatively constant over the range 0.85 - 1.0 V (see Figure VII-2). Scan reversal at 0.9 V gives an $E_{1/2,rs}$ of about 0.64 V, or 140 mV negative of the $E_{1/2,fs}$. As the positive limits are increased above 1.0 V, three effects are observed. The first of these effects is the development of three potential regions on the reverse scan: two potential-dependent regions and a potential-independent region. For $E_a < 1.2$ V, Δi on the reverse scan simply decreases from the value that Δi had at the positive potential scan limit. For $E_a > 1.2$ V, a Δi plateau is also obtained on the reverse scan and this Δi is very much a function of the scan limit. But for $E_a > 1.2$ V, there is an additional potential-dependent region that gives an initial rapid decrease in Δi until the potential has decreased to 1.15-1.20 V. The second of these effects is a positive shift in $E_{1/2,rs}$ as E_a becomes more positive. The $E_{1/2,rs}$ for $E_a = 1.0$ V is 5-10 mV positive of $E_{1/2,rs}$

for $E_a = 0.9$ V; the $E_{1/2rs}$ for $E_a = 1.1$ V is 30 mV positive of the $E_{1/2,rs}$ for $E_a = 1.0$ V; and so on. The third effect is the arrest in the decrease in Δi on the forward potential scan that occurs at about 1.3 V. This last effect can be seen on Figure VII-1, but is even more clearly seen on Figure VII-2. The only difference in experimental parameters is that the scan rate used to record the $\Delta i-E_d$ curves on Figure VII-2 was 100 mV min^{-1} . The slower scan rate allows slightly more positive potentials to be attained with minimum of noise. The ringing phenomenon described previously is clearly marked on Figure VII-2. It should again be emphasized that ringing begins only after scan reversal. It is significant that Δi begins to increase at precisely the same potential that oxygen evolution begins. It would seem that simultaneous $\text{O}_2(\text{g})$ evolution modifies in some manner the kinetics of As(III) oxidation.

The most likely qualitative explanation for the shape of these $\Delta i-E_d$ curves is that the kinetics of As(III) oxidation is determined in some manner by the nature and amount of Pt oxide on the surface, but that the rate of oxidation also can be enhanced by simultaneous oxygen evolution. Scanning the potential beyond 0.85 V leads to an increased oxide coverage. The surface oxide does not completely passivate the electrode, as is the case with many anodic reactions, but does become somewhat less active with potential and/or coverage. Oxygen evolution "reactivates" the electrode surface, with the extent of reactivation again dependent on the rate of oxygen evolution and/or potential. The rapid decrease in Δi following scan reversal at potentials greater than 1.3 V is due to the rapid decrease in the rate of oxygen evolution as the potential



Conditions: 0.1 V min^{-1}

$0.5 \text{ M HClO}_4 + 0.200 \text{ mM As(III)}$

..... 1.4 V

———— 1.5 V

- · - · - · 1.6 V

Figure VII-2. SHMRDE voltammogram of As(III) at Pt at high values of E_a

becomes less positive; this phenomenon is known from numerous studies of the oxygen evolution reaction on Pt (51, 280-282). However, as Damjanovic and Jovanovic (284) have pointed out, oxide growth does continue during oxygen evolution, although at a somewhat lesser rate. The additional oxide growth that occurs in the oxygen evolution region leads to additional decreases in the magnitude of Δi on the reverse scan. It must be pointed out that for a given E_a , the normalized modulated current, using the Δi plateau values and Δi at 0.85 V, is a much smaller fraction than the normalized current obtained by normal cyclic voltammetry. It would appear that oxide age is also an important factor. Additional details on the mechanism of As(III) oxidation on Pt will be discussed in Section VIII.

In addition to these voltammetric results, some experiments were performed in which Δi was recorded as a function of time following a potential step. The disc potential was stepped from 0.0 V to potentials from 0.8 V to 1.6 V in 0.1 V increments. The results were consistent with the voltammetric results. A potential step to 0.8 V gave a large Δi that decayed slowly as a function of time. Potential steps to 0.9 V, 1.0 V, 1.1 V, and 1.2 V resulted in successively smaller Δi that decayed at successively greater rates. The Δi -t behavior for a potential step to 1.3 V is essentially identical to that for a step to 1.2 V. For steps to 1.4 V, 1.5 V, and 1.6 V, successively greater Δi are obtained that decay at successively smaller rates. Equivalent Δi -t curves are obtained for potential steps to 0.8 V and 1.6 V.

C. Brief Study of As(V) Electrochemistry on Pt
Utilizing SHMRDE

As stated in Section V.B, it was initially believed that an As(V) voltammogram on a Pt RDE was totally determined by surface reactions. Surface reactions do not give a Δi response; therefore, it was predicted that an As(V) Δi - E_d voltammogram would be flat. Indeed, such a voltammogram at the same Δi sensitivity as used in the As(III) experiments gave no discernible Δi response. Two more voltammograms, one at a 10 times greater Δi sensitivity and the same lock-in amplifier time constant, and the second at a 10 times greater Δi sensitivity and a much lower time constant were recorded. Both of these actions greatly increased the base line noise. It is now known that the small quantity of As(V) that undergoes an underpotential deposition on Pt is transported from the bulk solution (see Section V.B). In retrospect, it now appears probable that a small cathodic Δi , not attributable to electronic noise, is present at E_d between 0.2 V and 0.3 V. The reason that a larger Δi was not observed is that the As(V) flux was large, due to the As(V) concentration (0.19 mM) and the rotation speed ($\omega_0 = 2000$ rpm). It is now predicted that at a much smaller As(V) flux that a cathodic Δi signal could be generated. This technique might prove useful in determining if other up processes proceed through prior adsorbed states.

D. Study of As(III) Oxidation on Ir
Utilizing SHMRDE

In the case of Pt, the most positive potential that could be used was about 1.7 V. This limit is evidently related to the relative magnitudes of the dc background current due to oxygen evolution and the ac signal resulting from convective-diffusion processes. Iridium, being a much better oxygen evolution catalyst than platinum (219,318), has a correspondingly lower positive potential limit. This limit is about 1.5 V.

The Δi - E_d behavior of As(III) oxidation on Ir is relatively straightforward, compared to Pt. On the forward scan, oxidation begins at 0.85 V. The modulated current Δi steadily increases as the potential continues to scan toward more positive potentials. A limiting Δi is reached at ca. 1.25 V. The shape of the Δi - E_d wave appears to be much less reversible than the wave on Pt. Recall that on Pt, $E_{2/3}$ - $E_{1/3}$ was 20 mV on the forward scan; on Ir, $E_{2/3}$ - $E_{1/3}$ is 90 mV. The limiting Δi does not immediately begin to decrease with increasing potential, as is the case on Pt. In fact, a limiting Δi plateau is obtained on the forward scan until E_d reaches 1.4 V. At $E_a > 1.4$ V, Δi decreases very rapidly with potential, with $\Delta i \approx 0$ at $E_d = 1.5$ V. Immediately upon scan reversal, however, Δi rapidly increases as the potential decreases, attaining the limiting value at 1.4 V. The Δi on the reverse scan essentially retraces the limiting Δi plateau formed on the forward scan. For $E_a < 1.3$ V, the $E_{1/2,rs}$ is 30 mV negative of $E_{1/2,fs}$. For $E_a = 1.4$ V, $E_{1/2,rs}$ shifts to a

value that is 20 mV positive of $E_{1/2,fs}$. For $E_a = 1.5$ V, $E_{1/2,fs}$ and $E_{1/2,rs}$ are coincident at 1.07 V. Note that while $E_{1/2,rs}$ does shift with E_a on an Ir anode, the shifts are much smaller than those observed on a Pt anode.

Perhaps the most striking feature of these experiments is the very dramatic effects observed at $E_d > 1.4$ V. As discussed in section II.B, the nature of the anodic films on Ir makes the assignment of oxide stoichiometry difficult. Nevertheless, Kim, Sell, and Winograd (161) claim to have detected IrO_3 by XPS on electrodes held at high potentials. Buckley and Burke (210) state that at 1.6 V vs. RHE (ca. 1.36 V vs. SCE), the further oxidation (to Ir(VI)) of the outer oxide layers is the source of the small amount of corrosion that occurs at these high potentials. Burke and O'Sullivan (213) maintain that oxygen evolution on iridium oxide involves the partial conversion to a hydrated IrO_3 . Thus, it is at least suggested that the sharp decrease in electrode activity at $E_d > 1.4$ V vs. SCE is related to a conversion of the iridium oxide to a higher oxidation state.

E. Brief Comments on As(III) Oxidation on Au and Glassy Carbon

Results of As(III) oxidation on the Au using SHMRDE were not consistent with results of conventional cyclic voltammetry (see Section II.B). The source of the inconsistency was determined to be the very small ($\ll 10^{-6}$ M) Cl^- present in the 0.5 M $HClO_4$ supporting electrolyte. This has a very large effect on Δi because the very slow potential scan

rate required by SHMRDE results in a substantial accumulation of Cl^- adsorbed on the electrode surface. The adsorbed Cl^- appears to both block the electrode surface and influence the reaction kinetics. However, results recently obtained at Iowa State in 0.5 M H_2SO_4 supporting electrolyte, using an analogous technique in which the electrode is modulated in a square wave pattern should be noted (378). Since Au is a poorer electrocatalyst for oxygen evolution than is Pt, a positive potential limit of 1.8 V can be attained. On the forward scan, a very sharp anodic wave is obtained, with $E_{1/2,fs} = 0.878$ V. The quantity $(E_{2/3} - E_{1/3})$ is equal to 13 mV. This is a remarkable result, since theory predicts that $E_{2/3} - E_{1/3}$ should be 17.8 mV for a reversible, two-electron oxidation. This is a strong piece of evidence in support of a catalytic mechanism of As(III) oxidation. A limiting plateau Δi_{lim} is obtained on the forward scan in the range 0.86 V - 1.08 V. At 1.08 V, bulk oxide formation begins on the electrode surface and Δi begins to decrease very rapidly; this phenomenon can be observed also in conventional cyclic voltammetry experiments. At ca. 1.35 V, Δi has a very small, anodic value. At $E_d > 1.35$ V, Δi increases linearly with potential; at $E_d = 1.8$ V, $\Delta i / \Delta i_{lim} = 0.24$. The modulated current rapidly returns to 0 upon scan reversal and remains at 0 until the Au phase oxide is electrochemically reduced at about 0.88 V, giving a small anodic Δi peak. The additional information provided by this hydrodynamic modulation technique is that As(III) oxidation on a Au(III) oxide surface is enhanced by simultaneous oxygen evolution. This behavior is somewhat similar to that observed on a Pt anode, but very different from that observed on Ir.

Square-wave hydrodynamically modulated voltammetry was also applied to the oxidation of As(III) on glassy carbon. Earlier studies of the reaction of As(III) on glassy carbon were inconclusive, primarily because of the large residual currents obtained at all potentials on glassy carbon. This residual current is due primarily to double-layer charging, although other surface reactions may occur. These residual currents are eliminated in hydrodynamic modulation experiments just as the oxide formation currents are eliminated when noble metals are used. The extent of the irreversibility of As(III) oxidation on glassy carbon is remarkable. There is no Δi until the potential is 1.62 V, or 1.3 V positive of the standard reduction potential. Oxygen evolution is a very irreversible reaction on glassy carbon, but does begin at about 1.1 V. It is clear that any information on the oxidation of As(III) on glassy carbon can be obtained only by using a hydrodynamic modulation technique, since the reaction occurs only in the oxygen evolution region. The Δi increases slowly with potential at $E > 1.62$ V, peaks at about 1.83 V, and then decreases slowly as the potential is scanned to the positive limit of 1.92 V. The Δi decreases linearly with potential on the reverse scan and $\Delta i = 0$ at 1.62 V, the same potential where oxidation began on the forward scan. According to Bard and Faulkner (328), the following equation can be used to obtain kinetic parameters for systems in which mass transfer effects are important:

$$\eta = \frac{RT}{\alpha_a nF} \ln(i_0/i_{l,a}) + \frac{RT}{\alpha_a nF} \ln(i/i_{l,a} - i) . \quad \text{VII-17}$$

In Equation VII-17, η is the overpotential, α_a is the anodic charge transfer coefficient, i_0 is the exchange current density, and $i_{l,a}$ is the limiting anodic current. A plot of E vs. $\ln(i/i_{l,a} - i)$ is linear (with some data scatter) for potentials up to about 1.77 V; at greater potentials, there is a significant deviation from linearity. The slope of the line for $E < 1.77$ V is 0.055 V; this gives a value for $\alpha_a n$ of 0.47. In this case, n really represents the number of electrons in the rate-determining step. For most multi-electron reactions, only one electron is transferred in the rate-determining step (328). The anodic charge transfer coefficient would be the coefficient for the rate-determining step; a value of 0.47 is very reasonable.

VIII. THE MECHANISM OF As(III) OXIDATION ON Pt
AND OTHER NOBLE METAL ELECTRODES

A. Introduction

The oxidation of As(III) proceeds under mixed control (i.e., commensurate rates of mass transport and electrochemical conversion) on rotating disc electrodes of Pt, Ir and Pd. The oxidation of As(III) on Au proceeds under mass transport control at potentials less than about 1.1 V, but proceeds under mixed control at potentials greater than 1.1 V. In Section IV, it was shown that $i-\omega$ data obtained from a reaction proceeding under mixed control at a RDE can be fitted to an equation of the form

$$i^{-1} = B\omega^{-1/2} + Z \quad \text{IV-35}$$

for four different kinds of kinetic processes. These kinetic processes are characterized by the following: (1) a slow, heterogeneous charge-transfer step; (2) a slow, homogeneous, preceding chemical reaction that produces an electroactive specie; (3) nonlinear diffusion to "active sites" on a macroscopically inhomogeneous electrode surface; and (4) a slow, heterogeneous reaction not involving an electron transfer. A linear plot of i^{-1} vs. $\omega^{-1/2}$ is of itself not sufficient evidence on which to assign any one of the four possible kinetic processes as the cause of the observed mixed control. In this section, each of the kinetic processes listed above will be examined in turn. It will be shown that the first three of these processes cannot account for key experimental observations and therefore must be discounted when formulating an overall mechanism. It will be shown that the data can be understood in terms of mechanism

which has as its central feature a chemical reaction that occurs on the electrode surface and which does not involve a charge transfer. The rate constant of this surface reaction is influenced in several ways by the oxide coverage. Additionally, the rate of the surface reaction is influenced by the surface densities of the reactants, which are under certain circumstances potential-dependent quantities.

Most of the following discussion will deal with the oxidation of As(III) on Pt. The electrochemistry of Pt has been studied to a much greater extent than the other noble metals and is the most commonly used of the noble metals. Platinum has many characteristics (e.g., corrosion resistance) that are important from a practical standpoint. However, the important similarities and differences between Pt and other noble metals will be discussed in order to develop a more general mechanism for anodic reactions on noble-metal electrodes.

B. Slow Heterogeneous Charge Transfer

Cyclic voltammograms obtained at a Pt RDE have, for sufficiently positive values of E_a , a potential region on the negative scan of several hundred millivolts (depending on the positive potential scan limit) where the anodic current is essentially independent of potential; see Figures V-3 and VI-1. This simple observation leads to the conclusion that the rate determining step in the oxidation of As(III) on Pt cannot be a heterogeneous charge-transfer step within that potential region. The classical and well-known Butler-Volmer formulation of electrode kinetics has the form

$$i = nFAk^0[C_s \exp(\alpha_a nF(E-E^0)/RT)] \quad \text{VIII-1}$$

for an irreversible anodic reaction. In Eq. VIII-1, k^0 is the standard rate constant, C_s is the surface concentration of the electroactive specie, α_a is the anodic transfer coefficient, and E^0 is the formal electrode potential for the redox couple. It is clear from Eq. VIII-1 that the current is an exponential function of the applied potential. Since the observed current on the current plateau of i - E curves is both less than the mass-transport limited current and is independent of potential over a wide potential region, one must conclude that a heterogeneous charge-transfer step is not responsible for the mixed control observed in the oxidation of As(III) on Pt within the potential range that defines the current plateau. This same conclusion can be drawn from a simplified consideration of electron tunneling (379). The theory of electron tunneling predicts that the current will be an exponential function of the applied overpotential. Recently, Schultze and Habib (380) have collected several examples of redox reactions that occur on electrodes completely covered by oxide films. At any given overpotential, $\log i$ is a linear function of the oxide thickness d , as expected for a tunneling phenomenon. At a greater overpotential, however, the entire $\log i$ - d curve shifts to greater values of i . Thus, both from theory and from experimental results, one cannot rationalize the entire i - E behavior observed for As(III) in the cyclic voltammograms with a heterogeneous charge-transfer step.

In light of these observations, the analysis of the oxidation of As(III) on Pt given by Catherino (40) must be rejected. Catherino simply assumed that all other steps preceding and subsequent to the electron-transfer reaction were fast. His analysis of $\log i$ vs. E at the foot of wave led him to conclude that two consecutive one-electron transfers occurred. While Catherino was aware of the "passivating" influence of the Pt oxide at higher potentials, he failed to consider the current due to oxide formation at the foot of the wave. He also appears to have ignored the contribution to total current from the oxidation of chemisorbed As(III). For all of these reasons, the mechanism proposed by Catherino (40) cannot be accepted as correct for the entire range of experiments described in this dissertation.

It is interesting to consider briefly the oxidation of Br^- at a Pt electrode. Rubinstein (366) has determined the mechanism and kinetic parameters for the oxidation of Br^- on an "oxide-covered" Pt electrode, formed by polarizing the electrode for 10 s at 0.80 V vs. mercury sulfate reference electrode. From the potentiostatic work of Gilroy (113), it is estimated that the oxide coverage θ would be approximately 2.0 (i.e., a monolayer of PtO) under these conditions. The heterogeneous rate constant is given by the equation (328)

$$k = k^0 \exp[\alpha_a nF(E - E^0)/RT] \quad \text{VIII-2}$$

Rubinstein gives a value for k^0 of about 0.010 cm s^{-1} and α_a of 0.43 for the oxidation of Br^- on an oxidized Pt electrode. Assuming that the formal reduction potential in 0.5 M HClO_4 is approximately the standard

reduction potential (0.85 V vs. SCE), the values of $(E-E^0)$ varied from 0.25 V - 0.45 V in the experiments described in Section VI. Substituting these values into Eq. VIII-2 gives values for k of 0.66 cm s^{-1} for $E = 1.1$ V, 3.50 cm s^{-1} for $E = 1.2$ V, and 18.6 cm s^{-1} for $E = 1.3$ V. The experimental values of the rate constant for Br^- oxidation were 0.233 cm s^{-1} for $E = 1.1$ V, 0.176 cm s^{-1} for $E = 1.2$ V, and 0.173 cm s^{-1} for $E = 1.3$ V (Table VI-7). The conclusion to be drawn is that even though a charge-transfer step may be the rate-determining step at low overpotentials, the rate constant for the charge transfer step can become so large at high overpotentials that some other elementary step must be rate limiting if the observed current is less than the transport limited value.

C. Slow Homogeneous Chemical Reaction

The possibility of a slow, preceding, homogeneous chemical reaction also can be eliminated as the slow kinetic step in the oxidation of As(III) on Pt. From Tables VI-2, VI-3, VI-4 and VI-6, it is clear that the experimental k is potential dependent, k decreasing as the applied potential is made more positive. The influence of potential on the experimentally-derived k is both direct and indirect, depending on the oxide coverage and the actual value of potential (see Section VII.B). In either case, such variations in k cannot be rationalized as consistent with a slow, homogeneous chemical reaction.

A homogeneous reaction preceding the oxidation of As(III) can also be eliminated by other lines of reasoning. The most common preceding

homogeneous reactions that are important with respect to subsequent electrochemical reactions are protonation, deprotonation, loss of a ligand to give an electroactive form, and dehydration to give an electroactive form. An example of a preceding dehydration reaction occurs in the reduction of formaldehyde at a Hg electrode in aqueous solutions. A non-reducible form, $\text{H}_2\text{C}(\text{OH})_2$, is in equilibrium with the reducible form, H_2CO . Given the structure of As(III) in acidic and basic solutions (4,5) and the $\text{p}k_a$ values of the As(III) species ($\text{p}k_1 = 8.62$, $\text{p}k_2 = 12.13$ and $\text{p}k_3 = 13.40$), none of the typical homogeneous reactions listed above can be considered as likely. In addition, Eq. IV-27 predicts that the intercept of a plot of i^{-1} vs. $\omega^{-1/2}$ should be proportional to $(D^{1/2}K(k_1 + k_2)^{1/2})^{-1}$. For solutions of different ionic strength, the product of the intercept and $D^{1/2}$, and a correction factor to account for the variation of the rate constant with ionic strength (381), should be constant. This variation arises due to changes in the activity coefficients. The correction factor was calculated based on a formula of the form

$$\log \gamma_{\pm} = \frac{A\sqrt{I}}{1 + J\sqrt{I}} + Bc + D'c^2 \quad \text{VIII-3}$$

given by Harned and Owen (382), where A, B, C, D' and J are constants and γ_{\pm} is the mean activity coefficient. These products were not constant for I of 0.5M, 2.75M and 5.0M.

D. Nonlinear Diffusion to Active Sites

It is conceivable that in the course of Pt oxide formation, small areas of a polycrystalline electrode might be relatively less susceptible to oxidation than the surface of the electrode as a whole. These small areas might be extremely active sites for the oxidation of As(III) by virtue of their ability to adsorb As(III), their proximity to especially active oxide species, or other favorable steric effects. For an As(III) to be oxidized, it would be necessary for the As(III) specie to not only diffuse across the familiar diffusion layer but also to diffuse along the electrode surface until an active site is encountered. This additional diffusion length has the same effect as a slow kinetic step and can cause a case of mixed control at a RDE. It was established in Section VI (see Table VI-1) that the mixed control exhibited in the oxidation of As(III) on Pt is not solely due to nonlinear diffusion on a macroscopically inhomogeneous electrode surface, i.e., diffusion to isolated active sites. This was done by showing that the product of D and the intercept of a plot of i^{-1} vs. $\omega^{-1/2}$ was not constant for various values of D . This product is a constant for a true case of nonlinear diffusion, as verified by Scheller, Landsberg and Wolf (338). The theory developed by Landsberg and coworkers (see Section IV) assumes that the number and distribution of active sites on the electrode is constant. There are two ways in which the number and distribution of active sites within the oxide film might be changed by the variation in ionic strength. The first of these is if the kinetics of oxide growth is in some way a function of ionic strength at a

constant pH. If the rate of Pt oxide formation increased with ionic strength, then the oxide coverage at a given time would increase with ionic strength and there would therefore be a decrease in the number of active sites. Unfortunately, there are no known studies of this kind in supporting electrolytes where the anion does not specifically adsorb. However, since ClO_4^- does not specifically adsorb to any significant extent, it does seem reasonable to assume that any effects of the ionic strength of the supporting electrolyte on Pt oxide growth are minimal. The second way in which the number and distribution of active sites might have been altered is by the co-adsorption of Cl^- present as a contaminant in the NaClO_4 used to adjust the ionic strength. Since the amount of Cl^- present in the supporting electrolyte would be directly proportional to concentration of NaClO_4 , it is conceivable that Cl^- adsorption on the active sites would lead to smaller numbers of available sites as the ionic strength is increased. However, Lown (364) has shown that Cl^- concentrations well in excess of ca. 0.1 ppm, the level present in these experiments, has a relatively small effect on the As(III) anodic current obtained at a Pt anode. It is concluded that Cl^- adsorption on active sites would not significantly reduce the number available for the oxidation of As(III) in the experiments described here. In light of the facts that the products of D and the intercept of the plots of i^{-1} vs. $\omega^{-1/2}$ are not constant for various values of D and the number and distribution of active sites (if they existed) is not likely to be a function of ionic strength, it is concluded that the oxidation of As(III) on Pt does not proceed by process involving nonlinear diffusion.

A comparison of the results of the hydrodynamic modulation experiments obtained at Pt, Au and Ir also tends to argue against an "active site" mechanism. If such active sites did exist in an oxide film, it is expected that the number and distribution of these sites would be comparable for polycrystalline Pt, Au, and Ir surfaces under comparable conditions. However, the sinusoidal hydrodynamic modulation experiments (for Pt and Ir) and the square-wave hydrodynamic modulation experiment (for Au) exhibit dramatically different behaviors when phase oxides are formed or already present in the surface. The results obtained on Pt (see Figure VII-1), where Δi gradually decreases with increasing potential and therefore increasing oxide coverage, leads one to conclude that the number of active sites decreases relatively slowly with increased oxide coverage. On Au and Ir, however, there are very sharp decreases in Δi over very small potential ranges (see Sections VII.D and VII.E). On Au, Δi decreases very rapidly as soon as the potential is sufficiently positive to form a phase oxide on the surface. If the reaction on Au proceeded through active sites, one would conclude that the number of sites decreased very rapidly with phase oxide coverage. On Ir, Δi decreases very rapidly when the potential is positive enough to convert a lower oxide (probably Ir(IV)) to a higher oxide (probably Ir(VI)). Since the number of active sites, if such sites do exist would be expected to respond to oxide growth in similar manners for the three different metals, it is reasonable to conclude that active sites do not play a significant role in the oxidation of As(III). It is much more logical to assume that differences observed in the hydrodynamic modulation experiments are due to

properties of the respective oxides rather than active sites within the oxide films.

E. Slow Heterogeneous Reaction Not Involving Charge Transfer

The vast majority of the data obtained on the oxidation of As(III) at noble metal electrodes is consistent with a mechanism in which the overall rate is limited by the rate of a chemical reaction that occurs on the electrode surface and that does not involve the transfer of an electron. The rate constant of this surface reaction is strongly influenced by the oxide coverage. The rate of this surface reaction also is influenced by the surface densities of the reactants, quantities which are potential dependent. The most likely surface reaction is one that involves either a strongly- or weakly-adsorbed $\text{As}(\text{OH})_3$ and an oxygen-containing surface specie. Under most circumstances, this will be an adsorbed hydroxyl radical. As reviewed in Section II.C, there is a considerable amount of evidence that adsorbed hydroxyl radicals participate in surface reactions with a wide range of adsorbed reactants. In fact, in almost all of the reactions discussed in Section II.C, the surface reaction involving the OH_{ads} is the rate-determining step.

In order to explain all of the results obtained for As(III) oxidation from conventional cyclic voltammetry, hydrodynamically-modulated voltammetry, and the potentiostatic experiments, it is necessary to propose a mechanism in which both a charge-transfer reaction and a slow surface reaction not involving charge transfer are involved in the rate-

determining step. For the most part, the parameter k that was used to characterize the mixed control observed in oxidation of As(III) is concluded to be related to the surface combination reaction between $(OH)_{ads}$ and an adsorbed arsenic species. This conclusion is valid under conditions where the surface reaction is the rds (e.g., on the current plateau of an i - E curve, at 1.1 V in a potentiostatic experiment). The rate of the surface reaction is strongly influenced by the oxide coverage via changes in the surface concentrations, the type of oxygen-containing reactants and the nature of the As(III) adsorption sites. In general, the rate constant k of the surface reaction is expected to vary as a smooth function of θ , but for discussion purposes one can consider the rate of the surface reaction to fall into 3 regimes. At low coverages by the oxide, i.e., $\theta < 1$, the rate of the surface reaction is very fast, and may in fact be fast enough to give mass-transport limited currents (i.e., $D/k \ll \delta$ in Eq. VI-3). At intermediate coverages by the oxide, defined as $1 < \theta < 2.5$, the surface reaction proceeds at a significantly slower rate. At high coverages, i.e., $\theta > 2.5$, the value of k is very small; there may even be a change in the nature of oxygen-containing species that acts as a reactant at $\theta > 3$. The reasons for these regimes will be discussed in terms of the nature of oxide films on noble metals.

In addition to the facts that the proposed mechanism is consistent with the results from a wide variety of electrochemical techniques and is consistent with a large body of literature, it can be used to explain at least some of the differences in electrochemical behavior observed on different noble metal electrodes. The important theoretical

considerations and experimental observations that were used to develop and to test this mechanism will be discussed now in some detail.

F. Detailed Discussions of the Mechanism of Anodic Oxidation

The role that surface oxides or the precursors in the production of surface oxide play as electrocatalysts is crucial. As has been pointed out previously, the standard reduction potential for the As(III,V) couple is 0.32 V vs. SCE. The fact that only small anodic currents are obtained until the potential up to 400 millivolts positive of 0.32 V is evidence that the uncatalyzed oxidation of As(III) is either very irreversible or inhibited by a surface film of some sort or both. It was established in Section V.B.3 that As(III) chemisorbs on a reduced Pt surface, and Loucka (44) has presented evidence that As(III) also chemisorbs on Au. It might be reasonable to assume that the oxidation of As(III) is inhibited by the presence of a monolayer of chemisorbed As(III). It is difficult, however, to understand why the oxidation of the chemisorbed As(III) would be even more irreversible (with respect to the overpotential required to initiate oxidation) than the oxidation of As(III) that is not chemisorbed. The experiment performed using a glassy carbon electrode illustrates both the "true irreversibility" of the oxidation of As(III) and the importance of surface oxides (Section VII.E).

At a glassy carbon surface, the consequences of As(III) adsorption and electrocatalysis via surface oxides are eliminated. As discussed in Section VII.E, a huge overpotential (ca. 1.3 V) is required to oxidize

As(III) in the absence of any electrocatalytic effects. It would appear that a direct electron transfer from $\text{As}(\text{OH})_3$ is a very demanding electrochemical reaction. It is very likely that the oxidation will proceed along any alternate path that becomes available at an overpotential less than the ca. 1.3 V required for direct electron transfers to the carbon electrode.

The anodic wave for As(III) at a Pt electrode occurs at a potential that is several hundred millivolts positive of the E^0 , yet has the shape of a reversible wave. These facts are especially obvious in the results of the hydrodynamic modulation experiments (Figures VII-1 and VII-2). The electrocatalysis of the oxidation by $(\text{OH})_{\text{ads}}$ can rationalize this apparent logical contradiction. The behavior on a Pt electrode will be considered first. In essentially all cyclic voltammograms (conventional and hydrodynamically modulated), the negative potential scan limit was set sufficiently negative to reduce the Pt oxides formed on the previous positive scan. It has been conclusively shown that As(III) chemisorbs on Pt, giving a full monolayer coverage within a few seconds (see Figure V-10) under the conditions of As(III) bulk concentration and rotation speed that were used typically. Therefore, the electrode surface is covered with a complete layer of adsorbed As(III) at essentially all values of $E_d < 0.75$ on the positive scan. The adsorbed As(III) inhibits the oxidation of the Pt surface for quite logical reasons: any adsorbed H_2O is simply desorbed when the As(III) adsorbs, and when the As(III) monolayer is complete, there are simply no Pt sites that can be oxidized to the corresponding oxide. At $E_d = 0.75$ V a small number of the strongly-

adsorbed As(III) species, probably those at surface sites having an especially high surface energy (e.g., kinks, grain boundaries, or edge dislocations) are oxidized by electron transfer to As(V), which is not adsorbed. The direct oxidation of As(III) to As(V) in this case is not in contradiction with the results obtained on glassy carbon. It is reasonable that a direct electron transfer would be significantly easier at a Pt electrode than at a glassy carbon electrode for three reasons: 1) the As(III) orbitals are in a favorable position for electron transfer by virtue of the preceding adsorption; 2) the As(III) has already been stabilized by an amount of free energy equivalent to the free energy of adsorption; and 3) that surface states of especially high energy do exist on Pt and probably do not exist on glassy carbon. Once a few of the adsorbed As(III) species are oxidized and desorbed, the following events can occur in rapid succession. The potential at this point ($E_d \approx 0.75$ V) is ca. 200 mV positive of the potential where Pt surface oxidation would begin in the absence of adsorbed As(III). The most likely event to occur at the bare Pt site just formed is to discharge H_2O to give PtOH. The situation on the surface now is that a few PtOH are present but are essentially surrounded by adsorbed As(III). A surface reaction between the PtOH and the adsorbed As(III) gives As(V) and two bare Pt sites. These sites quickly are re-oxidized to PtOH, which can then react with other As(III) species that are adsorbed on the nearest neighboring Pt atoms. A situation emerges in which expanding two-dimensional islands of PtOH are being formed. Since both the reactions to form PtOH and the reaction of PtOH with $As(III)_{ads}$ on the adjacent Pt atoms are relatively

fast, the surface is transformed from one completely covered with $\text{As(III)}_{\text{ads}}$ and therefore not reactive toward oxidation of As(III) from the bulk solution to one covered by Pt oxides and, therefore, reactive (to a greater or lesser extent) toward oxidation of As(III) from the bulk solution. This explains why the oxidation wave simultaneously occurs at a potential several hundred millivolts positive of the E^0 , yet has the shape of a reversible wave. The same argument can be applied to the As(III) oxidation wave on Au, although the situation on Au is somewhat simpler. While there is some evidence for As(III) adsorption on Au (44), the results of cyclic voltammograms (see Figure V-16) establish that the extent of adsorption on Au is small relative to the extent of adsorption on Pt. At the As(III) concentrations typically used in this research, the amount of adsorbed As(III) is much less than 1 monolayer. As soon as the potential is sufficiently positive, AuOH is formed on those sites not occupied by As(III) . As soon as AuOH is formed, the surface reaction between AuOH and As(III) can occur rapidly. This reaction is the rds, but is nevertheless fast enough to give a mass-transport limited current. Careful analysis of the results of Landsberg's group, as cited by References 334-340, reveals that a mass-transport limited current can be obtained even if the coverage of the active sites is relatively small. This explains why a mass-transport limited current is attained within a few millivolts of the onset of AuOH formation. The current remains at the mass-transport limited value for approximately 150 mV, or until the formation of a Au(II) phase oxide begins. A limiting-current plateau over a wide range of potential is obtained on Au but not on Pt because of

differences in the conversion of $(OH)_{ads}$ species to higher oxides under the influence of potential and/or time. The higher oxide of Au is a severe inhibitor to oxidation of As(III), while the higher oxide of Pt has a finite catalytic effect. The effect of oxidation of the gold surface to the Au(III) oxide will be discussed later.

Attention is turned now to the variation in k as a function of the oxide coverage θ . It does not appear to be possible to identify a single parameter that varies as a function of θ and that directly influences k . Rather, as θ changes in either potentiostatic or potentiodynamic experiments, at least three factors change that influence the rate of the surface combination reaction. However, under specific conditions, the change in one of these factors may predominate over all of the others, at least to the extent that the trends in k as a function of θ can be semi-quantitatively rationalized.

As illustrated in Figure V-3, there is a clear relationship between the value of the anodic current plateau and the positive potential scan limit E_a in conventional cyclic voltammetry. This relationship can be seen for more positive values of E_a in the hydrodynamic modulation experiments illustrated by Figures VII-1 and VII-2. It is clear from Figure V-3 that θ is a function of E_a when an oxidizable substance is present in the bulk solution, just as it is in the absence of oxidizable substances (57). However, it is not possible to determine if θ for the absence of As(III) is the same as θ for the presence of As(III) because the mixed current in the potential region around 0.75 V makes accurate integration of the oxide reduction peak impossible when As(III) is

present. In fact, at a fixed scan rate, θ is usually a linear function of E_a , with small breaks in the slope at $\theta = 1$ and at $\theta = 2.4$ (55). From Figure 2 of reference 55, it can be determined that for cyclic voltammetry at 6.0 V min^{-1} , $\theta = 1$ at $E_a = 0.86 \text{ V}$, $\theta = 2$ at $E_a = 1.16 \text{ V}$, $\theta = 3$ at 1.43 V , and $\theta = 4$ at 1.71 V , where $\theta = 1$ corresponding to a monolayer of PtOH. It is known from many potentiodynamic studies of Pt oxide growth that further oxide growth ceases immediately upon scan reversal. It can hardly be a coincidence that θ is a function of E_a , and is fixed at that value as soon as the potential begins to scan in the negative direction, and that the As(III) anodic current plateau decreases as a function of E_a and yet is, by definition, independent of E_d for several hundred millivolts for a given value of E_a .

Further evidence that links k and the oxide coverage θ is obtained from potentiostatic experiments. At a given potential and As(III) flux, k is a linear function of $\log t$. It is well known from potentiostatic studies of Pt oxide growth (113) that θ is a linear function of $\log t$, the slope increasing with applied potential. Before examining the relationship of k and θ in detail, several causes for the decrease in k with θ will be suggested.

The rate of oxygen evolution on noble-metal oxides is frequently cited as being a function of the thickness of the oxide film. Note: oxide thickness is simply another way of expressing the quantity of oxide, as is θ . Gilroy (116) has given 3 possible explanations for this phenomenon:

- 1) A variation in the adsorption energy of hydroxyl radicals with the degree of coverage; Gilroy believes this to be valid only for the first two monolayers.
- 2) The work function of the surface is directly related to the degree of oxidation.
- 3) The density of suitable electron acceptor levels in the surface is diminished by oxidation.

In his first point, Gilroy refers to generalized adsorption site, S . It is not clear in reference 116 whether Gilroy means that $(OH)_{ads}$ are formed on the Pt atoms in the oxide film, analogous to the theory of $O_2(g)$ evolution on Ir given by Gottesfeld and Srinivasan (219), or that $(OH)_{ads}$ is formed on the oxygen atoms in the oxide film, in accordance with the theory given by Damjanovic and Jovanovic (284). In any case, the variation in adsorption energy with coverage is doubly important in the case of As(III) oxidation by $(OH)_{ads}$. The rate of the surface reaction must be proportional to product of the surface concentrations of $(OH)_{ads}$ and As(III). The free energy of adsorption energy of As(III) is undoubtedly also effected by the oxide coverage, especially at θ where some place-exchange has occurred. It is reasonable to assume that free energy of As(III) adsorption on Pt atoms within a PtO film is much less than that on a Pt metallic surface, and that this free energy would decrease even further as the oxide film becomes thicker. In other words,

the "sticking probability" of As(III) on the electrode surface decreases with increasing θ , and this surely effects the rate of the surface reaction. A discussion of the variation of the work function and the density of electron acceptor states with θ is beyond the scope of this dissertation, but these factors are expected to be of no importance with respect to the rate of the surface reaction itself. However, these factors certainly are important in any charge-transfer reactions that precede or follow the surface reaction and can under certain circumstances effect the overall rate.

Two other factors that are likely to influence the rate of the surface reaction, and that are related to the oxide coverage, can be identified. The first of these is the distance between the adsorbed As(III) and the active oxygen specie. For $\theta < 1$, this distance can, as a minimum, be the distance between nearest Pt neighbors. Note that the number of nearest Pt neighbors is dependent on the crystallographic surface; in the polycrystalline electrodes that were used, there is probably a random distribution of the three major crystallographic surface across the surface of the electrode. For $\theta > 2$, where place-exchange has occurred, the minimum distance can be that of next-nearest neighbors. Orbital overlap and therefore the rate constant of the surface reaction certainly must be effected by the distance between the reactants. The second factor that influences k is the kind of oxygen-containing reactant present at various θ . For $\theta < 1$, this is certainly $(OH)_{ads}$, designated "PtOH". At somewhat higher θ , the surface density of $(OH)_{ads}$ is considerably less, but when $O_2(g)$ evolution is occurring the surface

density of $(\text{OH})_{\text{ads}}$ is again probably very high. Even at values of θ for which the surface density of $(\text{OH})_{\text{ads}}$ is expected to be very small, there is still some reactivity of the oxide, indicating that lattice oxygens can participate in the surface reaction, albeit at a significantly lower rate than for $(\text{OH})_{\text{ads}}$. It should be noted that direct participation of lattice oxygen has been documented in a wide variety of cases: the gas-phase oxidation of a wide variety of organic substances by heterogeneous catalysts made from transition-metal oxides (383); the oxidation of U(IV) to U(VI) by PbO_2 , MnO_2 , and NaBiO_3 (384) and the oxidation of sulfite by MnO_2 (385) in aqueous solutions; and the electrochemical evolution of $\text{O}_2(\text{g})$ on Pt (289,290). Another way of looking at the reactivity of oxygen-containing species is to consider the effects of increasing E_a on the reduction potential of Pt. It is well known that the reduction peak potential shifts negatively as E_a becomes more positive. This can be interpreted as an increase in strength of the average Pt-O bond. It is reasonable that any process involving the breakage of a Pt-O bond should occur less rapidly as the average Pt-O bond strength increases.

It was mentioned in Section VI that k is related to $\log t$ for large values of t (> 100 s) in potentiostatic experiments. It was noted that this implied the existence of a relationship between k and the oxide coverage, since the relationship between the quantity of oxide Q_{Ox} and $\log t$ under potentiostatic conditions is well known (55, 113). The relationship between k , Q_{Ox} and t will be examined in more detail now.

An interesting relationship between k and Q_{Ox} can be discerned from data obtained by cyclic voltammetry. As illustrated in Section V.A, the

anodic current plateau on the reverse scan is a function of both the rotation speed and the positive scan limit. It is a simple matter to combine these two dependencies to obtain values for k as a function of Q_{Ox} if one assumption is made. As discussed in Section V.A, it is not possible to obtain an accurate value for Q_{Ox} by integrating the area of the Pt oxide reduction peak of cyclic voltammograms recorded when As(III) is present. However, accurate values of Q_{Ox} can be obtained by this technique if As(III) is absent. It was assumed that the amount of oxide formed in the presence of As(III) is the same as that formed in the absence of As(III) for identical supporting electrolytes, positive scan limits, and scan rates. This assumption is justified based on the observations that all of the $As(III)_{ads}$ is oxidatively removed on the forward potential scan and that the oxide growth rate appears to greater than normal once the oxidation of the surface does begin. The data are generated by determining Q_{Ox} for a given positive scan limit in the absence of As(III), and then determining k for the same scan limit by varying the rotation speed of the electrode and plotting i^{-1} vs. $\omega^{-1/2}$. A plot of $\log k$ vs. $\log Q_{Ox}$ has two linear regions: the first region is for $Q_{Ox} < \underline{ca.} 540 \mu\text{Coul cm}^{-2}$, and the second region is for $Q_{Ox} > \underline{ca.} 750 \mu\text{Coul cm}^{-2}$. The slope of the region at high Q_{Ox} is twice that at low Q_{Ox} . The intersection of the two linear regions occurs at about $660 \mu\text{Coul cm}^{-2}$. In terms of θ , the first significant deviation from linearity occurs at $\theta = 2.5$, the intersection of the extrapolations for the two linear regions is at $\theta = 3.0$, and the second linear region begins

at $\theta \approx 3.4$. Clearly, the relationship between k and θ undergoes a transition in the region between $\theta = 2.5$ and $\theta = 3.4$.

These results can be interpreted in light of the structure of the Pt oxide as θ increases. According to Tilak *et al.* (58), a value of $\theta = 1$ corresponds to a completely place-exchanged layer of PtOH; Pt atoms and hydroxyl radicals alternate in the two layers above the metallic Pt substrate, rather than complete monolayer of $(OH)_{ads}$ on an undisturbed Pt substrate. A value of $\theta = 2$ (*i.e.*, PtO) corresponds to the oxidation of the hydroxyl radicals to oxide ions in the oxide lattice. Again, Pt ions and oxide ions alternate within the two layers above the substrate. Further oxidation of the surface beyond $\theta = 2.0$ is accomplished by the formation of $(OH)_{ads}$ on the Pt ions in the outermost layer of the oxide film. All of the Pt ions in the outer layer are covered by $(OH)_{ads}$ when $\theta = 2.5$. It appears that a significant change in the mechanism occurs at that oxide coverage where there are no "uncovered" Pt atoms on the surface of the oxide.

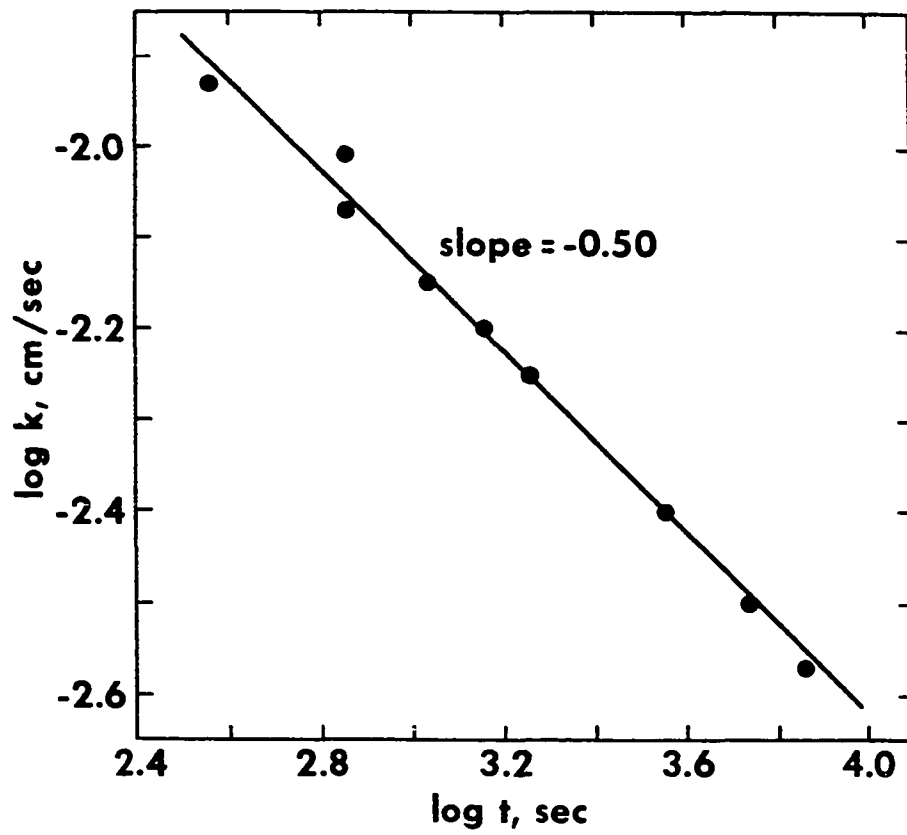
The importance of $\theta = 2.5$ also can be seen in the SHMRDE data (Figure VII-1). According to Belanger and Vijn (55), a coverage of 2.5 is obtained in a potentiodynamic experiment when the applied potential reaches 1.20 V. On Figure VII-1, a positive scan limit of 1.20 V results in a potential-dependent Δi on the reverse scan. The appearance of a Δi plateau occurs only when the positive limit is great enough to form an oxide coverage greater than 2.5, again showing that some change in the way that As(III) is oxidized has occurred.

The relationship between k and t was examined briefly in Section VI. In general, the values for k obtained at long times decreased as a linear function of $\log t$. The relationship between k , t , and the As(III) flux now will be examined in more detail.

The values of k given in Table VI-8 were obtained in a potentiostatic experiment at polarization times from 6 min to 120 min. In Section VI it was stated that k and $\log t$ are related by the equation

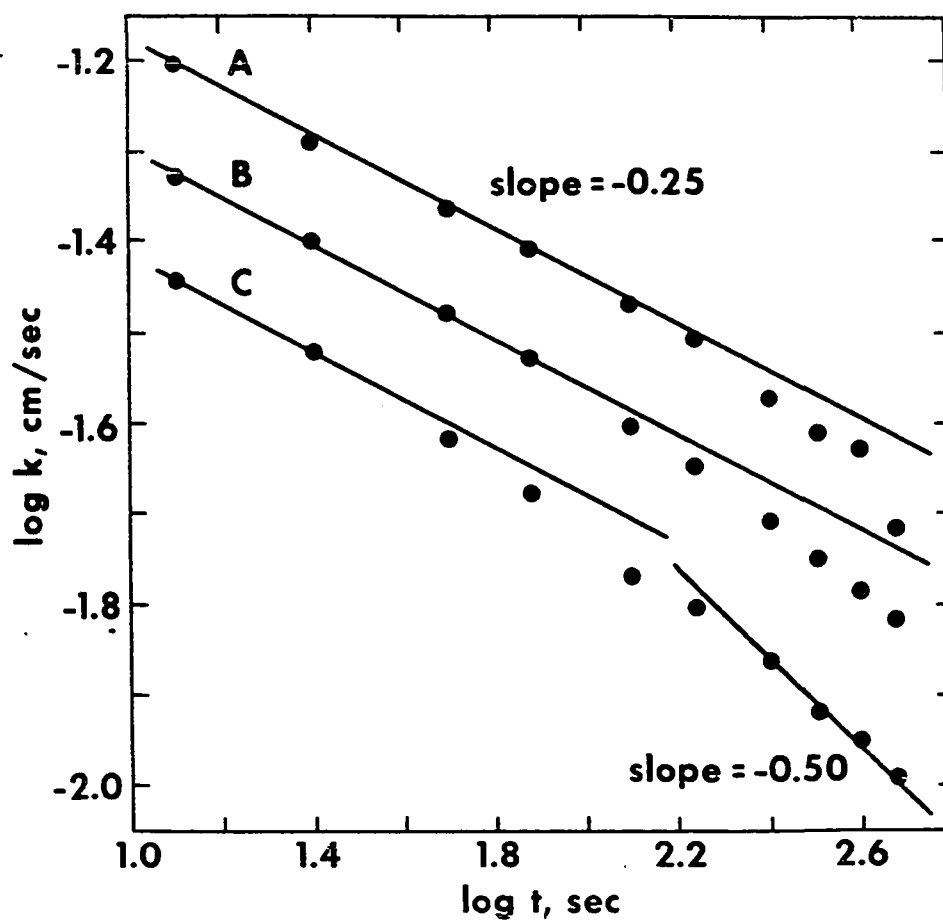
$$k \text{ (cm s}^{-1}\text{)} = 0.0415 - 0.0166 \log t \text{ (min)}$$

These data were obtained by rapidly scanning the rotation speed from 300 rpm to 5000 rpm at each of the polarization times given in Table VI-8. The bulk concentration of As(III) in this experiment was 0.515 mM. These data also can be fitted to a linear equation relating $\log k$ and $\log t$; Figure VII-1 is a plot of the data in this form, with t converted from minutes to seconds. The slope of this plot is -0.50. These data have been replotted in this way in order to facilitate a comparison with the data obtained at shorter times in other potentiostatic experiments. It also was stated in Section VI that a good fit was obtained for k as a function of $\log t$ for $t > 100$ s in the potentiostatic data given on Figures VI-1 and VI-2; the parameters of the linear regressions are collected in Tables VI-10 and VI-11, respectively. The data from Figure VI-1 for t from 12.5 s to 475 s has been replotted in Figure VIII-2 as $\log k$ vs. $\log t$ for three of the As(III) bulk concentrations. Data from Figure VI-2 have been replotted in the same manner for two of the rotation speeds and is given in Figure VIII-3. Figures VIII-2 and VIII-3 illustrate the effect that the As(III) flux has on the relationship of



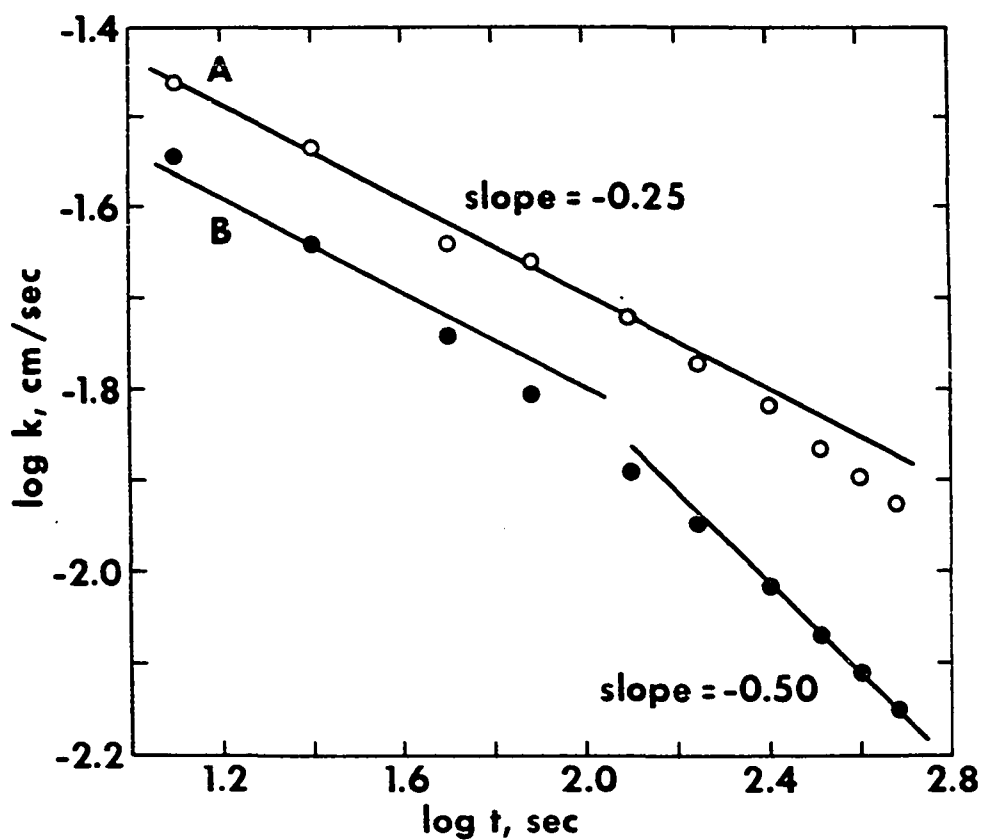
Conditions: 0.5 M HClO_4 + 0.515 mM As(III)
 E_d 1.1 V

Figure VIII-1. Plot of $\log k$ vs. $\log t$ for long times



Conditions: 955 rpm
 0.5 M HClO_4
 E_d 1.1 V
 A 0.515 mM As(III)
 B 1.026 mM As(III)
 C 2.039 mM As(III)

Figure VIII-2. Plot of $\log k$ vs. $\log t$ for short times as a function of $[\text{As(III)}]$



Conditions: 0.5 M HClO_4 + 2.039 mM As(III)

E_d 1.1 V

A 5.00 $\text{rad}^{1/2} \text{ s}^{-1/2}$

B 25.00 $\text{rad}^{1/2} \text{ s}^{-1/2}$

Figure VIII-3. Plot of $\log k$ vs. $\log t$ for short times as a function of ω

$\log k$ vs. $\log t$. At low As(III) flux (e.g., curve A), the slope has a value of -0.25 for low values of $\log t$. Deviation from linearity begins at $\log t \approx 2.2$. As the flux increases, the deviation from a slope of -0.25 begins at lower values of $\log t$. At high values of As(III) flux and at long times, the slope of a plot of $\log k$ vs. $\log t$ is -0.50 (curve C on Figure VIII-2 and curve B on Figure VIII-3). This slope is the same as that given on Figure VIII-1 for very long times. Figures VIII-2 and VIII-3 are further support of the observation that k is not only a function of the applied potential and the time, but is a function of the As(III) flux as well. They also show why good correlations between k and $\log t$ were obtained only for $t > 100$ s.

Unfortunately, it is not possible at this time to give a quantitative interpretation of the slopes of plots of $\log k$ vs. $\log t$ or of k vs. $\log t$. The rate of the surface reaction can be effected by the oxide coverage in many ways, as described above. The effects of θ on $k_{s,r}$ and on the surface densities of the reactants obviously combine in a complex manner, giving a slope that cannot be interpreted in any simple manner. There is, for example, no simple theoretical interpretation for a slope of -0.5 in a plot $\log k$ vs. $\log t$ at the highest As(III) fluxes used. Had a much higher As(III) flux been used, it is likely that a more negative slope would have been obtained.

While an exact quantitative relationship between k , t , and the As(III) flux cannot be derived for comparison with experimental values, it is possible to suggest qualitative explanations. It is clear that for a given potential and polarization time, a higher As(III) flux results in a

lower value of k . Another anodic reaction that decreases with time under potentiostatic conditions is the evolution of oxygen. Gottesfeld and Srinivasan (219) have discussed the decrease in the rate of the oxygen evolution reaction on Ir under potentiostatic conditions. According to them, oxygen evolution on Ir proceeds by a mechanism in which an active site in the oxide-electrolyte interface is oxidized, via an adsorbed OH intermediate, to a higher metastable oxidation state. Oxygen gas is produced as the result of a surface reaction between two molecules of the metastable oxide, thus regenerating two active sites. According to Gottesfeld and Srinivasan, deactivation occurs when active sites are "lost" due to a "stabilization" of the higher oxide structure. In the case of As(III) oxidation on Pt under potentiostatic conditions, the general trend of decreasing electrode activity with time is, in some respects, similar to the decay in the oxygen evolution current on Ir. If the rate at which Pt sites in the oxide film were stabilized in a higher oxidation state was a function of the number of reactions at those sites per unit time, then the overall rate of deactivation would be a function of the As(III) flux. This possible explanation is judged to be relatively unlikely under the conditions employed, primarily the value of applied potential. Although a stable Pt(IV) oxide can be formed anodically (75, 83-90), this occurs only when the potential is about 1.9 V. Therefore, it does not seem likely that any appreciable amount of Pt(IV) oxide could be formed in potentiostatic experiments recorded in Figures VI-1 and VI-2.

Another possible explanation for the dependence of k on flux is that the total electrode activity is related to the homogeneity of the

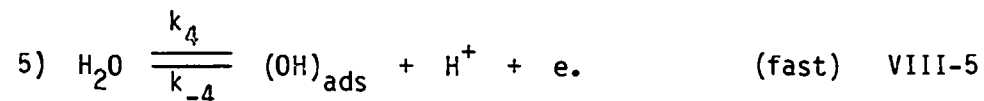
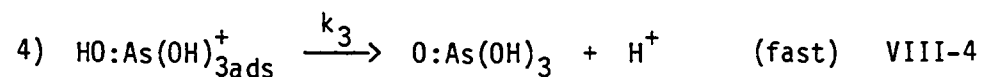
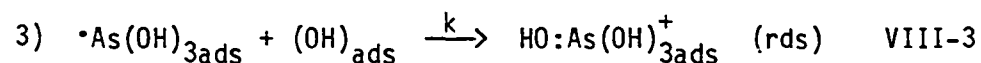
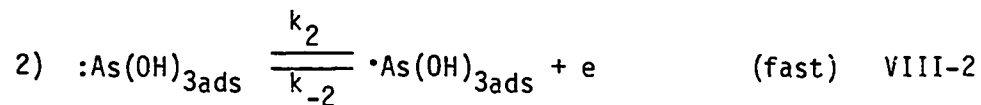
electrode surface and that the homogeneity of the electrode surface is influenced by the rate at which As(III) is being oxidized on the surface. A mechanically polished, polycrystalline electrode is quite clearly inhomogeneous on a microscopic scale. Even though there is some value for average oxide coverage θ_{av} which can be calculated based on the geometric area of the electrode, the distribution of surface states around grain boundaries, edge dislocations, polishing marks, et cetera, assures that there are microscopic regions with $\theta < \theta_{av}$ and other regions with $\theta > \theta_{av}$. There will be, therefore, some areas that will be more catalytically active than others. In other words, there will be active regions on a microscopic level. Note that this is quite a different case than that developed by Landsberg's group (see Section IV and References 334-340); that theory deals with a macroscopically inhomogeneous surface in which the area that is not "active" is totally inactive. The diffusion layer thickness for the highest rotation speed used was $\sim 6.6 \times 10^{-4}$ cm; this is so large on a microscopic scale that any deviation from uniform accessibility is negligible. It has been proposed that the oxidation of As(III) "consumes" either $(OH)_{ads}$ or lattice oxygen, depending on the state of the oxide. A high As(III) flux would tend to limit the growth of local active sites, due to the high rate of the reaction and therefore a high rate of consumption of "active" oxide. The oxide film as a whole would tend to be somewhat more homogeneous and inactive. The observed current density can be thought of as the sum of the current densities for each microscopic area. If microscopic areas of especially high current density are eliminated, the total current density will be less. A good

analogy is the growth of precipitates and the improvement in precipitate quality obtained by "aging" the precipitate. Precipitates formed very rapidly are often characterized by very poorly developed crystals having a large number of defects, dislocations, dendrites, and so on. Analogous defects within a Pt oxide film are probably areas of high electrocatalytic activity. Precipitate aging, which allows for many successive dissolutions/reprecipitations, leads to well-formed and much more homogeneous crystals. This would be analogous to repeated consumption and reformation of the Pt oxide when a high flux of As(III) is present. A more homogeneous anodic film results, a film having a smaller number of sites that have a greater than average electrocatalytic activity.

An experiment was described in Section VI for which the rate of decay of current with time at a given potential was determined to be independent of the total oxide coverage. These results can be interpreted in light of the relationship between k and the oxide coverage. These data were obtained from a double potential-step experiment. Gilroy (113) also performed double potential-step experiments in his study of oxide growth on Pt. In experiments where the potential of the first step was positive of the potential of the second step, Gilroy observed that after a certain amount of time at the second potential the slope of Q_{Ox} vs. $\log t$ was the same as that obtained when the potential was simply stepped to second value. In other words, the plot of Q_{Ox} vs. $\log t$ for the double potential-step experiment eventually became parallel to the plot of Q_{Ox} vs. $\log t$ for a simple potential-step experiment to the second (lower) potential, but was, of course, displaced to higher values of Q_{Ox} . Since

the rate of oxide growth eventually becomes the same in double potential-step experiments having the same final potential, the rates of decay of As(III) anodic current with time also will be the same.

In light of all of the evidence presented thus far, the following detailed mechanism for the oxidation of As(III) on noble-metal electrodes is proposed:



In this mechanism, the reactive oxygen-containing specie in 3) is denoted by $(\text{OH})_{\text{ads}}$, but the slow transfer of an oxygen atom from the oxide lattice is also possible, and, in fact, is probably the predominant reaction occurring at very high oxide coverages. Up to this point, most of the experimental results recorded in potentiodynamic and potentiostatic experiments have been explained in terms the effect that the applied potential and the oxide coverage have on the surface density of $(\text{OH})_{\text{ads}}$ and value of k . The oxide coverage also exerts an influence on the overall mechanism by effecting the adsorption of As(III) and the rate

constant of step 2 via changes in the work function and the availability of suitable electron acceptor levels. The experimental observation of potential-dependent regions for $E_d > \sim 1.3$ V and for $E_d < \sim 0.95$ V on the reverse scan have not been discussed up to this point; these dependencies are most easily seen in the hydrodynamic modulation data (Figures VII-1 and VII-2). The potential dependence of the As(III) anodic current for $E_d > 1.3$ V can be explained in terms of the dramatic changes in the surface density of $(OH)_{ads}$ that occurs during $O_2(g)$ evolution (284). This large increase in surface density evidently more than compensates for the decrease in the rate caused by the additional oxide growth that is simultaneously occurring. The effect that this additional oxide growth has on the overall rate is readily apparent by the magnitude of anodic current after oxygen evolution ceases. The rapid decrease in current with potential on the negative scan reflects the rapidity with which the rate of the oxygen evolution reaction decreases with decreasing overpotential (280).

The origin of the potential dependence of k at $E_d < 0.95$ V on the negative potential scan is somewhat less straightforward. Two different factors probably are responsible for this decrease in the overall rate with potential. As previously discussed, one of the factors that determines the magnitude of k is the strength of the interaction between the oxygen-containing reactant and the electrode surface. The Pt-OH interaction is less than the Pt-O and the $(OH)_{ads}$ is correspondingly more reactive. For E_a of 1.1 V to 1.6 V, the peak potential for Pt oxide reduction varies from about 0.53 V to about 0.4 V. It is clear from

Figures VII-1 and VII-2 that the anodic current begins to decrease at a potential where only a small fraction of the oxide film has been reduced. It is entirely likely, however, that the oxide that is reduced at potentials positive of the oxide peak potential is precisely the oxide that is most catalytically reactive in the oxidation of As(III). The decrease in the rate with potential is due to a potential-dependent removal of the most active oxygen-containing reactants. This argument is applicable also to those cases in which lattice oxygen is the reactive specie.

The surface density of the other reactant in step 3), $\cdot\text{As}(\text{OH})_{3\text{ads}}$, is potential dependent also. At very positive potentials, the equilibrium in step 2) is driven to the right. In this case, the surface density of $\cdot\text{As}(\text{OH})_{3\text{ads}}$ is limited by $:\text{As}(\text{OH})_3$ adsorption isotherm, which in turn is certainly effected by the oxide coverage. As the potential becomes less positive, the equilibrium of step 2) must begin to shift toward the left. Since the E°' of step 2) is unknown, it is not known how much the equilibrium of step 2) is shifted. If this E°' is considerably negative of 0.95 V, then the effect of potential on the surface density of $\cdot\text{As}(\text{OH})_{3\text{ads}}$ and therefore on the rate of step 3) would be negligible. Conversely, if this E°' was only slightly negative of 0.95 V, then the effect of potential in this manner would be significant. It is likely that changes in the reactivity of the oxide and changes in the surface density of $\cdot\text{As}(\text{OH})_{3\text{ads}}$ both contribute to the potential dependence of the anodic current at $E_d < 0.95$ V.

A few general comments can be made concerning the oxidation of As(III) on the other noble metals in acidic solutions. The oxidation mechanism on Au is in some respects analogous to the mechanism of Pt. As previously stated, the limiting-current plateau obtained on the forward scan is related to the relatively large range of potential in which AuOH exists. A major difference in the behaviors of Au and Pt is the activity of oxide having the next highest oxidation state. A monolayer of AuO displays essentially no activity in the oxidation of As(III). There are several possible explanations for this behavior. The free energy of adsorption of As(III) on Au is apparently much less than the corresponding energy on Pt; therefore, it is likely that As(III) adsorption on AuO occurs to a very small extent indeed. Another contributing factor may be the surface density of $(OH)_{ads}$ on AuO. This surface density may be very low on AuO relative to equivalent surface coverage for PtO. The Au-O bond strength may be strong enough to completely preclude any direct oxygen-atom transfer, whereas PtO can participate catalytically, albeit at a slow rate. It is interesting to note that the hydrodynamic modulation experiment showed an increase in electrode activity when the potential was scanned into the oxygen evolution region. It is in the oxygen evolution region that the surface density of $(OH)_{ads}$ again becomes large and the surface oxide is converted to $Au(OH)_3$ (306).

There does seem to be a good deal of evidence for a Pd electrode that points to the electroformation of PdOH and to the further oxidation to PdO. In this sense, Pd is very similar to Pt. However, in their study of CO oxidation, Blurton and Stetter (310) estimated that the coverage of the

active metal-OH species on Pd was several orders of magnitude less than that on Pt. Capon and Parsons (234,248) have pointed out that there is almost a complete lack of strongly-adsorbed intermediate products when Pd is exposed to simple organic molecules. Both of these factors undoubtedly contribute to the very low activity of Pd for the oxidation of As(III).

Evidence was presented in Section VI for an Ir electrode that showed that the anodic current obtained at an Ir electrode was significantly larger than that obtained Pt electrode and was much less time dependent under potentiostatic conditions. The fact that the current is less time dependent is undoubtedly due to the fact that continuing oxide growth does not occur on Ir unless the potential is cycled into the hydrogen region (220,221). The relatively high currents obtained on Ir are certainly due in part to the large real surface area of Ir oxide films caused by their extremely porous nature (223-225). On the negative side, however, it is known that Ir-O bonds are stronger than either Pt-O or Au-O bonds (224), so oxygen-atom abstraction from the oxide lattice is less likely to occur on Ir than on Pt or Au.

While the proposed mechanism (Equations VIII-1 to VIII-5) does account qualitatively for the vast majority of the experimental results, two sets of data cannot be explained at this time. The data obtained as a function of pH at constant ionic strength (Table VI-9) establishes that k decreases as the pH increases above 0.5. A decrease in the rate constant with an increase in pH is usually interpreted as meaning that H^+ is a reactant in a pre-equilibrium step, i.e., in chemical steps leading to and including the rds. Polish workers (46) have invoked hydronium ions as

reactants in a pre-equilibrium step, but their scheme cannot be accepted as correct in light of true structure of As(III) species in solution (4,5). Neither the proposed mechanism nor any other mechanism that was contemplated in the course of this research can account for this pH dependency. Similarly, the dependence of k on ionic strength at a constant pH (Table VI-1) cannot be explained on the basis of the proposed mechanism. For a given polarization time, t_1 , a plot of k vs. I is linear; a plot of k vs. I for a different time, t_2 , is parallel to the plot for t_1 . As far as is known, there are no other data of this kind for an electrode reaction in which a surface reaction is the rds. Even though the structure of the diffuse layer and the outer Helmholtz layer are likely to be modified by fairly large changes in I , it is not obvious how changes in I could effect a reaction occurring at the inner Helmholtz plane.

Several attempts were made in the course of this research to examine by Auger electron spectroscopy and secondary-ion mass spectrometry the surface of electrodes having various amounts of adsorbed or deposited As. None of these attempts was successful. The reason for this lack of success was identified by Sutyagina et al. (43) as arising from the rapid oxidation of the As in air to form As_2O_3 , which is volatile. From the data compiled by Stull (386), it is clear that the vapor pressure of As_2O_3 is quite low (e.g., T for 1 mm vapor pressure = 212°C for As_2O_3 , but is 2148°C for Al_2O_3). Meaningful surface analysis could be obtained only if the electrode was transferred via an apparatus that excluded oxygen. Dickinson et al. (101) have constructed just such an apparatus.

IX. SUMMARY

The purpose of this research was the study of the anodic oxidation of As(III) on Pt and several other noble metals in an attempt to gain a detailed understanding of the heterogeneous electrochemical process. Of specific interest was the role of surface oxides that are anodically formed on noble metals at positive potentials.

A wide variety of electrochemical techniques were used in the study of this oxidation; among these were potentiodynamic and potentiostatic experiments at rotating disc electrodes and rotating ring-disc electrodes. A relatively new technique, hydrodynamically-modulated voltammetry, also was used in one of its' first applications as a means of investigating an electrode reaction.

Cyclic voltammograms at a Pt rotating disc electrode are complex, exhibiting some potential regions in which the rate of As(III) oxidation is potential dependent and other regions in which this rate is potential independent. Onset of As(III) oxidation does not occur until the applied potential is nearly 400 mV positive of the thermodynamic potential; yet once oxidation begins, the current increases rapidly with potential. This combination of high overpotential and a rapid increase in current with potential is highly unusual and can be explained only in terms of an "electrocatalytic" mechanism. The onset of As(III) oxidation is accompanied by the oxidation of the electrode surface; this is strong evidence of the catalytic nature of the surface oxides. However, further oxidation of the electrode surface causes a decrease in the rate of

As(III) oxidation, thus showing that the surface oxides can act as oxidation inhibitors. This behavior is particularly evident on a Au electrode.

A mechanism for the anodic oxidation of As(III) on Pt is proposed that is consistent with the vast majority of the data. At the heart of this mechanism is a surface reaction between an adsorbed hydroxyl radical, or an oxygen atom in the oxide lattice, and an adsorbed arsenic specie; this surface reaction is the rate-determining step (rds). There is no transfer of charge across the electrode interface in the rds. The rate constant of this surface reaction is a complex function of the oxide coverage. Techniques were developed that gave values of rate constant under a variety of experimental conditions. The potential dependence of the rate of As(III) oxidation under certain conditions is explained in terms of the surface densities of the reactants in the surface reaction described above.

The general nature of the mechanism proposed for the oxidation of As(III) on Pt is demonstrated in discussions of the anodic behavior of As(III) on Au, Pd, and Ir.

X. SUGGESTIONS FOR FUTURE RESEARCH

This research, as does most scientific research, has answered some questions but has generated a great many more. Only a few of the more exciting areas for future research will be given here.

All of the experiments performed in this research were conducted on polycrystalline electrodes. There are considerable differences in reactivity among the principle crystallographic surfaces for many electrode reactions. It would be of some interest, therefore, to examine the oxidation of As(III) on two or more electrodes made from single crystals.

Folquer et al. (130) and Arvia (131) have shown that the properties of oxide films can be altered significantly by "potentiodynamic aging". The reactivity of such films toward the oxidation of a wide variety of substances should be investigated.

A great deal of work has been done in the area of electrocatalysis by ad-atoms of various metals on noble-metal substrates. This has not been applied to anodic oxidations of inorganic species to any extent. Two particularly attractive systems are Sn ad-atoms on Pt and Ru ad-atoms on Pt.

It should be possible, by the combination of a very high oxide coverage, a very high As(III) concentration, and a high rotation speed, to observe a truly "kinetically-controlled" rate of As(III) oxidation, i.e., the anodic current is independent of rotation speed. This should be verified.

The development of hydrodynamically-modulated voltammetry should continue, especially in its use as a means of elucidating reaction mechanisms in those cases where surface reactions introduce complications. A detailed analysis of the instrumental limitations of sinusoidal hydrodynamic modulation and computer-controlled square-wave hydrodynamic modulation should be undertaken in order to determine if one technique is superior to the other over a wide range of criteria.

As discussed in Section V.E, the surface reactions that occur on Pd obscure the electrochemistry of As(III) on Pd. Hydrodynamic modulation experiments using a Pd electrode would do much to increase the general understanding of the mechanism of As(III) on noble metals.

Use has been made of labelled oxygen in experiments designed to determine the mechanism of the oxygen evolution reaction on Pt. Similar techniques could be applied to oxidation of As(III); however, the rate of oxygen exchange between arsenate and H₂O would have to be carefully evaluated.

The heterogeneous reaction between As(III) and (OH)_{ads} has been proposed in this dissertation. It would be extremely interesting to examine the reaction rate of analogous homogeneous reaction. This could be done by using the technique of pulse radiolysis, in which a beam of high-energy electrons impinges on an aqueous solution. Hydroxyl radicals are formed in high yield in this procedure, and other energetic species such as solvated electrons can be scavenged by working in acidic solutions or by the addition of N₂O.

XI. BIBLIOGRAPHY

1. Arnold, J. P.; Johnson, D. M. Talanta 1969, 16, 1191.
2. Tomilov, A. P.; Chomutov, N. E. In "Encyclopedia of Electrochemistry of the Elements"; Bard, A. J., Ed.; Marcel Dekker: New York, 1974; Vol. II, Chapter 2.
3. Pourbaix, M. "Atlas of Electrochemical Equilibria in Aqueous Solutions"; Oxford: London, 1966; p. 516.
4. Loehr, T. M.; Plane, R. A. Inorg. Chem. 1968, 7, 1708.
5. Szymanski, H. A.; Marabella, L.; Hoke, J.; Harter, J. Appl. Spectrosc. 1968, 22, 297.
6. Susic, H. V.; Pjescic, M. G. J. Electroanal. Chem. 1972, 34, 535.
7. Myers, D. J.; Osteryoung, J. Anal. Chem. 1973, 45, 267.
8. Elenkova, N. G.; Tsoneva, R. A. Zh. Anal. Khim. 1974, 29, 1344.
9. El Shayeb, H. A. J. Electroanal. Chem. 1979, 102, 257.
10. Zhdanov, S. I.; Kryukova, T. A.; Vasil'eva, E. G. Electrokhimiya 1975, 11, 767.
11. Watson, A. In "Polarography of Molecules of Biological Significance"; Smyth, W. F., Ed.; Academic: London, 1979; Chapter 10.
12. Goparishnan, V.; Gnanasekaran, K. S. A.; Narasimham, K. D.; Udupa, H.V.K. Trans. SAEST 1976, (2), 251; Chem. Abstr. 1976, 85, 168831.
13. Meites, L. J. Am. Chem. Soc. 1954, 76, 5927.
14. White, M. C.; Bard, A. J. Anal. Chem. 1966, 38, 61.
15. Votava, J.; Bartusek, M. Coll. Czech. Chem. Comm. 1977, 42, 620.
16. Toropova, V. F.; Polyakov, Yu. N.; Soboleva, L. N. Zh. Anal. Khim. 1977, 32, 985.
17. Henze, G. Mikrochim. Acta 1981, 2, 343.
18. Holak, W. Anal. Chem. 1980, 52, 2189.
19. Trushina, L. F.; Kaplin, A. A. Zh. Anal. Khim. 1970, 25, 1616.

20. Kaplin, A. A.; Veits, N. A.; Stromberg, A. G. Zh. Anal. Khim. 1973, 28, 2192.
21. Forsberg, G.; O'Laughlin, J. W.; Megargle, R. G.; Koirtyohan, S. R. Anal. Chem. 1975, 47, 1586.
22. Kaplin, A. A.; Veits, N. A.; Mordvinova, N. M. Electrokhimiya 1978, 14, 227.
23. Krapivkina, T. A.; Roizenblat, E. M.; Nosacheva, V. V.; Zaretskii, L. S.; Utenko, V. S. Zh. Anal. Khim. 1974, 29, 1818.
24. Kaplin, A. A.; Veits, N. A.; Mordvinova, N. M.; Glukhov, G. G. Zh. Anal. Khim. 1977, 32, 687.
25. Kuwabara, T.; Suzuki, S.; Araki, S. Bull. Chem. Soc. Jpn. 1973, 46, 1690.
26. Kolthoff, I. M.; Probst, R. L. Anal. Chem. 1949, 21, 753.
27. Cozzi, D.; Vivarelli, S. Anal. Chim. Acta 1951, 5, 251.
28. Haight, G. P. J. Am. Chem. Soc. 1953, 3848.
29. Vasilyeva, E. G.; Zhdanov, S. I.; Krjukova, T. A. Electrokhimiya 1968, 4, 439.
30. Atanasiu, I. A.; Neata-Balescu, M. Rev. Chim. (Bucharest) 1974, 25, 826.
31. Aleksyeev, D. J. Russ. Phys-Chem. Soc. 1909, 41, 1155.
32. Lloyd, S. J.; Kennedy, A. M. Trans. Am. Inst. Chem. Engrs. 1924, 16, 29.
33. Lloyd, S. J.; Kennedy, A. M. Chem. Met. Eng. 1925, 32, 624.
34. Essin, O. A. Z. Electrochem. 1929, 35, 234.
35. Brown, O. W.; Hatfield, J. E.; Church, J. M. Trans. Electrochem. Soc. 1936, 70, 323.
36. MacNevin, W. M.; Martin, G. L. J. Am. Chem. Soc. 1949, 71, 204.
37. MacNevin, W. M.; Baker, B. B. Anal. Chem. 1952, 24, 986.
38. Baker, B. B.; MacNevin, W. M. J. Am. Chem. Soc. 1953, 75, 1476.

39. Zakharov, V. A.; Songina, O. A. Russ. J. Phys. Chem. 1964, 38, 412.
40. Catherino, H. A. J. Phys. Chem. 1967, 71, 268.
41. Daniels, M. J. Phys. Chem. 1966, 70, 1338.
42. Woods, R.; Kolthoff, I. M.; Meehan, E. J. J. Am. Chem. Soc. 1964, 86, 1698.
43. Sutyagina, A. A.; Kuznetsova, T. I.; Il'chenko, N. I.; Vovchenko, G. D. Elektrokhimiya 1977, 13, 1204.
44. Loucka, T. J. Electroanal. Chem. 1973, 47, 103.
45. Zakharov, V. A.; Songina, O. A., Kal'nitskaya, L. P. Elektrokhimiya 1971, 7, 1702.
46. Kedzierzawski, P.; Szklarska-Smialowska, Z. J. Electroanal. Chem. 1981, 122, 269.
47. Agapova, L. Ya.; Orgoratinikov, Yu. I.; Ponomareva, E. I. Kopleksn Ispol'z Miner. Syr'ya 1982, 1, 12; Chem. Abstr. 1982, 96, 112261.
48. Loodma, V. R.; Past, V. E. Elektrokhimiya 1967, 3, 260.
49. Nikitin, E. V.; Kazakova, A. A.; Parakin, O. V.; Galyametdinov, Yu. G.; Chernokal'skii, B. D.; Kargin, Yu. M. Dokl. Akad. Nauk SSSR 1980, 250, 899.
50. Nikitin, E. V.; Kazakova, A. A.; Parakin, O. V.; Chadaeva, N. A.; Kargin, Yu. M. Isv. Akad. Nauk SSSR, Ser. Khim. 1981, 9, 2168.
51. Hoare, J. P. "The Electrochemistry of Oxygen"; Interscience: New York, 1968.
52. Hoare, J. P. In "Advances in Electrochemistry and Electrochemical Engineering"; Delahay, P., Ed.; Interscience: New York, 1967; Vol. 6.
53. Gilman, S. In "Electroanalytical Chemistry"; Bard, A. J., Ed.; Marcel Dekker: New York, 1967; Vol. 2.
54. Gilman, S. Electrochim. Acta 1964, 9, 1025.
55. Belanger, G.; Vijn, A. K. In "Oxides and Oxide Films"; Vijn, A. K., Ed.; Marcel Dekker: New York, 1977; Vol. 5.
56. Feldberg, S. W.; Enke, C. G.; Bricker, C. E. J. Electrochem. Soc. 1963, 110, 826.

57. Angerstein-Kozłowska, H.; Conway, B. E.; Sharp, W. B. A. J. Electroanal. Chem. 1973, 43, 9.
58. Tilak, B. V.; Conway, B. E.; Angerstein-Kozłowska, H. J. Electroanal. Chem. 1973, 48, 1.
59. Conway, B. E.; Gottesfeld, S. J. Chem. Soc., Faraday Trans. I 1973, 69, 1090.
60. Goldstein, M. D.; Zalkind, T. I.; Veselovskii, V. I. Elektrokhimiya 1974, 10, 1533.
61. Srinivasan, S.; Gileadi, E. Electrochim. Acta 1966, 11, 321.
62. Conway, B. E.; Angerstein-Kozłowska, H. Acc. Chem. Res. 1981, 14, 49.
63. Vetter, K. J.; Schultze, J. W. J. Electroanal. Chem. 1972, 34, 131.
64. Vetter, K. J.; Schultze, J. W. J. Electroanal. Chem. 1972, 34, 141.
65. Schultze, J. W. Z. Phys. Chem., N.F. 1970, 73, 29.
66. Visscher, W.; Devanathan, M. A. V. J. Electroanal. Chem. 1964, 8, 127.
67. Ord, J. L.; Ho, F. C. J. Electrochem. Soc. 1971, 118, 46.
68. Biegler, T.; Woods, R. J. Electroanal. Chem. 1969, 20, 73.
59. Mayell, J. S.; Longer, S. H. J. Electrochem. Soc. 1964, 111, 438.
70. Fleischman, M.; Mansfield, I. R.; Wynne-Jones, W. F. K. J. Electroanal. Chem. 1965, 10, 511.
71. Vijh, A. K.; Conway, B. E. Z. Anal. Chem. 1967, 224, 160.
72. Tyurin, Yu. M.; Volodin, G. F. Elektrokhimiya 1970, 6, 1186.
73. Khanova, C. A.; Kasatkin, E. V.; Veselovskii, V. I. Elektrokhimiya 1972, 8, 451.
74. Woods, R. J. Electroanal. Chem. 1969, 21, 457.
75. Balej, J.; Spalek, O. Coll. Czech. Chem. Comm. 1972, 37, 499.
76. Visscher, W.; Blijlevens, M. J. Electroanal. Chem. 1973, 47, 363.
77. Parsons, R.; Visscher, W. J. Electroanal. Chem. 1972, 36, 329.

78. Biegler, T.; Rand, D. A. J.; Woods, R. J. Electroanal. Chem. 1971, 29, 269.
79. Vinnikov, Y. Y.; Shepelin, V. A.; Veselovskii, V. I. Electrokhimiya 1973, 9, 649.
80. Momot, E.; Bronoel, G. C. R. Acad. Sc. Paris 1972, 275, 721.
81. Momot, E.; Bronoel, G. J. Chim. Phys. 1973, 70, 1651.
82. Icenhower, D. E.; Urbach, H. B.; Harrison, J. A. J. Electrochem. Soc. 1970, 117, 1500.
83. Bagotskii, V. S.; Lukjanytschewa, W. J.; Osche, A. J.; Tichomirov, W. J. Dokl. Akad. Nauk SSSR 1964, 159, 644.
84. Ershler, B. Disc. Faraday Soc. 1947, 1, 269.
85. Shibata, S. Bull. Chem. Soc. Japan 1963, 36, 525.
86. Shibata, S. Bull. Chem. Soc. Japan 1967, 40, 696.
87. Kozawa, A. J. Electroanal. Chem. 1964, 8, 20.
88. James, S. D. J. Electrochem. Soc. 1969, 116, 1681.
89. Shibata, S.; Sumino, M. P. Electrochim. Acta 1971, 16, 1089.
90. Visscher, W.; Blijlevens, M. Electrochim. Acta 1974, 19, 387.
91. Shibata, S. Electrochim. Acta 1972, 17, 395.
92. Burke, L. D.; Roche, M. B. C. J. Electroanal. Chem. 1982, 137, 175.
93. Shibata, S.; Sumino, M. P. Electrochim. Acta 1981, 26, 517.
94. Shibata, S. Electrochim. Acta 1977, 22, 175.
95. Reddy, A. K. N.; Genshaw, M. A.; Bockris, J. O'M. J. Electroanal. Chem. 1964, 8, 406.
96. Greef, R. J. Chem. Phys. 1969, 51, 3148.
97. Kim, S. H.; Paik, W.; Bockris, J. O'M. Surf. Sci. 1972, 33, 617.
98. Vinnikov, V. V.; Shepelin, V. A.; Veselovskii, V. I. Electrokhimiya 1973, 9, 1557.

99. Kim, K. S.; Winograd, N.; Davis, R. E. J. Am. Chem. Soc. 1971, 93, 6296.
100. Allen, G. C.; Tucker, P. M.; Capon, A.; Parsons, R. J. Electroanal. Chem. 1974, 50, 335.
101. Dickinson, T.; Povey, E. F.; Sherwood, P. M. A. J. Chem. Soc., Faraday Trans. I 1975, 71, 298.
102. Bancroft, C. M.; Adams, I.; Coatsworth, L. L.; Bennewitz, C. D.; Brown, J. D.; Westwood, W. D. Anal. Chem. 1975, 47, 586.
103. Deglass, W. N.; Hughes, T. R.; Fadley, C. S. Cat. Rev. 1970, 4, 179.
104. Hammond, J. S.; Winograd, N. J. Electroanal. Chem. 1977, 78, 55.
105. Köver, L.; Ujhely, Cs.; Berenyi, D.; Varga, D.; Kadar, I.; Köver, A.; Miller, J. J. J. Electron Spec. Related Phenom. 1978, 14, 201.
106. Johnson, W. J.; Heldt, L. A. J. Electrochem. Soc. 1974, 121, 34.
107. Shibata, S. Electrochim. Acta 1972, 17, 395.
108. Ord, J. L.; De Smet, D. J.; Hopper, M. A. J. Electrochem. Soc. 1976, 123, 1352.
109. Appleby, A. J. J. Electrochem. Soc. 1973, 120, 1205.
110. Appleby, A. J. J. Electroanal. Chem. 1975, 68, 45.
111. Fujihara, M.; Kuwana, T. Electrochim. Acta 1975, 20, 565.
112. Battalova, Yu. V.; Smirnova, L. A.; Volodin, G. F.; Tyurin, Yu. M. Electrokhimiya 1975, 11, 1276.
113. Gilroy, D. J. Electroanal. Chem. 1976, 71, 257.
114. Fleischmann, M.; Thirsk, H. R. In "Advances in Electrochemistry and Electrochemical Engineering"; Delahay, P., Ed.; Interscience: New York, 1963; Vol. 3.
115. Ward, A.; Damjanovic, A.; Gray, E.; O'Jea, M. J. Electrochem. Soc. 1976, 123, 1599.
116. Gilroy, D. J. Electroanal. Chem. 1977, 83, 329.
117. Shibata, S. J. Electroanal. Chem. 1978, 89, 37.

118. Yamamoto, K.; Kolb, D. M.; Kotz, R.; Lehmpfuhl, G. J. Electroanal. Chem. 1979, 96, 233.
119. Damjanovic, A.; Yeh, L-S. R. J. Electrochem. Soc. 1979, 126, 555.
120. Angerstein-Kozłowska, H.; Conway, B. E.; Barnett, B.; Mozota, J. J. Electroanal. Chem. 1979, 100, 417.
121. Damjanovic, A.; Yeh, L-S. R.; Wolf, J. F. J. Electrochem. Soc. 1980, 127, 1945.
122. Damjanovic, A.; Yeh, L-S. R.; Wolf, J. F. J. Electrochem. Soc. 1980, 127, 1951.
123. Damjanovic, A.; Yeh, L-S. R.; Wolf, J. F. J. Electrochem. Soc. 1982, 129, 55.
124. Damjanovic, A.; Yeh, L-S. R.; Wolf, J. F. Electrochim. Acta 1981, 26, 825.
125. Damjanovic, A.; Ward, A. T. In "MTP Int. Review of Sci., Phys. Chem."; Bockris, J. O'M., Ed.; Butterworths: London, 1976; Series 2, Vol. 6.
126. Verway, E. J. W. Physica 1935, 2, 1059.
127. Bagotzky, V. S.; Tarasevich, M. R. J. Electroanal. Chem. 1979, 101, 1.
128. Slygin, A.; Frumkin, A. Acta Physicochim. URSS 1935, 3, 791; 1936, 4, 911; 1936, 5, 819.
129. Temkin, M. I. Zh. Fiz. Khim. 1941, 15, 296.
130. Folquer, M. E.; Zerbino, J. O.; de Tacconi, N. R.; Arvia, A. J. J. Electrochem. Soc. 1979, 126, 592.
131. Arvia, A. J. Acta Cient, Venzolana 1980, 31, 496.
132. Facci, J.; Murray, R. W. J. Electroanal. Chem. 1980, 112, 21.
133. Shibata, S.; Sumino, M. P. Electrochem. Acta 1981, 26, 517.
134. Novak, D. M.; Conway, B. E. J. Chem. Soc., Faraday Trans. I 1981, 77, 2341.
135. Conway, B. E.; Mozota, J. J. Chem. Soc., Faraday Trans. I 1982, 78, 1717.

136. Conway, B. E.; Novak, D. M. J. Electrochem. Soc. 1981, 128, 956.
137. El Wakkad, S. E. S.; El Din, A. M. S. J. Chem. Soc. 1954, 3098.
138. Brummer, S. B.; Makrides, A. C. J. Electrochem. Soc. 1964, 111, 1122.
139. Brummer, S. B., J. Electrochem. Soc. 1965, 112, 633.
140. Schultze, J. W.; Vetter, K. J. Ber. Bunsenges. Phys. Chem. 1971, 75, 470.
141. Dickertman, D.; Schultze, J. W.; Vetter, K. J. J. Electroanal. Chem. 1974, 55, 429.
142. Ferro, C. M.; Calandra, A. J.; Arvia, A. J. J. Electroanal. Chem. 1974, 50, 403.
143. Ferro, C. M.; Calandra, A. J., Arvia, A. J. J. Electroanal. Chem. 1974, 55, 291.
144. Ferro, C. M.; Calandra, A. J.; Arvia, A. J. J. Electroanal. Chem. 1975, 59, 239.
145. Ferro, C. M.; Calandra, A. J.; Arvia, A. J. J. Electroanal. Chem. 1975, 65, 963.
146. Capon, A.; Parsons, R. J. Electroanal. Chem. 1972, 39, 275.
147. Cadie, S. H.; Bruckenstein, S. Anal. Chem. 1974, 46, 16.
148. Goldstein, M.D.; Zalkind, T. I.; Veselovskii, V. I. Elektrokhimiya 1971, 8, 606.
149. Goldstein, M. D.; Zalkind, T. I.; Veselovskii, V. I. Elektrokhimiya 1973, 9, 699.
150. Gruneberg, G. Electrochim. Acta 1965, 10, 339.
151. Hoare, J. P. Electrochim. Acta 1964, 9, 1289.
152. Hoare, J. P. Electrochim. Acta 1966, 11, 311.
153. Bonewite, R. A.; Schmid, G. M. J. Electrochem. Soc. 1970, 117, 1367.
154. Sirohi, R. S.; Genshaw, M. A. J. Electrochem. Soc. 1969, 116, 910.
155. Vinnikov, Y. Y.; Shepelin, V. A.; Veselovskii, V. I. Elektrokhimiya 1972, 8, 1229.

156. Vinnikov, Y. Y.; Shepelin, V. A.; Veselovskii, V. I. Electrokhimiya 1972, 8, 1384.
157. Horkans, J.; Cahan, B. D.; Yeager, E. Surf. Sci. 1974, 46, 1.
158. Lazorenko-Manevich, R. M.; Stoyanovskaya, T. N. Electrokhimiya 1972, 8, 982.
159. Lazorenko-Manevich, R. M.; Stoyanovsky, T. N. Electrokhimiya 1972, 8, 1113.
160. Takamura, T.; Takamura, K.; Nippe, W.; Yeager, E. J. Electrochem. Soc. 1970, 117, 626.
161. Kim, K. S.; Sell, C. D.; Winograd, D. In "Electrocatalysis"; Breiter, M. W., Ed.; Electrochemical Society: Princeton, 1974.
162. Lohrongal, M. W.; Schultze, J. W. Electrochim. Acta 1976, 21, 957.
163. Schultze, J. W.; Lohrongal, M. W. Ber. Bunsenges. Phys. Chem. 1976, 80, 552.
164. Sotto, M. J. Electroanal. Chem. 1976, 70, 291.
165. Sotto, M. J. Electroanal. Chem. 1976, 72, 287.
166. Sumino, M.; Shibata, S. Denki Kagaku 1976, 44, 425; Chem. Abstr. 86:35645.
167. Clavilier, J.; Huong, C. N. V. J. Electroanal. Chem. 1977, 80, 101.
168. Ganon, J.-P.; Huong, C. N. V.; Clavilier, J. Surf. Sci. 1979, 79, 245.
169. Tucceri, R. I.; Posadas, D. J. Electroanal. Chem. 1982, 131, 377.
170. Rath, D. L., private communication, IBM Watson Research Center, 1982.
171. Chao, F.; Costa, M.; Tadjeddine, A.; Abeles, F.; Lopez-Rois, T.; Theye, M. L. J. Electroanal. Chem. 1977, 83, 65.
172. de Tacconi, N. R.; Zerbino, J. O.; Folquer, M. E.; Arvia, A. J. J. Electroanal. Chem. 1977, 85, 213.
173. Cordova, R.; Martins, M. E.; Arvia, A. J. J. Electrochem. Soc. 1979, 126, 1173.

174. Cordova, R.; Martins, M. E.; Arvia, A. J. Electrochim. Acta 1980, 25, 453.
175. Martins, M. E.; Cordova, R.; Arvia, A. J. Electrochim. Acta 1981, 26, 1547.
176. Huong, C. N. V.; Hinnen, C.; LeCoeur, J. J. Electroanal. Chem. 1980, 106, 185.
177. Fujishima, A.; Masuda, H.; Honda, K.; Bard, A. J. Anal. Chem. 1980, 52, 682.
178. Kirk, D. W.; Foulkes, F. R.; Graydon, W. F. J. Electrochem. Soc. 1980, 127, 1069.
179. Watanabe, T.; Gerischer, H. J. Electroanal. Chem. 1981, 117, 185.
180. Watanabe, T.; Gerischer, H. J. Electroanal. Chem. 1981, 122, 73.
181. Masuda, H.; Fujishima, A.; Honda, K. Bull. Chem. Soc. Jpn. 1980, 53, 1542.
182. Burke, L. D.; McRann, M. J. Electroanal. Chem. 1981, 125, 387.
183. Burke, L. D.; Lyons H. E.; Whelan, D. P. J. Electroanal. Chem. 1982, 139, 131.
184. Newman, R. C.; Burstein, G. T. J. Electroanal. Chem. 1981, 129, 343.
185. El Wakkad, S. E. S.; El Din, A. M. S. J. Chem. Soc. 1954, 3094.
186. Hickling, A.; Vrjosek, G. Trans. Faraday Soc. 1961, 57, 123.
187. Hoare, J. P. J. Electrochem. Soc. 1964, 111, 610.
188. Cadle, S. H. J. Electrochem. Soc. 1974, 121, 645.
189. Llopis, J. F.; Gamboa, J. M.; Victori, L. Electrochim. Acta 1972, 17, 2225.
190. Rand, D. A. J.; Woods, R. Anal. Chem. 1975, 47, 1481.
191. Capon, A.; Parsons, R. J. Electroanal. Chem. 1972, 39, 275.
192. Rand, D. A. J.; Woods, R. J. Electroanal. Chem. 1971, 31, 29.
193. Tarasevich, M. R.; Vilinskaya, V. S.; Burstein, R. Kh. Electrokhimiya 1971, 7, 1200.

194. Morcos, I. J. Electrochem. Soc. 1977, 124, 13.
195. Fortung, R.; Genesca, J.; Victori, Lluís Afinidad 1981, 38, 91; Chem. Abstr. 1981, 95, 122799.
196. Genesca, J.; Victori, Lluís Afinidad 1981, 38, 205; Chem. Abstr., 1981, 95, 140685.
197. Gossner, K.; Mizera, E. J. Electroanal. Chem. 1981, 125, 347.
198. Chierchie, T.; Mayer, C.; Lorenz, W. J. J. Electroanal. Chem. 1982, 135, 211.
199. Kim, K. S.; Gossmann, A. F.; Winograd, N. Anal. Chem. 1974, 46, 197.
200. Bold, W.; Breiter, M. W. Electrochim. Acta 1961, 5, 169.
201. Otten, J. M.; Visscher, W. J. Electroanal. Chem. 1974, 55, 1.
202. Otten, J. M.; Visscher, W. J. Electroanal. Chem. 1974, 55, 13.
203. Rand, D. A. J.; Woods, R. J. Electroanal. Chem. 1974, 55, 375.
204. Damjanovic, A.; Dey, A.; Bockris, J. O'M. J. Electrochem. Soc. 1966, 113, 739.
205. Kurnikov, B. D.; Zhurin, A. I.; Chernyi, V. V.; Vasil'ev, Yu. B.; Bagotskii, V. S. Electrokhimiya 1973, 9, 833.
206. Kurnikov, B. D.; Vasil'ev, Yu. B. Electrokhimiya 1973, 9, 1203.
207. Kurnikov, B. D.; Vasil'ev, Yu. B. Electrokhimiya 1973, 9, 1845.
208. Kurnikov, B. D.; Vasil'ev, Yu. B. Electrokhimiya 1974, 10, 77.
209. Podlovchenko, B. I.; Epstein, N. A. Electrokhimiya 1973, 1194.
210. Buckley, D. N.; Burke, L. D. J. Chem. Soc., Faraday Trans. I 1975, 71, 1447.
211. Buckley, D. N.; Burke, L. D. J. Chem. Soc., Faraday Trans. I 1976, 72, 2431.
212. Buckely, D. N.; Burke, L. D., Mulcahy, J. K. J. Chem. Soc., Faraday Trans. I 1976, 72, 1896.
213. Burke, L. D.; O'Sullivan, E. J. M. J. Electroanal. Chem. 1981, 117, 155.

214. Burke, L. D.; Wheelan, D. P. J. Electroanal. Chem. 1981, 124, 333.
215. Michell, D.; Rand, D. A. J.; Woods, R. J. Electroanal. Chem. 1977, 84, 117.
216. Woods, R. Isr. J. Chem. 1979, 18, 118.
217. Frazer, E. J.; Woods, R. J. Electroanal. Chem. 1979, 102, 127.
218. Schubert, C. C.; Page, C. L.; Ralph, B. Electrochim. Acta 1973, 18, 33.
219. Gottesfeld, S.; Srinivasan, S. J. Electroanal. Chem. 1978, 86, 89.
220. Zerbino, J. O.; de Tacconi, N. R.; Arvia, A. J. J. Electrochem. Soc. 1978, 125, 1266.
221. Zerbino, J. O.; Arvia, A. J. J. Electrochem. Soc. 1979, 126, 93.
222. Glarum, S. H.; Marshall, J. H. J. Electrochem. Soc. 1980, 127, 1467.
223. Mozota, J.; Conway, B. E. J. Electrochem. Soc. 1981, 128, 2143.
224. Mozota, J.; Conway, B. E. Electrochim. Acta 1983, 28, 1.
225. Mozota, J.; Conway, B. E. Electrochim. Acta 1983, 28, 9.
226. McCallum, C.; Pletcher, D. J. Electroanal. Chem. 1976, 70, 277.
227. Gilman, S. J. Phys. Chem. 1964, 68, 70.
228. Gibbs, T. K.; McCallum, C.; Pletcher, D. Electrochim. Acta 1977, 22, 525.
229. Watanabe, M.; Motoo, S. J. Electroanal. Chem. 1975, 60, 275.
230. Motoo, S.; Shibata, M.; Watanabe, M. J. Electroanal. Chem. 1980, 110, 103.
231. Motoo, S.; Watanabe, M. J. Electroanal. Chem. 1980, 111, 261.
232. Bilmes, S. A.; de Tacconi, N. R.; Arvia, A. J. J. Electrochem. Soc. 1980, 127, 2184.
233. Jolson, J. D. Diss. Abstr. Int. B 1982, 42, 3705.
234. Capon, A.; Parsons, R. J. Electroanal. Chem. 1973, 44, 239.

235. Adzic, R. R.; Popov, K. I.; Pamic, M. A. Electrochim. Acta 1978, 23, 1191.
236. Adzic, R. R.; O'Grady, W. E.; Srinivasan, S. J. Electrochem. Soc. 1981, 128, 1913.
237. Beden, B.; Lamy, C.; Leger, J. M. J. Electroanal. Chem. 1979, 101, 127.
238. Vassiliev, Yu. B.; Bogotzky, V. S.; Osetrova, N. V.; Mikhailova, A. A. J. Electroanal. Chem. 1979, 97, 63.
239. de Tacconi, N. R.; Leger, J. M.; Beden, B.; Lamy, C. J. Electroanal. Chem. 1982, 134, 117.
240. Sobkowski, J.; Zelenay, P. J. Electroanal. Chem. 1978, 91, 309.
241. Conway, B. E.; Angerstein-Kozłowska, H.; Czartoryska, G. Z. Phys. Chem. N.F. 1978, 112, 195.
242. Koch, D. F. A.; Rand, D. A. J.; Woods, R. J. Electroanal. Chem. 1976, 70, 73.
243. Kuliev, S. A.; Osetrova, N. V.; Bagotskii, V. S.; Vasil'ev, Yu. B. Elektrokhimiya 1980, 16, 1091.
244. Motoo, S.; Shibata, M. J. Electroanal. Chem. 1982, 139, 119.
245. Bagotzky, V. S.; Vasilyev, Yu. B. Electrochim. Acta 1964, 9, 869.
246. Bagotzky, V. S.; Vasilyev, Yu. B. Electrochim. Acta 1967, 12, 1323.
247. Sidheswaran, P.; Lal, H. J. Electroanal. Chem. 1972, 40, 143.
248. Capon, A.; Parsons, R. J. Electroanal. Chem. 1973, 45, 205.
249. Watanabe, M.; Motoo, S. J. Electroanal. Chem. 1975, 60, 259.
250. Mikhailova, A. A., Osetrova, N. V.; Vasil'ev, Yu. B. Elektrokhimiya 1977, 13, 518.
251. Hampson, N. A.; Willars, M. J.; McNicol, B. D. J. Chem. Soc., Faraday Trans. I 1969, 75, 2535.
252. Hampson, N. A.; Willars, M. J.; McNicol, B. D. J. Power Sources 1979, 4, 191.
253. Barradas, R. G.; Fletcher, S. Electrochim. Acta 1977, 22, 237.

254. Katayama, A. J. Phys. Chem. 1980, 84, 376.
255. Beden, B.; Lamy, C.; Kadrigan, F. J. Electroanal. Chem. 1982, 142, 171.
256. Bagotzky, V. S.; Vassilyev, Yu. B.; Khazova, O. A. J. Electroanal. Chem. 1977, 81, 229.
257. Sideheswaran, P.; Lal, H. J. Electroanal. Chem. 1973, 45, 152.
258. Raicheva, S. N.; Kalcheva, S. F.; Christov, M. V.; Sokolova, E. I. J. Electroanal. Chem. 1974, 55, 213.
259. Snell, K. D.; Keenan, A. G. Electrochim. Acta 1981, 26, 1339.
260. Dzhambova, A. G.; Sokolova, E. I.; Raicheva, S. N. Dokl. Bolg. Akad. Nauk 1981, 34, 815.
261. Rao, K. V.; Roy, C. B. Ind. J. Chem., Sec. A 1980, 19A, 840.
262. Vijh, A. K. Can. J. Chem. 1971, 49, 78.
263. Seber, J.; Vassiliev, Yu. B.; Bagotzky, V. S. Elektrokhimiya 1966, 2, 515.
264. Sidheswaran, P. Ind. J. Chem., Sec. A 1981, 20A, 570.
265. Kadrigan, F.; Beden, B.; Lamy, C. J. Electroanal. Chem. 1982, 136, 119.
266. Kadrigan, F.; Beden, B.; Lamy, C. J. Electroanal. Chem. 1983, 143, 135.
267. Sibille, S.; Moiroux, J.; Marot, J.-C.; Deycard, S. J. Electroanal. Chem. 1978, 88, 105.
268. Horyani, G. J. Electroanal. Chem. 1981, 117, 131.
269. Inzelt, G.; Szetey, E. Acta Chim. Acad. Sci. Hung. 1981, 107, 269.
270. Takamura, K.; Sakamoto, M. Chem. Pharm. Bull. 1979, 27, 254.
271. Sugawara, M.; Sato, M. Denki Kagaku Oyobi Kogyo Bursuri Kagaku 1976, 44, 498; Chem. Abstr. 1976, 86, 80762.
272. Alciaturi, C. E.; Marschoff, C. M. Electrochim. Acta 1980, 25, 353.
273. Levina, G. D.; Kolosova, G. M.; Vasil'ev, Yu. B. Elektrokhimiya 1977, 13, 1059.

274. Ginzburg, V. I. Zh. Fiz. Khim. 1959, 33, 1504.
275. Slaidens, G.; Actina, A. Latv. PSR Zinat. Akad. Vestis, Kim. Ser. 1980, (4), 497; Chem. Abstr. 1980, 93, 157778.
276. Appleby, A. J.; Pichon, B. J. Electroanal. Chem. 1979, 95, 59.
277. Seo, E. T.; Sawyer, D. T. J. Electroanal. Chem. 1964, 1, 184.
278. Comtat, M.; Mahenc, J. Bull. Soc. Chim. Fr. 1969, 11, 3862.
279. Audry, C.; Voinov, M. Electrochim. Acta 1980, 25, 299.
280. Damjanovic, A. In "Modern Aspects of Electrochemistry"; Bockris, J. O'M.; Conway, B. E., Ed.; Plenum: New York, 1969; No. 5, Chapter 5.
281. Damjanovic, A.; Ward, A. T. In "Electrochemistry - The Past Thirty and the Next Thirty Years"; Bloom, H.; Gutmann, F., Eds.; Plenum: New York, 1977; Chapter 6.
282. Burke, L. D. In "Electrodes of Conductive Metal Oxides"; Trasatti, S., Ed.; Elsevier: Amsterdam, 1980.
283. McNicol, B. D. In "Catalysis - Periodic Specialist Reports"; The Chemical Society: London, 1978; Chapter 10.
284. Damjanovic, A.; Jovanovic, B. J. Electrochem. Soc. 1976, 123, 374.
285. Miles, M. H.; Klaus, E. A.; Gunn, B. P.; Locker, J. R.; Serafin, W. E.; Srinivasan, S. Electrochim. Acta 1978, 23, 521.
286. Iwakura, C.; Fukuda, K.; Tamura, H. Electrochim. Acta 1976, 21, 501.
287. Burke, L. D.; McCarthy, F.; O'Meara, T. O. J. Chem. Soc., Faraday Trans. I 1972, 68, 1086.
288. Huang, C.-J. Diss. Abstr. Int. B 1977, 37, 6152.
289. Rozenthal, K. I.; Veselovskii, V. I. Dokl. Akad. Nauk USSR III 1956, 647.
290. Churchill, C. R.; Hibbert, D. B. J. Chem. Soc., Faraday Trans. I 1982, 78, 2937.
291. Erlikh, Yu. I.; Anni, K. L.; Palm, U. V. Elektrokhimiya 1978, 14, 1066.

292. Erlikh, Yu. I.; Anni, K. L.; Palm, U. V. Electrokhimiya 1979, 15, 1573.
293. Maximovitch, S. J. Electroanal. Chem. 1976, 72, 95.
294. Besenhard, J. O.; Parsons, R.; Reeves, R. M. J. Electroanal. Chem. 1979, 96, 57.
295. Gonzalo, P.; Aldaz, A.; Vazquez, J. L. J. Electroanal. Chem. 1981, 130, 209.
296. Van Effen, R. M.; Evans, D. H. J. Electroanal. Chem. 1979, 103, 383.
297. Van Effen, R. M.; Hui, B. S.; Evans, D. H. J. Electroanal. Chem. 1982, 135, 67.
298. Van Effen, R. M.; Evans, D. H. J. Electroanal. Chem. 1980, 107, 405.
299. Adzic, R. R.; Avramovic-Ivic, M. L. J. Electroanal. Chem. 1982, 134, 177.
300. Hauffe, W.; Heitbaum, J. Ber. Bunsenges. Phys. Chem. 1978, 82, 487.
301. Celdran, R.; Gonzalez-Velasco, J. J. Electrochim. Acta 1981, 26, 525.
302. Beltowska-Brzezinska, M. Electrochim. Acta 1979, 24, 247.
303. Beltowska-Brzezinska, M. Electrochim. Acta 1980, 25, 267.
304. Reynaud, J. A.; Malfroy, B.; Canesson, P. J. Electroanal. Chem. 1980, 114, 195.
305. Malfroy, B.; Reynaud, J. A. J. Electroanal. Chem. 1980, 114, 213.
306. Frankenthal, R. P.; Thompson, D. E. J. Electrochem. Soc. 1976, 123, 799.
307. Duncan, B. S.; Frankenthal, R. P. J. Electrochem. Soc. 1979, 126, 95.
308. Samec, Z.; Weber, J. Electrochim. Acta 1975, 20, 413.
309. Zakharov, V. A. Nov. Polyarogr., Tezisy Dokl. Vses. Sovesch. Polyarogr., 6th 1975, 119; Chem. Abstr. 1977, 86, 10026.
310. Blurton, K. F.; Stetter, J. R. J. Catal. 1977, 46, 230.

311. Zhirnova, M. I.; Vasina, S. Ya.; Manakova, G. S.; Petrii, O. A. Electrokhimiya 1979, 15, 1334.
312. Lu, P. W. T.; Ammon, R. L. J. Electrochem. Soc. 1980, 127, 2610.
313. Breiter, M. W. J. Electroanal. Chem. 1980, 109, 243.
314. Gossner, K.; Mizera, E. J. Electroanal. Chem. 1979, 98, 37.
315. Gossner, K.; Mizera, E. J. Electroanal. Chem. 1982, 140, 35.
316. Vol'fkovich, Yu. M.; Sedova, S. S.; Vassilyev, Yu. B.; Bagotsky, V. S. Electrokhimiya 1969, 5, 1195.
317. Bagotzky, V. S.; Vassiliev, Yu. B.; Khazova, O. A.; Sedova, S. S. Electrochim. Acta 1971, 16, 913.
318. Buckley, D. N.; Burke, L. D. J. Chem. Soc., Faraday Trans. I 1976, 72, 2431.
319. Hickling, A.; Hill, S. Trans. Faraday Soc. 1950, 46, 557.
320. Sanchez Cruz, M.; Fernandez Otero, T. An. Quim., Ser. A 1980, 76, 255; Chem. Abstr. 1980, 93, 194378.
321. Ureta Zanartu, M. S.; Fernandez Otero, T.; Sanchez Cruz, M. An. Quim., Ser. A 1981, 77, 94; Chem. Abstr. 1982, 96, 189535.
322. Hughes, S. Ph.D. Dissertation, Iowa State University, Ames, Iowa, 1982.
323. Nernst, W. Z. Physik. Chem. 1904, 47, 52.
324. Levich, V. G. "Physicochemical Hydrodynamics"; Prentice Hall: Englewood Cliffs, 1962; Chapter 2.
325. Riddiford, A. C. In "Advances in Electrochemistry and Electrochemical Engineering"; Delahay, P., Ed.; Interscience: New York, 1966; Vol. 4, Chapter 2.
326. Newman, J. J. Electrochem. Soc. 1966, 113, 501; 1966, 113, 1235.
327. Pleskov, Yu. V.; Filinovskii, V. Yu. "The Rotating Disc Electrode"; Consultants Bureau: New York, 1976; Chapter 3.
328. Bard, A. J.; Faulkner, L. R. "Electrochemical Methods"; John Wiley: New York, 1980.
329. Albery, J. "Electrode Kinetics"; Clarendon: Oxford, 1975.

330. Koutecky, J.; Levich, V. G. Zh. Fiz. Khim. 1958, 32, 1565.
331. Koutecky, J.; Levich, V. G. Dokl. Akad. Nauk SSSR 1957, 117, 441.
332. Saveant, J. M.; Vianello, E. Electrochim. Acta 1963, 8, 905.
333. Tong, L. K. J.; Liang, K.; Ruby, W. R. J. Electroanal. Chem. 1967, 13, 245.
334. Landsberg, R.; Thiele, R. Electrochim. Acta 1966, 11, 1243.
335. Haberland, D.; Landsberg, R. Ber. Bunsenges. Phys. Chem. 1966, 70, 724.
336. Scheller, F.; Muller, S.; Landsberg, R.; Spitzer, H.-J. J. Electroanal. Chem. 1968, 19, 187.
337. Scheller, F.; Landsberg, R.; Muller, S. J. Electroanal. Chem. 1969, 20, 375.
338. Scheller, F.; Landsberg, R.; Wolf, H. Z. Phys. Chem. (Leipzig) 1970, 243, 345.
339. Wolf, H.; Landsberg, R. J. Electroanal. Chem. 1970, 28, 295.
340. Lindemann, J.; Landsberg, R. J. Electroanal. Chem. 1971, 30, 79.
341. Nagy, F.; Horyani, G.; Vertes, G. Acta Chim. Acad. Sci. Hung. 1962, 34, 35.
342. Symthe, W. R. J. Appl. Phys. 1951, 24, 70.
343. Levart, E.; Schuhmann, D.; Contamin, O.; Etman, M. J. Electroanal. Chem. 1976, 70, 117.
344. Etman, M.; Levart, E.; Schuhmann, D. J. Electroanal. Chem. 1979, 101, 141.
345. Etman, M.; Levart, E.; Scarbeck, G.; Schuhmann, D. J. Electroanal. Chem. 1979, 101, 153.
346. Stonehart, P.; Kohlmayer, G. Electrochim. Acta 1972, 17, 369.
347. Albery, W. J.; Hitchman, M. L. "Ring-disc Electrodes"; Clarendon: Oxford, 1971.
348. Visco, R. E. In "Modern Electroplating", 3rd ed.; Lowenheim, F. A., Ed.; John Wiley: New York, 1974; Chapter 8.

349. Prater, K. B.; Bard, A. J. J. Electrochem. Soc. 1970, 117, 207.
350. Bruckenstein, S.; Napp, D. T. J. Am. Chem. Soc. 1968, 90, 6303.
351. Bruckenstein, S.; Feldman, G. A. J. Electroanal. Chem. 1965, 9, 395.
352. Grahame, D. C. Chem. Rev. 1947, 41, 441.
353. Gileadi, E.; Conway, B. E. In "Modern Aspects of Electrochemistry"; Bockris, J. O'M.; Conway, B. E., Eds.; Butterworths: London, 1964; No. 3.
354. Conway, B. E. "Theory and Principles of Electrode Processes"; Ronald Press: New York, 1965.
355. Conway, B. E.; Gileadi, E. Trans. Faraday Soc. 1958, 80, 2363.
356. Habib, M. A.; Bockris, J. O'M. In "Comprehensive Treatise of Electrochemistry"; Bockris, J. O'M.; Conway, B. E.; Yeager, E., Eds.; Plenum: New York, 1980; Vol. 1.
357. Cotton, F. A.; Wilkinson, G. "Advanced Inorganic Chemistry", 4th ed.; John Wiley: New York, 1980; p. 440.
358. Seanor, D. A.; Ambery, C. H. J. Chem. Phys. 1965, 42, 2967.
359. Kolb, D. M. In "Advances in Electrochemistry and Electrochemical Engineering"; Gerischer, H.; Tobias, C. W., Eds.; John Wiley: New York; Vol. 11.
360. Hubbard, A. T.; Osteryoung, R. A.; Anson, F. C. Anal. Chem. 1966, 38, 692.
361. Untereker, D. F.; Bruckenstein, S. Anal. Chem. 1972, 44, 1009.
362. Chagas, H. C. Can. J. Chem. 1979, 57, 2560.
363. Johnson, D. C.; Napp, D. T.; Bruckenstein, S. Electrochim. Acta 1970, 15, 1493.
364. Lown, J. A. Ph.D. Dissertation, Iowa State University, Ames, Iowa, 1979.
365. Johnson, D. C.; Bruckenstein, S. J. Am. Chem. Soc. 1968, 90, 6592.
366. Rubinstein, I. J. Phys. Chem. 1981, 85, 1899.

367. Miller, B.; Bellavance, M.I.; Bruckenstein, S. Anal. Chem. 1972, 44, 1983.
368. Johnson, D. C.; Bruckenstein, S. J. Electrochem. Soc. 1970, 117, 460.
369. Williams, W. J. "Handbook of Anion Determination"; Butterworths: London, 1979; p. 308.
370. Cadle, S. H.; Bruckenstein, S. J. Electroanal. Chem. 1973, 48, 325.
371. Lown, J. A.; Johnson, D. C. Anal. Chim. Acta 1980, 116, 41.
372. Miller, B.; Bruckenstein, S. Anal. Chem. 1974, 46, 2026.
373. Miller, B.; Bruckenstein, S. J. Electrochem. Soc. 1974, 121, 1558.
374. Tokuda, K.; Bruckenstein, S.; Miller, B. J. Electrochem. Soc. 1975, 122, 1316.
375. Tokuda, K.; Bruckenstein, S. J. Electrochem. Soc. 1979, 126, 431.
376. Kanzaki, Y.; Bruckenstein, S. J. Electrochem. Soc. 1979, 126, 437.
377. Albery, W. J.; Hillman, A. R.; Bruckenstein, S. J. Electroanal. Chem. 1979, 100, 687.
378. Austin, D. S., unpublished results, Iowa State University, 1982.
379. Bockris, J. O'M.; Reddy, A. K. N. "Modern Electrochemistry"; Plenum: New York, 1970.
380. Schultze, J. W.; Habib, M. A. J. Appl. Electrochem. 1979, 9, 255.
381. Adamson, A. W. "A Textbook of Physical Chemistry"; Academic: New York, 1973.
382. Harned, H. S.; Owen, B. B. "The Physical Chemistry of Electrolyte Solutions"; Reinhold: New York, 1950.
383. van der Wiele, K.; van den Berg, P. J. In "Comprehensive Chemical Kinetics"; Bamford, C. H.; Tipper, C. F. H., Eds.; Elsevier: Amsterdam, 1978; Vol. 20.
384. Gordon, G.; Taube, H. Inorg. Chem. 1962, 1, 69.
385. Halpern, J.; Taube, H. J. Am. Chem. Soc. 1952, 74, 380.
386. Stull, D. R. Ind. Eng. Chem. 1947, 39, 517.

XII. ACKNOWLEDGEMENTS

If I were to truly acknowledge the contributions of all of the people who have assisted me in my education, this section might well be as long as the dissertation itself. The best that I can do in a reasonable amount of space is to gratefully acknowledge some of those who have helped me in some very important ways.

Everyone expresses some gratitude to their major professor. I cannot express enough gratitude to mine. I have had two relationships with Professor Dennis C. Johnson. The first has been of a highly professional nature. His guidance in my research was exactly the correct combination of collaboration and benign neglect. One simply could not have asked for a better working atmosphere. The second relationship has been of a more personal nature and arose because of a sense of shared values and priorities. Right now I am hard pressed to say which relationship has been more important to me. His only fault was that he was not able to give me the golf tip that would cure my slice, but then neither has anyone else.

I was honored to receive the Colin Garfield Fink Summer Fellowship from the Electrochemical Society for the summer of 1982 and I gratefully acknowledge this source of financial support.

I would like to thank my parents and my wife's parents for their support in a large number of ways. They have made the stay at Iowa State more pleasant, more comfortable, and in some cases, even possible.

Glenn Leucke is to be thanked for his excellent and very timely analysis of the mathematics of nonlinear diffusion.

I have both enjoyed the company of and learned a great deal from the past and present members of the electroanalytical group. A special thanks goes to those that I have interacted with the most: Dr. Scott Hughes (who inspired us by his absence), Dr. Ron Tsang, and Deb Austin.

I also would like to thank Bob Barron for his scientific discussions and his friendship over the last five years.

The Jacksons provided us a place to live for the last three weeks of our time in Ames. Had it not been for them, a very trying time might well have been impossible.

Finally, I want to thank my wife for her support and her plain hard work. Her efforts in caring for me and our family probably have not been appreciated to the extent that they should have been. Without them, life would have been much more difficult and progress would have been much slower. I simply would not have had the patience to do many of the things that she has done. I look forward to the opportunities to adequately repay her.